Cell derived microvesicles: Novel preparative and characterization methods

Cherré, Solène

Publication date:
2016

Document Version
Publisher's PDF, also known as Version of record

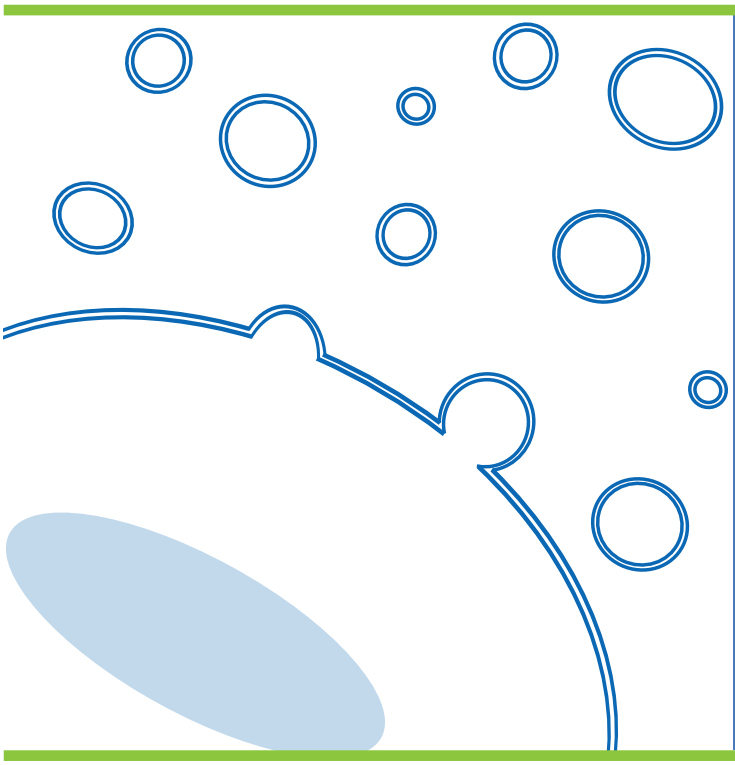

Cell derived microvesicles:
Novel preparative and characterization methods

Solène Cherré
PhD Thesis March 2016

DTU Nanotech
Department of Micro- and Nanotechnology

Cell derived microvesicles: Novel preparative and characterization methods

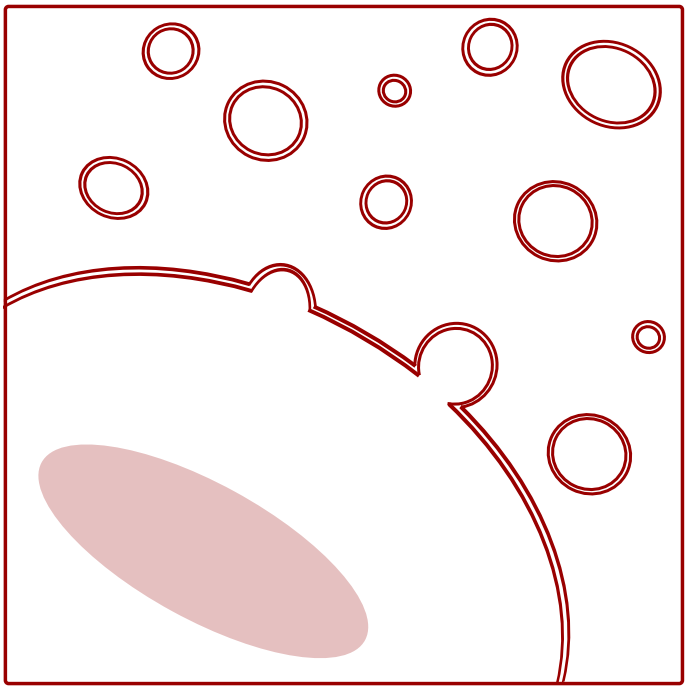

Solène Cherré

PhD thesis

DTU Nanotech
Department of Micro- and Nanotechnology

PHD THESIS

Cell derived microvesicles: Novel preparative and characterization methods

A thesis submitted in partial fulfilment of the requirements for the PhD degree of the Technical University of Denmark.

Author:
Solène Cherré

Supervisors:
Noemi Rozlosnik
Niels H.H. Heegaard

Technical University of Denmark
Department of Micro- and Nanotechnology
March 31, 2016

Preface

This thesis is submitted as partial fulfilment of the requirements to obtain the PhD degree of the Technical University of Denmark.

The PhD project has been conducted in the Department of Micro- and Nanotechnology (DTU Nanotech), in the research group Polymer Microsystems for Medical Diagnostics from April, 1st 2013 to March, 31st 2016. The work was supervised by Noemi Rozlosnik and co-supervised by Niels H.H. Heegaard (Statens Serum Institut, Copenhagen) and financed by a scholarship from DTU Nanotech.

A part of the project was also conducted in an external research stay at the International Iberian Nanotechnology Laboratory (Braga, Portugal) from May to July 2015 and October 2015, under the supervision of Elisabete Fernandes, Marta Oliveira and Prof. Paulo Freitas.

Kongens Lyngby, March 2016

Abstract

Cell derived microvesicles (MVs) are a type of extracellular vesicles released by a blebbing of the cell membrane. They have a diameter ranging from 50 to 1000 nm and carry the same phenotype (i.e. membrane receptors) as the parental cells. MVs play an important role in the cell-cell communication transferring signal molecules between cells. Moreover studies have shown that the number of MVs differs between healthy persons and patients with disease such as cancer, proinflammatory diseases and autoimmune diseases. Since MVs are easily accessible from body fluids, they have been proposed as novel circulating biomarkers. However, the conventional methods to isolate or characterize MVs are often not suited for such small and heterogeneous vesicles and the lack of standardization complicates the comparison between different studies. The goal of this PhD project was to investigate new methods for the characterization and isolation of MVs.

In the first part of the project, a population of MVs was generated from the human umbilical vein endothelial cells (HUVECs). The size distribution and the concentration of the MVs were characterized by atomic force microscopy (AFM) and nanoparticle tracking analysis (NTA). We compared the MVs released from HUVECs activated with the apoptosis-inducing chemical, staurosporine, and non activated HUVECs and found that the size distributions of the two MV populations were not significantly different, while the MV concentration was three times higher in the activated samples. The surface markers were analysed by an assay where MVs were captured on a surface functionalized with antibodies against the surface markers and then imaged by AFM. We found that this method can be used to select the MVs by their surface markers allowing the size characterization at the same time. In the rest of the project, HUVEC MVs were used as test MV population.

We addressed the challenges of the MV isolation by developing a diffusion-based microfluidic device separating MVs from contaminants. The separation occurred only according to size, thereby collecting all MVs above 50 nm. The size of the microfluidic channel was first determined by theoretical estimations and a finite element simulation. The device was then realised using microfabrication techniques. The results of the experimental testing were in good agreement with the simulated performances. Around 25% of the proteins could be removed from the sample. Moreover, the preliminary results with HUVEC MVs separated in the microdevice showed a recovery of approximately 60% compared to 30% with conventional centrifugation.

In a third part, we proposed the use of a magnetoresistive (MR) biosensor for the rapid and specific detection of MVs in the perspective of efficient diagnostics. This biosensor was based on sandwich assay where two probes recognized two different surface markers of the MVs. In this biosensor, the detection was performed within 40 minutes. The MR biosensor was able to discriminate between MVs from two different cell lines. This MR biosensor has a great potential for a multiplex detection to determine the MV profile in a given sample.

In conclusion, this work proposed two new methods for the isolation and characterization of MVs and provided a relevant step towards MV based diagnosis.

Resumé

Cell derived microvesicles (MVs) er en art ekstracellulær vesikel, som afsnører sig fra cellemembranen. De har en diameter fra 50 nm til 1000 nm og bærer de samme receptorer (phenotype) som modercellen. MVs er en vigtig del af kommunikationen mellem cellerne og overfører signalmolekyler til omkringliggende celler. Desuden har flere studier vist, at antal af MVs varierer mellem raske personer og patienter med forskellige sygdommme som cancer, proinflammatoriske sygdomme og autoimmun sygdomme. MVs er let tilgængelige og kan derfor bruges som ikke invasive biomarkører. De nuværende karakteriserings- og isoleringsmetoder er dog ikke velegnet til disse små og heterogene vesikler. Mangel på konsensus i metoderne komplicerer sammenligningen mellem forskellige studier. Formålet med dette projekt var at analysere nye metoder til karakterisering og isolering af MVs.

I den første del af projektet genereres en population af MVs fra endotelcellerne HUVECs. Størrelsen af MVs blev karakteriseret med atomar kraftmikroskopi (AFM) og nanoparticle tracking analysis (NTA). MVs fra aktiverede HUVECs og MVs fra uaktiverede HUVECs blev sammenlignet og størrelsesfordelingen af de to populationer var ikke signifikant forskellig. Men koncentration af aktivererede MV var tre gange højere end uaktiverede MVs. Overfladereceptorene blev analyseret med enzyme-linked immunosorbent assay (ELISA) og med et forsøg hvor MVs blev bundet på en overflade med specifikke antistoffer og visualiseret med AFM. Vi viste at denne metode kan bruges til at separere MVs baseret på deres overflademarkøre og samtidig karakteresere størrelsen. I den resterende del af dette projekt blev denne MV population brugt som test MV population.

I anden del af projektet beskæftigede vi os med udfordringerne ved af isolering af MVs. En mikrofluidik enhed blev udviklet, som fungerede ved hjælp af diffusion, og kunne isolerer MVs fra proteiner kun på baggrund af deres størrelse. MV større end 50 nm blev isoleret. Dimensionerne af kanalen blev først bestemt ud fra en teoretisk beregning og en finite element simulering. Enheden blev fremstillet med standard mikrofabrikationsmetoder. Resultaterne fra forsøget lignede meget resultaterne fra simuleringen. Næsten 25% af proteinerne kunne udtrækkes fra prøverne. Desuden viste tabet af MVs sig at være 20% mindre med mikrofluidik enheden end med standard centrifugeringsprotokollen.

I tredje del brugte vi en magnetoresistive (MR) biosensor til at detektere MVs til brug indenfor diagnostik. Denne biosensor fungerede som et sandwich assay, hvor to specifikke sonder genkendte to markøre på overfladen af MVs. Signalet er kvantitativt og biosensoren kunne detektere MVs på 40 minutter. MR biosensoren kunne skelne mellem MVs fra to forskellige cellelinjer. Denne MR biosensor har udvist et stort potentiale for at blive brugt i et multiplex detektionsskema for at bestemme flere typer af MVs i en biologisk prøve.

Dette projekt viser to nye metoder til isolering og karakterisering af MVs og bidrager hermed til at vi nu er et skridt nærmere anvendelsen af MVs i diagnostik.

Acknowledgements

During the three years of my PhD, I have learnt a lot and I am convinced that the new knowledge will accompany me for my future, while continuing growing. All along the way, I had the chance of working with and being surrounded by wonderful people, who all contributed to the fulfilment of the thesis. I would like to thank all of them.

First of all, I would like to express my deep gratitude to my supervisor Associate Professor Noemi Rozlosnik for giving me the opportunity to conduct my PhD thesis in her research group PolyMeDiag. You were very supportive all along the project, enabling me to follow my own ideas while guiding me on the PhD path. Your door was always open for a meeting, to answer questions or doubt. I would like also to thank you for giving me the idea and topic of the thesis, which I really enjoyed discovering.

I would also like to thank my co-supervisor Niels H.H. Heegaard and Ole Østergaard from the Statens Serum Institut in Copenhagen. Thank you very much for introducing me to the field of the microvesicles. You were always available to answer my questions and the project progressed significantly thank to your suggestions and guidance.

My greatest thanks go also to the former and present members of the PolyMeDiag group, especially Maria Dimaki, Julie Kirkegaard, Mark Holm Olsen, Johannes Daprá and Giulio Rosati. Our discussions allowed me to see my project from other perspectives and your suggestions certainly benefited the project immensely. Thank you very much to Maria Dimaki for all your help with the simulations, all your advice on this part of the work and all the time you took to explain me about microfluidics. Tusind og mere tak til Julie og Mark for den fantastisk atmosfære på kontoret. Vores videnskabelig diskussioner og jeres spørgsmål altid har givet mig mere motivation og nye ideer til projektet. Jeg vil også sige tusind tak for de ikke-videnskabelig diskussion og kaffeetid, og især for jeres støtte og uttalige forklaringen omkring den danske samfund. Det har altid været en stor hjælp, at jeg måtte komme med alle mine spørgsmål.

I would like to thank the students that I had the pleasure to supervise, especially Mathilde Granberg and Maël L'hostis. I also learnt a lot while teaching you and discussing with you. I am very grateful for your help in running some of the experiments included in the thesis.

I would like to acknowledge Christian Engelbrekt from DTU Kemi for introducing me to the nanoparticle tracking analysis instrument and giving me the possibility of using the instrument throughout the project. Without your help, a lot of experiments in the thesis would have been much more difficult to perform.

I would like to thank all my former and present colleagues at DTU Nanotech, who gave advice, shared some time in the lab, helped in a way or other. DTU Nanotech is a great place to work and conduct a PhD thesis. A special thank to the technician team, Lene, Lotte, Ole, Per and Jannik, for your help in any matter. Thanks to your great organization, my project was greatly facilitated. Thank you also to the administration team, always available to answer questions.

I am very grateful to the researchers and personnel of the International Iberian Nanotechnology Laboratory (INL) in Braga, Portugal for warmly welcoming me during the four months of my external research stay. I am very happy that I had the opportunity to conduct a part of

my project and I would like to acknowledge my supervisors from INL, Prof. Freitas, Marta Oliveira and specially Elisabete Fernandes, who did not count her time to help me. It was a great pleasure to work with you. You were always very good to keep the motivation up. I learnt a lot from you, especially regarding scientific thinking.

Finally, I would like to thank a thousand times my dear friends and loving family for their continuous support, their encouragements. I would like to thank all my family, especially my parents Françoise and Hubert and my brother Ronan; my friends from Denmark, Kat, Layla, Ritika, Silvia, Siyin, Åse; my friends from Berlin, Amandine, Jane, Kristin, Lydia, Mareen, Sophie, Vicky, Victoria; my friends from France, Marie, Noémie, Pauline; etc. Thank you very much for your patience with me.

And last but not least, I would like to give my loving thanks to my boyfriend, Joachim Habel. Your unconditional support really helped me to progress every day. You had great ideas and propositions. With your trust, I could keep going. Thank you very much for proof reading all the thesis. I hope that we will continue having opportunity to discover the world together.

List of publications and submitted manuscripts

Papers and book chapter

Cherré S, Fernandes E, Oliveira M, Rozlosnik N, Freitas P (2016) Rapid and specific detection of cell-derived microvesicles using a magnetoresistive biosensor. Manuscript in preparation for submission
This work is included in part IV. My contribution was the design of the study, the performance of the experiments, data analysis, the redaction of the manuscript.

Cherré S, Østergaard O, Heegaard NHH, Rozlosnik N (2016) Generation and characterization of cell-derived microvesicles from HUVECs. International Journal of Molecular Sciences, special issue "Focus on extracellular vesicles" Submitted
This work is included in part II. My contribution was the design of the study, the performance of the experiments (except MV array experiments), data analysis, the redaction of the manuscript.

Habel J, Ogbonna A, Larsen N, **Cherré S**, Kynde S, Midtgaard SR, Kinoshita K, Krabbe S, Jensen GV, Hansen JS, Almdal K, Hélix-Nielsen C (2015) Selecting analytical tools for characterization of polymersomes in aqueous solution. RSC Adv. vol.5, 97:79924–79946.
This paper is about different characterization tools that are available to measure polymersomes (vesicles made of polymers). 17 different techniques were used to characterize polymersomes based on amphiphilic polybutadiene-polyethylene oxide block copolymer. The aim was to provide users with a guide to select the best suited techniques to characterize polymersomes. In this paper, my contribution was the AFM and NTA analysis (measurement and data analysis) as well as some support in the other data analysis. This paper is not included in the thesis.

Cherré S, Rozlosnik N (2015) Polymer Based Biosensors for Medical Applications. In: Puoci F (ed) Adv. Polym. Med. Springer International Publishing Switzerland, pp 513–537
The aim of this book chapter was to describe recent advances about polymer based biosensors designed for medical applications. The chapter gives first an overview about the function principle of biosensors. In a second part the use of conductive polymers as electrode material in biosensors is discussed. Finally in a third part we presented the molecularly imprinted technology as an alternative for bioelements. I wrote the book chapter together with Noemi Rozlosnik. This book chapter is not included in the thesis.

Rosati G, Daprà J, **Cherré S**, Rozlosnik N (2014) Performance Improvement by Layout Designs of Conductive Polymer Microelectrode Based Impedimetric Biosensors. Electroanalysis 26:1400-1408.
This paper proposed a model to predict the performances of an electrochemical biosensor. The influence of the geometry of the electrodes and microchannels was evaluated using a computer simulation. The biosensor based on PEDOT:TsO electrodes were microfabricated to test the optimized biosensor design with the antibiotics ampicillin as analyte. I participated in the fabrication of the chips and in the generation of ideas. This paper is not included in the thesis.

Kiilerich-Pedersen K, Daprà J, **Cherré S**, Rozlosnik N (2013) High sensitivity point-of-care device for direct virus diagnostics. Biosens Bioelectron 49:374-9.
In this paper, an all-polymer biosensor was developed to detect influenza A viruses. The detection was based on a conductive polymer electrode where aptamers against influenza A were immobilized. The detection was based on an impedance signal and was quantitative. Clinically relevant concentrations of influenza A viruses were detected directly from saliva. I participated in the work involving the viruses as well as the functionalization of the chip. This paper is not included in the thesis.

Conference proceedings

Cherré S, Østergaard O, Heegaard NHH, Rozlosnik N (2014) Analysis of Cell-Derived Microparticles with Highly Precise Nanotechnological Methods. J. Nanomater Mol Nanotechnol. S2-004

Contribution to conferences

Cherré S, Fernandes E, Oliveira M, Rozlosnik N, Freitas P (2015) Detection of extracellular vesicles on a magnetoresistive sensor platform, First Iberian Meeting on Extracellular Vesicles, Porto, Portugal (Oral presentation)

Cherré S, Olsen M.H., Rozlosnik N (2015) Towards a diffusion based microfluidic device for the isolation of cell-derived microparticles, EMBS Micro- and Nanotechnology in Medicine, Oahu, USA (Poster)

Cherré S, Østergaard O, Heegaard NHH, Rozlosnik N (2014) Towards powerful analysis tools for cell-derived microparticles, 9th international summer school on nanosciences and nanotechnologies, Thessaloniki, Greece (Poster)

Cherré S, Østergaard O, Heegaard NHH, Rozlosnik N (2014) Analysis of cell-derived microparticles with highly precise nanotechnological methods, 5th International BioNanoMed, Krems, Austria (Oral presentation)

Cherré S, Rozlosnik N (2013) Production and characterization of cell-derived microparticles, Production and characterization of cell-derived microparticles, London, United Kingdom (Oral presentation)

Contents

List of Figures

List of Tables

List of Symbols

ρ	Density	kg/m^3
η	Dynamic viscosity	Ns/m^2
c	Concentration	mol/m^3
$c_{S_{inlet}}$	Concentration at sample inlet	mol/m^3
$c_{MV_{outlet}}$	Concentration at MV outlet	mol/m^3
$c_{WS_{outlet}}$	Concentration at waste outlet	mol/m^3
d	Diameter of particle	m
D	Diffusion coefficient	m^2/s
h	Height/depth of the channel	m
l	Length of the channel	m
Q	Volumetric flow rate	m^3/s
r	Radius of particle	m
t	Time	s
V	Volume	m^3
w	Width of the channel	m

Part I

General introduction

Chapter 1

Introduction

1.1 Motivation and aims of the thesis

Early diagnosis of diseases is a key to successful treatments of the patients. This requires very specific biomarkers that can be detected in the early stages of the disease and that are easily accessible for detection. Cell derived microvesicles (MVs) are novel biomarkers, which meet those requirements. They are now extensively investigated as seen by the exponential increase in publications since 1985 [1, 2].

MVs have first been described by Chargaff and West [3] who isolated a factor triggering blood clotting from plasma centrifuged at high speed. In 1967, Wolf [4] presented the evidence for the presence of particles originated from platelets in the blood. Further research has shown that MVs are not cellular debris but have an important biological function and are now accepted as diagnostics and prognostics biomarkers.

MVs are a class of extracellular vesicles (EVs) [5]. They are spherical vesicles with different sizes (from 50 nm to 1 µm). Nearly all types of cells are releasing MVs. The release of the MVs occurs through an outward budding of the cell membrane. MVs are formed of the membrane of the cell of origin. Therefore they carry the same surface receptor as the parental cell and their origin can herewith be identified [6]. Other types of EVs are among others exosomes (30 to 100 nm) and apoptotic bodies (1 to 5 µm).

MVs take an active part in the cell-cell communication and the cellular protection against external and internal stress [7]. The study of MVs provides novel insight into basic cellular pathways. Moreover many studies have focussed on the enumeration of MVs from body fluids. Significantly different MV levels were detected for several diseases such as autoimmune diseases [8], cancer [9, 10] or cardiovascular diseases [11].

However, the methods for characterization and isolation of MVs lack standardization [12]. This makes it difficult to compare the results of different investigations. The International society for extracellular vesicles (ISEV) has addressed the problem in numerous studies [13–15] and provided guidelines for consistent analysis and report of work with EVs [16]. Moreover, characterization and isolation methods are not yet well adapted for these heterogeneous vesicles in the complex body fluids [15]. For example the main method used for the characterization of MVs is flow cytometry, but this method is only well suited for objects larger than approximately 100 to 200 nm and relies on the availability of antibodies against the interesting markers. Therefore novel and reliable preparative and analytical methods are highly required to improve the results of MVs studies and bring MVs further towards a clinical application.

The goal of this project was to explore novel, state of the art isolation and characterization methods for MVs. The major focus was to develop simple methods in the perspective of a future clinical application.

In the first part, the aim was to obtain a well characterized population of MVs, which could be generated in a reproducible way for use as test population for further investigation and development of new microvesicle related techniques.

The goal of the second part of the thesis was to develop a microfluidic device for the purification of MVs in a simple, easy to use system to overcome the limitations of current isolation methods such as the need for large sample volume and the low recovery of MVs.

In the third part, the thesis approaches the diagnostics based on MVs. Our aim was to investigate if a magnetoresistive (MR) biosensor was able to detect MVs in a rapid way as well as discriminating different types of MVs.

From this work, we expect that the proposed solutions will significantly contribute to bring forward microvesicle based diagnosis.

1.2 Outline of the thesis

In the following, a brief description of the different parts of the thesis is given.

Part I describes the theoretical background of this work, focussing on the isolation and characterization methods used currently in EV research in general. Most isolation and characterization methods are indeed relevant and applied for all types of EVs including MVs.

Part II presents a study where MVs were generated from endothelial cells in a reproducible way. The focus was on the characterization of the MVs with atomic force microscopy (AFM) and with nanoparticle tracking analysis (NTA).

Preliminary results of this work were presented in an oral communication (title: Production and characterization of cell-derived microparticles) at the Society for Endocrinology-sponsored microparticles workshop 2013 (December, 16th 2013, London, United Kingdom). Part of this work was also presented in an oral communication (title: Analysis of cell-derived microparticles with highly precise nanotechnological methods) at the BioNanoMed 2014 (March, 26-28th 2014, Krems, Austria). A conference proceeding on the preliminary results was published under the title Analysis of Cell-Derived Microparticles with Highly Precise Nanotechnological Methods [17] in Journal of Nanomaterials & Molecular Nanotechnology. The original conference proceeding can be found in appendix B.2 on page 185.

Part III presents the development of a diffusion based microfluidic device for the separation of MVs at low forces. Theoretical calculations and experimental testing were performed.

Part this work was presented in a poster (title: Towards a diffusion based microfluidic device for the isolation of cell-derived microparticles) at the EMBS Micro and Nanotechnology in Medicine Conference (MNMC 14, Oahu, HI, USA). The experimental work (fabrication and testing of the device with standard samples) was realised by internship student Maël L'Hostis under my supervision.

Part IV reports the proof of concept study for the detection of MVs on a portable MR sensor platform. The results of the proof of concept study shows that the biosensor was able to discriminate between MVs isolated from two different types of cells.

This work has been performed during an external research stay at the International Iberian Nanotechnology Laboratory (INL, inl.int) together with Elisabete Fernandes and Marta Oliveira and under the supervision of Prof. Paulo Freitas. Part of this work was presented in an oral communication (title: Detection of extracellular vesicles on a magnetoresistive sensor platform) at the first Iberian meeting on extracellular vesicles on September, 30th 2015 in Porto, Portugal. Part of this work will be published. A manuscript is in preparation.

Part V concludes and summarizes the results as well as presents an outlook for future studies.

Chapter 2

Background about microvesicles

Extracellular vesicles (EVs) is a universally shared property between eukaryotes and prokaryotes [5, 12]. Cells release the EVs as a mean of communication between each other [12]. EVs are spherical and are enclosed by a lipid bilayer [5]. Their size range is between 30 nm and 5 µm [5]. EVs could be isolated from many different body fluids such as blood [18], urine [19], breast milk [20], saliva [21], cerebrospinal fluid [22]. The EVs concentrations in body fluids range from 10^6 to 10^{11}/ml [23–26]. The concentrations measured are very dependent on the characterization methods used [26]. EVs could also be isolated from cell culture [27, 28].

EVs have very important functions in the body. They participate in the intercellular communication by transferring molecules such as proteins, lipids or genetic material from one cell to another. Through the surface-receptors, the EV can be uptaken by other cells and influence the cellular processes [12]. For example, the up-take of genetic material (mRNA or microRNA) from EVs was shown to have modified the protein expression in the recipient cells [12]. Moreover, cells release EVs to protect themselves from toxic chemicals that are packaged into the EVs [7]. EVs play an important role in coagulation when their surfaces expose phosphatidylserine and tissue factor which promote the assembly of molecules from the blood coagulation cascade [29]. Many more functions of the EVs have been eludicated and are described in details in recent reviews [7, 12, 13].

The growing interest in EVs research is mostly related to their potential as noninvasive biomarkers [5] and to the fact that their study provides a better understanding of diseases.

In this chapter, three different types of EVs will be presented. The advances of the research for the use of MVs as biomarkers will be described. In a last part, we will describe the conventional and novel methods to isolate EVs and to characterize and detect EVs.

2.1 Microvesicles and other extracellular vesicles

2.1.1 Nomenclature

In the literature, different types of EVs have been described. However, their classification is subject to debate [5]. Authors have different definitions for the same term [14]. Confusion is also created by the difficulty to isolate pure EVs subpopulations. Improvement in the isolation and analysis methods will help to classify the different EV types [5]. The issue of the nomenclature is debated in the literature [14, 15]. Gould et al. [14] recommended to precisely define the

type of vesicles and describe the isolation method (speed of centrifugation, type of centrifuge) used in the papers.

Currently, three main types of EVs are described in the literature [12]: exosomes, microvesicles (MVs), also called cell-derived microparticles or sometimes ectosomes [30, 31] and apoptotic bodies. Some reviews also distinguished other types of vesicles such as the membrane vesicles [5] or exosome-like vesicles [6, 30]. Further investigations will verify if those are separate categories of EVs or associated with exosomes or MVs. In some cases EVs are also named according to the type of cells from which they have been released [5] such as oncosomes being released from cancer cells [32]. However naming the EVs according to their tissue of origin does not provide information about the release mechanism of the EVs [5, 13]. Currently many publications use the generic term of EVs.

In the following, we will describe the three main classes of EVs: exosomes, MVs and apoptotic bodies. Table 2.1 presents an overview of the three main categories of EVs with their main parameters and figure 2.1 presents a schematic representation of the release process of the three different types of EVs.

Table 2.1: Overview of the three main categories of EVs

	Exosomes	**Microvesicles**	**Apoptotic bodies**
Alternative names		Cell-derived microparticles, ectosomes	Apoptotic vesicles
Size range	30 to 100 nm	50 to 1000 nm	> 1 µm
Formation	Formation in multivesicular bodies that fuse with cell membrane to release the exosomes	Outward cell membrane budding	Apoptosis in cells, cell shrinkage, budding
Characteristic markers[1]	CD9, CD63, CD81	Phosphatidylserine, markers of cell of origin	Phosphatidylserine
Density	1.13 - 1.19 g/ml	not determined	1.16 -1.28 g/ml
Centrifugation conditions	>100000 × g	10000 to 20000 × g	
to pellet EVs	18 hours	30 to 45 min	

[1] Markers are not exclusive, i.e. their only detection on a vesicle is not enough to categorise the vesicles.

2.1.2 Exosomes

Exosomes are described in the literature as spherical vesicles of a size range of 30 to 100 nm [5] which is a more homogenous size range than MVs [33]. The density is reported to be from

1.13 to 1.19 g/ml [5, 30]. Most papers describe the isolation of exosomes by ultracentrifugation with a speed above 100000 × g for pelleting the exosomes [5]. Exosomes have been shown to express on their surface proteins of the tetraspanin familly such as CD9, CD63 and CD81 [15, 32] and others such as flotillins and TSG101. However none of these markers are enough to exclusively detect exosomes [5]. Exosomes are formed in multivesicular bodies inside of the cell. The multivesicular bodies fuse with the cell membrane to finally release the exosomes outside of the cell [5, 34].

2.1.3 Microvesicles (MVs)

MVs have also been isolated from almost all body fluids [5]. They have a size range of 50 nm to 1 µm [35], where some papers state them to be 100 to 1000 nm [34]. This size range is overlapping with the size range of exosomes which makes it very difficult to differentiate the two types of EVs. The phospholipid phosphatidylserine is often expressed on the surface of MVs [6]. However, growing evidence shows that not all MVs express phosphatidylserine [34, 36, 37]. For example, Latham et al. [38] reported that only 30 to 55% of the total MVs expressed phosphatidylserine when measured with flow cytometry and around 60% when measured with immuno-electronmicroscopy. The expression of phosphatidylserine is associated with the procoagulant activity of the MVs. Currently, there is no strictly specific MV marker.

The isolation of MVs is performed most of the time by a series of centrifugation steps. MVs are often reported to be pelleted at 10000 to 20000 × g [38–40] for approximately 30 to 45 min. However, some reports also used speeds above 100000 × g to isolate MVs [41].

The formation of MVs occurs by an outward blebbing of the membrane. This has the consequence that MVs have the same membrane as their cell of origin and express the same receptors [42]. This strategy is used to identify the origin of the MVs and qualify them as for example platelet MVs (released by platelets) or endothelial MVs (released by endothelial cells). The release of MVs appears to be triggered by cell activation and apoptosis [43], although healthy cells also release MVs. Burger et al. [6] reviewed the stimuli that were shown to lead to MVs formation in platelets, T-cell, monocytes, neutrophils and endothelial cells. The loss of the membrane asymmetry and the exposure of phosphatidylserine seem to be two major events leading to the budding of MVs [6, 29]. More detail about the molecular pathways leading to the release of the MVs can be found in the literature [29].

MVs have been shown to contain proteins, RNA and microRNA [42]. The content of MVs is highly dependent on the stimuli to release MVs and is packaged according through a regulated process [44].

2.1.4 Apoptotic bodies

Apoptosis is the process of programmed cell-death that maintains a constant cell number in the body [45]. Upon apoptosis, cells package some components into vesicles that are named apoptotic bodies [46]. These apoptotic bodies are then released from the cell membrane and removed in a non-inflammatory way by innate immunity cells [47]. Apoptotic bodies have a size of 1 to 5 µm [5] and a density of 1.16 to 1.28 g/ml [5]. They express phosphatidylserine on

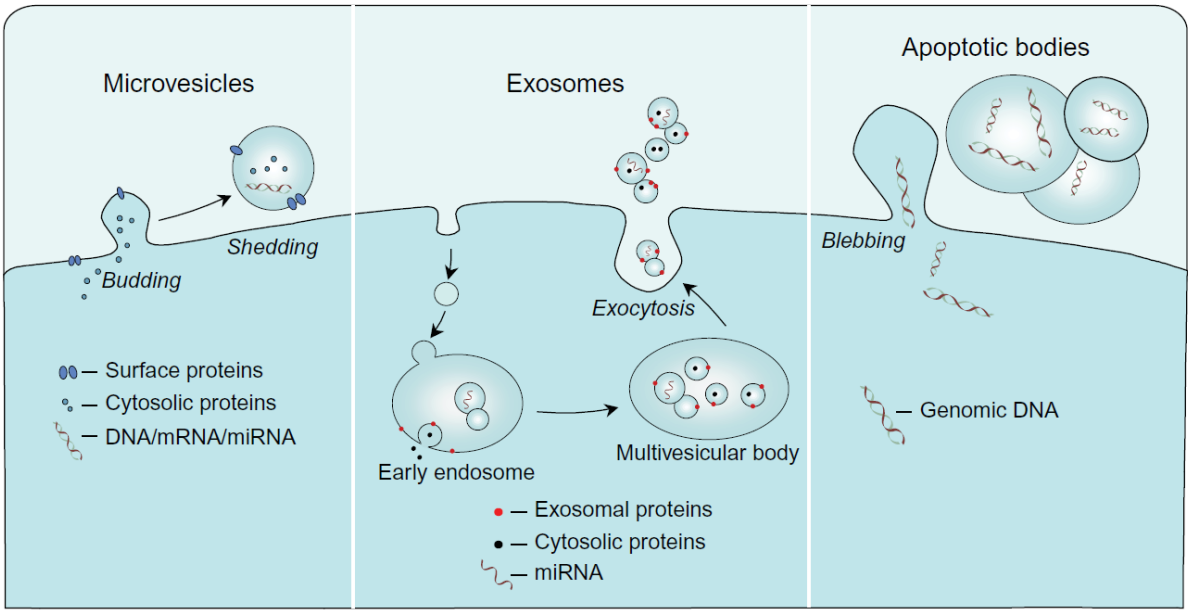

Figure 2.1: Schematic representation of the EVs release. Microvesicles are released from a budding of the cell membrane and carry the same surface proteins as the cell of origin. Exosomes are formed inside of the cell in multivesicular bodies and are released from the cell by exocytosis. Apoptotic bodies are formed during the apoptosis of the cell and contain genomic DNA. Image adapted from [2]

their membrane [42]. Characteristic for the apoptotic bodies is the presence of genomic DNA in the vesicles [1].

2.2 Microvesicles as prognostic and diagnostic markers

Even though the release of MVs is a process that happens in healthy cells, several studies have shown aberrant MV numbers in specific diseases [48]. Therefore MVs have been proposed as novel biomarkers [6]. As they are found in circulation in the blood or other body fluids such as urine [12], MVs are easily accessible biomarkers [5].

Nielsen et al. [23] compared the MVs in the plasma of systemic lupus erythematosus (SLE) patients and of healthy controls. They found significantly different concentrations of MVs in SLE patients and healthy controls. In general they found decreased levels of overall MVs but could identify two annexin V non binding MV populations that were increased in SLE patients. These observations are useful in the perspective of SLE diagnosis and furthermore also provide new valuable information about the disease. Similarly, Boilard et al. [49] showed that the immune complexes associated with MVs from platelets correlated with SLE disease activity.

MVs derived from cancer cells have also been proposed as biomarkers for disease and to follow the effect of treatments [9, 10, 50]. For example, Yoshioka et al. [51] have shown that serum from colorectal cancer patients had elevated levels of CD147 and CD9 double-positive EVs. Similarly, many studies have been published relating the level of subpopulation of MVs to different cardiovascular diseases as reviewed by França et al. [11]

MVs are unique biomarkers as they allow to identify pathological states in a minimal invasive way [5, 6]. After identification of the MV subpopulation relevant for the diagnostics of a defined disease, MV quantification can be used as a novel diagnosis method, also to be involved in early diagnosis [52]. However, many studies are impaired by the lack of standardization in isolation and characterization methods. Improvement of those methods will lead to data that are more accurate and can be compared between different laboratories.

2.3 Methods of isolation of microvesicles: State of the art

Even though correct isolation of MVs and other EVs is crucial for their further analysis [20, 53], currently there are no standard protocol for the isolation of MVs [33]. The main method used for the isolation of MVs from body fluids or cell culture supernatant is differential centrifugation. Different types of filtration are also employed. More and more attention is given to the isolation methods. Novel methods are developed and standard methods are compared to each other to evaluate performances, advantages and disadvantages [54, 55]. Moreover, pre-analytical variables such as plasma collection (among others: type of anti-coagulant tubes or collection needles) or storage of the samples are extensively studied to determine their influence on the further MV characterization [26, 56–58].

Even though some characterization methods are now able to detect MVs directly from the body fluid, isolation remains of advantage to avoid artefacts from other objects in the body fluids and increase the MV concentrations as required for some characterization methods such as western blot (WB) [59, 60].

In this section, we will present an overview of the isolation methods used for MVs, but also for EVs in general as most methods can be used for several types of vesicles. We will keep the nomenclature for the vesicles as used in the original publications. The description will be organized in three parts. The first part will describe the methods that isolate the vesicles according to their size. The second part will present techniques that isolate MVs depending on their surface markers. In the third part, a special focus will be made on microfluidic devices specially developed for the isolation of vesicles per size and surface markers.

Several reviews have been published recently and describe the challenges of MV isolation [35, 56, 61].

2.3.1 Isolation according to the size

Methods that isolate MVs by their size are differential centrifugation, filtration and size exclusion chromatography (SEC).

Differential centrifugation

Centrifugation is a process that is extensively used for the processing of all sort of samples for many years. A sample is placed in a tube which is rotated around an axis. This applies a centrifugal force onto the sample that is displaced outwards to the bottom of the tube. The rate of sedimentation is dependent on the size of the particle and on the density difference

between the surrounding medium and the particle. In principle, centrifugation accelerates the sedimentation of particles [62]. The settling velocity is derived from the Stokes law using the following formula [63]:

$$v = \frac{d^2 g(\rho_P - \rho_{medium})}{18\eta} \tag{2.1}$$

with d the diameter of the particle, g the gravitational acceleration constant, ρ_P the density of the particles, ρ_{medium} the density of the surrounding medium and η the viscosity of the surrounding medium. According to the equation 2.1, particles can be sedimented if they have a higher density than the surrounding medium. The higher is the centrifugation force, the smaller are the particles that can be collected in the bottom of the tube. Protocols usually indicate the centrifugation speed used in relative centrifugation force (RCF or g-force) such as $10000 \times g$. This value should be preferred over the indication of the revolution per minute (RPM) as RCF is independent of the radius of the rotor in the centrifuge.

Differential centrifugation is one of the most used method for the isolation of MVs and EVs in general [64]. The process involves different centrifugation steps at different speeds to obtain a suspension of MVs free of cell debris and free of small proteins or protein aggregates that can also be found in body fluids. After collection of the sample (body fluid or cell culture supernatant), large debris are removed by a centrifugation step with a speed between $1200 \times g$ to $4300 \times g$ [27, 65] for 5 to 15 min [27, 66]. This step is crucial because it sets the upper limit for the size of the objects that will be considered as MVs. After this first centrifugation step, the pellet is discarded and the supernatant is collected and further processed. The goal of the following step is to pellet the MVs from the supernatant and thereby removing all smaller vesicles or objects such as protein or protein aggregates. Centrifugation speeds used for this step ranges from $10000 \times g$ [30] to $20000 \times g$ [55, 61]. Often this step is repeated after removal of the supernatant and resuspension of the MVs in clean buffer. This allows to increase the purity of the MV suspension. However, many repeated centrifugation steps can results in a reduced yield of MVs. In the case of the exosomes, the centrifugation speed required to pellet them is $100000 \times g$ for 18 hours as developed in the gold standard protocol by Théry et al. [28, 30].

The difficulties related to the purification of MV by centrifugation lie in the overlapping size range of the different types of vesicles that makes it nearly impossible to find a protocol that will reach a sharp separation between the different types of EVs [64]. Besides, concern was raised regarding the damages and modifications such as aggregation and fragmentation encountered by MVs during centrifugation due to the centrifugation forces [26, 67, 68]. This is discussed in details in the introduction of part III on page 71.

Density gradient centrifugation has also been used for to separate EVs from other objects according to their density [35, 69]. Cantin et al. [70] successfully used this technique to separate exosomes from virus particles despite their close density. However, Yuana et al. [71] showed that EVs and high density lipoproteins were collected together on a KBr-gradient density ultracentrifugation due to their similar density [15].

Filtration

Filtration is also used for the isolation of MVs [72]. This isolation method is based on the size of the MVs but also on their ability to deform to pass through the pores of the filter [64]. Some protocols use filtration in combination with centrifugation as reviewed in [73]. Several studies used filtration through a 0.22 µm filter to remove a part of the EVs [39, 74]. The main concern in using filtration is the clogging of the filter pores due to the high content of proteins in the samples and the adhesion of the EVs to the filter membrane [69]. The use of low protein binding materials could improve this limitation [75]. Similar as with the centrifugation, vesicle fragmentation under filtration can happen [56] which results in smaller MVs increasing artificially their concentration.

Size exclusion chromatography

Size exclusion chromatography (SEC or gel filtration) is also used to purify extracellular vesicles from cell culture supernatants or body fluids [54, 76–79]. In SEC, the separation is achieved by the differences of the path length of the analytes in the column. The working principle is that small particles penetrate into the column material and have a longer path, hence a longer retention time in contrast to larger particles, which are eluted first from the column [61, 80]. For the isolation of EVs, separation on the SEC column is usually preceded by a centrifugation step to remove cells (e.g. platelets from blood plasma [81, 82]) or larger debris [61]. Böing et al. [81] analysed extensively the collection process and found that their home-made sepharose column could separate vesicles from proteins and high density lipoproteins with a good recovery of EVs. When they are isolated by SEC, EVs do not risk to aggregate as they are not subjected to high forces as in ultracentrifugation.

However, a problem with SEC is the dilution of the sample with separation buffer on the column. For example Welton et al. [83] loaded 1 ml of sample and collected the EVs in seven fractions of 0.5 ml, which corresponded to 3.5 fold dilution of the sample. Following the SEC isolation they investigated several concentration methods (ultracentrifugation, precipitation). The recovery of vesicles was however very poor (95% were lost) and this step remains to be optimized.

SEC is very promising method for isolation of EV as it is cheap, easy to perform, rapid [61, 81] and can be performed in the required buffer to ensure stability of the MV [80] and maintain the biologic activity of the MVs [15]. SEC is very efficient to separate the bulk proteins from the EV population. However, to our knowledge there is no study where EVs were separated in subpopulations by SEC. Also, SEC is time consuming and difficult to employ in studies with many samples.

2.3.2 Immunoaffinity based sorting

An important feature of MVs is the markers present on their surface. Purification of MVs based on those markers allows to selectively collect sub-population of EVs with a common marker expressed on the surface, disregarding the size differences of the vesicles [61]. Protocols involve the coating of magnetic beads with antibodies specific against the surface protein of

interest [35]. Therefore Oksvold et al. [84] described a protocol where exosomes were captured by magnetic beads functionalized either against CD9, CD81 or EpCAM. The capture of the exosomes was followed by a flow cytometry analysis and structural analysis by transmission electron microscopy (TEM) of the magnetic beads covered with the exosomes. Gieseler et al. [85] used commercially available annexin V functionalized magnetic beads to capture MVs exposing phosphatidylserine. Similarly, Arakelyan et al. [86] captured EVs directly from blood plasma with magnetic beads functionalized with antibodies against EV markers. The captured EVs were then collected inside a magnetic column. Recently, Wang et al. [87] used magnetic microbeads to capture specific populations of exosomes. They found that magnetic microbeads conjugated to anti-CD105 had the highest efficiency to isolate exosomes from endothelial cells.

The advantage of this technique is that the washing steps are simple by collecting the vesicles bound to magnetic beads inside a magnetic column or by a magnetic collector. However, elution of the vesicles from the magnetic beads is not trivial, though not always required for further analysis. Moreover, the ratio of magnetic particle to vesicles and the size of the magnetic particles relative to the vesicles should be chosen carefully to ensure a proper purification. It is also dependent on the expression of the surface protein. As there is currently no universal exosome or MV markers, the immunoaffinity based isolation collects defined subpopulations of EVs. This is a fundamental difference compared to size based methods and requires prior knowledge about the EV subpopulation of interest.

2.3.3 Microfluidic devices

The isolation of EVs could also be performed in microfluidics systems. Liga et al. [88] provided a comprehensive review of the microfluidic devices developed for the purification of exosomes. Here we present a few examples for this type of devices.

Some devices rely on the size of the vesicles for their isolation. Laki et al. [89, 90] presented a system based on the principle of deterministic lateral displacement to separate MV from cells. The device was composed of a channel with an array of pillars. Large particles, such as cells, more often hit on the pillars and their flowing trajectory is modified (i.e. the particles are displaced). The larger the particles are, the more they are displaced as shown in figure 2.2A. Several outlets at the end of the channel enable the collection of different fractions of vesicles. Fine tuning of the pillar sizes and position is required to obtain the correct collection of vesicles. Another device with pillars was developed by Wang et al. [91]. Cells and larger particles are trapped at the beginning of the channel, while particles in the submicron range enters the pillar area. Exosomes are trapped in the ciliated pillars while proteins and smaller particles flow unhindered through the channel. The ciliated pillars are later dissolved to release the trapped vesicles. Lee et al. [92] developed a microfluidic device where MVs were isolated using acoustic forces. They were able to separate exosomes from MVs. Similarly, Evander et al. [93] also used acoustic forces to separate MVs making use of seed particles. This acoustic nanofilter offers the advantage of label-free, non-contact isolation based only on the size of the vesicles. Davies et al. [94] presented a microfluidic filter with a porous polymer membrane with a pore size of 500 nm (figure 2.2C). The implementation of electrodes helped to attract a

larger proportion of EVs to the sample outlet. However the device clogged after filtration of 4 µl.

Immunoaffinity based devices were also developed. Chen et al. [95] developed a channel coated with antibodies against the exosomal protein CD63, where exosomes in serum were directly trapped on the channel surface. Later the same author presented an immuno-based paper device (figure 2.2D), where EVs were also captured in the paper device functionalized with anti-CD63 antibodies [96]. Ashcroft et al. [97] developed a microfluidic device where MV were captured on an anti-CD41 antibody coated mica surface placed in a microfluidic channel. After capturing, MVs were directly analysed by AFM (figure 2.2B). However the difficult release of intact MVs from the surface is a limitation to enable further analysis after isolation by this solid-phase capture. Shao et al. [98] developed a miniaturized nuclear magnetic resonance (NMR) system where MVs were isolated with capture on magnetic beads. Shao et al. [98] also presented a microfluidic platform where exosomes were enriched through binding to magnetic particles functionalized with anti-CD63 antibodies. This was used for on-chip exosomal RNA extraction and on-chip quantitative polymerase chain reaction (qPCR) (figure 2.2E).

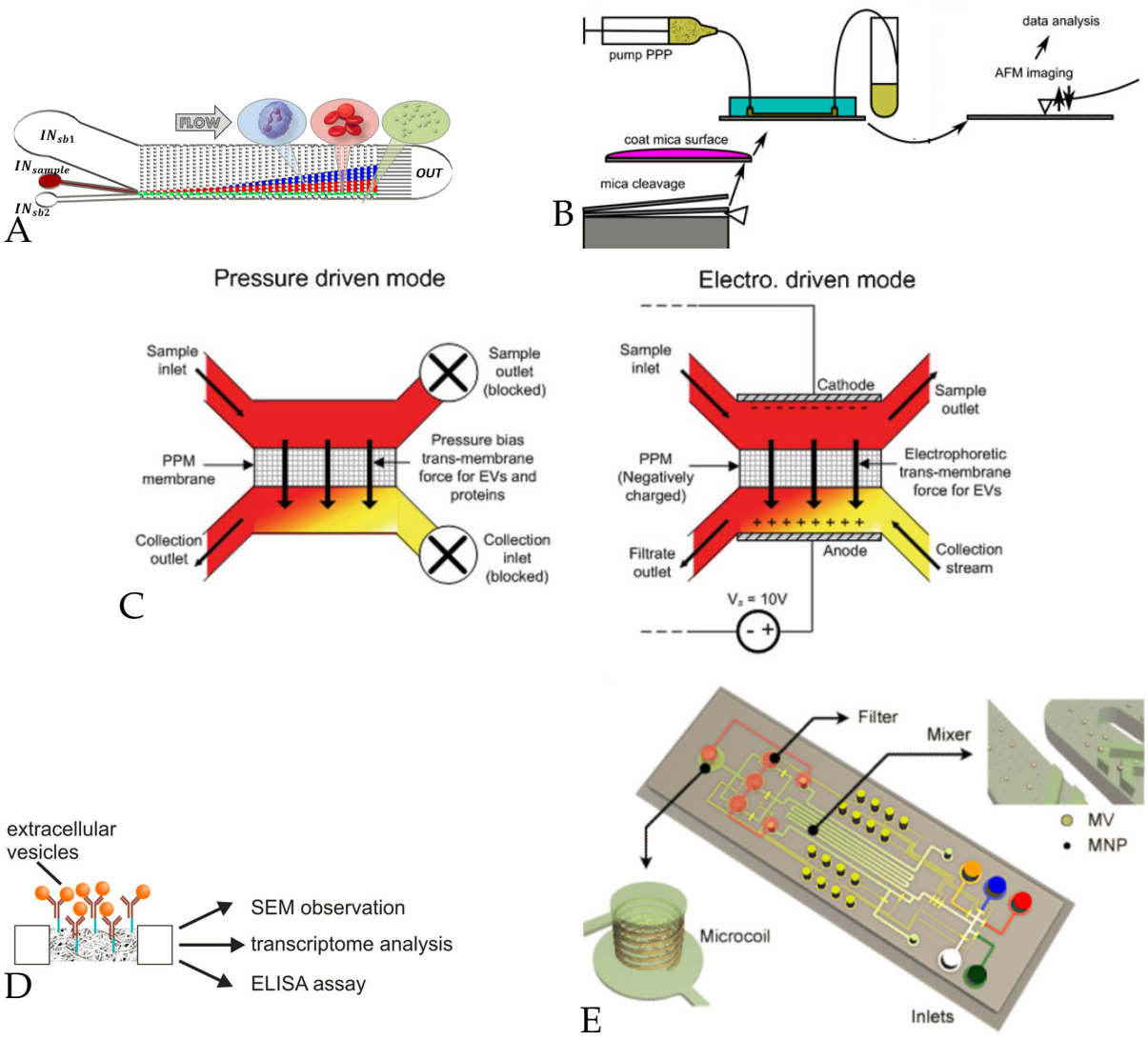

Figure 2.2: Overview of some of the microfluidic devices for isolation of EVs (A) Deterministic lateral displacement device, from [89]. Large particles such as cells are displaced laterally more than small particles which are collected in a separate outlet. (B) Scheme of the microfluidic filter, from [94] (C) Collection of MVs on a mica sheet coated with anti-CD41 antibodies and imaged directly with AFM, from [97] with PPP standing for platelet poor plasma (D) Paper based assay for the isolation of EVs, from [96]. After capture, EVs could be analysed by SEM, by transcriptome analysis and ELISA. (E) µNMR device, from [50]. After capture on magnetic beads, the proteins of the EVs were analysed by NMR.

2.4 Methods of characterization and detection of microvesicles: State of the art

Many methods are available to detect, characterize and enumerate MVs either directly from the collection fluid (body fluid or cell culture supernatant) or from a suspension of purified MVs. As for the isolation methods, the MV characterization methods are also applied for other types of EVs. Each method provide a different type of information such as size, structure or surface protein expression. As no method is able to cover a complete characterization of the MV, the use of several methods is recommended. Recently, ISEV published some requirements for the complete characterization of EV populations [16]. Complete EV characterization and detection remain difficult, especially the discrimination between EVs and non-vesicular proteins and the discrimination between the different types of EVs. The sensitivity of conventional methods does not always allow the detection of all vesicles owing to their small size and polydisperse nature [15]. To meet those challenges, conventional methods are being improved and novel methods are being developed.

We will describe here some methods for EV chracterization and detection. The methods are sorted according to the type of information they provide, i.e. size characterization (by imaging techniques or indirect measurement of the total population), detection of the surface proteins expressed, molecular composition of the vesicles and activity of the EVs. Figure 2.3 presents an overview of the characterization methods. The reader is moreover referred to recent reviews for more information [6, 15, 34, 99–101].

2.4.1 Imaging techniques to characterize the size

Electron microscopy (EM)

EM techniques are based on the interactions of electrons from an electron beam with the electron dense structures to create an image. The resolution of EM is in the subnanometer range. Different techniques based on EM have proven useful to characterize EVs.

In transmission electron microscopy (TEM) thin samples (< 500 nm) are imaged by an electron beam passing through the sample. Negative staining TEM is a simple method particularly useful for a first characterization of the EV isolates and determine the purity of those isolates. The sample preparation is relatively fast as it only includes the deposition of a sample on a TEM grid and the staining with with an electron-rich heavy metal salt such as osmium tetraoxide, accumulating around the structures in order to enhance its visualization contrast [102]. After washing and drying, the sample is ready for imaging in TEM. Negative staining TEM has short preparation times, however this imaging technique is quite unspecific and will show the structure of all objects in the sample. An isolated MV imaged by negative staining TEM is shown in figure 3.3 on page 42. To better preserve the native structure of the EVs, extensive preparation protocols are required. The different steps involve the fixation of the vesicles with a fixative such as glutaraldehyde, then the staining with a contrasting agent such as osmium tetraoxide, the dehydration of the sample, the embedding in a resin and finally the cutting of the sample in thin sections [27, 103]. This extensive preparation might affect the size of the vesicles to some

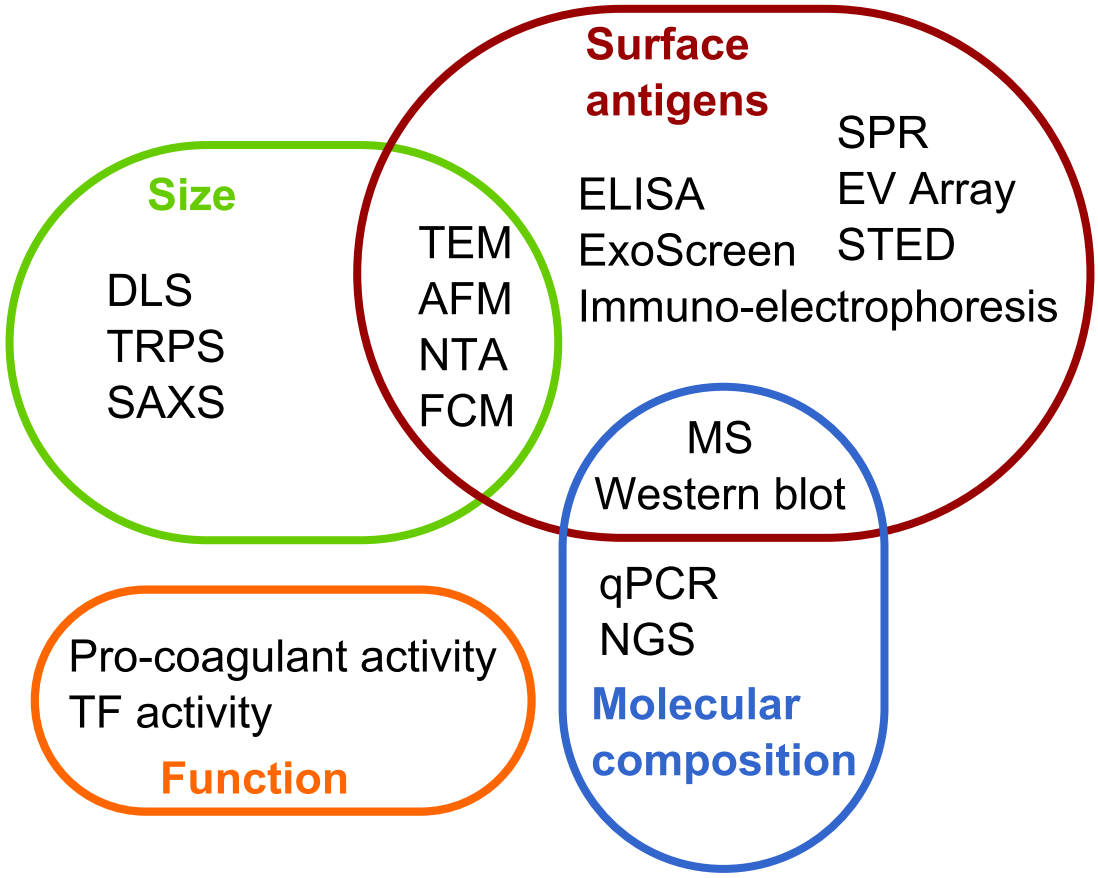

Figure 2.3: Overview of the characterization and detection methods for EVs. The methods are classified by type of information generated by the analysis. All abbreviations can be found in the abbreviation list (see page xix).

extend. As an alternative, cryo-TEM is able to image vesicles in their native state as they are frozen at extremely high freezing rate (12000 K/s [104]) with a cryoprotectant [55, 105]. TEM is an excellent tool to provide detailed information about the structure of the vesicles, their size and their shape. TEM is able to distinguish between vesicular and non-vesicular structures [56] as it can image the lipid bilayer constituting the membrane. As only surface-adsorbed EVs are imaged, overall concentrations cannot be determined easily [56, 101]. Van der Pol et al. [106] provided an estimation of the concentration assuming that all EVs would have adsorbed onto the grid. Information about the surface proteins of the vesicles can also be obtained with the use of immuno-gold labelling [38]. Those are gold nanoparticles conjugated to an antibody, which recognizes the surface proteins on the EVs.

Scanning electron microscopy (SEM) is also used in EV research. SEM provides 3D information about the topography of the sample. This was used by Combes et al. [27] to show the release of MVs from endothelial cells.

EM is a very relevant technique in EV research. However, analysis are time-consuming and requires trained personnel. EM is very good to provide an in-depth characterization of EVs, however it is less suitable for routine detection of EVs in clinical settings.

Atomic force microscopy

The measurement of MVs derived from platelets by atomic force microscopy (AFM) has been introduced by Siedlecki et al. in 1999 [107]. The AFM measurement principle relies on the scanning of a surface by a tip fixed at the free end of a cantilever. A laser beam is reflected from the back of the cantilever to a photodetector. Figure 2.4B shows an overview of the AFM setup. AFM has a resolution down to the Ångström range and therefore measures EVs with high accuracy. Even though AFM is mostly used for material characterization, this technique plays a growing role in biology to image for example the morphological changes of cells [108] or nanoparticles for drug delivery [109]. Different imaging modes are available with AFM [110], which are based on the van der Waals interaction between the atoms of the sample and the atoms of the tip.

In figure 2.4B, the van der Waals force is plotted as a function of the tip to sample distance. Three possible AFM modes are represented on this graph. In contact mode, the tip is brought in contact with the sample and the force between sample and tip is kept constant. The cantilever is deflected due to the repulsive forces. In non-contact mode, the tip is oscillating over the sample (a few hundreds of nanometers) and interactions are due to the attractive forces. In non-contact mode, only low forces are applied to the sample, which is particularly attractive for soft samples. The third common AFM mode is the intermittent (or tapping) mode, where the cantilever only gently taps the surface. This mode has become very important as it combines the high resolution of the contact mode with the low forces of the non-contact mode. Another advantage of AFM for biological samples is the possibility of imaging samples in liquid, i.e. in the native environment. This is used for example to image living cells [111]. For AFM imaging, the sample needs to lie on a flat surface such as a mica sheet or a silicon wafer.

Several reports have characterized MVs with AFM. Yuana et al. [39] immobilized anti-CD41 antibodies on a mica sheet where MVs isolated from plasma were then captured. Using liquid

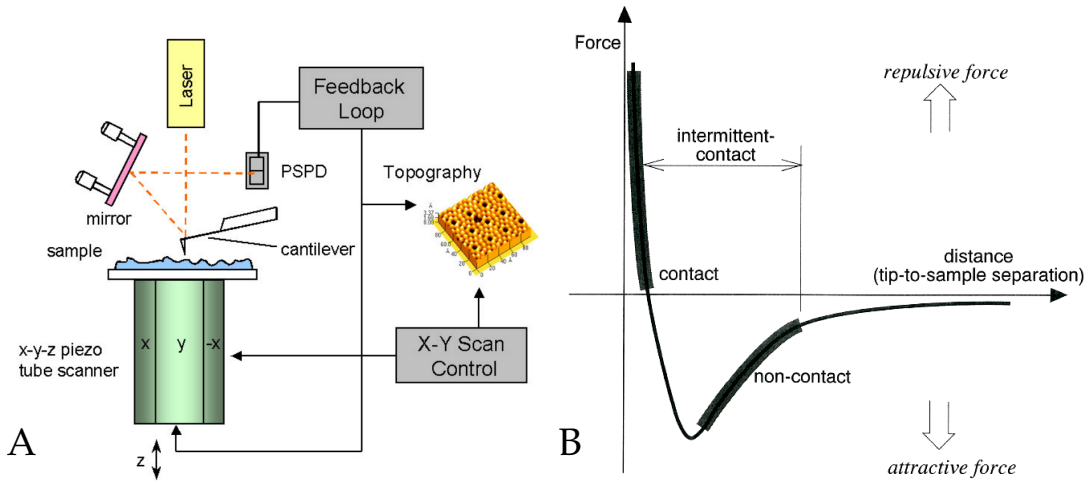

Figure 2.4: Working principle of AFM (A) Overall setup of a conventional AFM instrument. The sample is mounted on a piezoelectric scanner. A cantilever scans the surface while a laser beam is reflected on the back of the cantilever. The position-sensitive photodetector (PSPD) records the deflection of the cantilever and the software creates a topography image of the sample. Picture adapted from [112]. The AFM from the company Park Systems, which was used in this study has the x-y-scanners separated from the z-scanner. (B) Forces between the sample and the cantilever according to the distance between the sample and the tip. The different AFM modes are indicated corresponding to the type of forces. Picture adapted from [112].

tapping mode, they imaged MV and compared their results with flow cytometry (FCM). AFM enumerated 1000 fold more MVs than FCM. The interaction of the vesicles with the surface of the support modifies the shape of the vesicles, especially in the case of dried samples [60]. Yuana et al. [39] assumed a spherical shape of the MVs in liquid and a conservation of the total volume upon binding to the surface. Therefore they proposed to calculate the diameter of the MVs (d_{MV}) from their volume (V) measured by the AFM software according to the following formula:

$$d_{MV} = \frac{\sqrt[3]{6V}}{\pi} \tag{2.2}$$

With the same immobilization procedure, Ashcroft et al. [97] could image CD41 positive MVs directly from blood plasma. Using the immuno-labelled mica sheet allows to image specifically MVs expressing the corresponding surface marker. In those two studies, the mean diameter of the MVs was less than 100 nm which was below the detection limit of FCM. In their work, György et al. [59] compared the size of MVs measured by AFM, TEM and dynamic light scattering (DLS) and found good agreement between the different methods with a size range between 80 nm to 400 nm for MVs derived from plasma. Hardij et al. [113] compared the analysis of tissue factor positive EVs in air and liquid AFM. They found a significant decrease of the EV size when imaged in air which they attributed to a shrinkage during the drying process. They recommended to image EVs in liquid in order to respect the native environment of the EVs. Zhang et al. [114] used AFM to image the vesicles being released from the surface of the

cells. Exosomes were also imaged by AFM [21, 115, 116].

The main advantage of AFM for EVs analysis is its precision in measuring sizes and ultrastructures in a broad size range. Subpopulations can be detected accurately by capturing the EVs on a surface coated with antibodies (or other recognition molecules) against the relevant surface marker. However, AFM for EVs has some limitations. First of all the time required for an analysis is in the range of 1 to 3 hours [39, 97] and to operate the instrument users have to be trained. Similar as for TEM, the assessment of the EV concentration in the samples is based on the assumption that all vesicles absorb to the surface [39]. For a clinical use of AFM, the analysis should become automated and standardized to achieve reproducible results that are also easy to interpret. Moreover, appropriate materials to calibrate the instruments for EV analysis are necessary [60, 117].

2.4.2 Measurement of the size of EVs by bulk techniques

The methods described below analyse the EVs population as a whole, i.e. no image of the single EVs are created. Nanoparticle tracking analysis (NTA), dynamic light scattering (DLS) and tunable resistive pulse sensing (TRPS) analyse EVs in liquid state.

Dynamic light scattering

DLS also called photon correlation spectroscopy uses the scattered light pattern to calculate an average size distribution of the particles in suspension. The EV sample is illuminated by a laser. Because of the random motion (Brownian motion) of particles in suspension, the scattered light is detected [118]. Applying the autocorrelation function, the average hydrodynamic size of the particles can be calculated, assuming a spherical shape of the particles [119]. DLS can also be used to measure the zeta potential of the particles by applying an electric field across the sample [118]. DLS measurements are fast (few minutes) and the size range that can be measured is relatively broad ranging from 3 nm to 7 µm [120]. However, DLS does not give any indication about the EV concentration [119]. The size distribution is an average distribution calculated from an algorithm and not from each single particle. The concentration of particles in the sample has to be high enough to create enough light scattering [119]. DLS does not perform very well for polydisperse particle populations with low refractive index, which are often present in EVs samples [120], as larger particles scatter more light than small particles and therefore bias the measurement.

In their work, Lawrie et al. [120] could detect MVs from plasma samples in the expected size range. To overcome the limitation of DLS, György et al. [59] suggested the use of the coefficient of the autocorrelation function to describe the distribution of the population as they claimed that this was better appropriated to polydisperse populations. In their study they found that MVs and contaminants of MVs preparation overlap in the size distribution. This highlights that DLS cannot distinguish between MVs and other contaminants in the sample. No distinction between the subpopulation of EVs is possible. In their study, Gabriel et al. [118] used a novel DLS instrument called ISADE, which is a light-scattering instrument specifically developed for the measurement of EVs and where single particles are counted. They also found

that background contamination contributed to the signal. To conclude, DLS is a simple and rapid method for EVs characterization. However, the polydispersity of the samples leads to erroneous size distributions.

Nanoparticle tracking analysis

NTA instruments were first commercialized in 2006 but rapidly became extensively used for EVs characterization. The working principle of NTA is based on the direct visualization of the light scattering of the vesicle and the tracking of their Brownian motion. Figure 2.5B shows a picture of the NTA instrument. The sample is placed in a chamber where a focused laser beam is passed through the sample chamber. The optical setup is shown in figure 2.5A. The particles within the laser beam scatters light and moves in a random motion (Brownian motion). A video is recorded for usually 30 to 60 s. Figure 2.5C shows an example of a frame from a video recorded by NTA. The NTA software is then able to recognize and track the two-dimensional motion of the particles from frame to frame [121]. Using the Einstein-Stokes equation, the hydrodynamic diameter of the particles can be calculated as follow:

$$< x, y >^2 = \frac{k_B T t_s}{3\pi\eta d} \tag{2.3}$$

$< x, y >^2$ is the mean square displacement, k_B the Boltzmann constant, T the temperature in Kelvin, t_s the time of the video, η the viscosity of the medium and d the diameter of the particles [121]. With this technique, the diameter of each particle is determined individually.

To obtain accurate measurements, the software parameters and measurement settings have to be optimized. Gardiner et al. [121, 124] wrote a set of recommendations for proper use of this instrument: The concentration of EVs should be approximately between $1x10^8$ and $1x10^9$ /ml [99] to obtain an accurate measurement. A lower concentration would lead to poorer statistic (less particles tracked), while a too high concentration results in particles overlapping each other and their path [121]. The camera gain has to be set so that each particle can be seen. For the tracking, a detection threshold has to be defined to select which points are considered as particle.

For concentration measurements, the use of calibration beads is recommended. Those calibration beads need to have a similar refractive index as the vesicles measured. Van der Pol et al. [125] used NTA to determine the refraction index of EVs from human urine. They found an average refraction index of 1.37. Polystyrene beads have a refraction index of 1.59, while silica beads have a refraction index of 1.42 [121]. Therefore silica beads should be preferred for the calibration over polystyrene beads, before more suitable materials are developed for calibration for EVs measurements [121]. The calibration results in a factor built by the ratio of the expected concentration over the measured concentration of silica beads [117]. The concentration measured in the samples should then be multiplied by this factor [117].

NTA instruments can be equipped with laser of different wavelengths (405, 488, 532 or 638 nm). If the EVs are labelled with fluorescently labelled probes, subpopulations of EVs can be detected with fluorescence NTA (F-NTA) [121]. An important consideration for F-NTA is the photobleaching of the fluorophore while in the focused laser beam [15]. Techniques have to

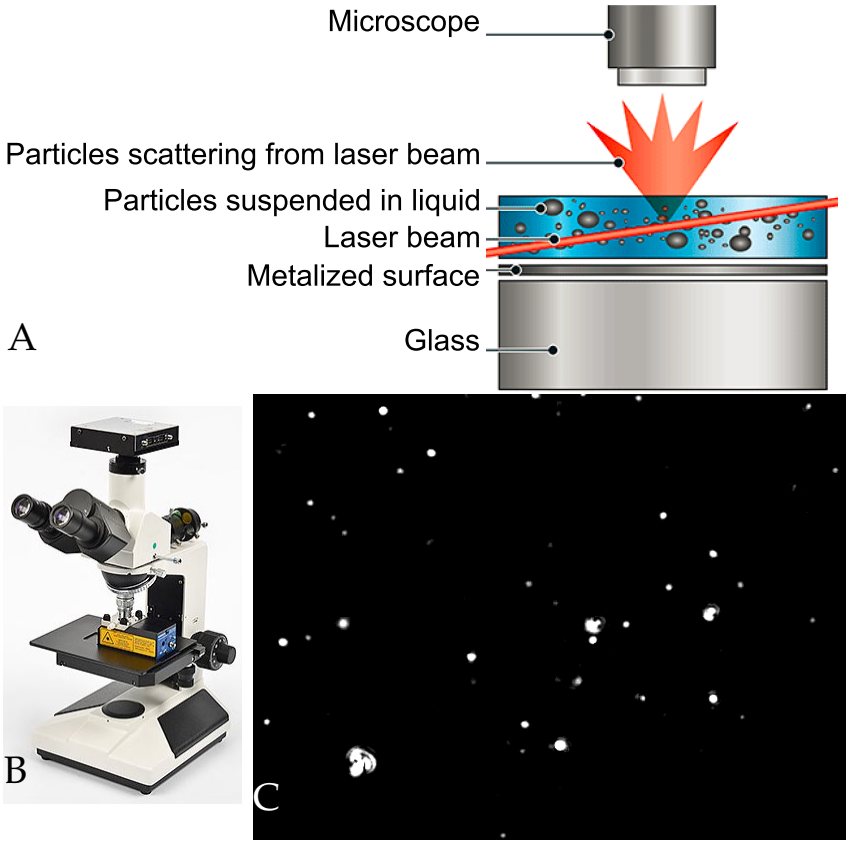

Figure 2.5: Working principle of NTA Figure A shows the optical setup of a NTA instrument. Picture adapted from [122]. Figure B is a photograph of a LM10 NTA instrument (adapted from [123]). The NTA system (sample chamber and laser) is mounted on a microscope equipped with a high speed camera. Figure C was extracted from a video recorded by the NTA during the measurement of MVs derived from endothelial cells. The white dots are the light scattering from the vesicles.

be improved to exclude artefact due to photobleaching. For example, the use of quantum dots conjugated to antibodies might be an attractive solution [78, 87].

NTA has a great potential for the routine characterization of EVs, especially when using the instrument with automated sample injection. Measurement times are relatively short. Its limit of detection is about 50 nm [126, 127] to 70-90 nm [106]. NTA suffers from the typical issues of light scattering methods in that sense that no distinction of the vesicle aggregates or large protein complexes can be performed [78, 128].

Tunable resistive pulse sensing

TRPS is a technique recently available on the market. It makes use of the coulter counter principle to measure the size of EVs [26]. It is independent of any optical properties. The instrument is composed of two chambers separated by a membrane with a single pore. A voltage is applied across the pore and the current is measured continuously. When a vesicle passes through the pore, the resistance increases and a dip peak in the current is recorded. The resistive pulse is calculated from this current drop and is proportional to the volume of the particle [129]. The size of the pore can be adapted to the size range of the vesicles. However reproducible pore size is highly important to obtain reproducible results [129]. Van der Pol et al. [106] needed to use two pore sizes to measure the complete size range of EVs. They showed that TRPS resulted in a broader size distribution compared to the reference, which once again could be attributed to aggregation of particles. In their experiments, Yuana et al. [26] showed good agreement in the concentrations obtained from NTA and TRPS. Maaset al. [130] also showed that TRPS and NTA obtained the same size for the EVs measured using as well two pore sizes. Limitations of TRPS also concerns the possible clogging of the pore [64, 127]. The analysis time is realtively long. Van der Pol et al. estimated an analysis time of 30 min for 1000 particles [15]. Currently no information about the phenotype of the EVs can be provided by TRPS, but development of techniques involving specific aptamer probes are envisaged [131, 132].

Small angle X-ray scattering

Other techniques are also available for characterization of the size of EVs, even though they are less used. Small angle X-ray scattering (SAXS) has been used to characterize EVs derived from erythrocytes [133]. SAXS can provide a reliable size determination as well as structural information of the lipid bilayer [99]. However this technique require a high concentration of EVs in the sample with a monodisperse distribution [133]. This technique requires highly specialized instrumentation only available in a few places worldwide [99].

2.4.3 Characterization and detection of surface antigens

The characterization of surface antigens of EVs provides information about the cellular origin of the vesicles. This information is crucial, especially regarding the biomarker potential of EVs. For example MVs derived from endothelial cells are thought to indicate damages of the tissue of origin [134]. Therefore great efforts are also made to develop rapid and reliable methods to characterize the surface proteins of the EVs as well as detecting EVs according to their surface

proteins. The characterization of the surface antigens is also sometimes referred to as phenotyping [100]. Some of the methods described previously such as NTA or TRPS also allow the characterization of the surface proteins along side with the determination of the size. In the following we will describe methods mainly aiming at phenotyping of EVs. All of these techniques rely on the availability and use of specific molecules such as antibodies that recognize the surface antigens [100, 135].

Flow cytometry (FCM)

FCM remains the most used method for the analysis of the different types of EVs [52, 136]. EVs are labelled with an antigen-specific antibody (or annexin V if the target is phosphatidylserine) conjugated to a fluorophore. The sample is then focussed in a stream (hydrodynamic focussing) of sheath fluid and EVs pass in front of the laser where they scatter the light. Scattered light and fluorescence signal are recorded. FCM instruments are extensively used in cellular biology and are readily available in many laboratories.

The main criticism to FCM is its limitations regarding the size limit of detection. The wavelength of the lasers (400 to 700 nm) is within the same size range as the vesicles measured. However, objects equal or smaller than the wavelength of the light cannot be measured correctly [137]. FCM is therefore only able to measure the larger EVs. Newer instruments can allow the measurement of EVs down to 150 to 190 nm [106]. Leong et al. [138] sorted MVs directly onto mica sheets which were then imaged by AFM. With this method they could show that FCM could detect vesicles smaller than 1 µm. In FCM, relevant events are identified in a gate. In the case of the EVs, calibration beads are used to identify the events with the expected sizes. Polystyrene Megamix beads of 500 and 900 nm were used in the literature [18, 74, 136, 139]. However the differences in refractive index between the standard beads and the EVs compromise the accuracy of the gate position [140] but could be taken into account to calculate the vesicle size [106]. The debate about the limit of detection of FCM is still on-going and great efforts are made to assure the measurement of the complete population of EVs.

Using FCM, the concentration of EVs can be evaluated using the number of events counted and the flow rate used [37] or comparing with known standard beads [18]. However, because FCM only detects larger EVs, it was estimated that FCM underestimated of about 300 times the concentration of vesicles using a conventional FCM and only 15 times for an instrument specially optimized for the detection of submicron particles [106]. Arraud et al. [37] determined that FCM could only detect 1% of the EVs compared to EM. Another source of error is the so-called swarm detection [64], which is the detection of multiple vesicles as single event. In contrast to this, Oksvold et al. [84] made use of this swarming to detect several exosomes captured on magnetic beads. This does not give any information about the single particles but about an average antigen expression in the vesicle population.

One of the main strength of FCM is the analysis of multiple antigens during one measurement. FCM instruments are usually equipped with several fluorescence detectors and can therefore detect signals coming from different fluorophores. This is extremely relevant for biomedical applications as a combination of markers is usually necessary to confirm the cellular origin or a particular condition. However, only few fluorophores can bind to the surface of

the EVs due to their small size [33, 135, 140]. It requires that the detectors are sensitive enough for the low signal. Labelling strategies also have a great influence on the analysis results.

In summary, FCM is a very relevant method for the analysis of EVs. However, standardizations of the protocols and improvment of the instruments towards accurate detection of small particles (< 100 nm) are highly necessary. Recently, some recommendations for FCM analysis were published [58, 140].

Enzyme-linked immunosorbent assay

Other methods of detecting EVs by their surface antigens are the solid phase assays. **Enzyme-linked immunosorbent assay (ELISA)** works by capturing EVs on a surface where antibodies against the antigen of interest were previously immobilized (capture antibody). A second pair of antibodies is used to bind on the surface of the EVs. This second antibody can be conjugated to the enzyme horseradish peroxidase (HRP) or the assay uses a third antibody recognizing the constant part of the second antibody and conjugated to HRP. A colorimetric reaction catalyzed by HRP allows the detection of the binding. Detecting a target between two probes is defined as a sandwich assay. With this technique, only the relative quantity between samples can be determined but not an absolute EV concentration [33]. Yari et al. [40] used an ELISA to measure the evolution of the expression of phosphatidylserine on the surface of platelet derived MV during the storage of the platelets. Welton et al. [83] used ELISA to measure the expression of CD9, CD81 and CD63 among others on the fractions collected from the SEC column. In this case no capture antibody was immobilized on the surface. The EVs were expected to adsorb unspecifically to the surface. The specificity of the assay came from the antibodies against CD9, CD63 or CD81 and the binding was detected with a sensitive fluorescence complex. ELISA is an assay that is relatively cheap but is time and reagent consuming [127]. To address those issues, Chen et al. [96] developed a paper based ELISA where EVs where captured between an anti-CD63 and an anti-CD9 antibody. They claimed that only 10 µl of serum sample was needed and that the results were ready within 10 min. Göhner et al. [141] recently developed an ELISA slightly modified to detect specifically syncytiotrophoblast EVs, which play a role in preeclampsia during pregnancy. In their assay, the EVs were captured on the surface by annexin V, a probe binding specifically to phosphatidylserine expressed on the surface of the EVs. The colorimetric reaction was then catalysed by the placental alkaline phosphatase present specifically on the surface of this type of EVs.

Further ligand binding assays

In the following section, we will describe other types of assay to detect and characterize the EVs according to their surface markers.

Surface plasmon resonance (SPR) is a technique able to detect the binding of molecules on a surface. It is label free and very sensitive [142]. A surface is functionalized with a capture probe (e.g. an antibody). The SPR system detects the binding of the target, which is happening in close proximity of the surface. Several publications used SPR to detect exosomes. Rupert et al. [143] captured exosomes on an anti-CD63 functionalized surface. Grasso et al. [82] used SPR

to detect the molecular profile of exosomes using the capture with antibodies against exosomal or cancer markers. Zhu et al. [144] developed an array of antibodies to capture exosomes with different surface markers directly from cell culture supernatants. Im et al. [145] developed a high throughput device based on transmission SPR. With this system, they identified exosomes from ovarian cancer based on the expression of two surface markers.

Stimulated emission depletion (STED) microscopy is a super-resolution microscopy with a resolution far beyond the diffraction limit of 200 nm (16 nm) [126]. Koliha et al. [146] established a protocol to visualize EVs captured on glass slides functionalized with specific antibodies and fluorescently labelled antibodies binding later on the EVs (sandwich type assay). STED could reveal the heterogeneity of the expression of proteins on the surface of EVs.

Jørgensen et al. [147, 148] developed and optimized an **EV Array** to detect exosomes from body fluids (plasma) or cell culture supernatants. Antibodies against the surface proteins were immobilized on the glass slides by microarray prining. After incubation with the sample, a mixtures of biotinylated antibodies (against CD9, CD63 and CD81) followed by a fluorescently labelled streptavidin were incubated on the slide. This mixture of antibodies was used, rather than only one type to ensure the detection of all exosomes. Up to 60 different antigens could be detected simultaneously. The method could detect exosomes coming from as little as approximately 10^4 cells. Gagni et al. [149] developed a similar microarray, but combined it with a label-free detection based on interferometric measurement, which allowed to quantify the amount of EVs bound to the surface.

Other ligand binding assays were performed developed with the vesicle sample in suspension. Yoshioka et al. [51] developed the so-called **ExoScreen assay** where exosomes are captured by two different beads (acceptor and donor) functionalized against two different surface proteins. The detection occurred via a luminescence reaction triggered by the proximitty of the acceptor and donor beads. The sample volume was as little as 5 µl of serum and the analysis time was only 1.5 hours. Akagi et al. [150] proposed an **on-chip immunoelectrophoresis** chip. EVs decorated with antibodies specific for their surface proteins showed a shift in the zeta potential and therefore in the electrophoretic velocity. This technique is very promising as the zeta potential change does not scale with the size of the EVs. Recently, Zhao et al. [151] introduced the ExoSearch chip, where exosome isolation and multiplex detection were performed on the microfluidic chip. Exosomes were captured by magnetic beads conjugated to exosome specific antibodies. This is followed by the incubation with fluorescently labelled antibodies against the exosome markers. A CCD camera captured the fluorescence signal from the exosome-bead complexes. The system was used to detect exosomes associated with ovarian cancer.

2.4.4 Molecular composition

In EVs research, not only the receptors on the surface are of interest, but also the content of the vesicles provides a lot of relevant information about the biochemical pathways involved in EVs release.

Western blot/immunoblotting

Western blot is a standard molecular biology technique to identify proteins [152]. The proteins in the EVs sample are separated by gel electrophoresis according to their size [153]. After transfer onto a membrane (blotting), specific antibodies are used to recognize the protein of interest [78]. After incubation with a secondary antibody conjugated with HRP, a colorimetric reaction is used to identify the protein and quantify it relatively between samples. Western blot is a very useful technique in EV research. It can be applied both for MVs [153] and for exosomes [21]. It allows the detection of intravesicular proteins as well as proteins expressed on the membrane of the EVs [100]. However it requires a high amount of protein. Therefore ultracentrifugation steps are needed to pre-concentrate the samples before analysis [100, 154].

Proteomics methods

Mass spectrometry (MS) is a very sensitive method to identify and quantify proteins in a wide range of samples. It has been extensively used to identify proteins in exosomes [155] and MV samples [156]. MS analyses the vesicles in bulk, therefore no information about size or about the single vesicles can be obtained. Østergaard et al. [157] identified a set of 334 proteins that were present in all healthy controls. Moreover, they proposed the use of the signal from cytoskeletal proteins to normalize signal from other proteins when comparing different conditions (healthy controls and patients). Østergaard et al. [158] used MS to identify proteins specifically associated with MVs from SLE patients.

Nucleic acids composition

Many studies have shown that exosomes as well as MV contains nucleic acid material such as mRNA or microRNA. Standard RNA collection methods and qPCR are used to identify and quantify the RNA content in EVs [100]. Next-generation sequencing (NGS) was also used to identify precisely the isolated microRNA [159].

Data collected about the protein and RNA content of EVs are continuously catalogued into different databases such as ExoCarta [160–163].

2.4.5 Pro-coagulant activity

Another information that can be measured especially from the MV samples is their pro-coagulant and tissue factor (TF) activity [164, 165]. Those functional assays are performed as solid phase assays in ELISA plates. The pro-coagulant assay capture the MVs on the surface of the plates using annexin V. A thrombin generation assay is then performed as described in [166] measured by a colorimetric reaction. The concentration of thrombin generated is dependent of the phosphatidylserine concentration on the MVs. This assay has been first described in 1997 by Aupeix et al. [167]. The TF activity assay measures the pro-coagulant activity of the phosphatidylserine together with the triggering effect of TF [165]. In that case, MVs are captured on the plate by anti-TF antibodies and it is a Factor Xa generation assay that is performed [166]. A

drawback of those assays is that it only provides information about one biochemical activity of the bulk sample [6].

Part II

Microvesicles derived from cell culture

Introduction and aim

This part of the work introduces the generation and characterization of cell-derived MVs from the endothelial cell line Human Umbilical Vein Endothelial Cells (HUVECs). The aim of this study was to obtain a population of MVs that could be use for the testing of new characterization or isolation methods for MVs. In the literature, vesicles isolated from urine have been used as standard vesicles to compare different characterization techniques [106] and to optimize a TRPS measurement protocol [129]. However, body fluids always contains a mixture of MVs coming from the different types of cells in this body fluid or the cells adjoining the body fluid (e.g. endothelial MVs in blood). MVs isolated from conditioned medium of a defined cell line have the advantage of coming from only one type of cell and thus presenting a defined phenotype. The generation of MVs from cell culture has been presented from different cell lines such as Jurkat human leukemic T cells [168, 169], HUVECs [27, 170] or MDA-MB-231 breast cancer cells [103, 113]. Similarly, exosomes have also been isolated from conditioned medium in order to test analysis techniques [147] or isolation techniques [171].

The goal of this work was to obtain a reliable protocol for the generation of MVs from HUVECs and to assess the reproducibility of the protocol. The advantage of using an *in vitro* system is that we could study the cells releasing the MVs as well as the complete environment during generation of the MVs, and finally characterize the MVs. In this study, we characterized the size of the MVs by NTA and AFM, according to the minimum characterization requirements described by ISEV in [16]. This work is divided in two parts. In a first chapter, preliminary experiments are presented. Those experiments were used to establish some of the correct conditions for HUVECs culture. In the second chapter, further results are presented in form of the submitted manuscript to International Journal of Molecular Sciences.

Chapter 3

Preliminary experiments

In this chapter, the results of four experiments are described. First, HUVECs were incubated with different concentrations of the chemical staurosporine to analyse the morphological changes of the cells due to this treatment. Then, HUVECs were cultivated on a silicon wafer using different surface coatings to determine which one would lead to the best adherence of the cells. Finally, two different characterization methods of MVs are presented: staining with annexin V in an assay in suspension and imaging of the MVs via negative staining transmission electron microscopy (TEM). Those two characterization methods were only briefly investigated in this work.

3.1 Material and methods

3.1.1 Materials

All chemicals were purchased from Sigma Aldrich (Germany), unless otherwise stated.

3.1.2 HUVECs culture

The cells HUVEC-C (HUVECs, CLR-1730, ATCC, Sweden) were purchased from ATCC and were cultivated in Ham's F-12K nutrient mix (Gibco, Denmark) supplemented with 10% fetal bovine serum (FBS, Biowest), 50 µg/ml endothelial cell growth supplement (ECGS), 0.1 mg/ml heparin and 1% Penicillin/streptomycin (Stock concentration: 10000 Units Penicillin/10 mg streptomycin per ml). The medium was changed every alternate day and cells were passaged when 80% confluency was reached (approximately twice a week).

According to the manufacturer, this HUVEC cell line produces relatively heavy cells debris as well as viable suspension cells in addition to the cell monolayer. Therefore the cell culture supernatant was collected and centrifuged at 150g for 5 min. The pellet was resuspended in complete cell culture medium. In the meantime, the cell monolayer was rinsed twice with phosphate buffered saline (PBS). Trypsin/ ethylenediaminetetraacetic acid (EDTA) was added to the cell monolayer (1 ml was used for a 25 cm^2 cell culture flask and 2 ml for a 75 cm^2 cell culture flask) to detach the cells. The cell monolayer was coated homogeneously with the trypsin/EDTA and approximately 50% of the solution was removed. The cell flask was incubated for 5 min at 37°C. The detachment of the cells from the bottom of the cell flaks was verified in an optical microscope (Axiovert25, Zeiss, Germany) using a 10X objective and phase contrast. The trypsin/EDTA was inhibited by the addition of complete medium. The

suspension cells were added to the adherent cells and the cells were counted in a cell counting chamber (FastRead 102 counting chamber, Immune Systems, United Kingdom). The chamber factor was 10^4. HUVECs were diluted at an appropriate concentration in complete cell culture medium and were seeded at a cell density of 1×10^4 cells/cm^2. 5 ml of cell suspension were used for a 25 cm^2 cell culture flask and 15 ml for a 75 cm^2 cell culture flask. The HUVECs were incubated in a humidified incubator (HeraCell150, Thermo electron corporation, USA) at 37°C with 5% CO_2.

3.1.3 Observation by optical microscopy of the apoptosis induced by different concentrations of staurosporine

A HUVECs suspension was prepared according to the procedure described in 3.1.2. 3×10^3 HUVECs were seeded in the wells of a 12 well plate. After four days of incubation, the medium was removed and the cell monolayer was rinsed with PBS. Complete cell culture medium was supplemented with different concentration of staurosporine : 1 µM, 100, 10 and 1 nM. The medium was then added to the cell monolayer. A control well was also prepared with normal cell culture medium. The well plate was incubated in a humidified incubator at 37°C with 5% CO_2. The cell monolayer was observed by optical microscopy (Axiovert25, Zeiss, Germany) with a 10X objective and phase contrast up to eight hours after the start of the treatment.

3.1.4 Cultivation of HUVECs on silicon wafers with different surface coatings

The aim of this experiment was to investigate which coating material was the most appropriate to cultivate HUVECs on silicon wafer. A silicon wafer was patterned with a grid motif by photolithography. The silicon wafer was kindly prepared by Maria Dimaki (DTU Nanotech) in the DTU Danchip clean room facilities. The patterned silicon wafer was cut in small pieces (approximately 1×0.5 cm^2 with a diamond knife. The pieces were rinsed in milliQ water to remove cutting debris and placed in 70% ethanol for 15 min for sterilization. The pieces of silicon wafer were deposited in the wells of a 24-well plate (one piece per well). 200 µl of a coating solution were added in each well. Four coating solutions were prepared: 10 µg/ml fibronectin, 20 µg/ml laminin, 1.25% gelatin, 0.2 mg/ml poly-L-lysine. All solutions were prepared in PBS. A control well was prepared with 200 µl PBS. The coating solutions were incubated for three hours at room temperature in the cell culture cabinet. The coating solution was then removed. HUVECs were then seeded onto the coated silicon wafers at a cell density of 1×10^4 cells/well. 1 ml of cell medium was used per well. The well plate was incubated for 48 hours in the incubator at 37°C with 5% CO_2. The cell monolayer was observed with an upright microscope (Axio imager M1m, Zeiss, Denmark) with a 20X objective and differential interference contrast (DIC).

3.1.5 Characterization of microvesicles by negative staining transmission electron microscopy

A 200 mesh carbon grid (Agar scientific, United Kingdom) was glow discharged (Leica Coater ACE 200) for 15 s at 6 mA and used immediately. Apoptotic MVs were prepared from HUVECs

according to the procedure described in section 4.2.5 on page 48. 10 µl of MVs sample was applied on the grid for one minute. The excess of sample was blotted with a filter paper. 5 µl of negative staining dye (2% phosphotungstic acid) was applied on the grid and incubated for one minute. The excess of dye was blotted away. The grid was quickly rinsed with milliQ water and dried in air. The grid was imaged by transmission electron microscopy (TEM) using a CM100 (FEI,USA) instrument. This experiment was performed at core facility for integrated microscopy (CFIM, Copenhagen University, Denmark) with the help of Klaus Qvortrup.

3.1.6 Annexin V staining of MVs

50 µl of MVs from HUVECs (preparation of MVs see 4.2.5) were thawed and centrifuged at 18800 × g for 30 min. The pellet was resuspended in PBS with 2.5 mM calcium chloride (PBS-Ca). 5 µl of annexin-V-biotin was added. The solution was incubated for 20 min at room temperature (RT). 1 µl of a FITC-streptavidin solution (final concentration: 10 µg/ml) was added to the vesicles. After 15 min of incubation in the dark at RT, the vesicles were pelleted at 18800 × g for 30 min, then resuspended in 50 µl PBS-Ca. The fluorescence intensity was measured by a plate reader (laser: 488 nm, Victor3. Perkin Elmer, Denmark). Three negative controls were prepared: annexin was omitted in a control and apoptotic MV sample and a blank sample without MV was performed..

3.2 Results and discussion: HUVECs as parental cells for microvesicles

3.2.1 Observation of the apoptosis induced in HUVECs by different staurosporine concentrations

Apoptosis was induced in HUVECs treated with different concentrations of staurosporine (1 µM, 100 nM, 10 nM and 1 nM). The morphological changes on the HUVECs were observed by optical microscopy up to eight hours after the start of the treatment. Figure 3.1 on page 39 presents a representative picture at each observed time. After one hour of treatment, morphological changes are clearly visible in the cells treated with 1 µM and 100 mM of staurosporine. The cells started to lose attachment to the bottom of the well and shrank together. Later, this loss of adhesion continued. It can be observed that after four hours the cells treated with 1 µM staurosporine were quite round. Some membrane debris were visible on the surface. In contrast to this, the cells treated with 100 nm staurosporine still presented some elongated morphology after the four hours of treatment. Incubated with 10 nM staurosporine, HUVECs showed a clear change of morphology only after 4 hours of treatment. With 1 nM of staurosporine, it was only after eight hours that the cells started to shrink and lose adhesion to the substrate. On the pictures of the non-treated HUVECs, the cells did not present any change in morphology. Some cell debris (black dots) can be found over cell monolayer. This is in agreement with the description of the manufacturer [172]. To sum up, we could observe a concentration dependent morphological change during staurosporine induced apoptosis in HUVECs. HUVECs lost their

adhesion from the surface and shrank, which has been described as a characteristic morphological change in early apoptosis [46]. We could see morphological changes of HUVECs after eight hours of treatment with all tested concentrations. This shows that HUVECs were sensitive to staurosporine at concentrations as low as 1 nM. With the higher staurosporine concentrations, morphological changes were already visible after one hour. Previous studies by Kabir et al. [173] have shown in detail that staurosporine acts by disrupting the adhesion of the cells from their substrate. Moreover, they could also show that treated with 1 µM staurosporine the endothelial cells used in their study were also in apoptosis after one hour. In this experiment, the effect of the apoptosis inducing chemical was only evaluated according to the morphological changes. However further analysis on the biochemical level would provide more detailed information about the onset time of the apoptosis with the different staurosporine concentrations.

For the generation of MVs from apoptotic HUVECs, a staurosporine concentration of 5 µM was used, as Ullal et al. [169] showed that the release of MVs was higher using concentrations of staurosporine between 1 and 10 µM.

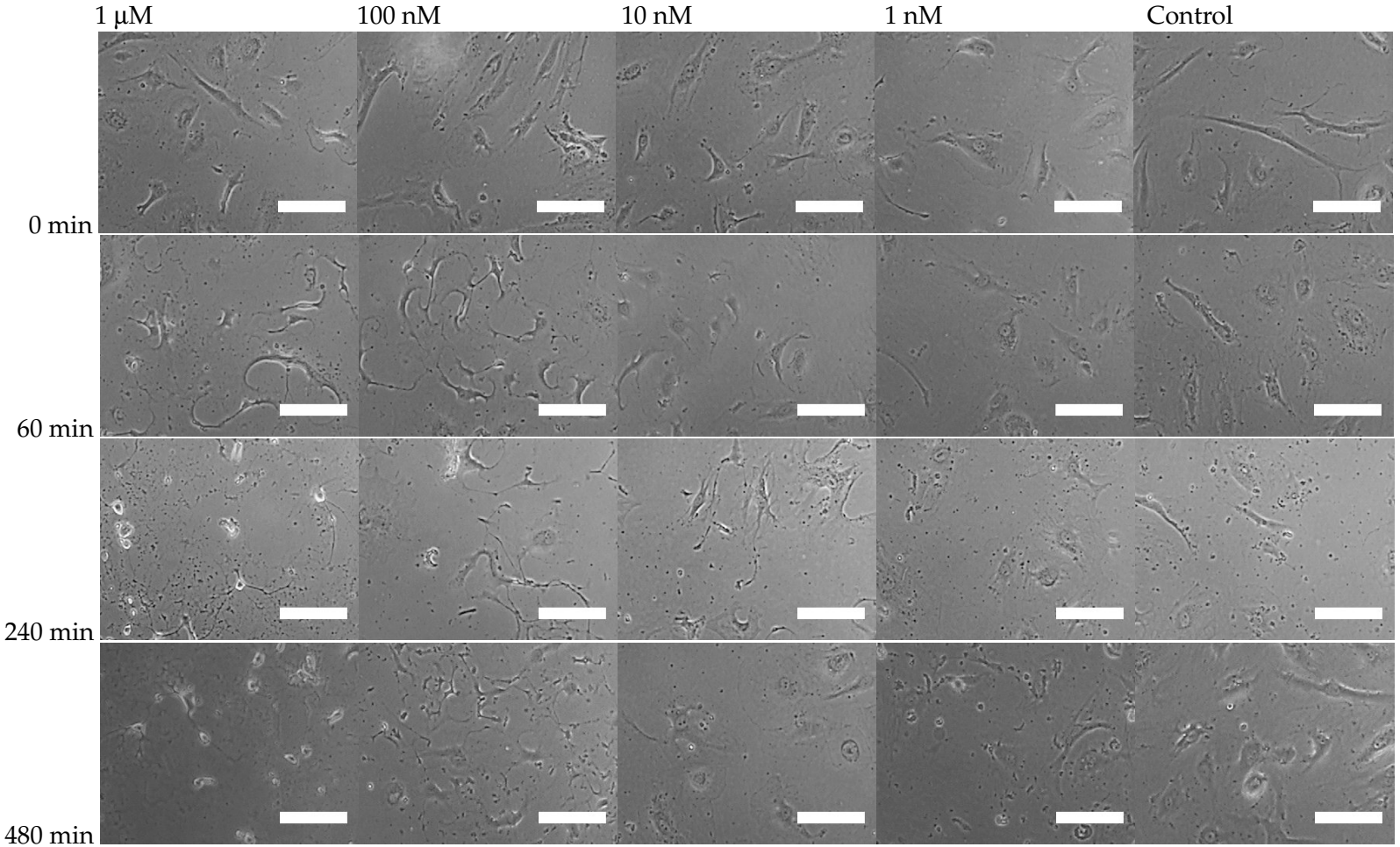

Figure 3.1: HUVECs undergoing staurosporine induced apoptosis from the start of the treatment and up to eight hours later. The morphological changes on HUVECs can be observed depending on the staurosporine concentrations used to induce apoptosis. The images were obtained in an optical microscope with phase contrast. The scale bar is 50 µm.

3.2.2 Cultivation of HUVECs on silicon wafers coated with different coating materials

To image biological samples using AFM, it is required that the support is extremely flat. Freshly cleaved mica sheets are often used. As an alternative, silicon wafers are also useful. However HUVECs did not grow well on blank silicon wafers as it can be seen in figure 3.2A. It seems that the cells would not attach and spread on the wafer as they did on a cell culture dish (see in figure 3.1 the control cells). Therefore different coatings (poly-L-lysine, gelatin, laminin and fibronectin) were tested on the silicon wafer to improve the adhesion of HUVECs according to the procedure described in 3.1.4. After 48 hours of incubation of the HUVECs, the adhesion was evaluated by microscopical observation. Surfaces coated with poly-L-lysine (figure 3.2B), gelatin (figure 3.2C) and laminin (figure 3.2D) did not allow a proper attachment of the cells onto the substrate. We could observe rounded cells that did not adhere onto the substrate. When the substrate was previously coated with 10 µg/ml of fibronectin (figure 3.2E), the morphology of the cells was comparable to the morphology of HUVECs on a standard cell culture dish. The cells adhered on the wafer and were spread, showing elongations on the surface. Thus, out of the four different coatings that we tested, we found that fibronectin was the most appropriate to promote HUVEC adhesion (see figure 3.2). Our results are in good agreement with results presented previously in [174, 175]. It has been shown that the active site of fibronectin is the arginine-glycine-and aspartic acid (RGD) motif [176]. This RGD-motif is recognized by integrins, involved in the adhesion of HUVECs. Laminin also contains a RGD motif that promotes endothelial cell attachment [177]. However we could not observe a proper attachment of the HUVECs on the laminin coated surface. As suggested in [174], it could be that the concentration used was not high enough or that the RGD motif was hidden and did not allow the cell attachment.

As a conclusion for the further experiments with HUVECs cultivated on silicon wafer, we used fibronectin as coating material prior of seeding the HUVECs. The intention with using patterned silicon wafer was to be able to perform fluorescence microscopy (for example with the annexinV/propidium iodide apoptosis detection assay) and then image per AFM the same cells to correlate the fluorescence image with the topography of the cells measured by AFM.

3.3 Results and discussion: Characterization of microvesicles derived from HUVECs

3.3.1 MVs from apoptotic HUVECs imaged by negative staining transmission electron microscopy

Electron microscopy is a widely used method for imaging of extracellular vesicles thank to its excellent resolution [106]. In this work, we used negative staining TEM to image the MV suspension. Figure 3.3 shows two representative images of a apoptotic MV preparation suspension. We could observe spherical objects surrounded by a membrane, which corresponded to the MVs released by HUVECs. Moreover we could observe other smaller elongated structures. As negative staining TEM is an unspecific method, we cannot with certitude identify

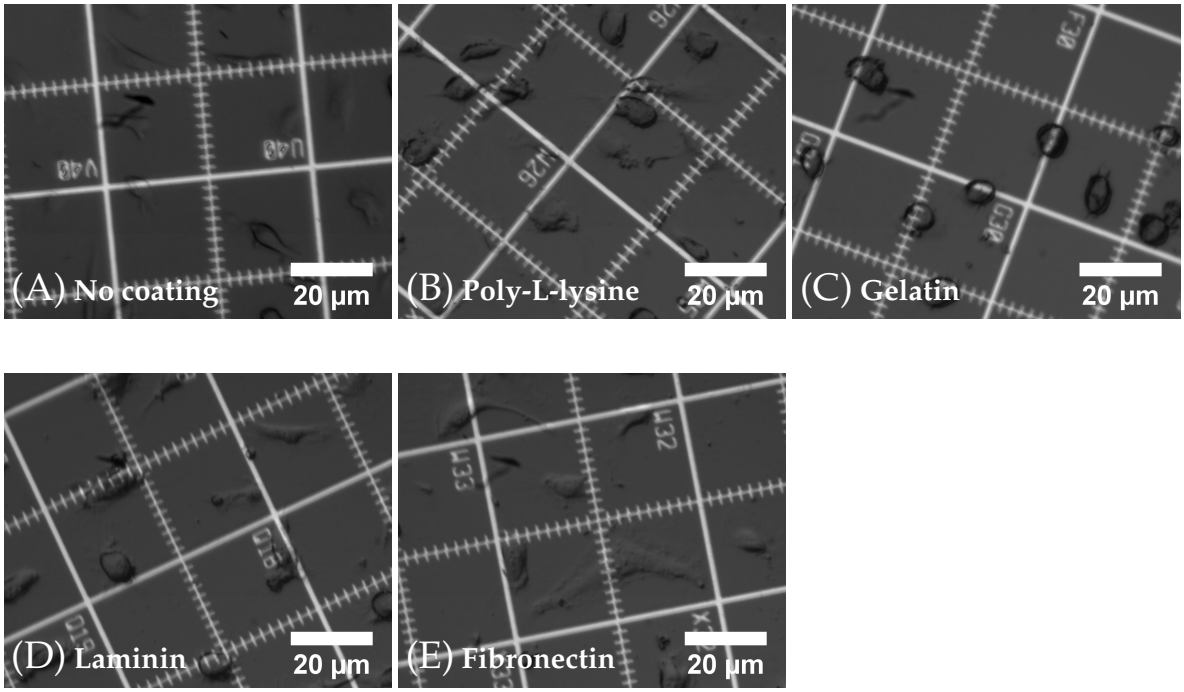

Figure 3.2: HUVECs cultivated on a silicon wafer coated with different adhesion molecules. HUVECs attached and spread best on a silicon wafer coated with fibronectin. The images were obtained in an upright optical microscope.

those structures. However, we can suppose that they were some small cellular debris that were pelleted together with the MVs or some artefacts from the buffer used. The electron dense points on the images 3.3A and 3.3B corresponded to dye aggregates. Nonetheless this investigation allowed us to confirm that our preparation contained vesicles. Moreover their sizes were around 100 nm, which is in good agreement with the values from AFM and NTA (see section 4.3.4 on page 54).

3.3.2 Expression of phosphatidylserine on microvesicles derived from HUVECs

Phosphatidylserine is a membrane phospholipid that translocates out of the cell in the early stages of the apoptosis. It has often been detected on the surface of microvesicles [65, 178] as it is exposed during vesiculation [38]. As we investigated vesicles released by apoptotic cells, we were interested in measuring the expression of phosphatidylserine on the membrane of the MVs derived from control and apoptotic HUVECs. A fluorescence MV staining assay was developed with annexin V as marker of phosphatidylserine. Briefly, MVs were incubated with annexin V-biotin then with streptavidin-FITC. In this assay, both targets (the MVs) and labelling molecules were in solution, and therefore were likely to get into close contact. Therefore, the labelling efficiency was expected to be higher than on a solid phase assay where MVs have to be captured on the bottom of a well. Figure 3.4 shows the staining principle for this assay. After a step of centrifugation to remove the unbound material, the fluorescence intensity was measured using a plate reader. A standard curve of streptavidin-FITC (figure 3.5A) was measured for streptavidin-FITC concentrations between 0.014 and 10 µg/ml. A linear fit was

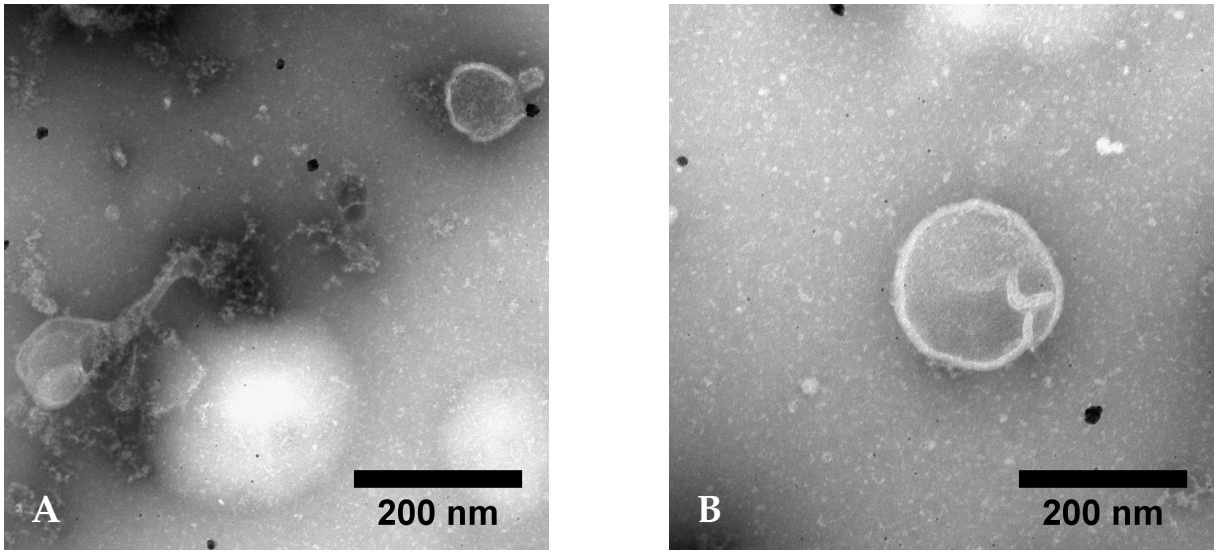

Figure 3.3: Apoptotic microvesicles imaged by negative staining TEM MVs are seen as structure enclosed by a membrane. Some other cellular debris of smaller size could also be observed in the sample.

applied to calculate the streptavidin-FITC concentration in the samples. The regression equation obtained was Streptavidin – FITC concentration = $1.3 \times 10^{-4} \times$ Fluorescence intensity – 0.12 with R^2= 0.999. The fluorescence intensity indicates the annexin V-biotin that is bound to MVs and therefore the expression of phosphatidylserine on the surface of the MVs.

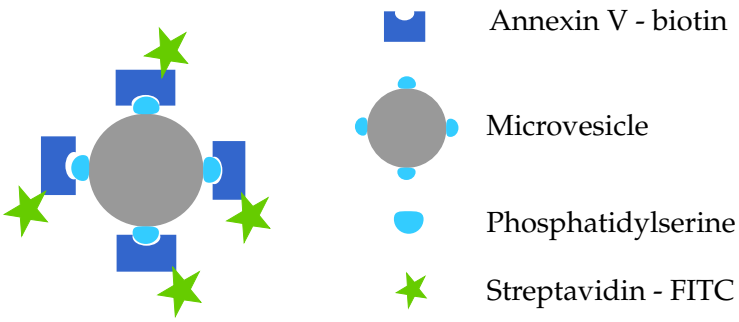

Figure 3.4: Principle of annexinV-FITC staining assay for MVs. MVs were incubated with annexinV-biotin, then with streptavidin-FITC. After washing the fluorescence intensity was measured.

Figure 3.5B presents the results for a representative sample measured during this assay. The concentration of streptavidin-FITC measured in the apoptotic MV sample (1 µg/ml) was approximately three times higher than in the control MV sample (0.3 µg/ml). However the controls where either no annexin V or no (apoptotic or control) MVs were added showed a streptavidin-FITC concentration approximately as high as in the control MV sample as shown in figure 3.5B. This high level of streptavidin-FITC in the controls was surprising. This indicated a high background fluorescence level in the assay and that further washing steps were

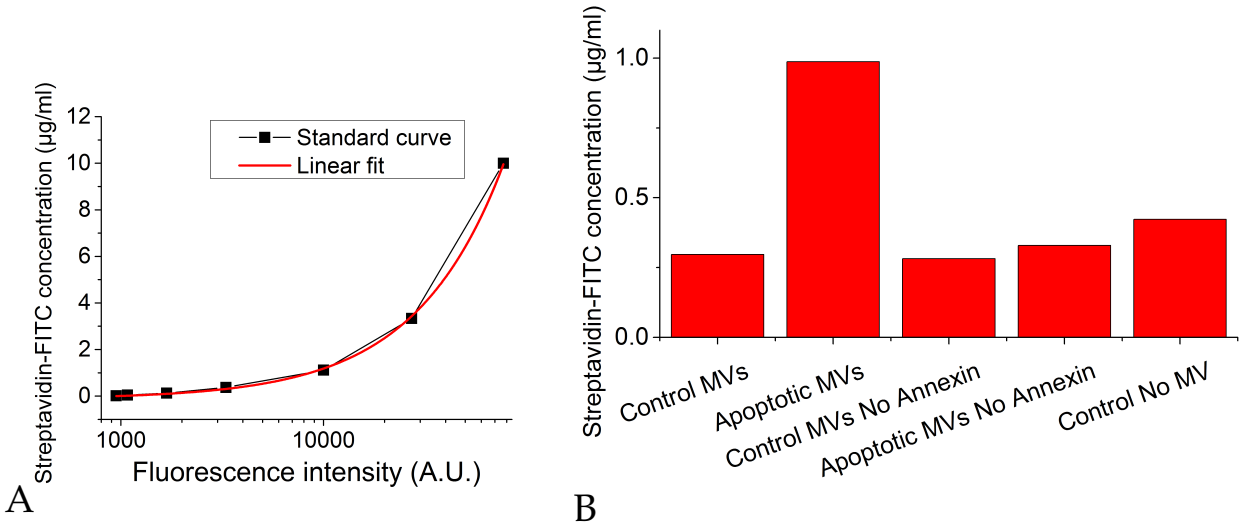

Figure 3.5: Fluorescence based assay for the measurement of the expression of phosphatidylserine on MVs Figure A shows the standard curve of streptavidin-FITC. The fluorescence intensity of streptavidin-FITC was measured between the concentrations 0.014 and 10 µg/ml. After subtraction of a blank value, a linear fit was applied. Figure B presents the results of the assay for a representative sample of apoptotic and control MVs and the corresponding controls.

required. It could also indicate that due to the use of a phosphate based buffer together with calcium ions, microprecipitates of calcium phosphate could form. Larson et al. [179] investigated the calcium phosphate microprecipitates and found that they behave similarly to the MVs leading to false positive signal. This assay could be improved by the use of HEPES based buffer instead of PBS. Furthermore, higher sensitivity might be achieved with the use of lactadherin as marker of phosphatidylserine instead of annexin V [38]. Due to time restriction, this assay was not further investigated.

Chapter 4

Generation and characterization of cell-derived microvesicles from HUVECs

This chapter is the article that has been submitted for publication in International Journal of Molecular Sciences, special issue "Focus on extracellular vesicles". The original submitted manuscript can be found in appendix B.1 on page 163. The experiments of the MV array were performed by master student Mathilde Granberg under my supervision.

Abstract

Background and aim: Microvesicles (MVs) have gained a large interest in the biomedical field as novel diagnostics biomarkers. However MV research is still impaired by the lack of standardization of the analysis methods. In this study, our goals were to develop a method for the reproducible generation MVs population from cell culture as a tool for standardization and validation of novel analysis methods, compare the sizing of MVs by atomic force microscopy (AFM) and nanoparticle tracking analysis (NTA) and develop an MV array allowing the sizing and phenotyping of MVs simultaneously.
Methods: MVs were isolated from apoptotic Human Umbilical Vein Endothelial Cells (HUVECs) by high speed centrifugation. Size and concentration of the MVs were characterized by AFM and NTA. The endothelial surface markers were analysed by an enzyme-linked immunosorbent assay (ELISA) and by the newly developed MV array, where MVs were captured according to their phenotype and imaged per AFM.
Results: MVs isolated from the cells undergoing apoptosis had a mean size of 115 nm as measured by AFM and of 197 nm as measured by NTA. MVs isolated from apoptotic and control HUVECs could not be distinguished by their size ($p>0.05$). HUVECs and their released MVs shared the same phenotype (positive for the endothelial markers CD31 and CD146 and negative for the platelet marker CD42b).
Conclusion: Our method generated MVs with a concentration reproducible within 20% range. This is a relevant model systems for medical applications. The size of the MVs was slightly larger as measured per NTA compared to AFM. The MV array proved to be an efficient tool to

characterize the surface markers of MVs and has the potential to identify the profile of MVs in patient samples

4.1 Introduction

Cell-derived microvesicles (MVs), also called cell-derived microparticles are a type of extracellular vesicles discovered in 1967 by Wolf, who named them "platelet dust" [4]. In contrast to exosomes which are formed inside the cells and released by exocytosis [34, 88], MVs are shed from cells by an outward blebbing of the cell membrane [6]. They are characterized by their diameter ranging from 50 to 1000 nm and the expression of receptors of the cell of origin on their surface. MVs play a central role in the cell-cell communication [180] and in the transfer of signal molecules such as microRNA from cell to cell [181, 182].

In the recent years, numerous studies have been published that showed that the concentration of MVs in the blood is altered in various pathological conditions such as systemic lupus erythematosus [23] and inflammatory diseases [183]. Therefore it has been proposed that MVs could be implemented as novel diagnostics markers [6]. Moreover the analysis of MVs could help to provide new insight in the pathogenesis of the diseases [184].

The main method used for MV analysis is flow cytometry, a method where the size and fluorescently stained surface molecules of each object are measured. Flow cytometry is a widely used analysis method with instruments available in most laboratories. However, flow cytometry is limited to measure objects larger than approximately 200 nm. Moreover lack of standardization in the measurement protocol leads to large variation in the results [185]. Therefore, other analysis methods have been developed to better understand and validate the potential of MVs as biomarkers. On one hand, attempts have been made to improve the flow cytometry techniques to adapt it to MVs such as the use of calibration beads [138, 186]. On the other hand, techniques based on light scattering such as dynamic light scattering (DLS) [120] and nanoparticle tracking analysis (NTA) [124] are attractive alternatives for MV measurement. NTA in particular was shown to be more sensitive than flow cytometry and could detect vesicles as small as 50 nm [25]. Imaging methods based on electron microscopy [105] and atomic force microscopy (AFM) [39] have been developed for MVs and allow a precise and accurate size and shape determination of MVs. The surface proteins of MVs can be accurately measured by an enzyme-linked immunosorbent assay (ELISA) and their pro-coagulatant function can be evaluated by a pro-thrombinase assay [103]. However solid phase assay such as ELISA do not deliver information concerning the particle size. Proteomics methods [157] are also available to characterize the protein content of MVs. The reader is referred to recent reviews [6, 101, 126] for a broader overview of the analysis techniques for MVs.

The development of new analysis methods for MVs requires their test, optimization and validation. For this purpose, standard MV populations are required. Synthetic beads such as polystyrene or silica beads have been developed as standards for the calibration of instruments measuring extracellular vesicles [117, 186]. However those can only be used for size and concentration calibration. Previous studies used urine MVs as standard sample in the comparison of different analysis techniques [106, 129]. Using *in vitro* cell lines to release MVs is a great tool

to obtain defined MV populations harbouring the phenotype, i.e. the surface markers, of the cells of origin. Apoptosis is one of the processes by which the release of MVs is induced [187, 188] and it can be implemented easily *in vitro* to activate cells. Combes et al. were able to activate the MV release from Human Umbilical Vein Endothelial Cells (HUVECs) using tumour necrosis factor-α (TNF-α)[27]. Similarly Šimák et al. studied the release of endothelial MVs when inducing the apoptosis in HUVECs with camptothecin [170]. Staurosporine induced apoptosis was used to activate Jurkat cells to release MVs [168, 169].

In the present study, we aimed at developing a standard method for the reproducible *in vitro* generation of a population of MVs derived from HUVECs. We focused on sizing and characterizing the MVs as well as on the reproducibility of the protocol. This well-characterized MV population can then be used to test and validate new analysis methods. The second aim of the study was to compare the sizing of MVs by AFM and NTA. To our knowledge, this is the first report comparing AFM and NTA sizing of biological MVs. Moreover we combined the array from Jørgensen et al. [147, 148] and the AFM imaging of MVs captured on antibodies by Yuana et al. [39] to obtain an MV array to characterize the MV phenotype as well as the size of the MVs.

4.2 Materials and Methods

All chemicals have been purchased from Sigma Aldrich, Denmark, except if stated otherwise. All antibodies have been purchased from Abcam, United Kingdom. The buffer phosphate buffered saline (PBS) used for all experiments with MVs was filtered through a 0.1 µm filter (VWR, Denmark).

4.2.1 Cell culture

HUVECs (Human umbilical vein endothelial cells , CLR-1730, ATCC, Germany) were purchased from ATCC and were cultivated in complete growth medium composed of Ham's F-12K nutrient mix (Gibco, Denmark) supplemented with 10% FBS, 50 µg/ml Endothelial cell growth supplement (ECGS), 0.1 mg/ml heparin and 1% penicillin/streptomycin (Stock concentration: 10000 Units penicillin/10 mg streptomycin per ml). The cells were seeded at a cell density of $1{\times}10^4$ cells/cm^2. The medium was changed every alternate day and cells were passaged when 80% confluency was reached (approximately twice a week).

4.2.2 Apoptosis detection assay of the HUVECs

HUVECs were seeded in a 24 well plate with $2.5{\times}10^4$ cells/well. 48 hours after seeding, the apoptosis was induced with medium supplemented with 5 µM staurosporine. After 4 and 8 hours, a well was stained with the Annexin V-FITC and PI (FITC Annexin V Apoptosis Detection Kit I, BD Pharmingen) with 5 µl of each dye in 1X binding buffer incubated for 15 min in the dark at room temperature. The cells were imaged using a fluorescent microscope (Nikon Eclipse Ti-S, DFA A/S, Denmark) with a 20X objective.

4.2.3 Atomic force microscopy of the apoptotic HUVECs

After rinsing with milliQ water, fragments (2×2 cm^2) of silicon wafer (Topsil, Denmark) were placed in 70% ethanol for 15 min for sterilization. They were then placed in a 24 well plate and coated with fibronectin (10 µg/ml in PBS) for three hours at room temperature. HUVECs were seeded on the fragments of silicon wafer at a density of 2×10^4 cell/well. 48 hours after seeding, apoptosis was induced as previously described (see 4.2.2). Samples were taken after 0, 4 and 8 hours. The cells were rinsed twice with PBS, then fixed in formaldehyde (3.7% in PBS) for 30 min at room temperature. The cells were then dehydrated in increasing concentrations of ethanol (30, 40, 50, 60, 70, 80, 90 and 99% (two times)) and finally dried in air. The cells were imaged with an AFM system (XE-150, Park Systems, Korea) in tapping mode. The images had a resolution of 512×512 pixel (scan area: 50×50 μm^2) and were acquired with a scan rate of 0.25 Hz. The AFM probe had a force constant of 40 N/m and a resonance frequency of 300 kHz (Budget Sensor, Bulgaria). The capture and analysis software were respectively XEP (version 1.7.70) and XEI (version 1.8.0) (Park Systems, Korea). The images were flatten using the linear regression method.

4.2.4 Immunostaining of HUVECs

An immunostaining assay was performed to verify the expression of the endothelial markers CD31 (Platelet endothelial cell adhesion molecule (PECAM-1)) and CD146 (Melanoma cell adhesion molecule (MCAM) or MUC18 or S-endo) on HUVECs. HUVECs were seeded on cover glasses. After two days of incubation, the cells were fixed in 3.7% formaldehyde for 30 min at room temperature. After rinsing twice in PBS, the remaining binding sites were blocked with 1% Bovine Serum Albumin (BSA) in PBS+0.1% tween®-20 (PBST) for 30 min. The HUVECs were incubated with the primary antibodies anti-CD31 (anti-CD31 antibody [JC/70A]) or anti-CD146 (anti-CD146 antibody [P1H12]) at 4°C over night. As isotype control an anti-CD42b antibody was used. The primary antibodies were diluted in 1% BSA in PBST to a concentration of 1 µg/ml (anti-CD146), 2 µg/ml (anti-CD42b) and 1 to 100 diluted for anti-CD31 antibodies. A negative control was prepared without primary antibodies. After rinsing (three times in PBS 5 min under gentle agitation (120 rpm)), the cells were incubated with a secondary antibody goat anti-mouse IgG1 FITC diluted in 1% BSA in PBST for one hour under gentle agitation (120 rpm). After rinsing the cells were counterstained with the DNA staining dye 2-(4-Amidinophenyl)-6-indolecarbamidine dihydrochloride (DAPI, final concentration 0.5 µg/ml) for one minute. The cells were rinsed twice in PBS and imaged right away in a confocal microscope (LSM 700, Zeiss, Germany) using a 50X objective.

4.2.5 Preparation of MVs from HUVECs

HUVECs were seeded in a cell flask at a density of 8×10^3 cells/cm^2. 5 days after seeding, when the confluence had reached approximately 70%, the cell medium was changed to cell medium supplemented with 5 µM staurosporine, an apoptosis inducing chemical. 24 hours later, the supernatant containing the apoptotic MVs was collected. The MVs were purified from the cell culture supernatant using a procedure adapted from the literature [23, 65, 189] to specifically

isolate MVs. A first centrifugation step at 1250 × g for 5 min removed the large cell debris. The MVs were then pelleted by centrifugation at 18800 × g for 30 min. 95% of the supernatant was removed and the MVs were resuspended in PBS. The MVs were then pelleted a second time. After removal of 95% of the supernatant, the pellet was resuspended into a volume corresponding to 10% of the initial volume. The aliquots were stored at -20°C. Each aliquot was thawed only once, directly before analysis. Control samples were prepared in the same way with complete medium.

4.2.6 Measurement of the MVs with AFM in tapping mode

According to [190], fragments (2×2 cm^2) of p-doped single sided polished silicon wafer (Topsil, Denmark) were coated with N-(6-Aminohexyl)aminopropyltrimethoxysilane (1 ml in 40 ml isopropanol and 1 ml milliQ water, Abcr GmbH, Germany) for three hours at room temperature. The fragments were rinsed in isopropanol and milliQ water and blow dried. 10 µl MV solution was placed on a fragment of silicon wafer for 1 min. The MV solution was then rinsed with milliQ water three times and blow dried with air. The MVs were imaged with AFM in tapping mode using cantilevers and software as previously described (see 4.2.3). The image size was 5x5 cm^2 with 256×256 pixel and a scan rate of 1 Hz was used. After flattening of the image, the MVs were detected using the upper threshold method. Assuming that the MVs were spherical, the diameter of the particles was calculated from the measured volume with the following formula : $d = 2 * (\frac{3V}{4\pi})^{\frac{1}{3}}$

4.2.7 Measurement of the MVs with NTA

Samples of MVs were diluted 10 times in PBS to suit into the recommended concentration range for NTA, i.e. between 2 to 10×10^8 MVs/ml [25, 191]. Samples were then introduced manually with a 1 ml syringe into the chamber of the Nanoparticle Tracking Analysis instrument (LM10, Nanosight, United Kingdom). The instrument was equipped with a laser with a wavelength of 638 nm and with the NTA software version 3.1. The camera level was adjusted to 11. For each samples, three videos of 60 s with a frame rate of 30 frames/second were recorded. For the analysis, the threshold level was set at 3, blur size was automatic. Between each measurements, the chamber was dismounted and washed thoroughly with milliQ water. For verification of the measurements, latex beads (size: 1000 to 50 nm , Molecular probes, USA) were used (data not shown).

4.2.8 ELISA assay for CD31 detection on the MVs

An enzyme-linked immunosorbent assay (ELISA) was performed to measure the level of CD31 (PECAM1) on the isolated MVs. A one step ELISA kit (Abcam, United Kingdom) according to the manufacturer's instruction. Briefly, the CD31 standard was reconstituted by adding 500 µl of sample diluent NS. A dilution serie of the standard was prepared from 50 to 4.4 ng/ml. MV samples were thawed. 50 µl of MV sample or standard aliquot was added to the wells of the pre-coated 96 well plate. A blank (only sample NS dilluent) was also prepared. Each measurement was made in duplicate. 50 µl of antibody cocktail was added into each well.

After one hour incubation on a shaker (400 rpm), the wells were rinsed three times with 1X wash buffer (diluted in milliQ water). 100 µl of 3,3',5,5'-Tetramethylbenzidine (TMB) substrate was added to each well and incubated for 10 min in the dark on a shaker (400 rpm). 100 µl of stop solution was then added and mixed for one minute on a shaker (400 rpm). The absorbance was then measured at 450 nm with a plate reader (Victor3, Perkin Elmer, USA).

4.2.9 MV array imaged by AFM to characterize the surface markers of MVs

To determine the surface markers present on the surface of the MVs, a MV array was developed with three antibodies (two antibodies against endothelial markers (anti-CD31 antibody [JC/70A] and anti-CD146 antibody [P1H12]) and one antibody against a platelet marker (anti-CD42b antibody [VM16d]) according to the experimental setup shown in figure 4.1. 10 nm titanium and 100 nm gold were deposited on a silicon wafer using Wordentec QCL 800. The silicon wafer were diced with a dicing saw (Disco Automatic dicing saw, model DAD321). Antibodies were immobilized onto the gold surface according to the procedure described by Fernandes et al. [192] and Martins et al. [193]. Briefly, the gold substrate was cleaned for three times 10 min in a UV/ozone photoreactor (UVP, USA). The linker sulfo-LC-SPDP (sulfosuccinimidyl 6-(3'-(2-pyridyldithio)propionamido)hexanoate, ThermoFisher Scientific, USA) was incubated on the gold substrate for 20 min in a humid chamber at room temperature. The concentration of the sulfo-LC-SPDP linker was 2 mg/ml in PBS. The gold substrate was rinsed with PBS and milliQ water and blow-dried. The antibodies were spotted manually (with a pipette) on the gold substrate with a concentration of 250 µg/ml. Each spot had a volume of 1.5 µl. The incubation of the antibodies was performed overnight at 4°C. The gold substrate was rinsed in PBS. The remaining binding sites were blocked in BSA (1% in PBS) for 30 min at room temperature in a humid chamber. After rinsing in PBS, apoptotic MVs (10 times diluted in PBS) were incubated on the functionalized gold substrate for 15 min at room temperature. The excess of MVs was rinsed with PBS and milliQ water. The gold substrate was blow-dried and immediately imaged by non-contact AFM (Park Systems, Korea). Each spot was imaged on at least three representative positions. The images had a a scan size of 5×5 μm^2 and a resolution of 256×256 pixels.

4.2.10 Statistical analysis

The data representation and statistical analysis were performed using the software OriginPro 9.0.0 (OriginLab, USA). The normality of the samples was tested with a Kolmogorov-Smirnov test ($p<0.05$). The comparison of means was performed with a one-way ANOVA test. The difference was determined statistically significant if $p<0.05$. SD denotes the standard deviation. We also indicated the standard deviation as the ratio between the standard deviation and the mean value.

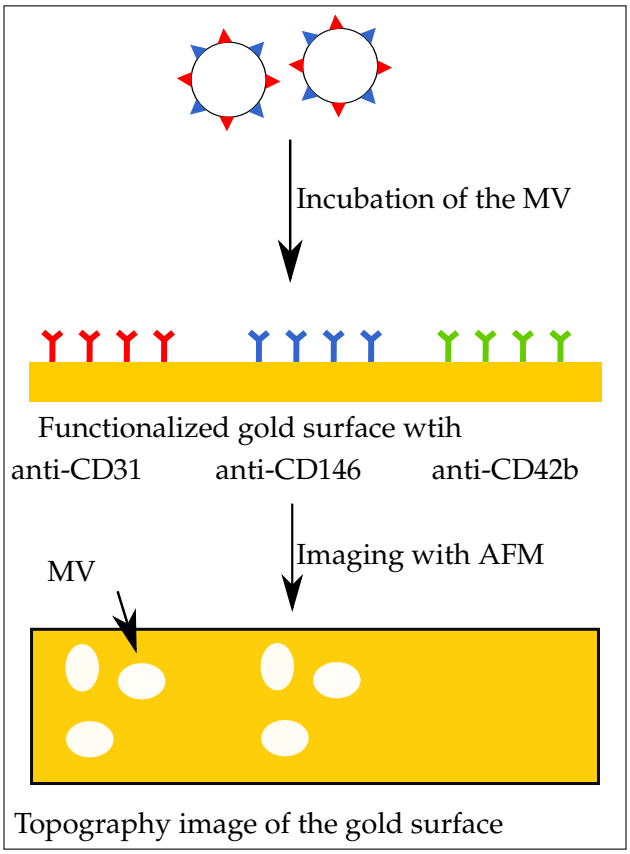

Figure 4.1: Experimental setup of the MV array A gold surface is functionalized in discrete spots with antibodies anti-CD31, anti-CD146 and anti-CD42b. MVs are incubated over the functionalized surface. The bound MVs are imaged by AFM.

4.3 Results

4.3.1 Morphological changes of HUVECs undergoing apoptosis induced by staurosporine

Stauropsporine, a potent protein kinases inhibitor was used to induce apoptosis in HUVECs. Throughout the study, we aim to compare HUVECs treated with staurosporine (apoptotic HUVECs) with non-treated HUVECs (control HUVECs). Figure 4.2 shows HUVECs undergoing apoptosis. In the phase contrast images (4.2A to 4.2C) the changes in morphology of the HUVECs can be observed, while the pictures 4.2D to 4.2F show the corresponding fluorescence images of the standard fluorescent apoptosis assay including the component annexin V-FITC (fluorescein isothiocyanate) and propidium iodide (PI). In those images, the green staining corresponds to annexin V-FITC binding to the membrane phospholipid phosphatidylserine, when it is translocated out of the cell, indicating an early apoptosis stage [46]. The red color corresponds to PI, that is able to stain the DNA inside the cells, only when the cell membrane has been perforated in late apoptosis stages [194]. At the time of apoptosis induction (figures 4.2A and 4.2D), the cells were well spread on the surface and no fluorescence signal could be detected. In the sample taken after four hours (figures 4.2B and 4.2E), we could observe that the cells have shrunk and some cells showed a positive signal for annexin V-FITC due to the

exposure of phosphatidylserine outside of the cells. Eight hours after the beginning of the treatment, we could see that the cells had shrunk further (figure 4.2C). More HUVECs had become positive for AnnexinV-FITC and PI signal could also be detected indicating that the cell membrane was perforated at this stage (figure 4.2F). In summary, treated with 5 µM of staurosporine the cells were in early apoptosis phase in the sample taken after four hours and had already reached a late apoptosis phase eight hours after the addition of staurosporine.

To confirm our findings of the annexin V-FITC/PI apoptosis detection assay, we imaged the HUVECs undergoing apoptosis using AFM in non-contact tapping mode. Figures 4.2G to 4.2I shows the topography image of HUVECs undergoing apoptosis. At the time point of the addition of the drug (figure 4.2G), the cells were widely spread on the surface showing numerous extensions and adhesion points evenly spread around the nucleus. After four hours of treatment with staurosporine, the membrane had lost many of these anchoring points and it seems that the cells had started to retract on themselves as illustrated by the representative cell presented in figure 4.2H. Moreover, protrusions appeared (highlighted in the red circles) that might indicate a blebbing of vesicles. Holes in the cell membrane had appeared which is a characteristic change of cells undergoing apoptotis [195]. The cells imaged after eight hours of treatment (figure 4.2I) had further retracted around the nucleus. The other structures on the surface corresponded to residues of the cell membrane.

4.3.2 Expression of CD31 and CD146 on HUVECs

The expression of CD31 (Platelet endothelial cell adhesion molecule 1 (PECAM1)) and CD146 (melanoma cell adhesion molecule (MCAM)) on the surface of HUVECs was verified by an immunoassay. Those two markers were chosen as they are often used to show the presence of endothelial cells [196, 197]. A secondary antibody conjugated to FITC was used so that the expression of the surface markers is indicated by the green color. The DNA of the cells was counterstained by 4',6-diamidino-2-phenylindole (DAPI) represented in blue. Figure 4.3A shows the expression of CD31 and figure 4.3B the expression of CD146. Both CD31 and CD146 were expressed on the surface of the HUVECs. The highest intensity was detected on the borders of the cells and also on the elongations of the cell membrane reaching to the neighbouring cells. The isotype negative control used was an antibody against a platelet surface marker (Platelet glycoprotein Ib alpha chain, CD42b) which was not expressed on HUVECs (figure 4.3C).

4.3.3 Release of MVs from HUVECs over time

The release of MVs over time was evaluated by collecting samples of cell culture supernatant at several times (1, 4, 8 and 24 hours) after addition of the medium supplemented with staurosporine. The samples were processed to collect the MVs according to the centrifugation procedure described in 4.2.5. Figure 4.4 shows the concentration of MVs in the different samples for the apoptotic MVs and control MVs. Until eight hours of treatment with staurosporine, the concentrations of isolated MVs in both apoptotic and control MV aliquots were similar. After 24 hours, the concentration of apoptotic MVs reached 1.3×10^{10} MVs/ml, while the concentration of MVs from the control cells was 5.9×10^{9} MVs/ml, only slightly higher than one hour

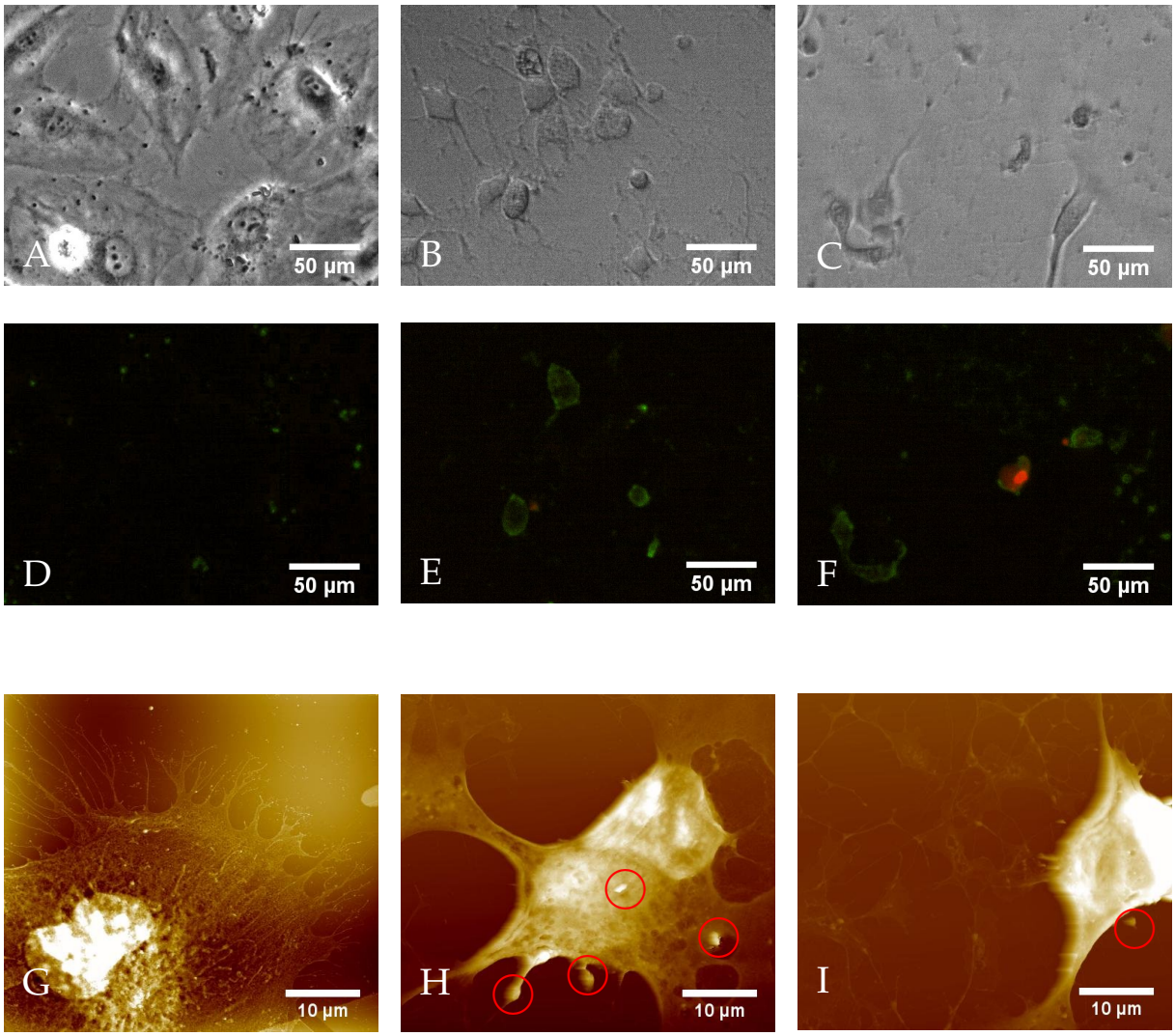

Figure 4.2: Morphological changes of HUVECs undergoing apoptosis induced by staurosporine after 0, 4 and 8 hours of treatment. (A to F) An Annexin V/PI apoptosis detection assay (Brightfield images with phase contrast: A to C and their corresponding fluorescence pictures: D to F) showed annexin V-FITC (green color) bound to the cells after four hours of treatment (E), showing that the exposure of phosphatidylserine started few hours after the addition of staurosporine. PI (red color) stained the DNA of some cells after eight hours (F). (G to I) The morphological changes of HUVECS were also observed by non-contact tapping mode AFM. The images represent the topography of a typical cells after 0 h (G), 4 h (H) and 8 h (I) of treatment. The color is representative for the height where the darkest color shows the lowest region and white the highest regions. HUVECs that were widely spread on the surface (G) lost their adhesion sites and shrunk around the nucleus (H and I) while undergoing apoptosis. The red circles indicate protrusion on the apoptotic cells that could correspond to the blebbing of MVs. The resolution of the images was 512×512 pixel.

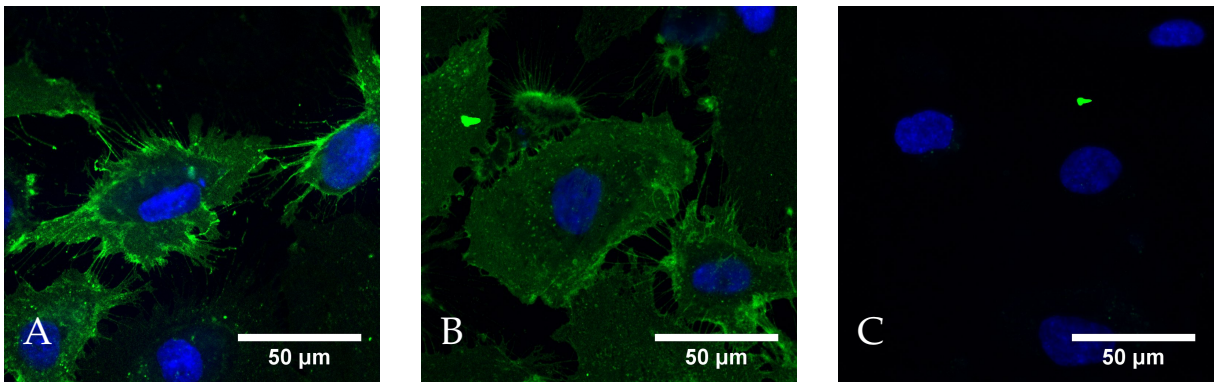

Figure 4.3: Expression of endothelial markers CD31 and CD146 on HUVECs. The cells were double stained for the endothelial markers CD31 (green, A) or CD146 (green, B) and DNA (blue). As isotype control, a platelet marker CD42b (C) was used and was negative on the HUVECs. The images were obtained with a confocal microscope.

after the medium was changed. The size distributions of the apoptotic MVs (figure 4.10) shows that the MVs that increased most had a diameter around 200 nm. For the control MVs (figure 4.10A), no significant change in the size distribution can be seen over the time.

4.3.4 Size characterization of MVs from HUVECs

Many methods for characterization of MVs are available as reviewed in [6, 101, 126]. In this work an imaging method (AFM) and a Brownian motion based method (NTA) were used to characterize and quantify MVs released from control and apoptotic HUVECs.

Measurement of MVs with AFM AFM was previously used to characterize extracellular vesicles from cell culture supernatant as well as extracellular vesicles isolated from complex body fluids [39, 97, 113]. AFM provides highly precise sizing of the vesicles. The sample preparation is relatively fast (up to five minutes) and does not require any specific equipment. Figure 4.5 shows the topography images of MVs on a silicon wafer measured by AFM. Those images provide structural information about the vesicles, which appeared as bell-shaped structures. Both apoptotic (figure 4.5A) and control MVs (figure 4.5B) appeared as round to rod-shaped structures. The MVs had a height of more than 50 nm.

A blank sample free of MV (PBS buffer) was prepared and imaged in the same way as sample with MVs to verify for contamination. Figure 4.5C shows a representative topography image of a blank sample. No objects with a size similar to the MVs were found. Few contamination could be imaged on the surface but their height (below 10 nm) was far lower than the threshold size for MVs.

Six independent samples (MVs from apoptotic and control HUVECs) were prepared and analysed by AFM. Around 200 MVs were imaged in each sample. The images were taken at representative positions on the sample. An average of five images were acquired per sample. Figure 4.6A shows the mean size distribution of each six samples with bin width of 50 nm. The mean size of apoptotic MVs was 115 nm (SD +/- 19, range: 12 to 409 nm), while the mean size

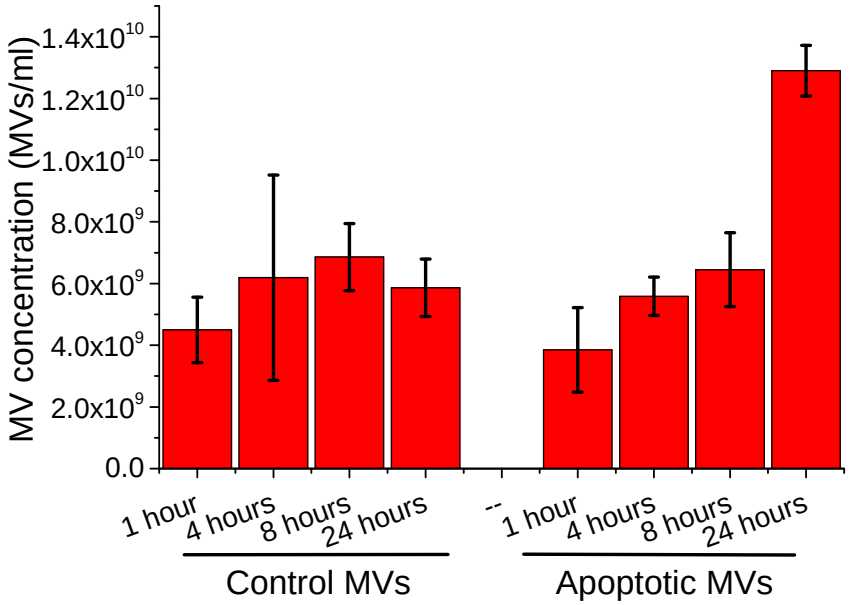

Figure 4.4: Release of MVs over time. The concentration of MVs isolated from apoptotic and control HUVECs after 1, 4, 8 and 24 hours was measured by NTA. In the first eight hours, the MV concentration in apoptotic and control samples was comparable. After 24 hours, the concentration of the apoptotic samples was clearly higher than in the control samples. We present an average of three measurements of a representative samples.

of control MVs was 139 nm (SD +/- 34, range: 26 to 393 nm). The mean sizes of the apoptotic and control MVs were not significantly different from each other (p = 0.16).

Measurement of the MVs with NTA The size of the MVs released from apoptotic and control HUVECs was also determined using NTA. With this technique the size of the vesicles is calculated from their Brownian motion in an analysis chamber. Figure 4.6A shows the average size distribution of six independent samples with bin width of 50 nm. Similar to the AFM, the size distribution of the apoptotic and control MVs were overlapping each other. Compared to the size distribution obtained by the AFM analysis, the NTA analysis lead to a more polydisperse size distribution evidenced as a wider peak in the size distribution graph. The maximum of the peak was located around 125 to 175 nm. The mean size of the apoptotic MVs as measured per NTA was 197 nm (SD +/- 28, range: 17 to 1381 nm) and the mean size of the control MVs was 192 nm (SD +/- 29, range: 13 to 959 nm). The difference between the mean sizes of apoptotic and control MVs measured with NTA was not significantly different (p = 0.7).

4.3.5 Measurement of the MVs concentration by NTA

NTA measurements give information not only about the size of the vesicles in the samples, but also about the concentration of the vesicles. Figure 4.6B reports the average MV concentration in five independent samples of MVs purified from control and apoptotic HUVECs. In the apoptotic samples, 1.22×10^{10} MVs/ml (SD +/- 2.8×10^{9}, corresponding to 23%) MVs were isolated, while 3.7×10^{9} MVs/ml (SD +/- 9×10^{8}, corresponding to 24%) were isolated from the

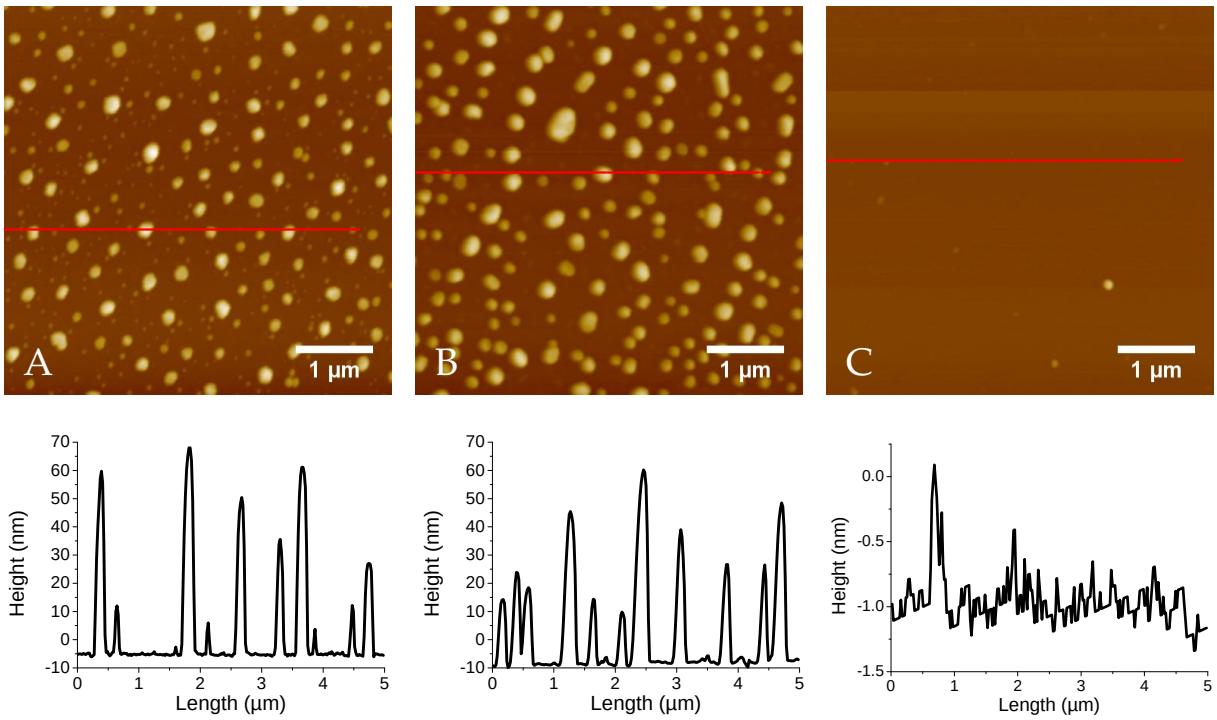

Figure 4.5: AFM imaging of MVs. Topography images of MVs derived from apoptotic HUVECs (A) and from healthy HUVECs (B) acquired with an AFM in tapping mode. A height profile along the red lines was represented for each AFM image. MVs isolated from HUVECs showed a height around 40 to 60 nm. Image C is the topography image of a blank sample (only buffer). No contamination was found in the buffer. The resolution of the images was 256×256 pixel.

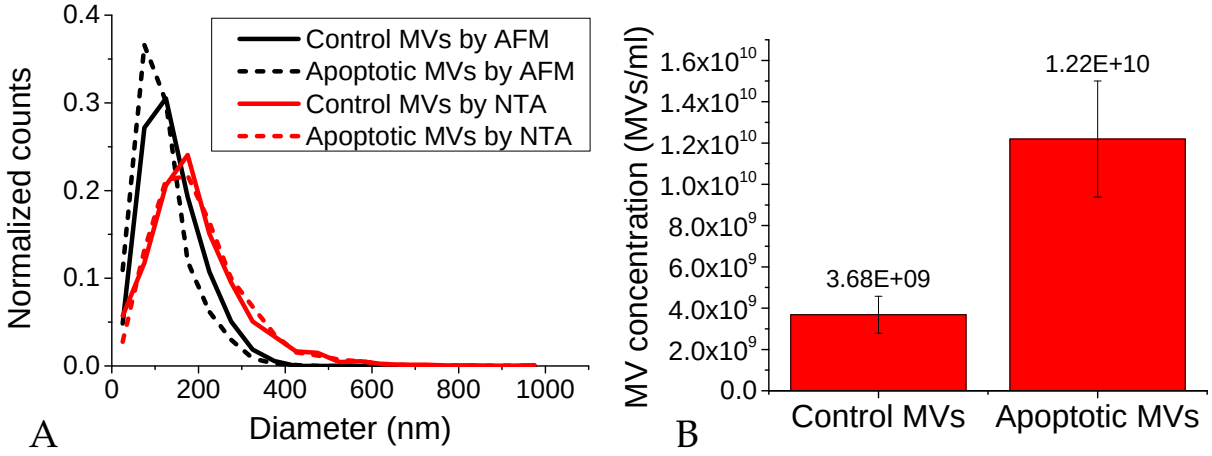

Figure 4.6: Size and concentration of HUVECs MVs. The size distribution (A) of MVs isolated from apoptotic and control HUVECs was measured by AFM and NTA for six independent samples. The average size distributions are presented. The size distributions for MVs measured by AFM and the size distribution of MVs measured by NTA respectively overlap each other. The size distribution obtained per NTA is wider and the mean larger than the size distribution obtained per AFM. Figure B reports the average concentration of MVs in the apoptotic and control aliquots for five independent samples. The measured concentration of apoptotic MVs was 3.3 fold higher than the control MVs concentration. The concentrations were significantly different ($p=2\times10^{-4}$). The error bars represent the standard deviation of the five independent samples.

cell culture supernatant of control HUVECs. Thus, in the apoptotic samples, 3.3 times more MVs could be measured compared to the control samples. The difference in concentration was statistically different with $p = 2\times10^{-4}$.

The complete growth medium and four of its components followed individually the same centrifugation protocol like the cell culture supernatants in order to evaluate if MVs or MV like structures could be isolated from the complete growth medium used to cultivate the cells. As shown in appendix A and in figure 4.9, the concentration of MVs in the complete growth medium corresponded to approximately 15% of the concentration of apoptotic MVs and most of those vesicles came from the FBS.

As we measured the MVs in the complete growth medium before incubation with the cells (see 4.6B), we can subtract the contaminating MVs (or background MVs) to calculate the MVs released per cell and we obtain that the concentration of apoptotic MVs and control MVs without the contaminating MVs from the medium were respectively 1×10^{10} MVs/ml and 1.9×10^{9} MVs/ml. Using the number of cells seeded in a cell flask (8000 cells/cm^2) of 75 cm^2 ($N_0 = 8000 \times 75 = 6 \times 10^5$) together with the number of days in culture (five days) and an estimated population doubling time of 30 hours [198], we could estimate the number of cells at the time of the apoptosis induction (N_{ind}) as follows:

$$N_{ind} = N_0 \times 2^{\frac{\text{duration}}{\text{doubling time}}} = 6 \times 10^5 \times 2^{(\frac{5 \times 24}{30})} = 9.6 \times 10^6 \text{ cells} \quad (4.1)$$

Using the average MV concentration in the apoptotic and control aliquots (with contaminating MVs subtracted), the up-concentration factor (UF) of the aliquots compared to the cell flask corresponding to UF=10, the total volume of the cell flask (V=15 ml), we obtain the number of MVs released per cell (MVs_{cell}) as follow:

$$MVs_{cell} = \frac{\text{MVs concentration} \times V}{UF \times N_{ind}} \tag{4.2}$$

which corresponded to 1625 MVs/cell for the apoptotic sample and 281 MVs/cell for the control samples, which was 5.8 fold more MVs released by an apoptotic cell compared to a healthy cell. Considering that the size distribution of the MVs had a maximum of the peak at 150 nm (considered as diameter of MVs (d_{MVs}) as measured by NTA and that the HUVECs had a diameter (d_{cell}) of 15 µm, we can calculate the part (P_{MVs}) of cell membrane used for the MVs as the ratio of the surface area of all the MVs released by one cell to the surface area of one cell, assuming that the cell is a sphere (surface area of a sphere=$4\pi r^2$):

$$P_{MVs} = \frac{MVs_{cell} \times area_{MVs}}{area_{cell}} = \frac{MVs_{cell} \times 4\pi(\frac{d_{MVs}}{2})^2}{4\pi(\frac{d_{cell}}{2})^2} \tag{4.3}$$

We obtain that the released MVs corresponded approximately to 16% of the total surface area of a HUVECs in the apoptotic samples and 3% of the total surface area of a HUVECs in the control samples.

4.3.6 Characterization of the surface markers on the surface of the cell-derived microvesicles

ELISA assay to measure the expression of CD31 on the MVs A one-step ELISA assay (see 4.2.8) was performed to measure the expression of CD31 (PECAM-1) on the surface of the MVs. The analysis was performed for five independent apoptotic and control samples. The cell culture supernatants (after first centrifugation at 1250 × g to remove larger debris) as well as washing steps after each centrifugation steps at 18800 × g were measured for a representative sample. The absorbance values measured for the supernatant of the control sample as well as all the washing steps were below the lowest value of the standard curve. Therefore it can only be concluded that the CD31 concentration in those samples was below 4.4 ng/ml, the lowest concentration measured in the standard curve. Figure 4.7A shows that in the apoptotic supernatant 7.4 ng/ml of CD31 was present, while after isolation of the MVs, the concentration of CD31 in the MVs preparation (70.5 ng/ml) was 9.53 times higher than in the apoptotic supernatant.

Figure 4.7B shows the average expression of CD31 per MVs in apoptotic MVs and control MVs preparations. Surprisingly the expression of CD31 was two fold higher on the apoptotic MVs (8.3×10^{-9} ng/ml, SD +/- 2.2×10^{-9} corresponding to 27%) than on the control MVs (3.8×10^{-9} ng/ml, SD +/- 7.5×10^{-10} corresponding to 20%). The difference between apoptotic and control MVs was statistically significant (p=0.0029).

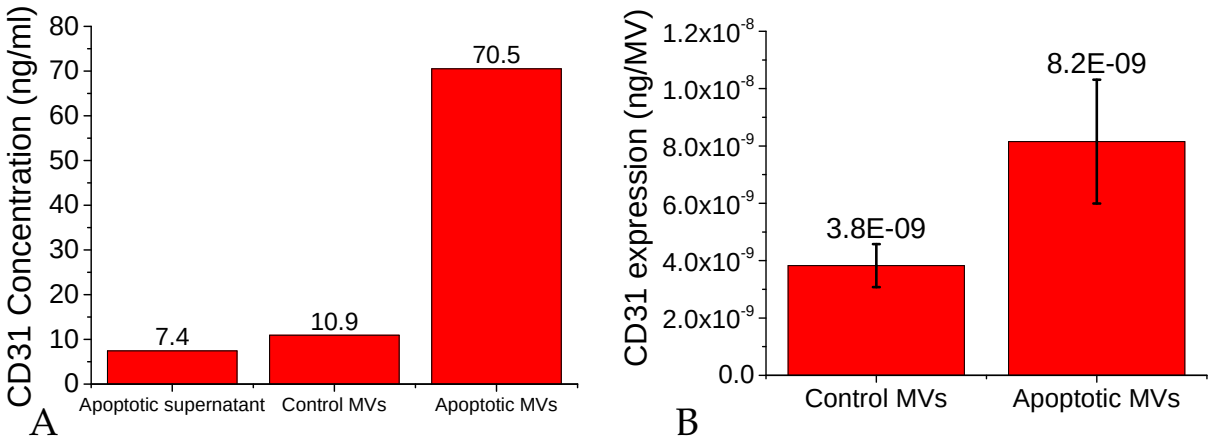

Figure 4.7: CD31 expression on the surface of the MVs derived from HUVECs measured. Figure A represents the concentration of CD31 as measured per ELISA in a representative sample: in the apoptotic supernatant before isolation of MVs and in the MVs (control and apoptotic) preparation after isolation. The CD31 concentration was approximately ten fold higher in the MVs aliquots compared to the apoptotic cell supernatant. This corresponded to the up-concentration factor of MVs during the isolation procedure. Figure B reports the expression of CD31 per MVs for five independent samples. The expression of CD31 was two fold higher on the apoptotic MVs compared to the control MVs. The error bars show the standard deviation. The difference of means was statistically significant ($p = 0.0029$).

Characterization of the surface markers of the MVs by a MV array To further characterize the surface markers present on the membrane of the MVs derived from HUVECs, antibodies were immobilized on a gold surface at discrete spots to create an MV array. After incubation of MVs isolated from apoptotic HUVECs, the functionalized gold surface was imaged by true non-contact mode AFM. Three positions were imaged in each antibody spot and the experiment was repeated with three independent MVs samples. Figure 4.8 shows the topography images of the representative regions on the substrate. Figures 4.8A and 4.8B are regions functionalized with antibodies against the endothelial markers CD31 and CD146. We found MVs captured on those regions. The MVs imaged here had a height of 40 to 60 nm, which is similar to the MVs imaged earlier without functionalization (see figure 4.5). This indicates that MVs carried on their surface CD31 as well as CD146. The region shown in figure 4.8C was functionalized with antibodies against the platelet marker CD42b. The profile of figure 4.8C shows a height of 2 to 3 nm. No MVs could be found on this marker in any of the independent experiments. This indicates that the MVs did not express CD42b as they were not captured by an anti-CD42b antibody.

4.4 Discussion

As MVs gain more and more significance in the biomedical field, adequate analysis methods are required. Great efforts are made to improve existing methods such as flow cytometry and to develop new characterization instruments with the objective of a rapid and reliable MVs

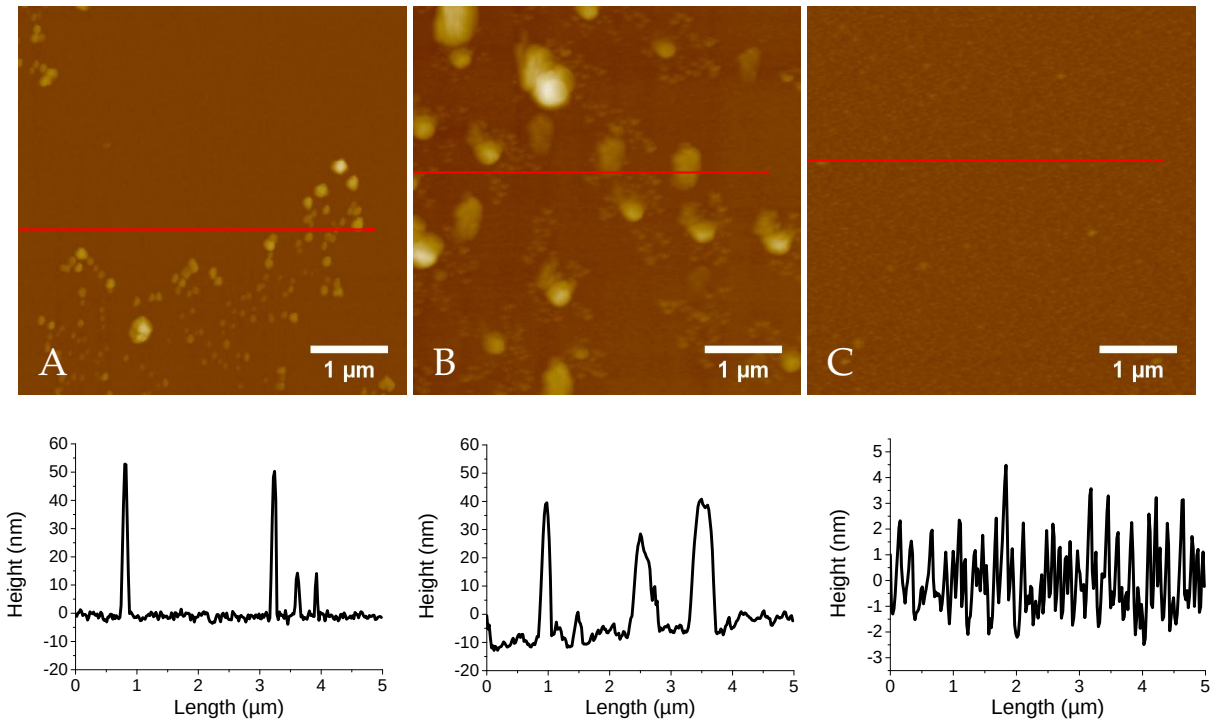

Figure 4.8: MV array. Topography AFM images of MVs derived from apoptotic HUVECs captured on a surface coated with antibodies against the endothelial markers anti-CD31 (figure A) and anti-CD146 (figure B). As negative control, a platelet marker anti-CD42b (figure C) was used and no MVs were detected on this spot. The height profile across each image is also shown. The captured MVs had a height of 40 to 60 nm. The resolution of the images was 256x256 pixel.

analysis. Our aim was to create a MVs population that could be used as a reference for the testing of new analysis methods. When investigating MVs released from a cell line, the complete system can be analysed, meaning that the precise phenotype (surface markers) of the parental cells can be determined, the release process of the MVs can be monitored and finally MVs can be isolated and characterized (size, concentration, surface markers). Therefore this is a very useful method to understand the biology behind the release of MVs.

4.4.1 Apoptosis as the mechanism to release MVs

In the present work, the release of the MVs was induced by incubating the endothelial cells (HUVECs) with 5 µM staurosporine for 24 hours. Staurosporine is known to induce apoptosis [199] and was previously used to activate jurkat cells to produce MVs [168, 169]. HUVECs were sensitive to staurosporine and went into apoptosis few hours after the start of the treatment as detected by the apoptosis assay (Figure 4.2). An homogeneous reaction was observed throughout the cell layer. In our experiments we could show by optical microscopy and AFM that the cells treated with staurosporine presented very clear morphological changes already few hours after the beginning of the treatment as previously shown by other studies [108, 173]. Perforation of the cell membrane was observed. This was similar to the results presented by Kim et al. [195]. A shrinkage of the HUVECs as well as the loss of their adherence to the cell culture substrate were later observed (see figure 4.2). These observations were in good agreement with the results presented by Kabir et al. [173], who described the effect of staurosporine on endothelial cells as a focal adhesion disassembly. Imaging cells in tapping mode AFM provided very detailed information regarding the morphology change of the cells. In our experiments, the blebbing of the cells could not be clearly imaged, even though this is characteristic for cells in apoptosis. The difficulty of observing the blebbing might be due to the preparation of the cells (fixing and drying) prior to imaging.

4.4.2 MVs in the cell growth medium

Contamination of the complete growth medium with vesicles prior to contact with the HUVECs was investigated. Our results showed that the vesicle concentration in the complete cell culture medium corresponded to less than 15% of the MVs concentration in aliquots of apoptotic MVs (figures 4.9 and 4.6B). The concentration of MVs in FBS was approximately ten times higher than in the complete growth medium (figure 4.9). As FBS is diluted ten times in the complete growth medium, we can conclude that those vesicles seemed to originate from the FBS used. The size distribution had a peak at 160 nm. The analysis was only performed by NTA. Further analysis with imaging methods should investigate the proper nature and shape of those NTA events. Removal of the contaminating vesicles prior to induction of MVs release could be achieved by overnight centrifugation at 120000 × g [200]. However the effect of this vesicle removal on the cell vitality needs to be assessed.

4.4.3 Concentration of MVs released: comparison between apoptotic and control samples

In the present study, MVs were released from HUVECs. Up to eight hours after the beginning of the incubation with staurosporine, the tendency was that the concentrations of MVs isolated from the control and the apoptotic cell culture supernatant were similar (figure 4.4). Ullal and Pisetsky reported an increase of the MVs released by jurkat cells within 20 min of treatment with staurosporine [169]. In our work, after 24 hours of treatment, a significant difference between the concentration of apoptotic and control MVs was found (figure 4.6B). Approximately three times more MVs could be isolated from the apoptotic cell supernatant than from the control cell supernatant. As measured by NTA, we obtained an average of 1625 MVs per apoptotic cell and an average of 281 MVs per control cell. In a previous study, Šimák et al. [170] measured using flow cytometry around 130 annexin V binding vesicles released per HUVECs activated with camptothecin and 20 annexin V binding vesicles from HUVECs treated with 0.5% DMSO. However, not all MVs are annexin V positive [38] and van der Pol [106] showed that flow cytometry underestimates MVs counts from 300 (standard flow cytometer) to 15 fold (dedicated flow cytometer) compared to NTA. The ratio of apoptotic MVs compared to control MVs was approximately 5.8, while Šimák et al. [170] found 6.5 in their work. Thus, the results of this study are comparable with previously reported work. The standard deviation corresponded to 23% of the mean MVs concentration for the apoptotic MVs samples and 24% for the control MV samples. This shows that our protocol can generate a population of MVs with a reproducible concentration.

4.4.4 Characterization of the size of MVs by AFM and NTA: a comparison

The size of MVs was characterized using two methods: AFM and NTA. No significant difference was found between the mean diameter of the apoptotic MVs and the mean diameter of the control MVs sized by AFM and NTA. Apoptotic MVs and control MVs could not be distinguished by their sizes. However, the difference in the mean sizes measured by AFM compared to the mean sizes measured by NTA were significantly different (figure 4.6). MVs measured by NTA were larger than MVs measured by AFM and showed a slightly broader size distribution. Both AFM and NTA measure objects that either have a certain topography (in case of the AFM) or scatter light (in the case of NTA). That is why the results have to be interpreted carefully. For instance our measurements showed that the smallest objects measured were below 30 nm. It raises the concern if those events really are vesicles and more particularly MVs. They may instead correspond for instance to protein aggregates or small protein debris. Other methods such as electron microscopy would be able to identify if those very small objects are vesicles. However, those objects accounted for less than 5% of the total population. Since we followed a protocol with a centrifugation speed (18800 $\times$ g) generally accepted to pellet MVs, we can thrust that the larger objects were MVs. To image MVs with AFM, the vesicles have to be deposited on a substrate. As previously described [138], MVs deposited on a surface are subject to a morphology change that causes the vesicles to collapse (reduce height) while spreading on the surface. This means that the height is under-representative of the diameter

while the area would overestimate the diameter of the MVs. However we can assume that the volume remained the same. Therefore sizing the MVs can be done by evaluating the volume of the measured MVs and calculating the diameter from this value [39, 138]. Apart from the size, AFM also provides structural information about the MVs. Other drawbacks of MVs study by AFM are the need of trained experimentators and the time required to image enough MVs for a representative analysis. Compared to AFM, NTA measures more vesicles per sample in a shorter time. However, NTA does not allow to verify that the scattered events tracked by the software really correspond to single MVs. Aggregates can therefore be reported as single vesicle and contribute to measurement of a larger MV population. Moreover it has been reported that NTA overestimate larger MVs [106]. This might be the reason why the sizes of the MVs measured are generally larger than with AFM (figure 4.6). However compared to AFM, the MVs measured by NTA were in liquid, i.e. in their native state. The MVs underwent no change before analysis and therefore their size distribution was less subject to artefacts due to preparation. Sizing MVs is always subjected to the advantages and drawbacks of each methods. The use of several characterization methods is therefore highly recommendable to gain a proper estimation of the size of the different MVs populations.

4.4.5 Characterization of the surface markers of the MVs

Further, we assessed if the surface markers present on the surface of the HUVECs could be detected on the surface of the MVs. As expected, CD31 and CD146 were detected on the membrane of HUVECs, while CD42b , a platelet marker was absent from the membrane of HUVECs. First, the concentration of CD31 on MVs from HUVECs was measured with an ELISA (figure 4.7). The CD31 concentration in apoptotic supernatant was approximately ten times lower than the CD31 in the apoptotic MVs aliquot after isolation by centrifugation (figure 4.7A). This factor of approximately 10 corresponds to the up-concentration factor of the MVs preparation (see 4.2.5). Since the washing steps did not contain a high concentration of CD31 (below detection limit of 4.4 mg/ml), this result suggests the CD31 measured in the non-centrifuged supernatant was only associated with the MVs pelleted during the isolation procedure and did not correspond to free CD31 in the cell culture supernatant. Moreover this result suggests that more than 95% of the MVs expressing CD31 in the supernatant could be isolated by the high-speed centrifugation protocol used.

The MV array presented in this study provided a method to determine the phenotype of MVs by imaging MVs captured on a surface functionalized with antibodies against surface markers of MVs. Thanks to the read-out by AFM, MVs can also be enumerated and sized. In the present work, MVs were captured on antibodies against CD31 and CD146 and were not captured on antibodies against CD42b, which is a platetelet marker. The height profile on the CD42b spot showed structures around 2 to 4 nm which corresponds to the height of an antibody coated surface as reported in [39]. Thus, we can conclude that the MVs released from apoptotic HUVECs expressed the endothelial markers markers CD31 and CD146 and did not express CD42b. This expression pattern was also shown on the HUVECs (figure 4.3). According to literature [42, 189], the combination of markers CD31 positive and CD42b negative confirms the endothelial origin of the MVs. Therefore we can conclude that the MVs present

in the MVs preparations had been released from the endothelial cells HUVECs. As endothelial MVs play a very central role in biological processes [42], our *in vitro* MVs population is highly interesting and relevant for medical applications. Further investigation of the phenotype of the MVs should include the expression of phosphatidylserine. This further investigation can be performed by the MV array presented here thanks to its flexibility in the surface functionalization.

4.5 Conclusions

In the present study, we showed that our method could generate MVs from HUVECs in a reproducible way. This validate the use of this MV population for the testing and optimization of novel analysis methods for MVs. AFM and NTA gave comparable results in the sizing of MVs. Combining the two methods helps to gain a correct idea of the size of the MVs. Moreover we introduced the use of an MV array to characterize simultaneously the phenotype (i.e. the surface proteins) and the size of MVs. With further development, this analysis tool will become very relevant to characterize MVs isolated from different type of body fluids.

Appendix A: Characterization of the complete growth medium for HUVECs culture

The different components of the complete growth medium of HUVECs were processed like the cell culture supernatants (centrifugation protocol described in 4.2.5) to assess if MVs or MVs like particles were present in the complete growth medium before culture with the cells. Figure 4.9A shows the concentration of MVs detected in the processed aliquots of the medium components as measured with NTA. In the complete growth medium, 1.8×10^9 MVs/ml (SD +/- 5×10^8, corresponding to 28%) were detected. The levels of MVs measured in Ham's F12K and the penicillin/streptomycin solution were below 10% of the level of MVs in the complete growth medium. However the level of MVs in the fetal bovine serum (FBS) reached 1.1×10^{10} MVs/ml (SD +/- 3.6×10^8, corresponding to 3%), that was approximately 10 times more than in the complete medium. The size distributions of the MVs from the complete growth medium and from the FBS (figure 4.9B) show both a main peak at 160 nm. Note that the buffer used (phosphate buffered saline, PBS) was filtered through a 0.1 µm syringe filter prior of use and also had a low level of MVs (1.1.^{8} MVs/ml).

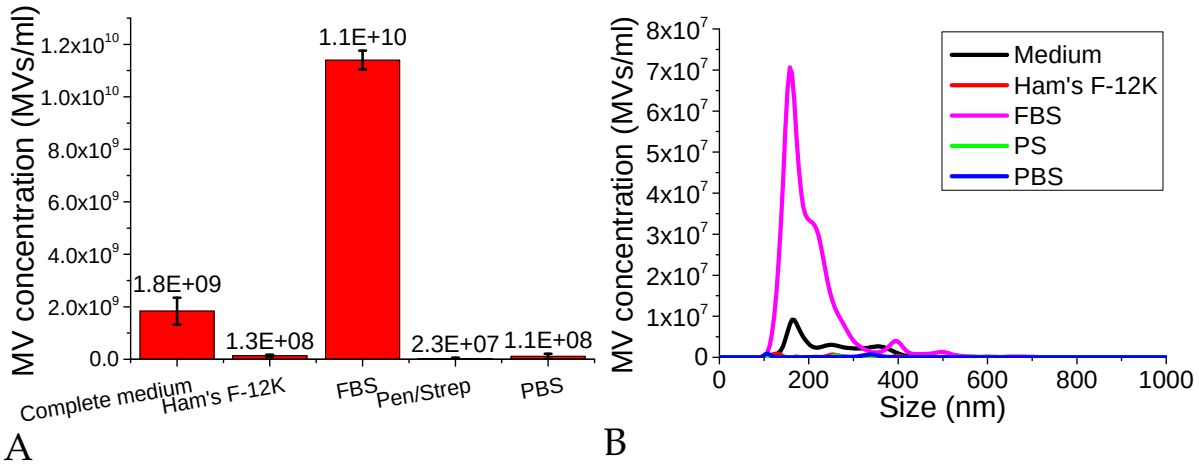

Figure 4.9: Concentration (A) and size distributions (B) of MVs isolated from the different components of the cell growth medium. The concentration and size distribution were obtained by NTA and are an average of three measurements of a representative sample. The error bars represent the standard deviation. The concentration of MVs found in the complete growth medium was approximately ten times lower than in the FBS, which corresponded to the dilution factor FBS in the complete growth medium. For the FBS and the complete growth medium, the size distributions were overlapping with both a peak around 160 nm. This suggests that the MVs from the medium were coming from the FBS. The other components did not contain a significant amount of MVs.

Appendix B: Size distributions of MVs released over time

Figure 4.10 presents the size distributions of the MVs isolated from apoptotic and control HUVECs at different times (1, 4, 8 and 24 hours) after the start of the staurosporine treatment.

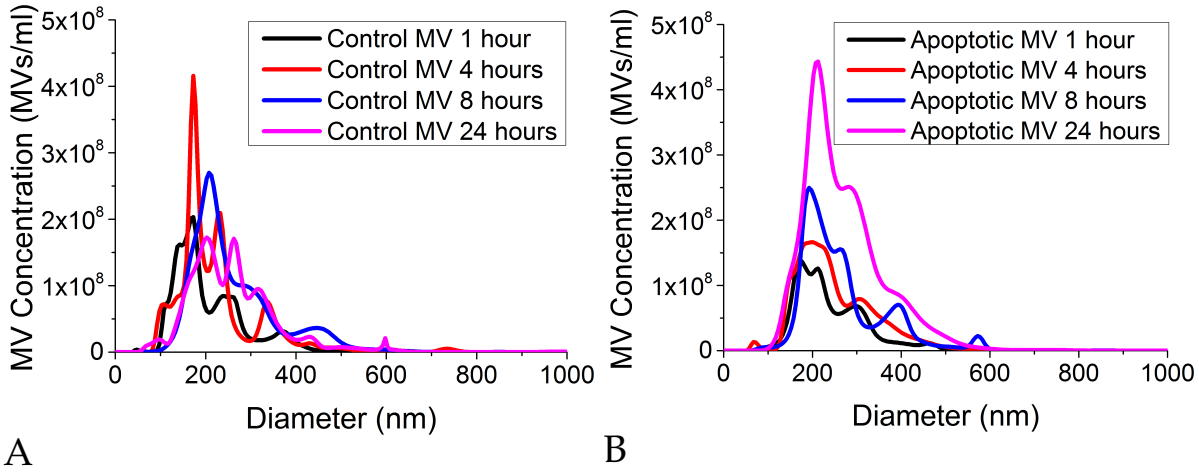

Figure 4.10: Release of MVs over the time. Size distributions of MVs isolated from control (A) and apoptotic (B) HUVECs after 1, 4, 8 and 24 hours of treatment with staurosporine. The size distribution was obtained by NTA and is an average of three measurements of a representative samples.

Conclusion

In this part of the work, HUVECs were used to generate MVs. The MVs were isolated from the cell supernatant using conventional differential centrifugation. Using MVs derived from a cell line allowed us to study the complete system around the MVs, i.e. the cells, the release process as well as the MVs.

The size of the MVs was characterized using AFM and NTA. Those two methods are highly complementary in the way the size is determined. NTA is a method analysing a large number of MVs in suspension in the buffer, while AFM images each single MVs when they are in contact with a surface. Size and structural information can be obtained from the AFM analysis. The MV size distribution obtained by NTA was generally slightly larger than the MVs size distribution obtained by AFM. Combining those two analysis methods helps to gain a proper insight into the content of the MVs suspension. Furthermore, the MV concentration was measured by NTA and apoptotic HUVEC MVs were three times more than control HUVEC MVs.

Apart from the size, the expression of two surface markers (CD31 and CD146) were also analysed. First we showed that those two markers were present on the HUVECs. Then we used an MV array, where the MVs were captured on immobilized antibodies against CD31 or CD146 and then imaged by AFM. We could capture MVs on the anti-CD31 and anti-CD146 antibodies. The specificity of the MV array was shown by an absence of MVs on anti-CD42b antibodies, which is a marker for platelet MVs. The combination of capturing MVs on specific antibodies followed by imaging with AFM allows to characterize the surface markers simultaneously with the size of MVs. This MV array could become a relevant tool to determine the phenotype of MVs simultaneously with their size and structure. The MV array is flexible as any probe can be immobilized on the surface. However, its broader use require that AFM imaging becomes faster and more automated.

MV populations derived from cell lines are an excellent tool to study the biological processes associated with MVs. Moreover after accurate characterization, such MV populations could be used to verify and optimize new analysis or preparative methods for MVs. However, procedures still remain to be standardized and need to follow precise guidelines such as the ones described in [56] to generate accurate populations of MVs.

Part III

Development of a diffusion based microfluidic device for the isolation of microvesicles

Introduction and aim

Isolation of MVs from body fluids such as blood or from cell culture supernatant is mostly performed by several steps of high-speed or ultra centrifugation or through filtration [154]. Currently there is no standard protocol for the correct isolation of MVs, even though this is crucial for the exact quantification and characterization of MVs. Different articles report that centrifugation affects particle counts or shape [154]. Dey-Hazra et al. [66] investigated different centrifugation protocols and showed significantly different MV counts depending on the speed and time of the first centrifugation step used to remove platelets. They concluded that small-size platelets might be left in the MV preparation if the first centrifugation step is not performed adequately. Some protocols perform the centrifugation steps at 4°C. Some groups claims that this might also affect the vesicle count as low temperature are able to activate platelets to release more vesicles [61].

During high speed centrifugation large forces are applied on the vesicles which could affect their structure or size. Linares et al. [68] showed the aggregation of extracellular vesicles after high speed centrifugation steps. The protein contamination of MV preparation is also of great concern. Protein aggregates can indeed be sedimented together with MVs [61]. György et al. [59] showed that immune complexes (ICs) are in a similar size range as MVs and during analysis they might be counted as MVs leading to false high MV counts. Regarding isolation by filtration, concerns have been raised that larger MVs could be fragmented resulting again in a false high MV count [61, 120, 154]. In the recent years, great efforts have been made to develop new methods that are better suited for the isolation of MVs. Recently, Böing et al. [81] introduced the use of size-exclusion chromatography columns to isolate MVs. Exosomes have also been isolated using magnetic beads. In that case, the isolation is based on the capture of the vesicles by specific antibodies immobilized on the magnetic beads [84]. Isolation would there be based upon the expression of the surface markers on the MVs instead of their size as with centrifugation or filtration. Those classical techniques require large volumes of sample which might not always be available.

Recently, more and more microfluidic-based technologies have been developed for biomedical applications [201]. Advances in the microfabrication techniques allow the creation of Lab-On-a-Chip systems where sample handling can be easily controlled and adapted to meet new biomedical challenges. Advantages of microfluidic devices comprise that only a small volume of sample is required, purification and analysis of samples can be integrated on the same platform reducing the space needed [35, 201]. This lead to a faster and more-sensitive analysis [35]. Several groups have proposed microfluidic devices for the isolation of MVs as described previously (see 2.3.3 on page 14). Compared to centrifugation, those microfluidic devices only

need few microliters of sample and are faster and easier to control.

In this work, we present the development of a simple microfluidic device for the isolation of MVs entirely through diffusion. Diffusion is a slow process that can be neglected in large systems but becomes very relevant in small channels with low Reynold numbers. The goal of the device was to remove protein aggregates and ICs slightly smaller than 50 nm from a MV sample where the larger cell debris had been previously removed. For this purpose, we used a well-known H-filter design proposed by Brody and Yager [202] in 1997. The authors were able to separate fluorescein from 0.5 µm polysterene beads. Other works have used the H-filter design to extract the cryoprotectant dimethyl sulfoxide (DMSO) from cell suspensions [203]. This design is also used extensively in micromixers to achieve a passive mixing of chemical substances [204]. Briefly the working principle is that the MV sample is introduced through one inlet of the device. Through a second inlet, an extraction buffer is introduced. The MV sample and the buffer flow next to each other in a laminar regime (no mixing of the bulk solutions) through the extraction channel. While travelling through the extraction channel, small objects such as the contaminating protein aggregates have time to diffuse from the MV sample into the extraction buffer. At the end of the extraction channel, the channel divides into two outlets. When the MV sample is collected, it is therefore depleted of a part of the contaminating proteins.

In this chapter, we introduce the governing equations describing the flows and the transport mechanisms in microfluidic channels. The working principle of the H-filter is presented in more details. As the geometrical parameters of the device are crucial for the separation performances, we performed a theoretical estimation of the required channel geometry. This theoretical estimation was confirmed by a finite element simulation. Finally the H-filter device was realised using standard microfabrication techniques. The H-filter was tested using polystyrene beads as model for the MVs and different types of proteins, as well as with MVs from HUVEC cell culture. The main advantage of this device is the gentle purification of the MVs that does not require the application of strong forces. Within 90 min, 200 µl of sample could be filtered.

Chapter 5

Theoretical work

5.1 Theoretical background

5.1.1 Fluid flow in a microfluidic channel

Microfluidics is a rapidly growing field dealing with devices in the micrometer range. Due to the small length scale, the fluid behaves differently compared to what we are used to in daily life at the macroscale and other parameters influence the fluid behaviour. For instance, the surface to volume ratio increases and mixing via diffusion becomes relevant [202, 205]. A fluid is defined as a material that will deform continuously under shear stress [206]. It is described as a continuum, meaning that the properties of the material such as density and velocity are changing continuously in the material [207]. This continuum approximation is considered as valid in microfluidics system as the characteristic length in microfluidic devices is much larger than spaces between molecules [205]. To describe the motion of fluids, we need the Newton's second law [206]:

$$m\ a = \sum_j F_j \tag{5.1}$$

This equation describes the sum of forces required to move an object of mass m with an acceleration a. In fluid dynamics, we use mass density (meaning that the mass is divided by the volume, obtaining the density ρ) and force densities [205, 208]. The Navier-Stokes equation is analogous to the Newton's second law to describe the motion of fluid [208] and reads [206]:

$$\rho(\partial_t v + v.\nabla v) = -\nabla p + \eta\nabla^2 v \tag{5.2}$$

On the left side, we find the inertial accelerations term [208], with $v.\nabla v$ the convective acceleration [208]. ∂_t is the partial time derivative [205]. On the right side of the equation, we find the terms related to the forces applied to the fluid. $-\nabla p$ describes the pressure gradient, while $\eta\nabla^2 v$ is the viscous term [209].

In general in a microfluidic channel, the liquids are considered as incompressible fluid because the density ρ is constant in space and time [206]. Therefore, we have the continuity equation for the conservation of mass [205]:

$$\nabla.v = 0 \tag{5.3}$$

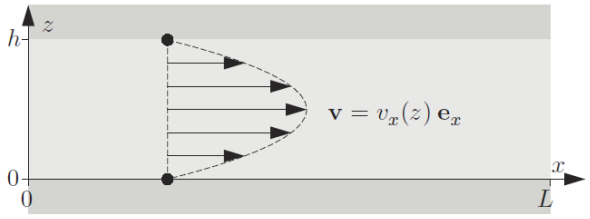

Figure 5.1: Poiseuille flow profile in an infinite flat channel. The fluid is flowing in the x-direction due to a difference of pressures between inlet and outlet. In the z-direction, the flow has a parabolic shape. Picture adapted from [206].

In microfluidic channels, the bulk solution is often moved by using a syringe pump. This is called a pressure driven flow. In a rectangular channel of infinite parallel plates and applying no slip boundary conditions (i.e. that at the wall of the channels, the fluid velocity is 0 [205].), we obtain one of the analytical solution of the Navier-Stokes equation [206]:

$$v_x = \frac{\Delta P}{2\eta L}(h - z)z \tag{5.4}$$

with h the height of the channel, L the length, η the dynamic viscosity and z the coordinate in the height direction of the channel as shown in figure 5.1. This equation describes a parabolic flow [206] as shown in figure 5.1. This pressure driven flow is also called Poiseuille flow [205].

An important dimensionless number is the Reynolds number (Re). This describe the ratio between inertial forces and viscous forces [209] and may be written as [205]:

$$\mathrm{Re} = \frac{\text{inertial forces}}{\text{viscous forces}} = \frac{\rho L_0 v_0}{\eta} \tag{5.5}$$

with L_0 the characteristic length of the system, for instance the diameter of a circular channel and v_0 the average velocity. For small Re numbers, the viscous force dominates over the inertial forces. If Re<1500, the flow is laminar, while for larger Re, the flow becomes turbulent [207] (i.e. what is happening at the macroscale). In the case of $\mathrm{Re} \ll 1$ which means that the viscous forces dominates over the inertial forces, the inertia term of the Navier-Stokes equation (equation 5.2) can be neglected [206] and the Navier-Stokes equation becomes the linear Stokes equation:

$$0 = -\nabla p + \eta \nabla^2 v \tag{5.6}$$

This flow is also called creeping flow [206]. In microfluidic devices, Re is usually smaller than 1 and therefore in the laminar regime [205]. A laminar flow means that the liquid flows in layers, without mixing. Thus, in a microfluidic channel, mixing only occurs via diffusion.

5.1.2 Transport of solute in microfluidic channels: diffusion and advection

Diffusion is the motion of the particles along a concentration gradient, from high concentration to low concentration. This is described by the Fick's law (also called diffusion equation) [205]:

$$\partial_t c = D\nabla^2 c \tag{5.7}$$

Where c is the concentration of the solute, $\nabla^2 c$ the concentration gradient in space and D is the coefficient of diffusion (in m^2/s). D is dependent on the size of the particles according to the Stokes-Einstein equation [209]:

$$D = \frac{k_B T}{6\pi\eta r} \tag{5.8}$$

with k_B the Boltzmann constant (equal to $1.38064852 \times 10^{-23}$ $m^2 kg\ s^{-2} K^{-1}$), T the absolute temperature (in Kelvin), η the dynamic viscosity (in $\frac{Ns}{m^2}$) and r the radius of the particle. This shows that the smaller the particle is, the larger the diffusion coefficient will be and therefore the faster the particle will diffuse.

The time t_{diff} for a particle to diffuse along a length l_{diff} is given by [206]:

$$t_{diff} = \frac{l_{diff}^2}{D} \tag{5.9}$$

Moreover, in a channel, solute can also be transported together with the bulk solution. That is called advection [205]. Advection is often wrongly being referred to as convection [205], which is not correct as convection describes all flows [205]. In practical situations, advection happens for example when a particle solution is transported through a channel using a syringe pump. Adding the fluid velocity as non zero, we obtain the convection-diffusion equation [205]:

$$\partial_t c + v.\nabla c = D\nabla^2 c \tag{5.10}$$

The time t_{adv} that it takes for the particles to move from the inlet to the outlet of the channel is defined as [206]:

$$t_{adv} = \frac{L}{v_0} \tag{5.11}$$

with L the length of the channel and v_0 the average flow velocity in the channel. The average flow velocity in a rectangular channel can be calculated as follows:

$$v_0 = \frac{Q}{h \times w} \tag{5.12}$$

with Q the volumetric flow rate, w the width of the channel.

5.2 Working principle of the isolation device

The device developed in this project is called a H-filter and was first introduced by Brody and Yager in 1997 [202]. The dimensions of the device have to allow a low Reynolds number ($Re \ll 1$), to assure that the flows will remain laminar through the complete channel. The device is composed of two inlet channels, a central channel and two outlet channels. A solvent (here: a buffer solution) and a solution of particles in the solvent are respectively introduced in the inlet channels, defined as buffer inlet and sample inlet. The buffer and particle solution flow through the channel via a pressure-driven flow. Those two streams meet in the central channel,

where they flow parallel to each other without mixing (laminar flow). This is defined as the extraction channel by Holl *et al.* [210]. At the end of the central channel, the streams separate equally into the two outlet channels, called waste (WS) outlet (containing the objects we want to extract from our sample) and the MV outlet. Figure 5.2 presents the geometry of the filter. In this device, the separation of ICs and smaller proteins from the MVs is achieved by diffusion that takes place in the extraction channel, where particles can diffuse from the particle stream to the buffer stream, i.e. a motion across the width of the channel, according to their size. As described in 5.1.2, particles will also move according to advection. An important point is that the device can extract maximum 50% of the ICs in one extraction round (i.e. the transport from the sample inlet to one of the outlets). The extraction by diffusion will take place indeed only if there is a concentration gradient. Once the concentration is equilibrated across the width of the channel, no more diffusion of this type of particle can take place and the concentration will correspond to half of the initial concentration in the sample inlet.

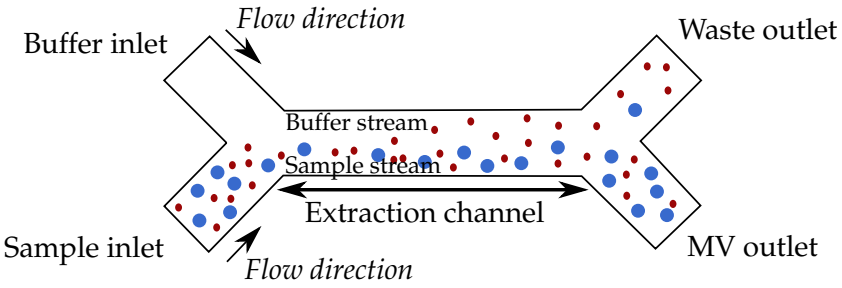

Figure 5.2: Scheme of the H-filter device The sample solution containing the MVs (large blue particles) and the contaminating proteins (small red particles) was introduced in the channel via the sample inlet. A buffer was introduced through the other inlet. In the extraction channel, small particles are extracted from the sample stream into the buffer stream. MVs are collected in the MV outlet and the solution contains less contaminating proteins.

5.3 Theoretical estimation

To gain a first idea of the performances and required geometry of the device and particularly of the extraction channel, we will try to estimate the behaviour in the fluidic device. We remind that our optimization problem aims to extract the maximum of ICs and smaller proteins possible from a sample flow containing MVs and ICs, while keeping all MVs between 50 and 1000 nm in the sample stream. According to the working principle described previously in 5.2, the situation of the maximum extraction of a particular particle (P) means that the concentrations in the outlets are equal and correspond to half of the initial concentration. It can be expressed as:

$$c_{MV_{outlet},P} = c_{WS_{outlet},P} = 0.5 c_{S_{inlet},P} \tag{5.13}$$

For this condition to be achieved, the time that the particle needs to be transported by the bulk fluid from the inlet to the outlet of the extraction channel (i.e. the advection time) had to

be equal (or longer) to the time that the particles need to diffuse from the particle stream to the buffer stream. The diffusion length is defined as half of the width of the channel, as this is the longest distance a particle can be located from the buffer stream. It would be in the case of a particle close to the wall of the channel. According to equations 5.9 and 5.11 [206]:

$$t_{diff,P} = t_{adv,P} \tag{5.14}$$

which is equivalent to:

$$\frac{(\frac{w}{2})^2}{D_P} = \frac{L}{v_0} \tag{5.15}$$

with w the width of the extraction channel, L the length of the extraction channel, D the diffusion coefficient of the particle P and v_0 the average flow velocity defined in equation 5.12. Solving for D, we obtain:

$$D_P = \frac{wQ}{4Lh} \tag{5.16}$$

This equation describes that for a channel with the defined geometrical parameters (L, h and w) and a volumetric flow rate Q, 50% of the particle P will be extracted to the buffer stream and therefore collected in the waste outlet. As the diffusion coefficient is dependent on the size of the particle according to the Stokes-Einstein equation (5.8), we can calculate the critical particle size for the filter, or cut-off size, that is the size of the particle P that will be extracted to 50% into the buffer stream as follows:

$$D_P = \frac{wQ}{4Lh} = \frac{k_B T}{6\pi\eta r_P} \tag{5.17}$$

Solving for d_P the diameter of the particle P with $r = \frac{d}{2}$, we obtained the following critical size (or cut-off size):

$$d_P = \frac{4k_B TLh}{3\pi\eta wQ} \tag{5.18}$$

5.3.1 Theoretical estimation: Design constraints

Before starting with further simulations and the experimental work, the geometry and working settings of the device have to determined.

The method of choice for the fabrication of the H-filter was micromilling on PMMA. The PMMA plates available in our lab were squares of 10x10 cm^2. For practical reasons, we defined the length of the extraction channel to a maximum of 6 cm, so that enough space was left for the side channels and fluidic connectors.

The fabrication by micromilling also presents limitations for the width and depth of the channels. The smallest milling tools available are around 50 to 100 µm in width. This means that the width cannot be smaller than 100 µm. When doing micromilling, the zero level on the surface is determined manually and therefore contains an error of approximately 10 to 20 µm. To obtain a reliable microfabrication process, the height of the channels should not be less than

200 µm. Moreover the fabrication by milling of narrow but deep channels is highly challenging. Therefore we restricted ourselves to fabricate channels with the width larger than the height (w>h).

For biomedical applications, the process time has to be reduced, so that analysis results can be provided relatively fast to the doctors and patients. Therefore, we aimed at obtaining a fast isolation of the MVs. For the calculation, we determine that we want to collect at least 200 µl in the MVs outlet within a maximum of 90 min. This correspond to a flow rate in the extraction channel of 266.7 µl/h. Moreover the syringe pumps also have a lower limit in the flow rate they can deliver. The pump used in this work could deliver 5 µl/min (corresponding to 300 µl/h or $8.3x10^{-11}$ m^3/s). This flow rate was used for the calculations.

5.3.2 Theoretical estimation: Calculations

To get a first idea of the correct dimensions of the extraction channel, a theoretical estimation was performed. According to the design constraints and equation 5.18, we calculated the cut-off sizes for different widths and heights of the extraction channel. The calculation was done for an experiment performed at room temperature (T = 293.15 K). Figure 5.3 shows the results of the calculation. There are only solutions in the above the diagonal line of equation w=h to satisfy the design constraints. We can observe on the graph that the largest particle that can extracted to 50% has a diameter of approximately 1.2 nm. This would correspond for example to a very small protein. Moreover we can see that the largest particles can be extracted if h=w, that is along the diagonal line through the graph. The wider the channel is for a given height, the smaller the particle has to be to be extracted to 50% into the buffer stream. The higher the channel is for a given width, the larger are the particles that can be extracted most efficiently. Considering the restriction due to the microfabrication and the results shown in figure 5.3, a channel of 300 µm wide and 200 µm high seems to be a possible device geometry.

This theoretical estimation has some limitations mainly due to the assumptions made for the calculation. To approach the reality better [211], a finite element simulation will be performed for this system.

5.4 Numerical modelling

For the numerical modelling we used a finite element simulation performed by the software COMSOL Multiphysics 5.0 (Comsol A/S, Denmark). The software solves partial differential equations after the considered geometry has been divided in small elements (meshing process). For this simulation, we fixed the depth of the central channel as 200 µm and the width as 300 µm. The length of the extraction channel as well as the flow rate were set to respectively 6 cm and 5 µl/min according to the design constraints described in 5.3.1. The simulation was performed in 2D for experiments performed at room temperature (293.15 K). To model the behaviour of the flow and the particles in the device, we used two types of physics: the creeping flow and the transport of diluted species. The aim of the simulation was to evaluate the separation efficiency for different relevant analytes in the H-filter of a given geometry.

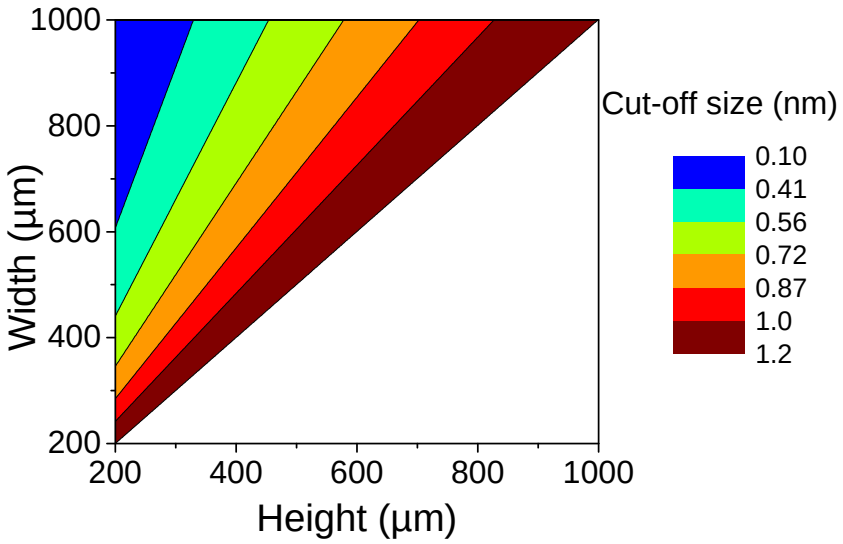

Figure 5.3: Theoretical calculations: cut-off sizes For different widths and heights of the extraction channels (length: 6 cm), the cut-off sizes of the H-filter were calculated, i.e. the sizes of the particles that would be extracted to 50% into the buffer stream. The flow rate allowed the filtering of 150 µl of MV sample in 90 min. The color scale represents the range of cut-off sizes. With those parameters, a 50% extraction can be reached with particles of a diameter of maximum 1.2 nm.

5.4.1 Fluid flow modelling: creeping flow interface

For this extraction channel, we can calculate the Reynold number (Re) according to equation 5.5. The fluid was an aqueous buffer with a density approximately equal to the one of water ($\rho = 1000\ kg/m^3$) and a viscosity also close to the one of water ($\eta = 0.001\ Ns/m^2$), the characteristic length of the system was the height of the channel (200 µm) and the average flow velocity v_0 could be calculated according to equation 5.12. We obtained:

$$Re = \frac{\rho h Q}{\eta h w} = \frac{\rho Q}{\eta w} = \frac{1000 \times 8.3 \times 10^{-11}}{0.001 \times 300x10^{-6}} = 0.42 < 1 \tag{5.19}$$

For this microfluidic device, Re < 1, however not much smaller than 1. So the inertia term will not be neglected to solve for the flow. In COMSOL Multiphysics, this type of flow is simulated by the creeping flow interface for incompressible flow, which solves for the Navier-Stokes equation (equation 5.2) and the continuity equation for the conservation of mass (equation 5.3).

We set the boundary conditions on the wall of the channel as no slip condition, which means that the fluid at the wall will have zero velocity [205]. Moreover we set two inlets where fluid is coming in with a laminar inflow and a flow rate of $\frac{Q}{2}$, so that from both side channels half of the flow rate comes in to add up to the flow rate of 5 µl/min in the extraction channel. Outlets were defined with a boundary condition of the pressure equal to 0 and backflow was suppressed. Moreover as described by Dimaki and Okkels [211], the influence of the height of the channel has to be considered in this 2D simulation. This lead to the addition of the damping force $\overrightarrow{F_{Da}}$ [211]:

$$\overrightarrow{F_{Da}} = \frac{-12\eta}{h^2}\vec{u} \tag{5.20}$$

with $\vec{u}$ the velocity field. With the addition of the body force, we use the term quasi-2D simulation because the effect of the channel height is considered.

Figure 5.4A shows the velocity magnitude in the direction of the flow in the side inlet channels and at the beginning of the extraction channel. The flow profile is parabolic in the flow direction because of the low aspect ratio ($\frac{w}{h} = 1.5$). The flow will have a parabolic shape both in the w- and in the h-direction. The maximum velocity magnitude was $9{\times}10^{-3}$ m/s in both side channels and doubled in the extraction channel to $18{\times}10^{-3}$ m/s. Moreover we investigated which distance was required for the flows coming from the side channels to reach a fully developed flow profile. In figure 5.4B, the velocity magnitudes across the channel at different distances from the intersection of the side channels with the extraction channel were represented. We can see that approximatively 100 µm from the intersection the flow profile was quasi fully developed to the level of the flow profile in the intersection channel. All along the channel no other change in the flow profile occurred until the separation of the extraction channel into the two outlet channels. At this point the flow profile splits to equal two parabolic flows, like the flows in the intet channels. This shows that the channel geometry allows for a collection of an equal volume of liquid in the outlets.

5.4.2 Separation of particles in the H-filter: Transport of diluted species

As discussed previously, transport of particles in the channel occurs through advection as well as diffusion and more particularly the separation of the different particles can happen thank to the different diffusion times of the particles (see 5.2 on page 75). The module Transport of diluted species was used to calculate the concentration of the particles in all points of the channel.

The velocity field was coupled to the creeping flow interface, meaning that the value of the velocity due to advection was coming from the solution of the flow interface. As boundary conditions, no flux was set on the walls. The channel was considered empty of the analyte before its entry. Inflow of the analyte was defined through the sample inlet at a concentration equal to 1 mol/m^3. Outflows were defined in the MV and waste outlets.

For this simulation, we identified seven samples that would be relevant for the MV isolation. First of all, we considered particles of 1 µm, 100 and 50 nm as representative for the MV population, then antibodies complexes immunoglobulin M (IgM, 750 kDa) and immunoglobulin G (IgG, 150 kDa) and the protein bovine serum albumin (BSA, 66.5 kDa) as representative for the contaminants in a MV sample isolated from plasma and small ions species such as Cl^-. The diffusion coefficients of the particles was calculated according to the Stokes-Einstein equation (see equation 5.8). The hydrodynamic radius R_H of the proteins (IgM, IgG and BSA) was estimated according to the formula developed by Erickson [212]:

$$R_H = 0.066M^{\frac{1}{3}} \tag{5.21}$$

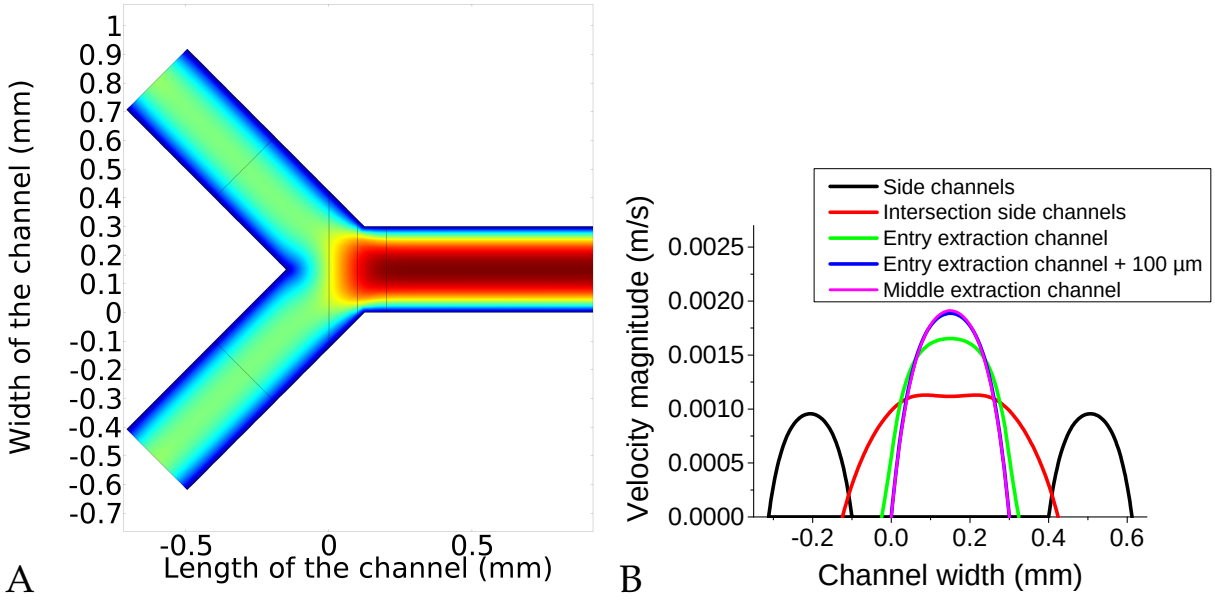

Figure 5.4: Velocity magnitude at the inlet of the extraction channel in the H-filter Figure A shows a surface plot of the velocity magnitude in the side channels and at the entry of the extraction channel. The color scale represents the velocity magnitude from 1.91×10^{-3} (red color) to 0 (blue color) in m/s. Figure B shows the velocity magnitude across the channel at the positions corresponding to the black lines on figure A. As expected by the aspect ratio ($\frac{w}{h}$ = 1.5, parabolic flow is observed in the direction of the flow. The maximum flow velocity of the side channels (approximately 0.9×10^{-3} m/s) add up into the extraction channel to the double value (approximately 1.8×10^{-3} m/s. The flow profile is quasi totally developed approximately 100 µm after entry into the extraction channel.

Table 5.1: Diffusion coefficients for seven analytes that were relevant for MV samples and therefore used in the simulation of the H-filter. We simulated three different sizes of MVs (1 µm, 100 nm and 50 nm), two types of antibody complexes (IgM and IgG), a protein (BSA), the cut-off particle for an extraction channel with 300 µm of width and 200 µm deep and a chloride ion. The diffusion coefficients of each of these analytes were calculated according to the Stokes-Einstein equation (see text for further explanations).

Sample	*unit*	**Particles** (diameter in nm)			**Antibody**		**Protein**	**Cut-off**	**Ion**
		1000	**100**	**50**	**IgM**	**IgG**	**BSA**	**0.8 nm**	**Cl^-**
Mass	*kDa*				750	150	66,5		
Radius	*nm*	500	50	25	6	3.5	2.7	0.4	
Diffusion coefficient	$\times 10^{-11}\ m^2/s$	**0.043**	**0.43**	**0.86**	**3.6**	**6.1**	**8**	**54**	**200**

with R_H the hydrodynamic radius (in nm) and M the mass of the protein in Da. From this calculated hydrodynamic radius, we calculated the coefficient of diffusion. The coefficient of diffusion of Cl^- was 2×10^{-9} m 2/s [206]. Table 5.1 presents the different diffusion coefficients for the seven analytes simulated through the channel. The numerical simulation was computed as a parametric sweep where the calculation was run separately for each analyte.

Figure 5.5 presents the concentration profiles of each analyte at the end of the extraction channel and in both outlet channels. The color legend represents the concentration where the darker blue represents 0, light green 0.5 and red 1 mol/m^3. The small ions (figure 5.5A) had enough time to diffuse the furthest and the concentration of Cl^- ions was equilibrated to half of the initial value. For particles with a diameter corresponding to the calculated cut-off size, the concentration profile was quasi homogenous at the outlets of the filter. The contaminant proteins (BSA (figure 5.5C), IgG (figure 5.5D) and IgM (figure 5.5E)) also diffused into the waste channel, however to a lesser extend than the small ions. The smaller the protein was, the higher the concentration of this protein was in the waste outlet channel. For the particles representative of the MVs (particles with diameter : 50 nm (figure 5.5F), 100 nm (figure 5.5G) and 1 µm (figure 5.5H)), nearly all particles were ending in the sample stream (red color) and their concentration in the waste channel was very low (blue color).

The concentration in the outlets relative to the initial concentration was calculated for each type of analyte and is represented in the graph (figure 5.6). The relative concentration are represented for both MV and waste outlet. For the particles representative of the MVs (particles from 1 µm to 50 nm), around 90% were estimated to elute in the MV outlet and only approximately 10% would have time to diffuse into the waste outlets. For the proteins such as immune complexes that we would like to extract gently from the sample, each extraction round through the H-filter is estimated to remove around 25% of those analytes from the MV stream. For particles with a diameter corresponding to the calculated cut-off size (0.8 nm) for this extraction channel (300 µm wide and 200 µm deep), 49% of the total concentration was found in the waste outlet. For the small chloride ions, the extraction reached the maximum possible in this kind of device and that is an extraction of 50% from the sample stream, thank to the small size and

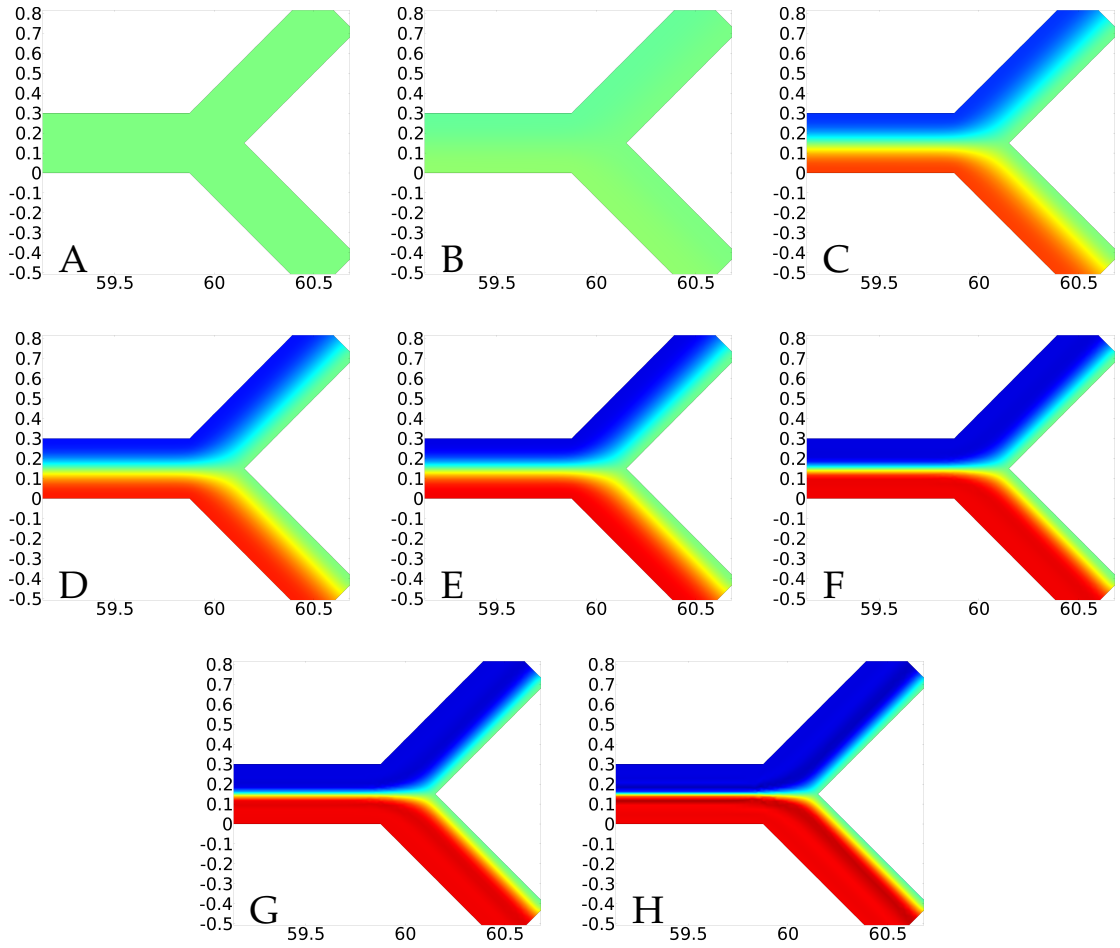

Figure 5.5: Concentration profiles of different analytes at the outlets of the H-filter The diffusion and advection behaviour of seven relevant analytes in the H-filter was analysed by a numerical simulation. The figure shows the concentration at the end of the extraction channel and in the outlet channels. The color legend shows the concentration of the analyte, where dark blue shows 0, light green 0.5 and red 1 mol/m^3. The smallest sample (Cl^-, figure A) was completely diffused at the outlets as the concentration was equal all over the channel. A particle of diameter 0.8 nm (cut-off sizes determined by the theoretical estimations, figure B) had been extracted to 49% into the buffer stream. The proteins (BSA (figure C), IgG (figure D) and IgM (figure E)) diffused in the waste channel to a lesser extend. The smaller the protein was, the more it had been extracted from the sample stream. The particles (50 nm (figure F), 100 nm (figure G) and 1 µm (figure H)) stayed nearly all in the sample stream and did not diffuse into the buffer stream.

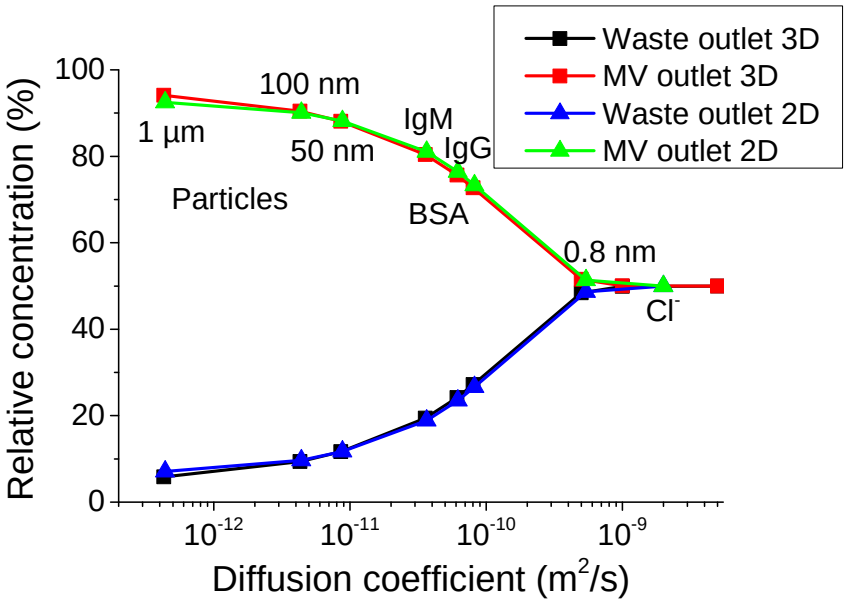

Figure 5.6: Estimation of the relative concentration of seven analytes at the outlets of the H-filter for a quasi-2D and a 3D simulation. According to the quasi-2D numerical simulation, the concentrations of each analyte relative to the initial concentration at the sample inlet was calculated. For the large particles (1 µm, 100 nm and 50 nm), approximately 90% were collected in the sample outlet. In every extraction round, up to 25% of the IgG (particles with a diameter of 7 nm) are extracted. With particles of 1.2 nm in diameter, 45% of extraction was calculated. The maximum extraction (i.e. 50% extraction) can be reached with small ions. The results of the 3D simulation fit very well with the quasi-2D simulation, indicating that the quasi-2D simulation is a relatively good approximation.

therefore the high diffusion coefficient of this analyte.

In parallel to the quasi-2D simulation, a 3D simulation was run to confirm the validity of the quasi-2D simulation. In figure 5.6, the relative concentrations according to the 3D simulation are presented compared to the results of the quasi-2D simulation. Both simulations gave similar results. The larger difference between the quasi-2D and the 3D simulation was obtained for the larger particle (1 µm in diameter) where the 3D simulation estimated that the concentration in the MV outlet would be 1.5% higher than estimated by the 2D simulation. This shows that the quasi-2D simulation with the addition of the body force was a valid approximation.

5.5 Discussion

The aims of the numerical simulation were to evaluate the potential of the H-filter for the isolation of MVs from complex samples and to determine the geometry of the device that would lead to the best possible extraction. The working principle of the H-filter is that particles diffuse across the channel from the sample stream to the buffer stream. At the end of the extraction channel, the sample stream has been depleted from the particles that diffused into the buffer stream. The extraction is dependent on the diffusion coefficient of the particles, i.e. on their sizes and on the time that the particles remains in the channel. It means that the separation

performances are highly dependent the geometry of the channel. Therefore it was important to determine the correct channel size considering certain fabrication constraints. At first a theoretical calculation was performed. We defined the cut off size as the size of the particles that would be extracted to 50% into the buffer stream. We could see that for a given depth, the larger cut-off was reached with channels with the smallest width. For a given width, the cut off became larger when the depth increased. This was due to the fact that the flow velocity decreases with an increasing depth (see equation 5.12). Therefore the particles would have more time to travel through the channel and therefore more time to diffuse into the buffer stream. For the further work, we chose to use an extraction channel with a width of 300 µm and a depth of 200 µm. Those dimensions were indeed possible to realise through micromilling as milling tools of 300 µm in width are available. For this channel dimensions, the cut-off size was 0.8 nm.

The precision of the results from the theoretical calculations is limited by the approximations used . For example, we use the average flow velocity through the device, neglecting the real parabolic flow profile (see figure 5.1). Moreover, the calculations do not take into account any effect of the height of the channel on the flow profile. This means that some particles will not be transported through the channel at the average flow velocity but at a slower flow velocity and will have therefore more time to diffuse. Secondly, we calculated the diffusion time for particles close to the wall of the channel and that have to travel by diffusion across the longest distance possible in the channel. However in the reality, not all particles will be located this position when entering the channel. Some will be much closer from the border of the two streams and therefore will diffuse faster to the buffer stream.

The finite element simulation (see 5.4) took velocity field into account to calculate the concentrations of the analyte at the outlets and was therefore closer to the reality. For the cut-off size, the simulation calculated that the concentration would be approximately 51% of the initial concentration in the MV outlet. This shows that the theoretical calculation and the finite element simulation were in good agreement despite the assumptions and limitations.

With this device, we obtained that particles in the size range of MVs (1 µm to 50 nm) would diffuse to approximately 10% in the waste outlet. This shows that some MVs would be lost during the separation process but in the same proportion throughout the size range of MVs. Therefore it would not affect further analysis of e.g. the size distribution. The concentration of contaminating proteins in the size range of antibodies complexes or BSA would be reduced of approximately 25% after flowing through the H-filter. The sample could be reintroduced into the H-filter to further reduce the concentration of contaminating proteins.

According to equation 5.18, a better extraction of the contaminating proteins in the MV samples can be achieved if either the depth or length of the channel were longer, or the width smaller. To respect the fabrication constraint, the width could be decreased three times to 100 µm even though this is already quite challenging to realise by micromilling. But in that case, the depth of the channel would also be reduced two times to 100 µm to have a channel whose depth is not larger than the width as this is preferable for micromilling. The length could be increased by creating for example a serpentine or zigzag channel. Hossain *et al.* [204, 213] investigated the effect of different channel geometries on the mixing at low Reynolds number

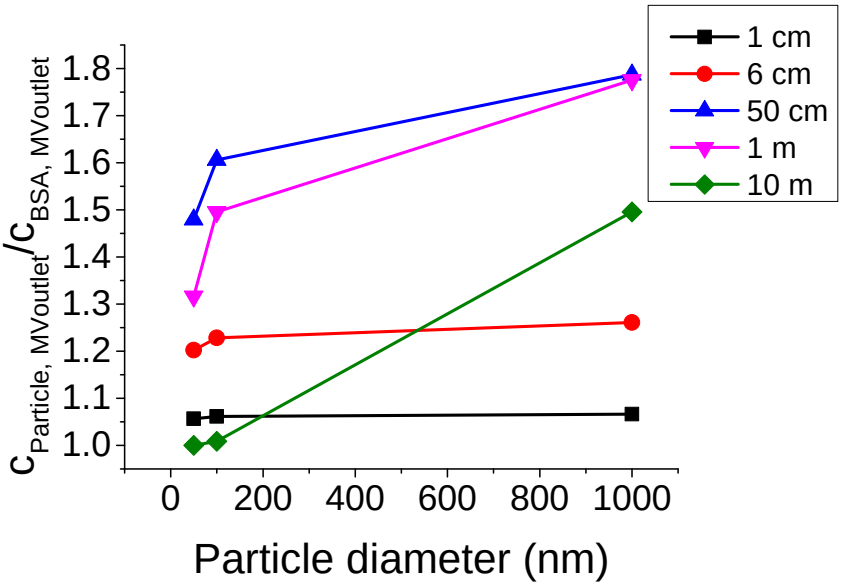

Figure 5.7: MV separation in channels of different lengths. The ratio of the particle concentration to the BSA concentration was calculated for channels of different lengths, using the results of the quasi-2D simulation. A straight line indicates that particles of the three sizes are collected with the same efficiency in the MV outlet. Very long channels would lead to a non-uniform collection of particles within the MV size range.

and found that only an increase of the residence time in the channel would improve the performances of the device because it gives more time to the species to diffuse across the channel. However, in the case of the separation of the protein complexes from the MVs, a longer channel would also give more time to the MVs to diffuse into the buffer stream and therefore be lost for further analysis. Figure 5.7 presents the ratio of concentration of the particles (50, 100 nm and 1 µm, corresponding to the MV size range) to the BSA concentration in the MV outlet in channels of different lengths. These ratios were calculated with the results from the quasi-2D simulation. For shorts channels (1 and 6 cm), the ratio was similar for the particles with a diameter of 50, 100 nm and 1 µm (quasi straight line). For the 6 cm long channel the ratio was higher than for the 1 cm channel. However, for longer channels, the ratio increased with the size of the particles. This shows that MVs would then not be collected homogeneously across the size range (more small MVs would be lost to the waste outlet compared to the large MVs). For very long channels (10 m), the smaller vesicles (50 and 100 nm) reached a concentration of 50% in both outlets and were therefore extracted to the same extend as the proteins. This would result in a strong modification of the MV size distribution and an exclusion of some MV subpopulation in the MV outlet. For a good separation, the MV to BSA ratio has to be as high as possible, while being constant for all MVs. The 6 cm long channel satisfied this condition. However, an optimization study could be performed to find the best length of the extraction channel to satisfy this criteria. Moreover a longer channel would result in a longer fabrication time for the technique envisaged for the microfabrication.

The implementation of active techniques based for example on dielectric, magnetic or acoustic forces [214] could be another possibility to improve the isolation of MVs in a microfluidic

channel. However this would increase the complexity of the system.

Chapter 6

Experimental work

The next step in the development of the microfluidic device for isolation of MVs was to realise the microfluidic device using microfabrication techniques and then test the device with different analytes separately. The real performances were compared with the expected separation from the numerical simulation previously presented. In the following part, we present the microfabrication techniques used to realise the device and the results of the different tests. In this work, we used the fluidic connector system created by Andrea Pfreundt [215] from the NaBIS group at DTU Nanotech.

6.1 Material and methods

6.1.1 Fabrication of the device

Design and material choice

For the microfluidic device we chose to use the polymer material Poly(methyl methacrylate) (PMMA). PMMA is a low-cost polymer that is easy to micromachine and has good optical properties (transparent) that will allow us to perform microscopy through the device. The device was essentially composed of three parts: the bottom part with the channel, the top part sealing the channel and the fluidic connectors. Figure 6.1A presents the general scheme of the device. The different parts were designed using AutoCAD 2015 (Autodesk, Inc, USA). The length of the extraction channel was 6 cm, the width and depth of the extraction channel and the side inlet and outlet channels were 300 µm and 200 µm respectively.

Micromachining of the polymer parts

The micromachining of the polymer parts was made using computer numerical control (CNC) micromilling as this technique is well suited for prototyping. The working principle of milling is that a tool removes material on the surface of a plate. Milling can be used for a wide range of material, both polymers and metals. Only few steps are required between design and the fabricated object, so that the final product can be rapidly tested [216]. Micromilling has a limitation in the size of the features that can be achieved which correspond to the size of the micromachining tools available. The smallest feature that can be accurately achieved by experienced users is around 50 µm [217]. The quality of the tools is of high importance for the result of the features[218]. For instance, a tool with a large erosion at the edges will create a feature smaller

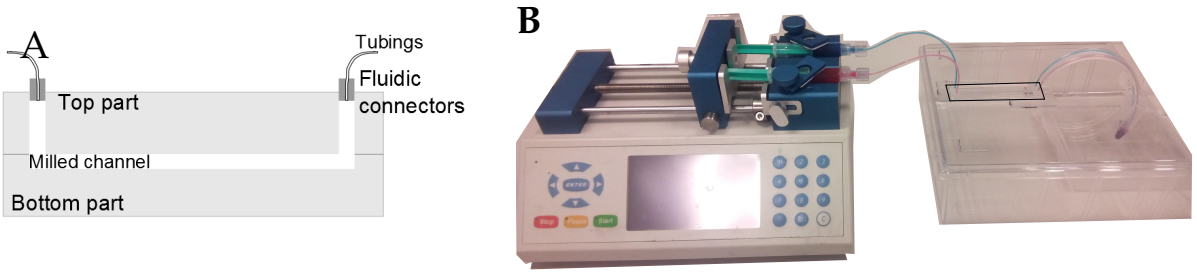

Figure 6.1: Experimental setup of the H-filter Figure A shows the scheme of the H-filter in cross-section. The H-filter was made of PMMA and composed of three parts: the bottom part with the channel, the top part with the fluidic connections and the fluidic connectors to connect tubings into the device. Figure B shows the complete experimental setup for the H-filter experiments with the syringe pump on the left, the H-filter in the middle and the outlet containers on the right.

than its nominal size. Other parameters that play an important role for the correct milling are the spindle speed (how fast the tool is rotated), the tool feed (how fast the tool is moved on the surface) and the depth of each milling steps (how much material is removed at each passage of the tool).

In this work the autoCAD drawings were converted into a G-code (i.e. a list of operations with trajectories and velocities to be read by the computer for communication with the micromilling machine) using the software EZ-CAM (Version 15, EZ-CAM solutions Inc, USA). The PMMA plate (10x10 cm^2, 2 mm thickness) was fixed onto the stage with a double-sided tape. Micromilling was performed on a Mini-Mill/3 (Minitech Machinery Corporation, USA). As coolant , soap water was used throughout the micromilling operation.

For the **bottom part**, we performed the following milling operations:

1. Face milling (to flatten the surface, tool: 3 mm endmill)
2. Milling of the channel (200 µm deep and 300 µm wide, tool: 300 µm endmill)
3. Milling of the alignment holes (diameter: 2.6 mm, tool: 2 mm endmill)
4. Cutting of the edges of the piece (tool: 2 mm endmill)

For the **top part**, we performed the following milling operations:

1. Milling of the fluidic connectors: socket parts according to [215]
2. Milling of the alignment holes (diameter: 2.6 mm, tool: 2 mm endmill)
3. Cutting of the edges of the piece (tool: 2 mm endmill)

The milling operations for the fludic connectors (part: plug) were performed according to the procedure described by Pfreundt et al. [215].

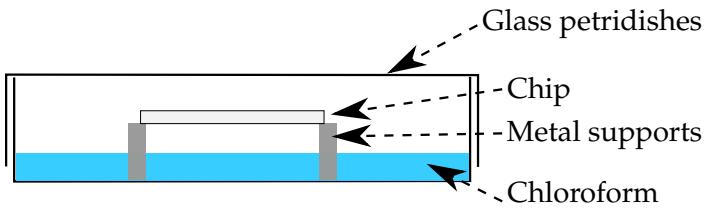

Figure 6.2: Experimental setup for the surface smoothing by chloroform vapours. The bottom part of chip was placed facing downwards above chloroform for 1 minute to reduce the surface roughness caused by the face milling operation.

Surface smoothing by chloroform vapours

The first milling operation of the bottom plate was a face milling operation where a thin layer of material was removed on all the surface of the PMMA plate in order to obtain a fully flat surface. However this operation increased the roughness of the surface so that the thermobonding of the bottom and top part of the H-filter was not possible anymore. Therefore a surface smoothing operation was introduced to reduced the roughness. The surface smoothing by solvent vapour was introduced by Ogilivie *et al.* [217, 219, 220]. As shown on the experimental setup (figure 6.2), the patterned piece of PMMA was placed above vapours of chloroform for one minute. It was then immediately thermobonded with a top part.

Assembly of the microfluidic chip

The assembly of the bottom and top parts of the H-filter was done by thermobonding. A top and a bottom part were placed under a UV-light (Dymax 5000-EC Series UV curing flood lamp, Dymax Corporation, USA) for one minute to activate the surface. The alignment spheres were placed in the alignment locations of the bottom part and a top part was aligned on top of it. The H-filter was placed in the pre-warmed (bottom and top hotplate of the bonding press heated to 85°C) bonding press (PW 10 H, P/O/WEBER, Germany). The bonding press was closed and a pressure of 11 kN was applied for 15 min. The H-filter was allowed to cool down in the press until 50°C before releasing the pressure.

6.1.2 Confocal imaging of the channel

After micromilling the bottom part with the channel were imaged in a confocal microscope to verify that the dimensions corresponded to the expectations. We used a confocal microscope (LSM 700, Zeiss, Germany) in reflection mode (laser: 405 nm, objective 20X). Z-stacks were recorded along the depth of the channel.

6.1.3 Experimental setup

The fluidic tubing (inner diameter: 0.8 mm, outer diameter: 1.6 mm, Bola, Germany) was connected to the two intlets and outlets of the H-filter through the fluidic connectors. All tubing had the same length. The inlet tubings were connected to 3 ml syringes via fluidic connectors

(Promepla, Monaco). The syringes were fixed on a syringe pump (Chemyx Fusion200, KR analytical, United Kingdom). Figure 6.1B on page 90 shows the experimental setup. The flow rate was set to be 2.5 µl/min at each syringe, so reaching a flow rate of 5 µl/min in the extraction channel.

6.1.4 Testing of the device: particles separation

The particle separation in the device was tested using six different analytes: fluorescently labeled polysterene beads (diameters: 1 µm, 100 nm and 50 nm, Fluoresbrite yellow green, Polysciences, Germany), anti-rabbit immunogloublin G (IgG) fluorescein isothiocyanate (FITC) conjugated (Sigma Aldrich, Germany), bovine serum albumine (BSA, Sigma Aldrich, Germany) and sodium chloride (NaCl, Sigma Aldrich, Germany). Each analyte was tested separately. The buffer syringe was filled with milliQ for NaCl as analyte and with phosphate buffered saline (PBS) for all other analytes. The sample syringe was filled with a solution of the analyte diluted in PBS (or milliQ water for the NaCl). The separation was performed in the channel and the liquids collected in the outlet containers. The concentrations of the analytes in the MV and waste outlets were measured using different methods. At least two independent separation runs were performed with every analyte. The outlet concentrations relative to the total collected concentration were calculated as follow:

$$\Delta c_{MVs} = \frac{c_{MV_{outlet}}}{c_{MV_{outlet}} + c_{WS_{outlet}}} \tag{6.1}$$

and

$$\Delta c_{WS} = \frac{c_{WS_{outlet}}}{c_{MV_{outlet}} + c_{WS_{outlet}}} \tag{6.2}$$

Measurement of the concentration of the fluorescently labelled beads and the FITC conjugated IgG antibody

The fluorescence intensity of the samples was measured in triplicate. We filled the well of a black well plate (flat bottom) and measured the fluorescence intensity using a plate reader (Victor 3, Perkin Elmer, USA). The fluorescence intensity was correlated to the respective concentration using a calibration curve (see Appendix A.3).

Measurement of the BSA concentration

The absorbance at 280 nm was measured with a spectrophotometer (Nanodrop 2000 with pedestal option, ThermoFisher, USA). Each solution was measured three times. The concentration of BSA in the solutions was obtained from the calibration in the Nanodrop software.

Measurement of the NaCl concentration

The conductivity of the solutions was measured with a self-made conductimeter (chamber size: $8 \times 5 \times 5$ mm, figure A.4A on page 161). A calibration curve was obtained to relate the conductivity to the concentration of the NaCl solutions (see Appendix A.4 on page 159).

6.1.5 Testing of the device: purification of MVs from HUVECs cell culture supernatant

Control MVs were produced from HUVECs according to the protocol described in the section 4.2.5 on page 48. The cell culture supernatant was collected and centrifuged at $1250 \times g$ for five minutes to remove the larger cell debris. One ml of cell culture supernatant was further processed with high speed centrifugation according to the MVs purification protocol described in the section 4.2.5 on page 48. The rest of the cell culture supernatant was diluted ten times in PBS previously filtered through a 0.1 µm filter and prepared in a syringe connected to the sample inlet of the H-filter device. Filtered PBS was prepared in the second syringe. 200 µl of sample were passed through the device with a flow rate of 2.5 µl/min at each syringe (so a total flow rate in the extraction channel of 5 µl/min). The outlet samples were collected and the MV concentration was measured with the NTA according to the measurement protocol described in the section 4.2.7 on page 49. The protein concentration was measured in the different solutions using a spectrophotometer as described in 6.1.4 on page 92. Two independent separation experiments were performed.

6.2 Results

6.2.1 Characterization of the size of the device

The microfluidic H-filter was fabricated using standard microfabrication techniques. Micromilling was used to create the channel in PMMA plates and thermo bonding was used to seal the channel and provide fluidic connections. Figure 6.1 provides an overview of the device. As discussed in the previous chapter (see chapter 5), the size of the extraction channel is determining the separation performances. We aimed to fabricate a H-filter with an extraction channel with a length of 6 cm, a width of 300 µm and a depth of 200 µm. The side channels had the same width and depth as the extraction channel. Figure 6.3A presents the 3D reconstruction of a stack of images recorded with a confocal microscope in reflection mode along the depth of the channel. The images were recorded at the intersection between the inlet side channels and the extraction channel. On the 3D reconstruction, we can see the top of the plate and the bottom of the channel. The lines visible on the surfaces were marks from the milling tool. It is also visible on the top of the plate because of the face milling operation used to flatten the plate. The roughness created by those structures was reduced by the solvent smoothing step. The side walls of the channel are not visible probably because the reflection from those was very little which indicates that the walls were straight as expected. The width of the extraction channel was approximately 316 µm, and the side channels had a width around 320 µm, that

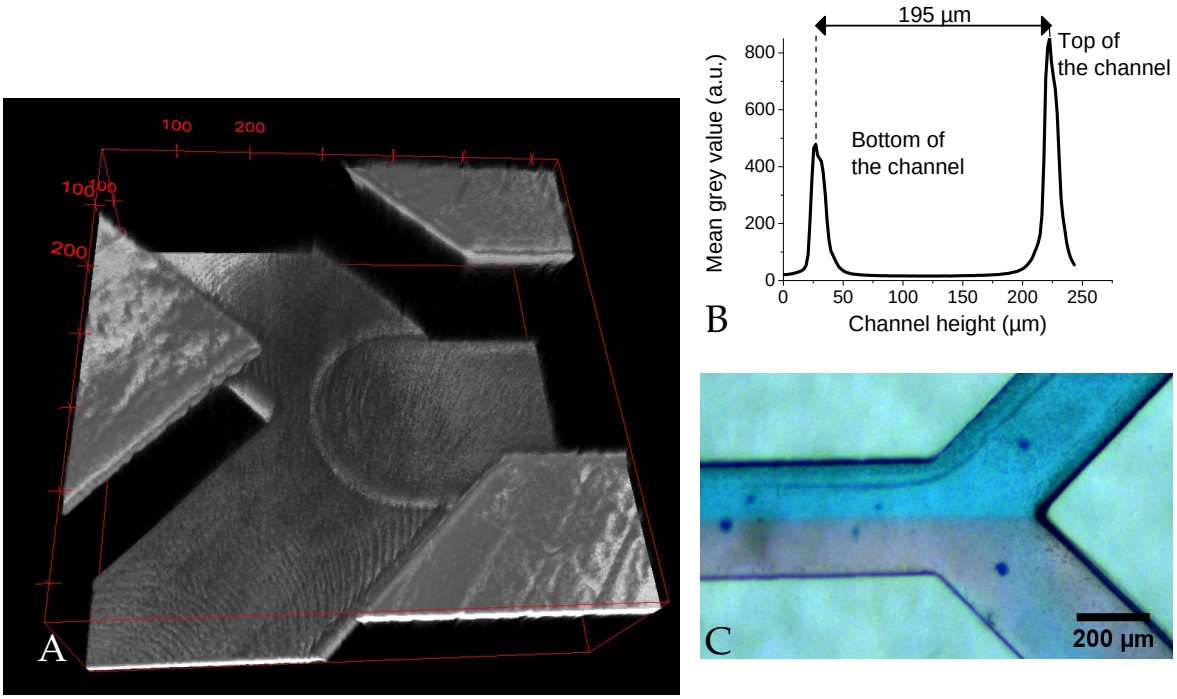

Figure 6.3: 3D reconstruction of the milled channel of the H-filter and laminar flow in the H-filter. Figure A presents the intersection of the inlet channels with the extraction channel. The image is a 3D reconstruction of a stack of images recorded along the depth of the channel. It was obtained with a confocal microscope in reflection mode after milling and smoothing of the surface. No reflection can be seen from the side walls showing that they were quite straight. The mean grey value was calculated for each image of the stack and represented in figure B. The two peaks represent the surfaces where a high reflection signal could be recorded. This allowed us to accurately determine the depth of the milled channel that was around 195 µm, i.e. 5 µm lower than the expected depth. Figure C shows the intersection of the extraction channel with the outlet channels when food dye solutions diluted in milliQ water were flowing through the channel. No mixing between the two solutions was seen which indicates that the flows were laminar in the channel. The image was captured with a stereomicroscope.

is 16 to 20 µm larger than expected. The mean grey value of each picture was evaluated and represented over the height of the channel (figure 6.3B). Two main peaks were visible, indicating two levels where structures were present. They corresponded to the bottom and the top of the plate. Determining the distance between the peaks allowed to verify the depth of the channel. For this device, the depth was 195 µm. The depth was measured at the end of the outlet channel as well and was 165 µm for this device.

Figure 6.3C show a microscopy picture of the H-filter at the outlet of the extraction channel. Two solutions of food dye diluted in water were introduced at the inlets with a flow rate of 500 µl/min. At the outlet of the extraction channel, the food dyes did not mix showing the flows were laminar in the device even at a flow rate 100 times higher than the flow rate that was used for the particle separation.

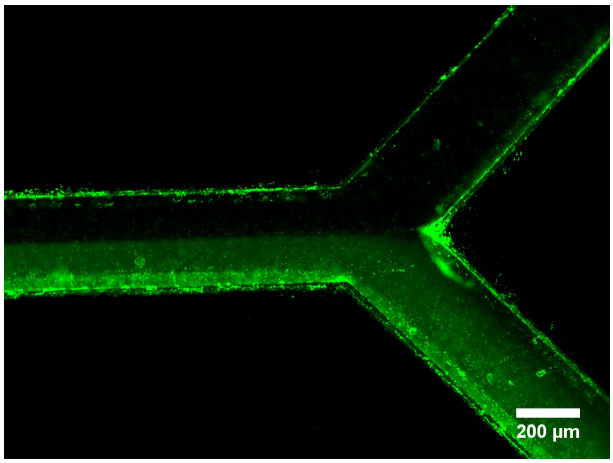

Figure 6.4: H-filter channel with 1 µm fluorescently labelled beads flowing through the channel The flow rate was 2.5 µl/min and the picture was recorded at the end of the extraction channel using a fluorescence microscope. The bulk fluorescence of the particle solution could be seen only in the sample stream. Hardly no fluorescence could be recorded in the waste channel (top channel on the right).

6.2.2 Particle separation

To test the separation performances of the fabricated device, six different analytes were introduced into the sample inlet and run through the channel at a flow rate of 2.5 µl/min. The analytes were representative for components found in a real sample To simulate MVs we used fluorescencently labeled beads of 1 µm, 100 nm and 50 nm of diameter. As protein contamination we used FITC conjugated IgG and BSA. As very small analyte, we used NaCl dissolved in water. Each analyte was tested separately and at least two independent experiments were run for each analyte. Figure 6.4 shows a fluorescence picture of the intersection of the extraction channel with the outlet channels during the experiment with the beads with a diameter of 1 µm. We were only able to image the bulk fluorescence of the beads solution instead of single particles. It can be seen that particles were only present in the sample stream. At the division of the extraction channel, the 1 µm particles are nearly all flowing to the MV outlet. A thin band of fluorescence is visible along the wall of the waste channel which might indicate that some particles are also going to the waste outlet. The fluorescence signal on the walls of the channel might be due to some reflection of the channel walls or to some particles trapped on the wall during filling of the channel.

For each experiment, 200 µl of solution was collected in the outlets and the concentrations of the analyte were measured. The relative concentrations at the outlets were calculated and plotted against the corresponding diffusion coefficients in figure 6.5. The values of each experiment were represented individually by a color. The values at the MV outlet were represented by a square and the values at the waste outlet with a disk. On the graph, we represented also the simulation results from figure 5.6 for those analytes (black symbol and dashed line). The particles with a diameter of 1 µm to 50 nm (representative for MVs) were all collected to approximately 90 to 80% in the MV outlet, which corresponded relatively well to the simulation results. The relative concentrations were comparable for all sizes of the beads representative

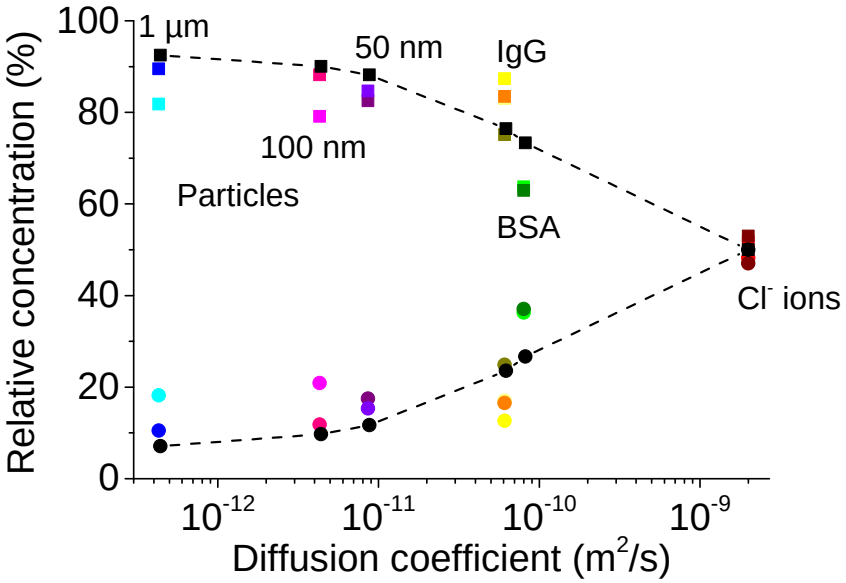

Figure 6.5: Relative concentration at the outlets of the H-filter The concentrations of six different analytes were measured at the MV (square symbols) and waste outlets (round symbols) after flowing through the device. The relative concentrations were calculated as the ratio between the MV (or waste) outlet concentration and total collected concentration. Each analyte was run separately through the H-filter and at least two independent experiments were run for each analyte. Each color represents the values of the MV and waste outlet for one given experiment. The black symbols represent the values of the relative concentrations in the MV and waste outlet from the numerical simulation. Generally the experimental results are in good agreement with the simulation. The particles between 1 µm and 50 nm were collected to 90% in the MV outlet, while approximately 36% of BSA was extracted from the sample stream.

for MVs. IgG were collected at a concentration between 75 and 87% in the MVs outlet, while the simulation predicted 76%. BSA diffused in our experimental results to 36% into the waste outlet, which was approximately 10% more than the results from the simulation. The small chloride ions were extracted to 48% into the waste outlet, which corresponded to the theoretical results.

6.2.3 Purification of MVs from HUVECs cell culture supernatant

Cell culture supernatant from non-treated HUVECs was collected and centrifuged for 5 min at 1250g. After being diluted ten times in PBS, it was injected into the sample inlet of the H-filter device. After flowing through the device, the samples in the MV and waste outlet were collected and characterized by NTA. An aliquot was purified using high speed centrifugation as comparison to the newly developed purification method. Figure 6.6 presents the results of this experiment. The size distributions of the MVs collected in the MV outlets were overlapping with the size distribution of the MVs introduced in the inlet of the device (see figure 6.6A). The mean sizes were around 210 nm and a main peak was between 130 and 230 nm. The size distribution of the MVs purified with the protocol with high speed centrifugation also showed

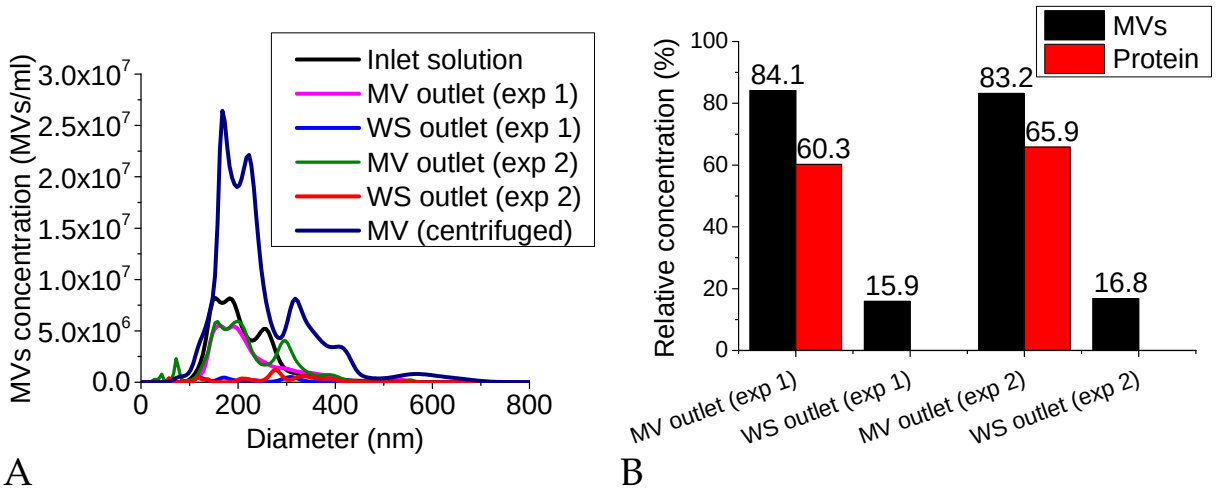

Figure 6.6: Purification of MVs with the H-filter Figure A presents the size distributions of samples collected in the MV and waste (WS) outlets as well as the size distribution of the inlet solution and of a sample purified by centrifugation. The size distributions of the MVs collected in the MV outlets overlap the size distribution of the MV solution injected in the inlet and had all a mean size around 210 nm. The MVs which were purified by centrifugation also had a main peak around 200 nm but presented an extra peak above 300 nm. Figure B shows the concentrations of MVs in the outlets relative to the total collected concentrations. In both experiments, around 84% of the MVs were collected in the MV outlet and 16% in the WS outlet. Figure B also shows the protein concentration in the MV outlet relative to the protein concentration in the inlet solution. Around 60% of the initial protein concentration was measured in the MV outlet. exp 1 stands for the experiment number 1 and exp 2 stands for the experiment number 2.

a peak around 200 nm but also a peak of vesicles with a diameter between 300 and 400 nm. The total MV concentration in the initial solution was 2.19×10^9 MVs/ml. The total concentration of MVs in the centrifuged aliquots (i.e. ten times up-concentrated compared to initial solution) was 6.54×10^9 MVs/ml, while the total concentrations in the MV outlets were respectively 1.61×10^8 MVs/ml and 1.1×10^8 MVs/ml, when the initial solution was diluted ten times before introduction into the channel. The percentages of MVs collected in the MV outlet were around 84% of the total collected MVs (figure 6.6B) and 16% in the waste outlets for both experiments. The protein concentration in the outlets solution was evaluated by measuring the absorbance at 280 nm. In the waste outlets the protein concentration was below 0.03 mg/ml which is below the limit for a reasonable detection as recommended by the manufacturer [221, 222]. Therefore those values could not be considered and the percentage of the protein concentration was calculated relative to the inlet solution. Approximately 60% of the initial protein concentration were found in the MV outlet in both experiments.

6.3 Discussion

The fabrication of the H-filter was realised in polymer by standard microfabrication methods: micromilling and thermobonding. Micromilling is well adapted for low cost and rapid prototyping [223]. However the use of micromilling imposed certain constraints on the geometry of the channel. The width of the channels was limited by the availability of small milling tools. Moreover the reproducibility of such small channels is subjected to variations due to the definition of the zero level of the milling tools on the plate. In our devices, we could observe some deviations of the expected channel dimensions. Variation in the depth of the channel was due to the fixation of the PMMA plate by a double sided tape onto the milling machine table. The use of the face milling operation helped to improve the flatness of the fixed PMMA plate. For further work requiring many devices with exactly the same dimensions, other microfabrication techniques involving a mold and its replication to obtain reproducible devices should be envisaged. All in all the fabrication of the H-filter is relatively easy as it only requires one channel with two inlets and outlets. This is faster and less expensive to realise than devices requiring the integration of electrodes such as the acoustic purification device developed by Lee et al. [92]. Moreover, the H-filter is less prone to clogging than devices with structures in the channel such as the deterministic displacement device from Laki et al. [89, 90] or the microfluidic filter of Davies et al. [94].

The flow in the device was shown to be laminar as expected from the flow simulation, so that the extraction of particles from the sample flow could only occur via diffusion. The volume of sample required to run the experiments (at least 500 µl) was here determined by the syringes and other fluidic connectors with a large dead volume to fill to assure the same fluidic resistance all over the system. Further development of the device will assure that even smaller sample volume can be used.

The separation efficiency was evaluated by calculating the concentration at the outlets relative to the total collected concentration at both outlets. The experimental separation results were generally in good agreement with the finite element simulation (see figure 6.5). The polystyrene beads representative for the MVs were all collected to approximately 90% in the MV outlet. There was no difference in the separation efficiency for the particles within the size range of the MVs. The experiments with IgG gave a variation of about 10% among the triplicates. Apart from one experiment, the relative IgG concentrations in the MV outlet were approximately 10% higher than expected from the simulation. BSA diffused more than expected in the device. A reason could be some denaturation of the protein when preparing or storing the solution that might result in particles with a smaller size than expected and therewith a faster diffusion.

Preliminary experiments were performed with MVs from non-treated HUVECs. In the two experiments about 84% of the MVs were collected in the MV outlet. This corresponded to the concentration values obtained with the beads with a similar size. The vesicles in the outlets showed the same size distribution than the MVs from the inlet solution, which proves that the size distribution of the MVs did not change while flowing through the channel. This confirms that the collection of the MVs in the H-filter had the same efficiency for all MVs within the

complete MV size range. Our system did not isolate mostly the large vesicles over the small ones but all particles with the same efficiency. In the two experiments, the MV recovery was 52 and 77% respectively (concentration in MV outlet relative to the initial MV concentration). After centrifugation, the recovery was only 30% (The centrifugation process up-concentrated ten fold the MV sample, which was taken into account for this calculation). This suggests that the purification through the H-filter is a method that enables a collection of a greater amount of MVs. We measured that only 60% of the initial protein concentration was found in the MV outlet. This suggests that 40% was extracted from the sample. However we used an unspecific protein characterization method which was not sensitive enough to quantify the protein in the waste outlet. Moreover, this analysis did not differentiate between the proteins associated with MVs and the free proteins such as ICs that we expect to extract from the sample. Further analysis is required to properly evaluate the reduction of contamination in the samples. Within 90 min, we were able to filter 200 µl of sample which is more than enough sample to perform further analysis on the MVs such as size characterization by AFM or TEM or surface marker characterization by ELISA or flow cytometry. If a greater reduction of the free protein and immune complexes reduction was required, the sample could be reloaded to run through a second round of extraction. This MV isolation device, however, depends upon the removal of cell debris or small cell components such as platelets prior of loading the solution into the filter.

Within those experiments, we were able to show that the device worked as we expected from the theoretical calculations. The separation was reproducible. Further development of the device could include the integration of the sample loading on the device to reduce the risk of contamination with potentially infectious patient samples. The sample collection on chip would also allow to reduce tubing and additional equipment after the outlet of the device. This would assure a greater stability of the device and better reproducibility of the performances.

Conclusion

In this part, we presented the development of a novel and low cost microfluidic device for the isolation of MVs. The working principle is based on the extraction of the small objects such as ICs or free proteins from the MVs samples by diffusion. This device called H-filter presents the advantage of isolating the MVs according to their size and not according to the expression of a marker on their surface. Therefore a collection of the complete population is expected to be achieved without exclusion based on biological function of the MVs. This method does not make use of strong forces on the MVs which presents the advantage that MVs will not aggregate or be disrupted during the isolation process. In our work we determined the geometry of the device for a suitable MV isolation using a finite element simulation. The results were confirmed by experimental testing of the device using defined samples such as polystyrene beads and BSA solution. Preliminary testing with MVs from cell culture showed that the isolation of MVs was possible while reducing the concentration of protein and ICs. Moreover the H-filter offered a better recovery than standard purification by high speed centrifugation. Further experiments will explore the possibility of a separation using several cycles through the H-filter. This device is easy to use and further technological improvement will enable the use of very small sample volumes.

Part IV

Detection of microvesicles on a magnetoresistive sensor platform: a proof of concept study

Introduction and aim

Aim of the work

In the recent years, great efforts have been made to develop novel analysis methods for exosomes and MVs. In chapter 2, section 2.4 on page 17 as well as in recently published reviews [64, 101] some of the conventional and novel MVs characterization methods are presented. Appropriate analysis methods are characterized by their ability of selectively detecting MVs, i.e. ensuring that the objects detected are MVs and not other contamination such as protein aggregates. To enable the application of MVs as biomarkers, the MV characterization methods have to also fulfil further criteria such as short analysis time and convenience of the performance in clinical settings.

Many MV analysis methods are based on the recognition of surface markers on the MVs. Probes (e.g. antibodies) against the corresponding surface markers are used either combined with a fluorophore (e.g. for detection in flow cytometry) or immobilized on a surface to capture the MVs (e.g. in ELISA assay). Characterizing the MVs through their surface markers can be used to determine their cell of origin as well as state of the cell at the moment of the release as long as the expression of the surface protein is specific for this particular condition. Some of the novel analysis methods require two different probes to complete the detection assay in a so-called sandwich detection strategy. This is for example the case of the exoscreen assay [51] where the exosomes were captured between two different beads functionalized with antibodies against the relevant surface proteins of the targeted exosomes. In a similar way, a paper-based ELISA captured exosomes between anti-CD63 and anti-CD9 antibodies [96]. Using two different probes helps to increase the selectivity of the detection and reduce the risk of detecting protein aggregates or cellular debris as MVs.

In this work, we addressed the demand for MV detection methods that are rapid, specific, reliable and easy to use in clinical settings. For this purpose, we proposed the use of a magnetoresistive (MR) sensor platform for the rapid detection of MVs based on their surface markers. This MR sensor platform works by detecting magnetic particles that are bound to the target, in our case the MVs. This study was designed as a proof of concept and aimed to show that this biosensor is able to discriminate between MVs derived from HUVECs and MVs coming from the epithelial cells from the cell line Michigan cancer foundation-7 (MCF7) at a physiological concentration. The detection was build up as a sandwich assay with two specific probes for the MVs from HUVECs. Two specific probes were chosen. The first one was annein V which binds to the phospholipid phosphatidylserine in the presence of calcium. The second one was an anti-CD31 antibody, as CD31 (also called Platelet endothelial cell adhesion molecule-1 (PECAM-1)) is a marker present on endothelial cells such as HUVECs as we showed in figure 4.3 on page 54. The working principle of the platform is further described in the next section.

The study is composed of three parts. First, the release of MVs from MCF7 cells was briefly investigated and the MVs from HUVECs and MCF7 cells were compared. Second, the detection strategy and some parameters of the assay were optimized using preliminary tests on gold substrates. Third, a proof of concept study was run on the MR sensor platform.

Description and working principle of the MR biosensor

Biosensors have gained great interest in the biomedical field since they have been introduced approximately 30 years ago [224, 225]. The working principle of a biosensor is that an analyte is recognized by a bioelement (antibody, aptamer, enzyme, etc.) and the recognition event generates a signal (such as fluorescence, colorimetric or electrical) that is detected by a transducer. In the case of the biosensor used in this study, the sensor was a magnetoresistive sensor. It detects the presence of magnetic particles due to a change in resistance of the magnetoresistive sensor [226, 227]. The magnetic particles bind to the target which again binds to the surface of the sensor (sandwich type assay). Recently, this type of biosensor became popular for biomedical applications because of the high sensitivity that they offer.

The MR biosensor used in this work was part of a portable platform that has been developed by Freitas and co-workers [228, 229]. It combines an array of spin-valve sensors, a microfluidic system to deliver the sample and an electronic read-out system to process the signal. A detailed description of the MR sensor platform was provided by Germano et al. [228]. Spin-valve sensors are a type of MR sensor composed of several layers of ferromagnetic material which are separated by a non-magnetic metal layer [229]. They are often used in sensing applications because of their high sensitivity [229]. The microfluidic system allows a controlled delivery of the liquids on the platform with a constant flow rate. Freitas et al. [229] showed that the detection made using the microfluidic system resulted in an increase of the signal compared to the same experiment but using the open-chamber. Using the microfluidic system to introduce the sample and washing buffer can also increase the reproducibility of the measurements and of the washing steps [230]. The electronic setup allows a rapid signal processing [228].

Several applications have already proven the versatility of this MR platform, especially regarding the types of analyte that can be detected. DNA hybridization studies [231, 232] were performed where a detection limit as low as 15 fM could be achieved [232]. Moreover, this platform was also used to detect larger analytes such as salmonella cells [192]. Combined with very specific bioelements, the MR platform was able to discriminate between different viability states of the salmonella cells. Salmonella typhimurium were also successfully detected on the platform [193]. The detection of analyte on this platform is quantitative, rapid (40 minutes) and highly sensitive.

Figure 6.7 shows an image of the platform as well as the detection strategy based on the sandwich assay developed by us. The main steps required to achieve the detection of the MVs are presented on 8.1A (page 118): 1) the functionalization of the magnetic nanoparticles (MNPs) with a MV specific probe, 2) the immobilization of a specific probe over half of the sensors (specific sensors) and of an unspecific probe (here BSA) over the other half of the sensors (control

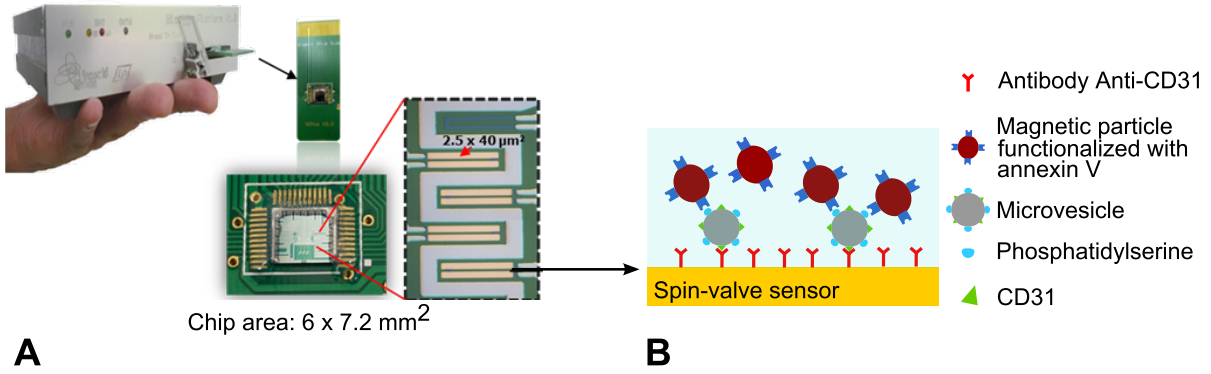

Figure 6.7: The magnetoresistive (MR) biochip (A) and the detection strategy (B) Figure A shows the portable platform and the biochip used in this study. The chip is organized in six groups of five sensors. The image was adapted from [233]. Figure B presents the sandwich assay where antibodies against CD31 were immobilized on the surface of the platform. MVs were incubated with magnetic nanoparticles (MNPs) functionalized with annexin V and introduced over the surface of the sensor. MV-MNP complexes were then captured by the anti-CD31 antibodies.

sensors), 3) the incubation of the functionalized MNPs with the MVs and 4) the introduction on the chip of the MV-MNP complexes. Once on the platform, the MV-MNP complexes are measured on the platform as follows: At the beginning (see figure 6.8A), a baseline signal is recorded in the absence of MNPs. After introduction of the magnetically labelled targets (in this study the MV-MNP complexes), the sensors detect the presence of magnetic particles and the signal decreases equally over the specific and control sensors as the sample is homogeneously distributed over all the sensors (see figure 6.8B). After 30 min of incubation where the MVs bind to their specific probe on the surface of the sensors, the unbound MNPs and unbound MV-MNP complexes are washed away and the remaining signal corresponds to the binding signal (see figure 6.8C). Ideally no MV-MNP complexes bind on the control sensors where the signal returns to the baseline level.

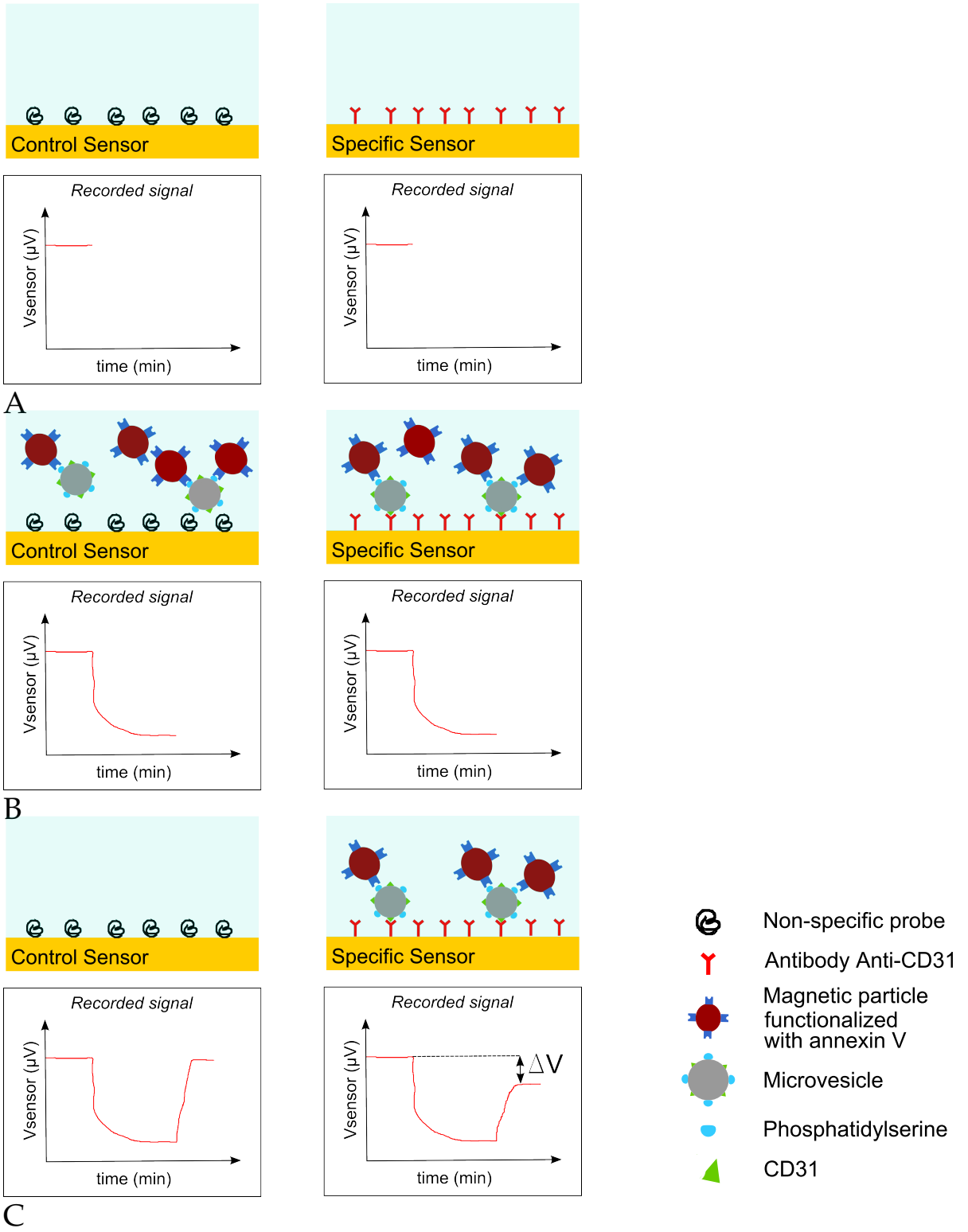

Figure 6.8: Detection steps on the MR platform. (A) Before the complexes are introduced, the recorded signal is equal over specific and control sensors (baseline level). (B) When MV-MNP complexes are introduced, the voltage decreases as the sensors detects magnetic particles. (C) After incubation, the surface of the sensors is washed and only the specifically bound MV-MNP complexes remain on the surface. The signal increases back to the baseline level on the non-specific sensor, while the difference between the baseline level and the signal after washing is the binding signal over the specific sensors.

Chapter 7

Comparison of microvesicles from HUVECs and MCF7 cells

For this work, two different populations of MVs were prepared: endothelial MVs released from HUVECs and epithelial MVs released from the cell line MCF7. The present chapter presents a brief study of the release of MCF7 MVs and the comparison of the size distribution profiles and concentrations between the HUVECs MVs and the MCF7 MVs. The HUVECs and their released MVs were prepared as described in chapter 4 on page 45.

7.1 Material and methods

7.1.1 Materials

All chemicals were purchased from Sigma Aldrich (Germany), except if otherwise stated.

7.1.2 MCF7 cell culture and passaging

The epithelial cell line MCF7 (Michigan cancer foundation 7, ATCC, Sweden) was cultivated in the ground medium DMEM (Dulbecco's modified Eagle's medium) supplemented with 10% FBS (Biowest, Denmark) and 1% Penicillin/streptomycin (Stock concentration: 10000 Units penicillin/10 mg streptomycin per ml). $1{\times}10^5$ cells/ml were seeded and cultivated in a T75 cell culture flask. MCF7 cells were passaged when approximately 70% confluency was reached. The cell monolayer was rinsed twice with PBS. 2 ml of trypsin/ethylenediaminetetraacetic acid (EDTA) was added to the cell medium and the cell flask was incubated for 5 min in a humidified incubator at 37°C with 5% CO_2. After optical control of the cell detachment, 5 ml complete medium was added to inhibit the trypsin. The cells were counted in a cell counting chamber and seeded in a new cell culture flask.

7.1.3 Induction of apoptosis in MCF7 cells

$1{\times}10^4$ cells/cm^2 were seeded in a T75 cell flask. After five days of incubation, the medium was changed with medium supplemented with 5 µM staurosporine. The change in morphology of the MCF7 cells was observed over 24 hours with a optical microscope (phase contrast, objective: 10X, Axiovert25, Zeiss, Germany)

7.1.4 Immunostaining of MCF7 cells

$4{\times}10^4$ cells were seeded in the wells of a 24-well plate. The immunostaining protocol was then performed according to the procedure described in 4.2.4 on page 48.

7.1.5 Generation, collection and characterization of microvesicles from MCF7 cells

The production and collection of MVs derived from MCF7 cells was performed as described for the MVs derived from HUVECs in the article "Generation and characterization of cell-derived microvesicles from HUVECs" (see section 4.2.5 on page 48). $7.5{\times}10^5$ MCF7 cells (density $1{\times}10^4$ cells/cm^2) were used for each experiment. Two flasks were prepared: one for the release of apoptotic MVs and one for the release of control MVs.

After purification, the MVs in the aliquots were analysed by NTA according to the procedure described in article "Generation and characterization of cell-derived microvesicles from HUVECs" (see section 4.2.7 on page 49).

7.2 Characterization of MCF7 cells: Results and discussion

7.2.1 Induction of the release of microvesicles from MCF7 cells

The release of MVs from MCF7 cells was activated in the same way as for the HUVECs. The apoptosis was induced with the introduction of 5 µM staurosporine in the cell culture medium over 24 hours. Figure 7.1 presents micrographs of the MCF7 cells treated with 5 µM staurosporine (apoptotic MCF7 cells, figures 7.1A to 7.1C) and micrographs of the non-treated cells (control MCF7 cells, figures 7.1D to 7.1F). MCF7 cells were growing in dense islands on the bottom of the flasks. Over the 22 hours of observation, it can be seen that the monolayer of MCF7 cells became denser when the cells were cultivated in culture medium (figure 7.1F). After fours hours of treatment with staurosporine (figure 7.1B), we observed that the cells were severely damaged as they had shrunk and many of them appeared to have been released from the surface. After 22 hours, the cell monolayer was further damaged and had a lot of cell debris (figure 7.1C). Compared to the apoptotic HUVECs (see figure 4.2 on page 53), many more debris were still left on the surface. The morphological changes of HUVECs and MCF7 cells during staurosporine treatment were slightly different. This suggests that the MCF7 cells reacted in a different way to staurosporine than HUVECs.

7.2.2 Immunostaining of MCF7 cells

Similar to the immunostaining presented for the HUVECs (see 4.3.2 on page 52), we verified the expression of CD31 and CD42b on the surface of the MCF7 cells. Figure 7.2 shows the results of the immunostaining. Three samples were prepared. In the first sample, we added primary antibodies against CD31, in the second sample primary antibodies against CD42b and in the third sample no primary antibody was given to the cells. The secondary antibodies were conjugated to FITC (green signal). The imaging parameters were kept the same as for the immnuostaining of the HUVECs presented in figure 4.3 on page 54. No green signal was

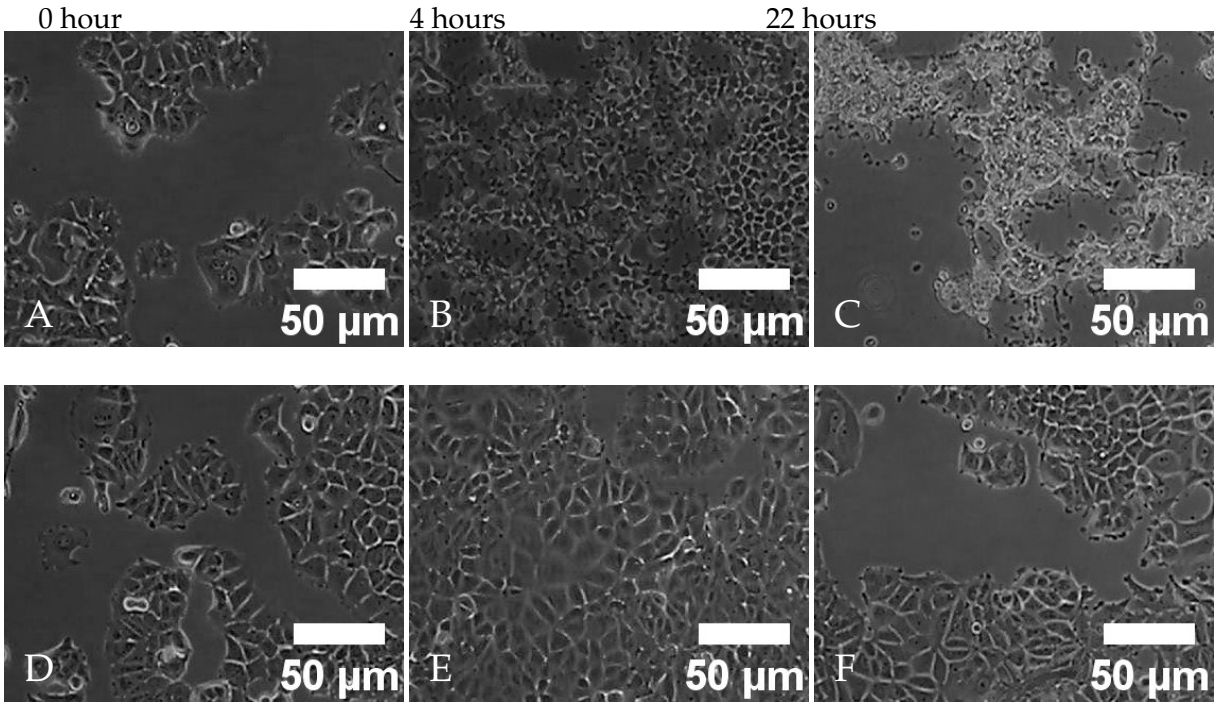

Figure 7.1: MCF7 cells undergoing apoptosis induced by staurosporine. The micrographs were captured 4 and 22 hours after the beginning of the treatment with staurosporine (figures A-C). Under staurosporine treatment, the cells detached from the surface and cell debris could be found in the medium. Figures D-F show control cells, which became slightly denser 22 hours after the start of the observation. The pictures were captured with an optical microscope with phase contrast.

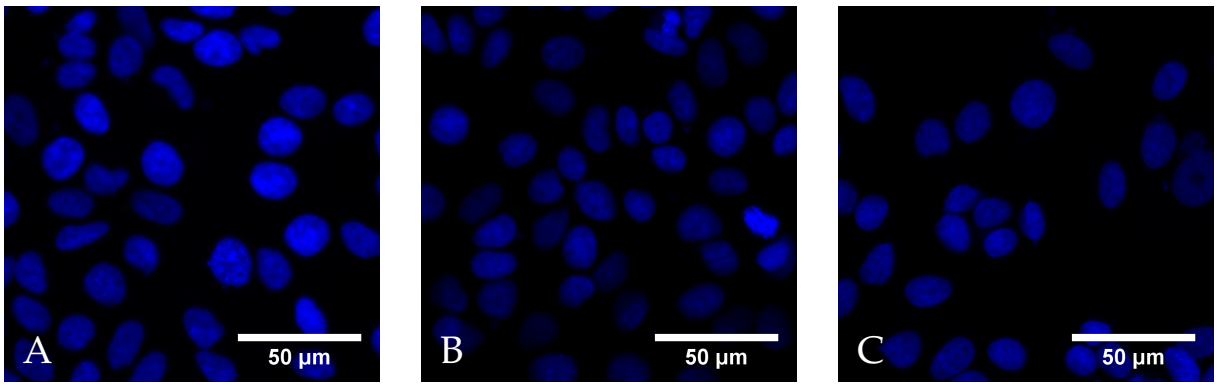

Figure 7.2: Immunostaining on MCF7 cells. The epithelial cells MCF7 were double stained for the endothelial marker CD31 (figure A) or a plaletet marker CD42b (figure B) and DNA (blue signal). Figure C is a negative control where no primary antibody was added. No green signal from the secondary antibody could be detected indicating that none of the two markers were expressed on the MCF7 cells, in contrast to the immunostaining of the HUVECs were CD31 was expressed (see figure 4.3 on page 54). The images were obtained with a confocal microscope.

detected from the secondary antibody for any of the three samples. This signifies that neither CD31 nor CD42b were expressed on the MCF7 cells. As MVs are formed from the membrane of the cell of origin, we expected that MVs would also be negative for those two markers, i.e. MVs from MCF7 cells would not express CD31 or CD42b on their surfaces.

7.3 Comparison of MVs from HUVEC and MCF7 cells: Results and discussion

The size distribution and concentration of the MVs were characterized using NTA. Figure 7.3A presents the size distribution of a representative MVs sample from HUVECs and a representative MVs sample from MCF7 cells. MVs showed a wide size distribution with a range between 100 and 700 nm and the mean size of 286 nm (+/- 14 nm) for the MCF7 MVs and 298 nm (+/- 7 nm) for the HUVEC MVs. Due to their similar size distribution, HUVEC MVs and MCF7 MVs could not be differentiated by their sizes.

Figure 7.3B presents the MVs concentration in two representative samples. The concentration of HUVEC MVs in the MVs preparation was 1.5×10^{10} MVs/ml, while the concentration of MCF7 MVs was around five times lower (2.9×10^{9} MVs/ml). This result suggests that the release procedure of MVs was less efficient for MCF7 cells.

7.4 Conclusion

For this proof of concept study, we needed a second population of MVs that would lack the expression of at least one of the two markers. An epithelial cell line (MCF7) was selected and the immunostaining assay performed on those cells showed that CD31 was not expressed on the surface of these cells. Therefore, they constituted a good source for the second population

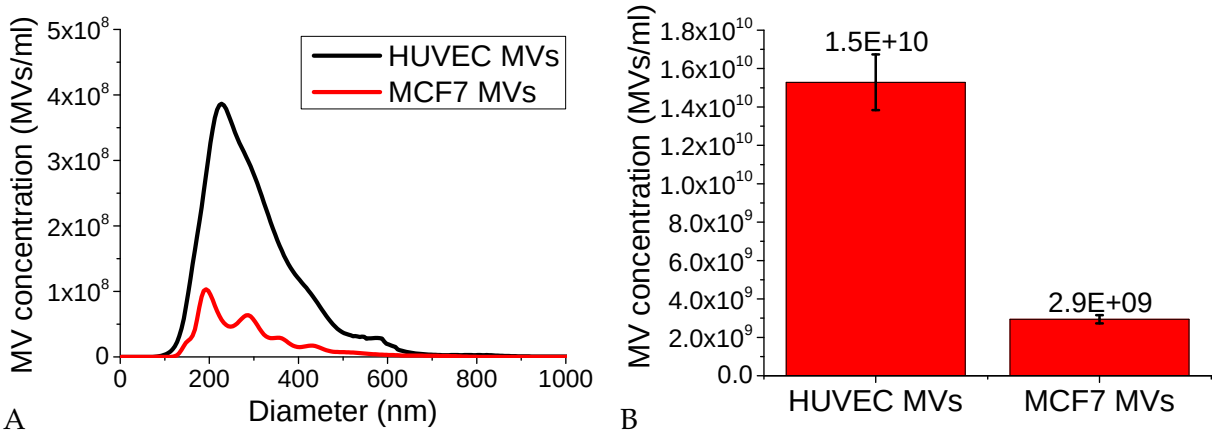

Figure 7.3: Size distribution (figure A) and concentration (figure B) of the MVs from HUVECs and MCF7 cells. HUVEC MVs and MCF7 MVs were overlapping in size with a mean size of 297 and 285 nm respectively. HUVEC MVs were higher concentrated than MCF7 MVs by a factor of 5. The graphs represent an average of three NTA measurements of a representative sample with the error bars representing the standard deviation.

of MVs. We showed that the MCF7 cells were also sensitive to the induction of the MV release with 5 µM staurosporine. Moreover, the size distribution profiles of the two MV populations were overlapping showing that a discrimination of the MVs by their size would not be possible. For the following work of this study, all MVs used were derived from apoptotic cells.

Chapter 8

Optimization of the detection strategy

The success of sandwich assays is dependent on many parameters such as the buffers or the incubation temperatures. The right combination of all these parameters has to be found to assure the specific detection of the analyte. In this chapter, we present preliminary tests that were performed to optimize the detection strategy. Three preliminary tests were performed: test of the pre- and post-capture strategy (test 1), test using different buffers (test 2) and test of the magnetic labelling of the MVs at different temperatures (test 3). The reproducibility of the optimized strategy was validated. Moreover, we investigated the effect of the buffers on the morphology of the MVs. For all those experiments, MVs isolated from the cell supernatant of apoptotic HUVECs were used.

8.1 Material and methods

8.1.1 Materials

All chemicals were purchased from Sigma Aldrich (Germany), except if otherwise stated.

8.1.2 Buffers

In this study, the following buffers were used:

Set 1: PB based buffers

- PB (0.205 mM $NaH_2PO_4 \cdot 2H_2O$, 1.24 mM Na_2HPO_4 in milliQ water, pH 7.4)
- PB-Ca (2.5 mM $CaCl_2$ in PB)
- PB-Tween (0.05% Tween®-20 in PB)
- PB-Ca-Tween (0.05% Tween®-20 in PB-Ca)
- 1% BSA in PB (0.1 g BSA in 10 ml PB)
- 5% BSA in PB (0.5 g BSA in 10 ml PB)
- 0.1% SH-PEG (1 mg/ml SH-PEG in PB)

Set 2: HEPES based buffers

- HEPES (10 mM HEPES (4-(2-hydroxyethyl)-1-piperazineethanesulfonic acid) in milliQ water, pH 7.4)
- HEPES-Ca (2.5 mM $CaCl_2$ in HEPES)
- HEPES-Tween (0.05% Tween®-20 in HEPES)
- HEPES-Ca-Tween (0.05% Tween®-20 in HEPES-Ca)
- 1% BSA in HEPES (0.1 g BSA in 10 ml HEPES)
- 5% BSA in HEPES (0.5 g BSA in 10 ml HEPES)

All buffers were filtered through a syringe filter (pore size: 0.2 µm) before use.

8.1.3 Preparation of the gold substrates

Fragments (7×7 mm^2) of silicon wafers coated with 3 nm chromium and 50 nm gold were used as model surfaces for the sensor. Gold substrates were prepared as described in [192]. The gold substrates were prepared in INL.

8.1.4 Test 1: Comparison of binding with pre- and post capture strategy

The aim of this test was to assess the efficiency of two detection strategies: the pre-capture or the post-capture. Figure 8.1 presents a schematic overview of the two strategies with their main steps. In this test, a specific probe, annexin V, and an unspecific probe, BSA, were immobilized on the gold surface. Anti-CD31 antibodies were immobilized on the MNPs. The immobilization of the probes on the gold substrate and the functionalization of the MNPs were performed with the same procedures for both strategies. In the next paragraphs, we describe the functionalization of the gold substrates and the MNPs, followed by the pre- and post-capture strategies.

Immobilization of the probes annexin V and BSA on gold substrates

The immobilization of the probes on the gold substrate was performed following a procedure previously published in [192, 193]. Briefly, the gold substrate was placed in a UV/ozone cleaner (Novascan Tecnologies, PSDP-UVT series, IA, USA) for 5 min at 50°C to remove rest of photoresist and organic contaminants. The linker Sulfo-LC-SPDP (sulfosuccinimidyl 6-[3´ -(2-pyridyldithio)-propionamido] hexanoate, Thermofischer, USA) was deposited all over the gold substrate at a concentration of 1 mg in 500 µl PB. After 20 min incubation at room temperature (RT) in a humid chamber, the gold substrate was rinsed with PB and milliQ water and blown dried. Annexin V and BSA were deposited manually (droplets of 1 µl) at distinct positions on the gold substrates. The concentration of annexin V in the droplet was 250 µg/ml. The immobilization of the probes was processed for two hours at RT in a humid chamber. The excess of probes was rinsed with PB. The remaining binding sites were blocked by incubating 0.1% SH-PEG all over the gold substrate for 30 min at RT. The gold substrate was rinsed with PB-Ca and kept wet with a drop of PB-Ca until further use.

Functionalization of the MNPs with antibodies anti-CD31

2 µl of streptavidin coated Nanomag MNPs (diameter: 250 nm, Stock concentration: 4.9×10^8 MNP/µl, micromod, Germany) were washed in 500 µl PB-Tween. After collection on a magnetic collector, the MNPs were incubated with 10 µg/ml anti-CD31 antibodies conjugated to biotin (clone clone WM59, IgG1, abcam, United Kingdom) for one hour on a shaker (100 rpm) at RT. The MNPs were washed with PB-Tween and incubated with 5% BSA in PB for 40 min at RT on a shaker (100 rpm) to block the remaining binding sites. The addition of the surfactant Tween®-20 helped to remove the unspecific binding. The MNPs were washed in PB-Tween and resuspended in PB in 2 µl.

Pre-capture detection strategy

As shown in figure 8.1, the MVs were first labelled with the functionalized MNPs prior of being put in contact with the functionalized gold substrate. The procedure was performed as follows: 1×10^7 MVs were incubated with 1 µl of the functionalized MNPs in 100 µl PB for 30 min at RT under agitation (100 rpm). The MV-MNP complexes were collected on the magnetic collector and resuspended in 30 µl of PB-Ca. They were then deposited over the whole surface of the functionalized gold substrate and incubated for 30 min at RT in a humid chamber. Next, the gold substrate was then rinsed with PB-Ca, PB-Ca-Tween and milliQ water and finally blow dried. The binding was observed in the stereomicroscope. Two replicates were prepared.

Post-capture detection strategy

In the post-capture strategy, the MVs were first incubated onto the functionalized gold substrate followed with adding functionalized MNPs on the surface. 20 µl of a suspension of MVs from HUVECs (concentration: 5×10^8 MVs/ml) in PB-Ca were deposited on the functionalized gold substrate. After the 30 min of incubation, the unbound MVs were washed from the surface with PB-Ca. 1 µl of anti-CD31 functionalized MNPs were diluted in 30 µl PB-Ca and then deposited over the gold substrate. They were incubated for 30 min in a humid chamber at RT. PB-Ca, PB-Ca-Tween and milliQ water were used to rinse the gold substrate before it was blow dried. The binding was observed in a stereomicroscope (Nikon SMZ 1500, Portugal). Two replicates were prepared.

8.1.5 Test 2: Comparison of the binding with different buffers

In the second test, we investigated the effect of calcium on the binding. Functionalization of gold substrate and MNPs was performed as the described procedure in test 1 (see section 8.1.4 on page 116), whereafter the pre-capture binding strategy was used.

Two sets with two gold substrates were prepared: one set used exclusively PB (or PB-tween when surfactant was required to remove unspecific binding) as buffer and one set was made using PB and PB-Ca as described in the protocol of test 1. In each set, there was one gold substrate, where the pre-capture binding strategy was performed with MVs and one excluding MVs of the procedure (blank sample). Two replicates were made for each condition.

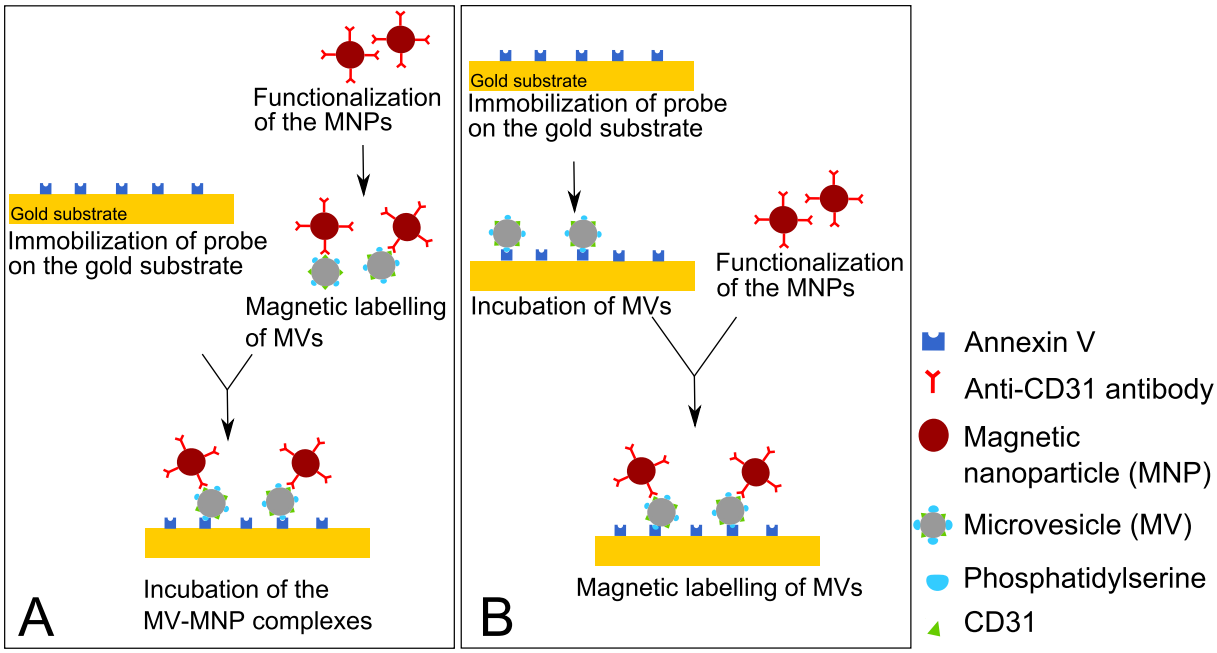

Figure 8.1: Schematic overview of the pre- (A) and post-capture (B) detection strategies. In both strategies, a specific probe (here annexin V) was immobilized on the gold surface and the MNPs were functionalized with a second specific probe (here antibodies against CD31) to the MVs. In pre-capture, the MVs were first incubated with the MNPs and then captured on the gold substrate. In post-capture strategy, the MVs were first incubated on the gold substrate and the functionalized MNPs were then introduced on the gold substrate. Tests 1 and 2 used the probes as represented on this picture. The pre-capture strategy used in test 3 inverted the probes, i.e. annexin V was functionalized on the MNPs and anti-CD31 antibodies were immobilized on the gold surface.

8.1.6 Test 3: Comparison of binding at different temperatures

For this test, HEPES based buffers (set of buffers 2, see section 8.1.2 on page 115) were used. In contrast to test 1 and 2, the gold substrate was functionalized with anti-CD31 antibodies (specific probe) and BSA (unspecific probe), while MNPs were functionalized with annexin V (see figure 6.7B on page 107). The pre-capture binding strategy was utilized again.

Immobilization of the probes (anti-CD31 and BSA) on the gold substrates

The immobilization procedure of the probes was performed according to the procedure described for the test 1 in section 8.1.4 on page 116. The following changes were made to the protocol:

- The set of buffers 2 were used, i.e. HEPES based buffer throughout the procedure.
- The specific probe was anti-CD31 antibodies (clone JC/70A, abcam, United Kingdom) used in the 1 µl droplet at a concentration of 250 µg/ml in HEPES.
- The blocking agent was 1% BSA in HEPES.
- The gold substrate were rinsed with HEPES at the end of the procedure (no calcium).

Functionalization of the MNPs with annexin V

The functionalization of the MNPs with annexin V was performed according to the procedure described in details in for the test 1 in section 8.1.4 on page 116. The following changes were made to the protocol:

- The buffers used were all from the set 2, i.e. HEPES based buffers.
- The probe immobilized on the MNPs was annexin V-biotin, used at a concentration of 1 ng/ml
- After functionalization and blocking, the MNPs were resuspended in 2 µl HEPES-Ca

Pre-capture binding strategy at different temperatures

For this test 3, the pre-capture strategy was used. This was performed as described for the test 1 in section 8.1.4 on page 116. The following changes were made to the protocol:

- The MVs and functionalized MNPs were incubated in HEPES-Ca.
- Three sets of gold substrates were prepared: for one set, the MVs and MNPs were incubated in the fridge (approximately 4-8°C), for the second set the incubation was at RT (approximately 20°C) and for the third set, the incubation was at 37°C. Each set contained two gold substrates: One MV sample (i.e. with MV-MNP complexes) and a blank sample (i.e. incubation of the MNPs without MV).
- After the incubation of the MV-MNP complexes on the gold substrate, the rinsing was done wtih HEPES-Ca, HEPES-Ca-Tween and milliQ water.

8.1.7 Image analysis

The binding on the gold substrates was evaluated by a semi-quantitative method using the software ImageJ (National Institute of Health, USA) on the image captured by the stereomicroscope. Each image was converted to 8bit grey scale. The average grey value of three areas outside of the spots (positions functionalized with a probe) was determined. This value constituted the background and was subtracted from the grey values of the entire image (background subtraction). A threshold was fixed to discriminate the the grey values corresponding to bound magnetic particles. The area around the spots was delimited. Using the plugin "Analyse Particles" from the software ImageJ, the surface coverage in each spot was calculated.

8.1.8 Statistical analysis

Statistical analysis was performed on independent samples. It was verified that the populations are normally distributed with a Kolmogorov-Smirnov test ($p<0.05$). The comparison of the means was performed with a Welch t-test. If $p<0.05$, the means were considered significantly different. The data representation and statistical testing were performed with the software OriginPro 9.0.0 (OriginLab, USA).

8.1.9 Influence of the buffers on the size distribution profile of the MVs

MVs derived from HUVECs were diluted in HEPES-Ca buffer. The size distribution and concentration of the MVs was measured by NTA according to the protocol reported in section 4.2.7 on page 49. The measurement was repeated at regular intervals during two hours, which were the maximum time for the MV detection.

8.2 Preliminary detection tests on gold substrates: Results and discussion

The success of sandwich assays is dependent on many parameters that have to be optimized to assure the specificity and selectivity of the assay. In this study, we performed optimization tests to investigate certain parameters and to determine the best detection strategy for the application of the platform. Similar studies were also used by Fernandes et al. [192] to investigate the binding for their application. We used fragments of silicon wafers coated with 50 nm gold as a model of the sensor surface. For those simulation tests, the functionalization of the MNPs and of the surface was conducted like for the experiments on the platform. The main difference concerned the read-out of the assay, which was only semi-quantitative on the gold substrates. After washing and drying, the MNPs that were bound to the gold surface appeared with a white spot as shown in figure 8.2. The semi-quantitative analysis was performed by evaluating the surface coverage over the spot after defining a threshold of the grey value corresponding to coverage. Although the above mentioned method was less precise and more prone to assay-to-assay variations as compared to the platform, this method is a rapid and simplified method for evaluating binding conditions to yield better results.

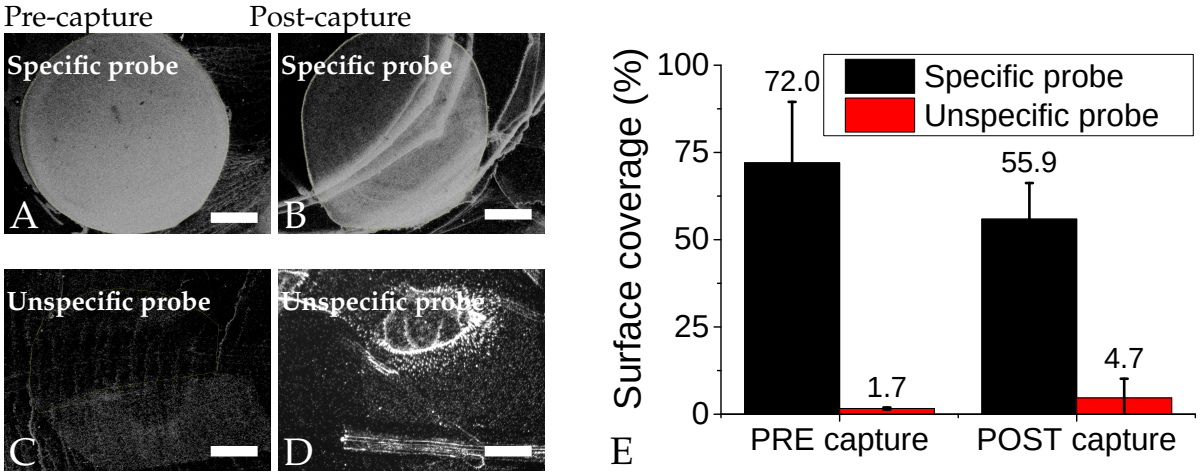

Figure 8.2: Analysis of the pre- and post-capture strategies on gold substrates. Figures A to D show representative spots on the gold substrates after the pre- (figures A and C) and post-capture (figures B and D) detection strategies of HUVECs MVs. White traces indicate the binding of the MV-MNP complexes. Strong binding was found on the spots functionalized with the specific probe annexin V. Some unspecific binding was seen on the spots functionalized with BSA. (Scale bar = 500 µm). The binding was quantified (figure E) and the tendency was that the pre-capture strategy resulted in a stronger binding. The average and standard deviation of two replicates are presented.

8.2.1 Test 1: Comparison of binding with pre- and post-capture strategy

The pre- and post-capture strategies are two different ways of performing the assay. Figure 8.1 shows a schematic overview of the main steps. The main difference lies in introduction of the MVs in the assay. In post-capture, MVs are first incubated onto the functionalized surface whereafter functionalized MNPs are introduced. In the pre-capture strategy, the MVs and functionalized MNPs are first mixed and then the resulting MV-MNP complexes are introduced on the functionalized surface. Figure 8.2 shows the results of the assay. On the control spot with BSA, the effective binding was < 5%, which can be regarded as negligible. On the specific spot, the surface coverage was relatively homogeneous with the pre-capture strategy (figure 8.2A). For the post-capture strategy, half of the spot was covered by MNPs that also reached beyond the spot borders (figure 8.2B). Those corresponded to MNPs that dried on the surface during the washing procedure. This part was not considered for the evaluation of the coverage. Analysis of the surface coverage showed that the pre-capture strategy had a tendency towards a higher surface coverage than the post-capture strategy (approximately 15% difference, figure 8.2E). For all the further experiments, the pre-capture strategy was therefore chosen. This strategy is also advantageous as the labelling of the MVs with the magnetic particles occurs out of the chip, therefore the target MVs can be up-concentrated and contaminants (other MVs, cell debris, proteins, protein aggregates) can be efficiently removed during the washing and collection processes of the MV-MNP complexes.

8.2.2 Test 2: Comparison of binding in different buffers

The aim of the second detection test was to investigate the influence of calcium on the binding. Therefore, we tested the binding under the use of the phosphate buffer with and without calcium. Table 8.1 summarizes the findings. When using calcium free buffer no binding was observed. Conversely, in the case of buffer with calcium, binding was found both on the sample incubated with MV-MNP complexes and on the blank sample. This shows that the addition of calcium was necessary to achieve the binding between annexin V and phosphatidylserine. This is in agreement with literature since the binding of annexin V to phosphatidylserine is reported to be calcium dependent [234, 235]. We attributed the unspecific binding on the blank sample to the reaction between phosphate ions and the calcium ions that creates solid precipitates.

Similar issues have been analysed by Larson et al. [179] with flow cytometry. They added fluorescently labelled probes such as annexin V to calcium-phosphate microprecipitates and showed that the fluorescence signal increased with an increasing calcium concentration in PBS. They concluded that the calcium-phophosphate microprecipitates gave a signal that overlapped with the signal from the MVs which led to false results. Therefore we used HEPES based buffer instead of the PB buffer for the further experiments. To avoid the corrosion of the sensors, we used sodium chloride free buffers [230].

Table 8.1: Binding in different buffers. The binding of MV-MNP complexes was reported for the specific (annexin V) and non-specific probe (BSA) for a blank sample and a sample with $1x10^8$ MVs/ml, when the MVs and MNPs were incubated with PB or PB-Ca. Without calcium, no binding was found, while with calcium in the phosphate buffer, binding was found on the gold substrate with MV-MNP complexes as well as on the blank sample (no MV).

	PB	PB-Ca
MVs	No binding	Binding
Blank	No binding	Binding

8.2.3 Test 3: Comparison of binding at different temperatures

The binding temperature of a probe to its target is an important parameter to assure an efficient binding while avoiding unspecific binding. Annexin V is a probe that binds to phosphatidylserine in the presence of calcium ions. Different reports recommend different incubation temperatures of annexin V with the target. For example, the material sheet of the apoptosis kit based on annexin V and propidium iodide (BD pharmingen, USA) that was used in the experiment reported in figure 4.2 (page 53) recommended incubating the cells with annexin V at room temperature [236]. Göhner et al. [141] developed an assay where extracellular vesicles were captured by annexin V on the surface at room temperature. The material data sheet of annexin V MicroBead kit (Miltenyi Biotech, Germany) recommended to incubate cells with annexin V labelled magnetic particles between 2 and 8°C to avoid unspecific binding [237]. Tong et al. [238] showed that the incubation of jurkat cells with annexin V at 37°C gave the highest signal for a annexin V based biosensor.

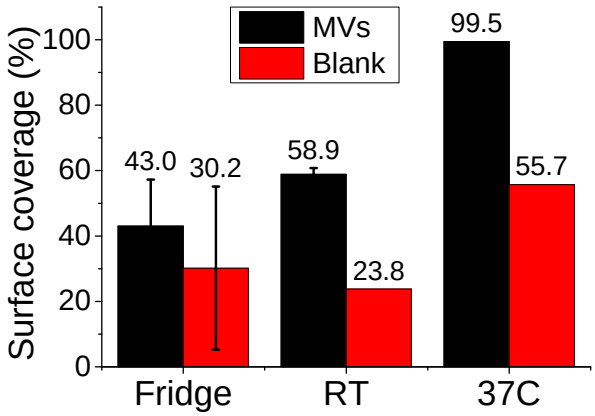

Figure 8.3: Incubation of MVs with MNPs at different temperatures. MVs were incubated with the annexin V functionalized MNPs at three different temperatures (fridge (approximately 4 to 8°C), RT (approximately 20°C) and 37°C). The surface coverage was evaluated over the spot where anti-CD31 antibodies had been immobilized. The higher the incubation temperature was, the higher the surface coverage was but also the unspecific binding of a blank sample increased with the increasing incubation temperature. The values are the average and the standard deviation of two replicates (except for the blank sample at RT, and both samples at 37°C).

Considering the different protocols available in the literature, we investigated the incubation of the MVs with the functionalized MNPs at three different temperatures: fridge temperature, RT, and 37°C for a sample with MVs and a blank sample (no MV). Using the pre-capture strategy enabled us to easily incubate the MVs with the MNPs at different temperatures. Figure 8.3 shows the results of the surface coverage over the anti-CD31 spot. The tendency was that the surface coverage increased with an increasing incubation temperature. After incubation in the fridge, the surface coverage of the MV-MNP complexes was approximately 40%, at RT 60% and at 37°C, nearly 100%. The unspecific binding also increased with the increase of the incubation temperature (from 30 to 56%). Incubation in the fridge was excluded for further experiments as the difference between the MV sample and the blank sample was only 1.4 fold. Finally, RT and 37°C were chosen for further experiments since they showed promising binding results with significant differences between MV and blank sample. Compared to test 1 (see figure 8.2), the surface coverage of the MVs sample was slightly lower in this experiment. This was probably due to the change in buffer (HEPES buffer instead of PB) and to the washing procedure which was performed manually and therefore difficult to reproduce from one experiment to another. The reproducibility of binding tests on the gold substrates could be improved by implementing a more automatised washing procedure for example by enclosing the gold substrate in a simple flow device subjected to a constant flow rate.

Since HEPES based buffer is different from the buffer used for the isolation of the MVs, i.e. PBS, the stability of the MVs in HEPES-Ca was analysed for the duration of the assay (two hours) and compared to the incubation of MVs in PBS. MVs from HUVECs were incubated in PBS and HEPES-Ca. The size of the MVs was measured by NTA. Figure 8.4 presents the size distribution of the MVs incubated in PBS and HEPES-Ca for two hours. For both buffers, the

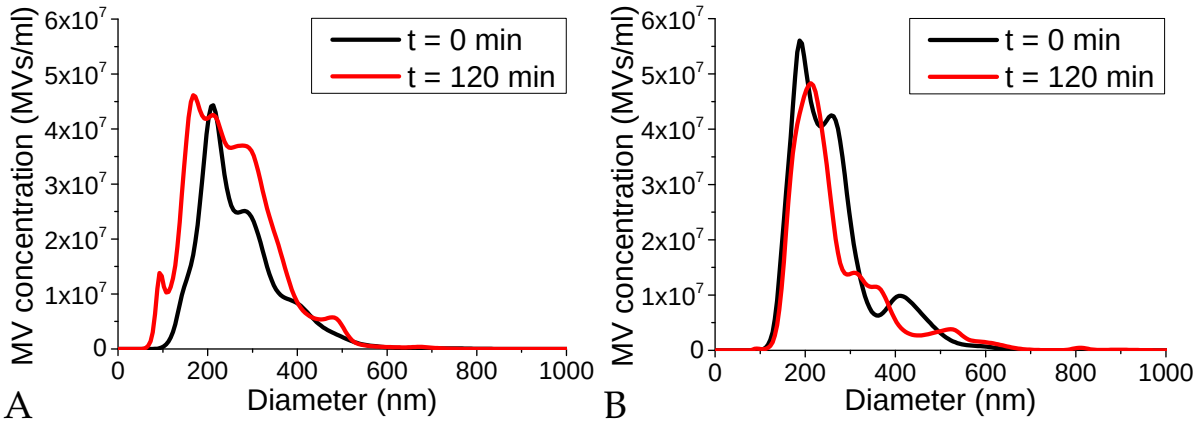

Figure 8.4: Influences of the buffers on the size of the MVs. MVs from HUVECs were incubated in PBS (figure A) or HEPES-Ca (figure B) for two hours, the maximum time required to perform the detection on the MR biosensor. The size distribution was measured by NTA at the beginning of the incubation (t = 0 min) and after two hours (t = 120 min). Incubation in the buffers did not affect the size distribution of the MVs. The graphs represent an average of three measurements of a representative sample. The error bars represent the standard deviation.

size distributions at t = 0 min and t = 120 min overlapped. The mode diameter at t = 0 min were around 210 nm in PBS (figure 8.4A) and around 188 nm in HEPES-Ca (figure 8.4B). After two hours of incubation, the mode diameter was around 193 nm in PBS (figure 8.4A) and around 204 nm in HEPES-Ca (figure 8.4B). These negligibly small size differences indicated that this buffer was suitable for the MV detection in this sandwich assay.

8.2.4 Final validation of the optimized binding strategy on gold substrates

Using the protocol established for the test 3, eight independent experiments were performed and the coverage density was evaluated for each of these experiments. This is reported in figure 8.5. The coverage density reached 69% for the specific probe while it was around 2% over the unspecific probe. For the blank sample, the coverage density was below 9% both on the specific and unspecific probe. This indicated that the pre-capture binding strategy with HEPES based buffer at RT was valid and reproducible.

8.3 Conclusion

In this part of the work, preliminary steps leading to the detection of MVs on the MR biosensor were investigated.

Preliminary tests on gold substrates were performed to optimize some parameters of the detection assay. We determined that the pre-capture binding strategy was more efficient than the post-capture strategy. We conclude that the combination of phosphate buffer and calcium ions was not adequate for these experiments. We have chosen HEPES-Ca buffer for the assay. Furthermore, we could prove that this buffer did not affect the stability of the MVs for at least

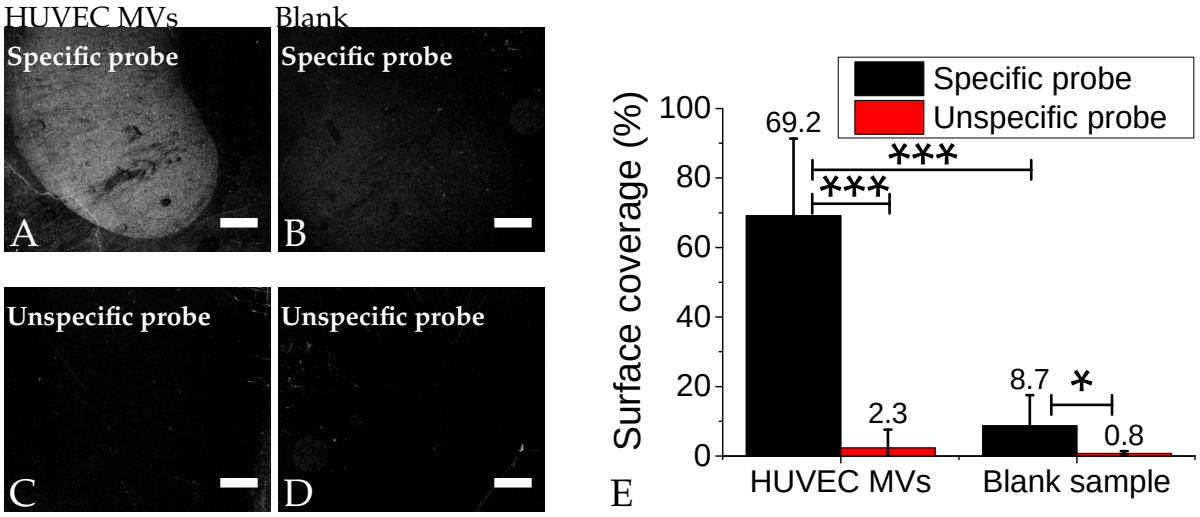

Figure 8.5: Validation of the binding strategy on gold substrates. Magnetically labelled HUVEC MVs and a blank sample (no MVs) were incubated on a Au substrate functionalized a two different spots respectively with a specific probe (anti-CD31) and a non specific probe (BSA). Figures A-D show representative pictures of the spots. The white spot was the MNPs specifically captured on the surface. It is only visible at the position functionalized with anti-CD31 antibodies for the sample with MVs. On the other samples, no binding of MV-MNP complexes can be seen. The images were captured with a stereomicroscope. (Scale bar = 500 µm.) The coverage density of the spots was evaluated for eight independent samples (figure (E)). On the specific probe spot, the incubation with magnetically labelled HUVEC MVs reached a high coverage (up to 69%) while on the other spots the coverage was less than 9%. The difference of means between specific and non specific probe was statistically significant (with *: $p < 0.05$ and ***: $p < 0.001$, Welch t-test).

two hours, which was the maximum required time for the assay. The test of the incubation temperatures of MVs with functionalized MNPs showed that room temperature and 37°C enabled a good binding on the gold substrates. At RT, the binding strategy was validated over eight independent experiments. Those preliminary tests constituted the pavement for the further tests on the MR platform.

Chapter 9

Detection of the MVs on a magnetoresistive biosensor

Having analysed the different detection parameters, we used the best conditions to perform the MV detection on the MR sensor platform. It means that the detection was performed according to the pre-capture binding strategy (main steps are shown in figure 8.1A on page 118), using the buffers based on HEPES. Two incubation temperatures for the binding of the MVs to the functionalized MNPs were tested: RT and 37°C. We tested the detection on the MR platform with HUVEC MVs and MCF7 MVs. Those experiments were built up as a proof of concept study to investigate if the MR sensors were able to discriminate between MVs coming from different cell lines. From the immunostaining of the MCF7 cells, we know that CD31 was not expressed on the MCF7 cells (see figure 7.2 on page 112). Therefore we expected that the MVs from MCF7 cells would not be able to bind to the surface of the sensors functionzalized with anti-CD31 antibodies.

9.1 Material and methods

9.1.1 Buffers used in this study

The buffers used in this study were all HEPES based buffers. We used 10 mM HEPES, HEPES-Ca, HEPES-Tween, HEPES-Ca-Tween, 5% BSA in HEPES and 1% BSA in HEPES. The precise composition of the buffers is described in section 8.1.2 on page 115.

9.1.2 MVs used in this study

MVs were derived from apoptotic HUVECs and MCF7 cells and isolated from the cell supernatant according to the protocols described in section 4.2.5 on page 48 and in section 7.1.5 on page 110.

9.1.3 MV detection on the MR platform

As the MR platform detects magnetic labels, it was necessary to bind MNPs to the MVs. MNPs were labelled with annexin V and the MVs were bound to the MNPs through the phosphatidylserine (present on the surface of the MVs) to annexin V interaction. The detailled

protocol for the magnetic labelling of the MVs is described in section 8.1.6 on page 119. After labelling, the MV-MNP complexes were resuspended in 5 µl HEPES-Ca.

The MR biochips were provided by INESC-MN. The microfabrication of the MR biochips is presented in details in [232]. The MR biochips are composed of 30 spin valves sensors. Those sensors are organized in two distinct regions of 15 sensors. On one region of sensors, the specific probe, anti-CD31 antibodies, was immobilized (specific sensors), while on the second region, the unspecific probe, 5% BSA, was immobilized on the sensors (control sensors). The immobilization procedure is described in details in section 8.1.6 on page 119. 1 µl of probe was used to cover all the sensors of one region.

After immobilization of the probes, the MR biochip was introduced in the portable platform. The microfluidic system (channel made in polydimethylsiloxane (PDMS) and tubing connected to a syringe pump) was set up over the sensors and the MV-MNP complexes were introduced into the tubing with a syringe pump (New Era Pump Systems, INC, USA) at a flow rate of 5 µl/min. The sensors were biased with a current of 1 mA and an external DC+AC magnetic field of 3 mT and 1.35 mT_{rms}, respectively, was applied. The voltage on the sensors was recorded over the time of the experiment. A baseline voltage was recorded for 10 min when the channel (total volume: 0.5 µl) was filled with the buffer HEEPES-Ca. The channel was then filled with MV-MNP complexes at a flow rate of 0.5 to 1 µl/min. The MV-MNP complexes were allowed to bind to the functionalized sensors for 30 min. The surface of the sensors was then rinsed with HEPES-Ca-Tween. The sensors have different baseline voltages due to variations in the microstructures. Therefore, a normalization of the binding signal was required to compare different sensors. The normalized binding signal was calculated as follow:

$$\frac{\Delta V_{binding}}{V_{baseline}} = \frac{V_{baseline} - V_{binding}}{V_{baseline}} \tag{9.1}$$

i.e. the binding signal after washing ($V_{binding}$) subtracted to the baseline signal of the sensor ($V_{baseline}$) and normalized over the baseline signal of the sensor ($V_{baseline}$). This normalized binding signal is proportional to the number of MNPs bound to the surface [192, 193]. The signal to noise ratio was approximately 50. The data were represented as the mean value with the standard deviation of the different sensors.

9.2 Results

The MV detection was performed on the MR platform with a MV concentration of $1{\times}10^8$ MVs/ml. The voltage at the sensors was recorded during the whole time of the assay. Figures 9.1A and 9.1B present a representative signal with HUVEC MVs of a specific and control sensor respectively. The time course was explained in figure 6.8 on page 108. A difference between the baseline signal and binding signal was only measured on the specific sensor.

The surfaces of the sensors were imaged after the assay. Figures 9.1C and 9.1D show micrographs of specific sensors and control sensors respectively. The black dots corresponded to the

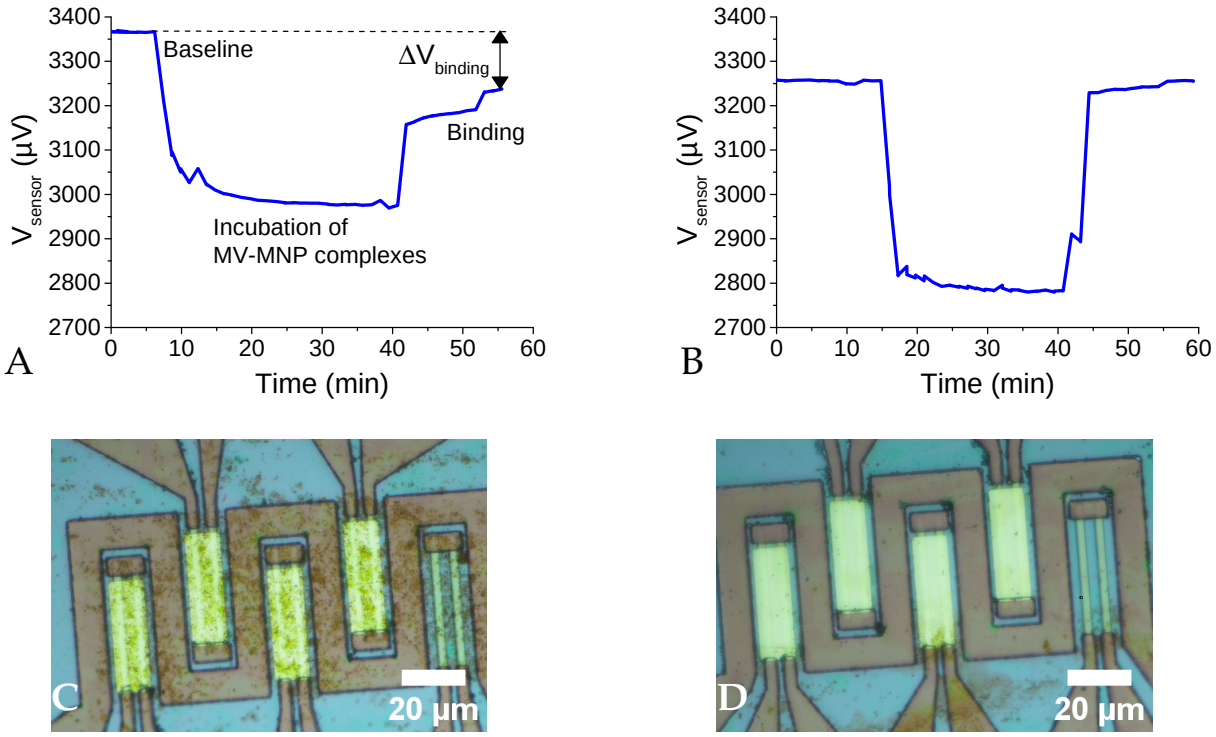

Figure 9.1: MVs detected on the MR platform Figures A and B present the MR sensor signal over the time for a specific sensor (figure A) and a control sensor (figure B). A baseline was first recorded. Then at the introduction of the MV-MNP complexes the signal decreased. After 30 min of incubation, the channel was washed and the unbound MNPs and MV-MNP complexes were removed. The signal on the control sensors (figure B) returned to the baseline level, while on the specific sensors (figure A), the difference between the signal after washing and the baseline signal was the binding signal. Figures C and D are microscopy images of specific (figure C) and control sensors (figure D) after the assay. Black dots representative for the MNPs could only be found on the specific sensors.

MNPs bound to the surface. It is clearly visible that the density was higher on the specific sensors than on the control sensors. Black dots were quasi absent from the surface of the control sensors.

The MV detection on the MR platform was performed with two types of MVs (HUVECs MVs and MCF7 MVs) and at two different temperatures for the incubation of the MVs with the functionalized MNPs (RT and 37°C). Figure 9.2 presents the normalized binding signal for the four different tested conditions. MVs from the endothelial cells HUVECs lead to a normalized binding signal of 0.041 at 37°C and of 0.028 at RT. MVs from the epithelial cells MCF7 showed a lower normalized binding signal (0.0076 at 37°C and 0.0051 at RT). At 37°C, the HUVEC MV signal was 5.4 higher than the MCF7 MV signal, and 5.6 higher at RT. The black line represents the highest normalized binding signal measured on the control sensors. This signal was never above 0.003.

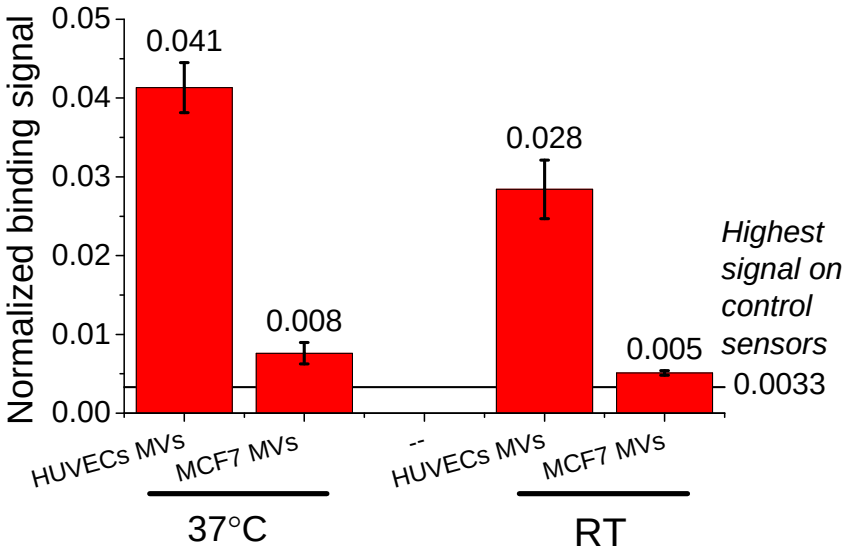

Figure 9.2: Normalized binding signal on the MR sensor. The MV detection assay was performed with MVs from HUVECs and MCF7 cells. The signals from the HUVEC MVs were approximately 5.5 times higher than the signal of the MCF7 signal. The error bars represents the standard deviation of at least four independent sensors. The horizontal black line represents the highest signal measured at the control sensors.

9.3 Discussion

The aim of this study was to present the possibility of detecting MVs from a defined cell type on a MR biochip. The use of MVs isolated from a cell line allowed us to control the number and origin of the MVs and therefore the surface markers present on the MVs. The detection strategy was designed to detect MVs positive for annexin V and CD31. This marker combination was used in clinically relevant cases [239, 240].

On the MR sensors, we could detect an approximately 5.5 times higher signal with the MVs derived from HUVECs than with the MVs from MCF7 cells. The signal obtained with the MVs derived from MCF7 cells was at the level of the signal on the control sensors. As epithelial cells do not express the marker CD31 (see immunostaining assay figure 7.2 on page 112), this shows that the MR biochip detected only MVs positive for both markers (annexin V and anti-CD31 antibodies).

Two incubation temperatures were investigated for the capture of MVs on the MNPs. However, we did not observe large differences. It could be that the increase in temperature does not increase the binding efficiency or that the binding efficiency is increased during the capture steps. But as the following steps (washing and measurement on the platform) are performed at RT, the weakly bound MVs would be released again from the MNPs when the temperature decreases.

In this sandwich type assay, the probes annexin V and anti-CD31 antibodies were proven to be suitable markers to discriminate between MVs from HUVECs and MVs from MCF7 cells because of the lack of CD31 on the surface of the MCF7 MVs. However, not all MVs express phosphatidylserine and therefore not all MVs bind to annexin V [36, 38]. As an alternative, CD9

[51] or CD81 [241] have been proposed as markers present on most EVs. Its use could therefore allow to capture a more complete MV population. CD31 is also not an exclusive marker for endothelial MVs as it is also for example expressed on the surface of platelet MVs [66]. CD144 for instance is a marker described as highly specific for endothelial MVs [189] and it could be therefore considered in this assay to very specifically detect only endothelial MVs.

The MVs concentration used (1×10^8 MVs/ml) in the assay was chosen within the dynamic range of MVs in body fluids (10^6 to 10^{11} /ml) as reported in the theoretical part of the thesis (see section 2.1 on page 7). This shows that the MR sensor could be used with clinical samples. Further work will include the investigation of dynamic range of the sensor to determine the lowest and highest MV concentration that can be detected on the MR biochip, with MVs isolated in buffers as well as directly from body fluids.

Further optimization of the detection of MVs on the MR platform should also include the investigation of the MVs to MNPs ratio. Imaging of the MV-MNP complexes using for instance TEM could reveal how many MVs bind to one MNPs. Further studies could focus on the influence of different ratios of MVs to MNPs on the binding signal. Moreover, it could be investigated if the detection is possible directly from body fluids in order to reduce the overall duration of the MV detection and to avoid artefacts from the MV isolation.

9.4 Conclusion

In conclusion, these experiments proved that the MR platform was able to detect MVs and to discriminate between MVs isolated from the endothelial cell HUVEC and MVs isolated from the epithelial cells MCF7. The detection was specific according to the surface markers of the MVs. It was performed within 40 min and the platform was sensitive for a physiologically relevant MV concentration. Further work will expand the possibilities of the MR platform for MV detection.

Conclusion

In this part of the thesis, we proposed a solution for a specific and rapid MV detection methods. For this purpose, we used a magnetoresistive (MR) biosensor adapted to a portable platform. The detection of the MVs was performed in a sandwich type assay using two distinct probes.

In the first part, we showed that MVs derived from HUVECs and from MCF7 cells displayed a similar size distribution. In the second part, several studies were conducted to optimize the binding strategy investigating different steps for magnetic labelling of the MVs, different buffers and incubation temperatures on gold substrates that mimicked the surface of the sensors. Finally, proof of concept detection was performed on the MR platform. The experiments showed that the MR platform is a suitable tool to detect MVs.

The platform presented the advantages of a rapid, specific and sensitive detection. Moreover, the organization of the biochip gives the possibility of a simultaneous detection of MVs from different cell types. Each group of sensors could be functionalized with markers specific for different populations of MVs. In further studies the feasibility of this multiplex detection will be investigated. This will give the possibility of determining the MVs profile in patient samples. After identification of the proper MVs and their corresponding markers, the MR biochip could be used as complementary diagnostic system.

Further, the MR biochip can be adapted to other types of analytes by changing the probes. Therefore other types of extracellular vesicles such as exosomes could also be envisaged to be quantified by this system.

Part V

General conclusion and outlook

The aim of this project was to explore the potential of new isolation and characterization methods for MVs to overcome the limitation of the conventional methods.

In the first part, we aimed to obtain a well characterized population of MVs, which could be generated in a reproducible way for use as test population for further investigation and development of new microvesicle related techniques.

MVs were isolated from the cell culture supernatant of apoptotic endothelial cells (HUVECs). After a conventional isolation using differential high speed centrifugation, the size of the MVs was characterized by AFM and NTA. We found that the main MV population had a diameter around 150 nm. The size distribution obtained by NTA was slightly larger than the one obtained by AFM. We concluded that the apoptotic HUVEC produced approximately three times more MVs than the control cells. An MV array was developed for the characterization of the surface markers. This array accurately showed that endothelial surface markers CD31 and CD146 were expressed on the MVs derived from HUVECs while a platelet marker was not present. Further development could give the possibility to characterize the phenotype of MV population along with the size distribution of these MVs.

Using a cell line to generate MVs allowed us to obtain a population of MVs from a single type of cells, in contrast to MVs isolated from body fluids which always contain MVs derived from many different types of cells. MV populations derived from single cell lines are therefore very useful tools to test new analysis methods. The protocol that we developed in this work proved to be very reproducible. The MV concentration was reproducible within a range of 20%. Moreover, we could study the complete system around the MVs and their release. Therefore we obtained a relevant model system of MVs. Further characterization of this population could include an evaluation of possible contamination by other types of EVs or from protein aggregates that might be co-isolated with the HUVEC MVs.

The goal of the second part of the thesis was to develop a microfluidic device for the purification of MVs in a simple, easy to use system to overcome the obstacles of the MVs isolation via differential centrifugation.

For this purpose, we developed an H-filter which is a microfluidic device separating analytes by diffusion. First we performed analytical calculations to determine the parameters required for the device. With these parameters, finite element simulation has been used for verifying the output concentrations. Based on these results, a H-filter device has been designed and tested with these samples. The results from the experimental work were in good agreement with the simulation results. Particles with a diameter in the range of 1 µm to 50 nm were all collected with an efficiency of 80 to 90%. Protein contamination was removed to an approximately 25% efficiency within 1.5 hour for 200 µl sample. The recovery of the MVs was around 60% in the H-filter while it was only 30% after high speed centrifugation. This suggested that the H-filter is better for collecting the MVs than the centrifugation. The small size of the channel enables the use of small volume of sample ($<$ 100 µl) which is attractive for the purification of MVs from body fluids, where only small volumes are available. A main advantage of the device is that no strong forces are applied on the MVs, thus the risk of MV aggregation or fusion during the isolation process is highly reduced.

In our experiments, the samples were analysed after one diffusion cycle through the H-filter. A more effective removal of the contamination could be achieved with several consecutive cycles. Further optimization of the device could allow the automation of the sample purification. The integration of electrodes to maintain all MVs in the sample stream via dielectric forces could be envisaged, though compromising the simplicity of the device. For use in the biomedical field, further development of the system is necessary with integration of the pumping system and sample loading and collection on the same platform. Further testing and optimization of the separation precision could establish the H-filter as a suitable alternative to conventional isolation methods.

In the third part, our aim was to develop the rapid and selective detection of MVs on a magnetoresistive (MR) biosensor.

We conducted a proof of concept study to demonstrate the potential of this biosensor. The method was based on a sandwich assay with the probes annexin V and anti-CD31 antibodies. Optimization studies were perfomed to determine the best parameters for the assay. We used MVs from HUVECs expressing both phosphatidylserine and CD31 and MVs from MCF7 lacking the expression of CD31. THE HUVEC MVs generated a high signal while the MCF7 MVs resulted in a significantly lower response on the similar level as the unspecific binding. This proved that the MR biosensor was able to discriminate between the two types of MVs. We showed that the detection was working at a physiologically relevant MV concentration.

The advantages of this platform are i) that the detection occurs only based on the surface markers independently of the heterogeneous size of the MVs and ii) that the signal from this biosensor is quantitative. Although this sensor is very promising, several parameters of the assay need to be analysed and optimized such as the ratio of magnetic beads to the number of MVs and the size of the magnetic beads compared to the MVs and the dynamic detection range of the sensor. The configuration of this biosensor would allow a multiplex detection of different subpopulations of MVs that could be quantified simultaneously. This would be very interesting to measure the profile of MVs in different samples.

In conclusion, the young but very active research field of MVs is moving fast forward elucidating new relations between MVs and disease states. The lack of appropriate preparative and analytical methods still hampers the clinical use of MVs for diagnosis. Great efforts are made by many research groups all around the world to improve methods and agree on standardized procedures. We think that this work could be a further step towards new highly appropriate methods for MV research in the perspective of efficient and non-invasive early diagnosis.

Bibliography

[1] E. van der Pol, "Detection of extracellular vesicles: size does matter". PhD thesis. University of Amsterdam, Amsterdam, The Netherlands, 2015.

[2] C. Lawson et al., *Microvesicles and exosomes: new players in metabolic and cardiovascular disease.* The Journal of endocrinology, 228 (2) **2016**, R57–71.

[3] E. Chargaff and R. West, *The biological significance of the thromboplastic protein of blood*. Journal of Biological Chemistry, 166 (1) **1946**, pp. 189–197.

[4] P. Wolf, *The Nature and Significance of Platelet Products in Human Plasma*. British Journal of Haematology, 13 (3) **1967**, pp. 269–288.

[5] R. Nieuwland, E. van der Pol, and A. Sturk, "Overview of Extracellular Vesicles in Health and Disease". In: *Extracellular Vesicles in Health and Disease*. Pan Stanford Publishing, Oxon, UK, May 2014, pp. 1–46.

[6] D. Burger et al., *Microparticles: biomarkers and beyond.* Clinical science (London, England : 1979), 124 (7) **2013**, pp. 423–41.

[7] R. Nieuwland and A. Sturk, *Why do cells release vesicles?* Thrombosis research, 125 (1) **2010**, S49–51.

[8] J. Perez-Hernandez, *Extracellular Vesicles as Biomarkers of Systemic Lupus Erythematosus*. Disease Markers **2015**, p. 613536.

[9] C. D'Souza-Schorey and J. W. Clancy, *Tumor-derived microvesicles: shedding light on novel microenvironment modulators and prospective cancer biomarkers.* Genes & development, 26 (12) **2012**, pp. 1287–99.

[10] C. J. Koch et al., *Microvesicles as a Biomarker for Tumor Progression versus Treatment Effect in Radiation/Temozolomide-Treated Glioblastoma Patients.* Translational oncology, 7 (6) **2014**, pp. 752–8.

[11] C. N. França et al., *Microparticles as potential biomarkers of cardiovascular disease.* Arquivos brasileiros de cardiologia, 104 (2) **2015**, pp. 169–74.

[12] M. Yáñez-Mó et al., *Biological properties of extracellular vesicles and their physiological functions*. Journal of Extracellular Vesicles, 4 **2015**, p. 27066.

[13] E. van der Pol et al., *Classification, functions, and clinical relevance of extracellular vesicles.* Pharmacological reviews, 64 (3) **2012**, pp. 676–705.

[14] S. J. Gould and G. Raposo, *As we wait: coping with an imperfect nomenclature for extracellular vesicles*. en. Feb. 2013.

[15] E. van der Pol et al., *Recent developments on the nomenclature, presence, isolation, detection and clinical impact of extracellular vesicles.* Journal of thrombosis and haemostasis, 14 **2015**, pp. 48–56.

[16] J. Lötvall et al., *Minimal experimental requirements for definition of extracellular vesicles and their functions: a position statement from the International Society for Extracellular Vesicles*. Journal of Extracellular Vesicles, 3 **2014**, p. 26913.

[17] S. Cherré et al., "Analysis of Cell-Derived Microparticles with Highly Precise Nanotechnological Methods". In: *Journal of Nanomaterials & Molecular Nanotechnology*. 2014, S2.

[18] E. F. Strasser et al., *Microparticle detection in platelet products by three different methods.* Transfusion, 53 (1) **2013**, pp. 156–66.

[19] F. Royo et al., *Different EV enrichment methods suitable for clinical settings yield different subpopulations of urinary extracellular vesicles from human samples*. en. Feb. 2016.

[20] M. I. Zonneveld et al., *Recovery of extracellular vesicles from human breast milk is influenced by sample collection and vesicle isolation procedures*. Journal of Extracellular Vesicles; Vol 3 (2014) incl supplements, 3 **2014**.

[21] V. Palanisamy et al., *Nanostructural and transcriptomic analyses of human saliva derived exosomes.* PloS one, 5 (1) **2010**, e8577.

[22] J. M. Street et al., *Identification and proteomic profiling of exosomes in human cerebrospinal fluid.* En. Journal of translational medicine, 10 (1) **2012**, p. 5.

[23] C. T. Nielsen et al., *Distinct features of circulating microparticles and their relationship to clinical manifestations in systemic lupus erythematosus.* Arthritis and rheumatism, 63 (10) **2011**, pp. 3067–77.

[24] A. S. Shet et al., *Sickle blood contains tissue factor-positive microparticles derived from endothelial cells and monocytes.* en. Blood, 102 (7) **2003**, pp. 2678–83.

[25] R. A. Dragovic et al., *Sizing and phenotyping of cellular vesicles using Nanoparticle Tracking Analysis.* Nanomedicine : nanotechnology, biology, and medicine, 7 (6) **2011**, pp. 780–788.

[26] Y. Yuana et al., *Handling and storage of human body fluids for analysis of extracellular vesicles*. en. Journal of Extracellular Vesicles, 4 **2015**, p. 29260.

[27] V. Combes et al., *In vitro generation of endothelial microparticles and possible prothrombotic activity in patients with lupus anticoagulant.* en. The Journal of clinical investigation, 104 (1) **1999**, pp. 93–102.

[28] C. Théry et al., *Isolation and characterization of exosomes from cell culture supernatants and biological fluids.* Current protocols in cell biology, 3 **2006**, pp. 3.22.1–3.22.29.

[29] O. Morel et al., *Cellular mechanisms underlying the formation of circulating microparticles.* Arteriosclerosis, thrombosis, and vascular biology, 31 (1) **2011**, pp. 15–26.

[30] C. Théry, M. Ostrowski, and E. Segura, *Membrane vesicles as conveyors of immune responses.* en. Nature reviews. Immunology, 9 (8) **2009**, pp. 581–93.

[31] E. Cocucci, E. Cocucci, and J. Meldolesi, *Ectosomes.* Current biology : CB, 21 (23) **2011**, R940–1.

[32] C. Ciardiello et al., *Focus on Extracellular Vesicles: New Frontiers of Cell-to-Cell Communication in Cancer.* en. International journal of molecular sciences, 17 (2) **2016**, p. 175.

[33] S. S. Antwi-Baffour, *Molecular characterisation of plasma membrane-derived vesicles.* Journal of biomedical science, 22 (1) **2015**, p. 68.

[34] B. György et al., *Membrane vesicles, current state-of-the-art: emerging role of extracellular vesicles.* Cellular and molecular life sciences, 68 (16) **2011**, pp. 2667–88.

[35] F. Momen-Heravi et al., *Current methods for the isolation of extracellular vesicles*. Biological Chemistry, 394 (10) **2013**, pp. 1253–1262.

[36] D. E. Connor et al., *The majority of circulating platelet-derived microparticles fail to bind annexin V, lack phospholipid-dependent procoagulant activity and demonstrate greater expression of glycoprotein Ib.* Thrombosis and haemostasis, 103 (5) **2010**, pp. 1044–52.

[37] N. Arraud et al., *Extracellular vesicles from blood plasma: determination of their morphology, size, phenotype and concentration.* Journal of thrombosis and haemostasis, 12 (5) **2014**, pp. 614–27.

[38] S. L. Latham et al., *Immuno-analysis of microparticles: probing at the limits of detection.* en. Scientific reports, 5 **2015**, p. 16314.

[39] Y. Yuana et al., *Atomic force microscopy: a novel approach to the detection of nanosized blood microparticles.* Journal of thrombosis and haemostasis, 8 (2) **2010**, pp. 315–23.

[40] F. Yari, S. Azadpour, and R. Shiri, *Platelet storage media change the expression characteristics of the platelet-derived microparticles.* Indian journal of hematology & blood transfusion : an official journal of Indian Society of Hematology and Blood Transfusion, 30 (3) **2014**, pp. 169–74.

[41] Y. Zhang et al., *Inflamed macrophage microvesicles induce insulin resistance in human adipocytes.* Nutrition & metabolism, 12 **2015**, p. 21.

[42] F. Dignat-George and C. M. Boulanger, *The many faces of endothelial microparticles.* Arteriosclerosis, thrombosis, and vascular biology, 31 (1) **2011**, pp. 27–33.

[43] S. Montoro-García et al., *Circulating microparticles: new insights into the biochemical basis of microparticle release and activity.* Basic research in cardiology, 106 (6) **2011**, pp. 911–23.

[44] L. V. Norling and J. Dalli, *Microparticles are novel effectors of immunity.* Current opinion in pharmacology, 13 (4) **2013**, pp. 570–5.

[45] K. Murphy, P. Travers, and M. Walport, *Janeway's immunobiology*. 7th ed. Garland Science, New York, NY, USA, 2008.

[46] S. Elmore, *Apoptosis: a review of programmed cell death.* Toxicologic pathology, 35 (4) **2007**, pp. 495–516.

[47] H. Kalra, G. P. C. Drummen, and S. Mathivanan, *Focus on Extracellular Vesicles: Introducing the Next Small Big Thing.* en. International journal of molecular sciences, 17 (2) **2016**, p. 170.

[48] C. T. Nielsen, *Circulating microparticles in systemic Lupus Erythematosus.* Danish medical journal, 59 (11) **2012**, B4548.

[49] E. Boilard et al., *Platelet-derived microparticles serve as an important source of autoantigens and discriminate between levels of disease activity in systemic lupus erythematosus*. Arthritis Research & Therapy, 16 (Suppl 1) **2014**, A17.

[50] H. Shao et al., *Protein typing of circulating microvesicles allows real-time monitoring of glioblastoma therapy.* Nature medicine, 18 (12) **2012**, pp. 1835–40.

[51] Y. Yoshioka et al., *Ultra-sensitive liquid biopsy of circulating extracellular vesicles using ExoScreen.* Nature communications, 5 **2014**, p. 3591.

[52] H. Julich et al., *Extracellular vesicle profiling and their use as potential disease specific biomarker.* Frontiers in immunology, 5 **2014**, p. 413.

[53] J. Van Deun et al., *The impact of disparate isolation methods for extracellular vesicles on downstream RNA profiling*. Journal of Extracellular Vesicles, 3 **2014**.

[54] I. M. Rood et al., *Comparison of three methods for isolation of urinary microvesicles to identify biomarkers of nephrotic syndrome.* Kidney international, 78 (8) **2010**, pp. 810–6.

[55] M. Sáenz-Cuesta, *Methods for extracellular vesicles isolation in a hospital setting*. Frontiers in Immunology, 6 **2015**, p. 50.

[56] K. W. Witwer et al., *Standardization of sample collection, isolation and analysis methods in extracellular vesicle research.* en. Journal of extracellular vesicles, 2 **2013**, p. 20360.

[57] R. Lacroix et al., "Preanalytical Variables". In: *Extracellular Vesicles in Health and Disease*. Oxon, UK: Pan Stanford Publishing, May 2014, pp. 139–157.

[58] P. Poncelet et al., *Tips and tricks for flow cytometry-based analysis and counting of microparticles.* Transfusion and apheresis science, 53 (2) **2015**, pp. 110–126.

[59] B. György et al., *Detection and isolation of cell-derived microparticles are compromised by protein complexes resulting from shared biophysical parameters.* Blood, 117 (4) **2011**, e39–48.

[60] Y. Yuana and S. Osanto, "Atomic Force Microscopy Measurement of Extracellular Vesicles Derived from Plasma". In: *Extracellular Vesicles in Health and Disease*. Oxon, UK: Pan Stanford Publishing, May 2014, pp. 223–234.

[61] R. Szatanek et al., *Isolation of extracellular vesicles: Determining the correct approach (Review)*. International Journal of Molecular Medicine, 36 (1) **2015**, pp. 11–17.

[62] S. Z. Lewin, *Centrifuges*. Journal of Chemical Education, 36 (5) **1959**, A269.

[63] PolysciencesInc., *Microspheres & Particles Handling guide*. Tech. rep., p. 16.

[64] E. van der Pol, T. van Leeuwen, and R. Nieuwland, "An Overview of Novel and Conventional Methods to Detect Extracellular Vesicles". In: *Extracellular Vesicles in Health and Disease*. Oxon, UK: Pan Stanford Publishing, May 2014, pp. 107–138.

[65] F. Angelot et al., *Endothelial cell-derived microparticles induce plasmacytoid dendritic cell maturation: potential implications in inflammatory diseases.* Haematologica, 94 (11) **2009**, pp. 1502–12.

[66] E. Dey-Hazra et al., *Detection of circulating microparticles by flow cytometry: influence of centrifugation, filtration of buffer, and freezing.* Vascular health and risk management, 6 **2010**, pp. 1125–33.

[67] V. Suštar et al., *Nanoparticles isolated from blood: a reflection of vesiculability of blood cells during the isolation process.* International journal of nanomedicine, 6 **2011**, pp. 2737–48.

[68] R. Linares et al., *High-speed centrifugation induces aggregation of extracellular vesicles*. Journal of Extracellular Vesicles, 4 **2015**, p. 29509.

[69] D. Wang and W. Sun, *Urinary extracellular microvesicles: isolation methods and prospects for urinary proteome.* Proteomics, 14 (16) **2014**, pp. 1922–32.

[70] R. Cantin et al., *Discrimination between exosomes and HIV-1: purification of both vesicles from cell-free supernatants.* Journal of immunological methods, 338 (1-2) **2008**, pp. 21–30.

[71] Y. Yuana et al., *Co-isolation of extracellular vesicles and high-density lipoproteins using density gradient ultracentrifugation.* Journal of extracellular vesicles, 3 **2014**, p. 23262.

[72] D. Gheldof et al., *Microparticle bearing tissue factor: A link between promyelocytic cells and hypercoagulable state.* Thrombosis research, 133 **2013**, pp. 433–439.

[73] Y. Sato-Kuwabara et al., *The fusion of two worlds: Non-coding RNAs and extracellular vesicles - diagnostic and therapeutic implications (Review).* International journal of oncology, 46 (1) **2015**, pp. 17–27.

[74] M. H. Nielsen et al., *A flow cytometric method for characterization of circulating cell-derived microparticles in plasma.* Journal of extracellular vesicles, 3 **2014**, p. 20795.

[75] M. L. Merchant et al., *Microfiltration isolation of human urinary exosomes for characterization by MS*. Proteomics – Clinical Applications, 4 (1) **2010**, pp. 84–96.

[76] D. D. Taylor, K. S. Lyons, and C. Gerçel-Taylor, *Shed membrane fragment-associated markers for endometrial and ovarian cancers.* Gynecologic oncology, 84 (3) **2002**, pp. 443–448.

[77] W. L. Dean et al., *Proteomic and functional characterisation of platelet microparticle size classes.* Thrombosis and haemostasis, 102 (4) **2009**, pp. 711–718.

[78] C. Gercel-Taylor et al., *Nanoparticle analysis of circulating cell-derived vesicles in ovarian cancer patients.* Analytical biochemistry, 428 (1) **2012**, pp. 44–53.

[79] M. T. Aatonen et al., *Isolation and characterization of platelet-derived extracellular vesicles*. en. Journal of Extracellular Vesicles, 3 **2014**, p. 24692.

[80] AmershamBioscicences, *Gel Filtration Principles and methods*. 2002.

[81] A. N. Böing et al., *Single-step isolation of extracellular vesicles by size-exclusion chromatography*. en. Journal of Extracellular Vesicles, 3 **2014**, p. 23430.

[82] L. Grasso et al., *Molecular screening of cancer-derived exosomes by surface plasmon resonance spectroscopy.* Analytical and bioanalytical chemistry, 407 (18) **2015**, pp. 5425–32.

[83] J. L. Welton et al., *Ready-made chromatography columns for extracellular vesicle isolation from plasma*. en. Mar. 2015.

[84] M. P. Oksvold, A. Neurauter, and K. W. Pedersen, *Magnetic bead-based isolation of exosomes.* Methods in molecular biology, 1218 **2015**, pp. 465–481.

[85] F. Gieseler et al., *Using annexin V-coated magnetic beads to capture active tissue factor-bearing microparticles from body fluids.* Cell biology international, 38 (2) **2014**, pp. 277–81.

[86] A. Arakelyan et al., *Antigenic composition of single nano-sized extracellular blood vesicles.* Nanomedicine : nanotechnology, biology, and medicine, 11 (3) **2014**, pp. 489–498.

[87] J. Wang, *The Novel Methods for Analysis of Exosomes Released from Endothelial Cells and Endothelial Progenitor Cells* **2016**.

[88] A. Liga et al., *Exosome isolation: a microfluidic road-map*. en. Lab Chip, 15 (11) **2015**, pp. 2388–2394.

[89] A. J. Laki et al., *Separation of Microvesicles from Serological Samples Using Deterministic Lateral Displacement Effect*. BioNanoScience, 5 (1) **2014**, pp. 48–54.

[90] A. J. Laki et al., "Microvesicle fractionation using deterministic lateral displacement effect". In: *The 9th IEEE International Conference on Nano/Micro Engineered and Molecular Systems (NEMS)*. IEEE, Apr. 2014, pp. 490–493.

[91] Z. Wang et al., *Ciliated micropillars for the microfluidic-based isolation of nanoscale lipid vesicles.* en. Lab on a chip, 13 (15) **2013**, pp. 2879–82.

[92] K. Lee et al., *Acoustic purification of extracellular microvesicles.* EN. ACS nano, 9 (3) **2015**, pp. 2321–7.

[93] M. Evander et al., *Non-contact acoustic capture of microparticles from small plasma volumes.* Lab on a chip, 15 (12) **2015**, pp. 2588–2596.

[94] R. T. Davies et al., *Microfluidic filtration system to isolate extracellular vesicles from blood.* en. Lab on a chip, 12 (24) **2012**, pp. 5202–5210.

[95] C. Chen et al., *Microfluidic isolation and transcriptome analysis of serum microvesicles.* Lab on a chip, 10 (4) **2010**, pp. 505–511.

[96] C. Chen et al., *Paper-based immunoaffinity devices for accessible isolation and characterization of extracellular vesicles*. English. Microfluidics and Nanofluidics, 16 (5) **2014**, pp. 849–856.

[97] B. A. Ashcroft et al., *Determination of the size distribution of blood microparticles directly in plasma using atomic force microscopy and microfluidics.* Biomedical microdevices, 14 (4) **2012**, pp. 641–9.

[98] H. Shao et al., *Chip-based analysis of exosomal mRNA mediating drug resistance in glioblastoma.* en. Nature communications, 6 **2015**, p. 6999.

[99] E. van der Pol et al., *Innovation in detection of microparticles and exosomes.* Journal of thrombosis and haemostasis, 11 Suppl 1 (1) **2013**, pp. 36–45.

[100] A. L. S. Revenfeld et al., *Diagnostic and prognostic potential of extracellular vesicles in peripheral blood.* Clinical therapeutics, 36 (6) **2014**, pp. 830–846.

[101] V. Sunkara, H.-K. Woo, and Y.-K. Cho, *Emerging techniques in the isolation and characterization of extracellular vesicles and their roles in cancer diagnostics and prognostics.* The Analyst, 141 (2) **2015**, pp. 371–381.

[102] S. De Carlo and J. R. Harris, *Negative staining and cryo-negative staining of macromolecules and viruses for TEM*. Micron, 42 (2) **2011**, pp. 117–131.

[103] D. Gheldof et al., *Thrombin generation assay and transmission electron microscopy: a useful combination to study tissue factor-bearing microvesicles*. en. 2013.

[104] J. Habel et al., *Selecting analytical tools for characterization of polymersomes in aqueous solution*. en. RSC Adv., 5 (97) **2015**, pp. 79924–79946.

[105] L. Issman et al., *Cryogenic transmission electron microscopy nanostructural study of shed microparticles.* PloS one, 8 (12) **2013**, e83680.

[106] E. van der Pol et al., *Particle size distribution of exosomes and microvesicles determined by transmission electron microscopy, flow cytometry, nanoparticle tracking analysis, and resistive pulse sensing*. Journal of Thrombosis and Haemostasis, 12 (7) **2014**, pp. 1182–1192.

[107] C. A. Siedlecki et al., *Platelet-derived microparticles on synthetic surfaces observed by atomic force microscopy and fluorescence microscopy*. Biomaterials, 20 (16) **1999**, pp. 1521–1529.

[108] J. A. Hessler et al., *Atomic force microscopy study of early morphological changes during apoptosis.* Langmuir, 21 (20) **2005**, pp. 9280–9286.

[109] D. A. Lamprou, V. Venkatpurwar, and M. N. V. R. Kumar, *Atomic force microscopy images label-free, drug encapsulated nanoparticles in vivo and detects difference in tissue mechanical properties of treated and untreated: a tip for nanotoxicology.* PloS one, 8 (5) **2013**, e64490.

[110] J. Grobelny et al., "Size Measurement of Nanoparticles Using Atomic Force Microscopy". In: *Characterization of Nanoparticles Intended for Drug Delivery*. Ed. by E. S. McNeil. Totowa, NJ, USA: Humana Press, 2011, pp. 71–82.

[111] C. A. Putman et al., *Viscoelasticity of living cells allows high resolution imaging by tapping mode atomic force microscopy.* Biophysical journal, 67 (4) **1994**, pp. 1749–53.

[112] ParkSystems, *XE-150 User's Manual Version 1.7*. 2007.

[113] J. Hardij et al., *Characterisation of tissue factor-bearing extracellular vesicles with AFM: comparison of air-tapping-mode AFM and liquid Peak Force AFM*. en. Aug. 2013.

[114] X. Zhang, Y. Chen, and Y. Chen, *An AFM-based pit-measuring method for indirect measurements of cell-surface membrane vesicles.* Biochemical and biophysical research communications, 446 (1) **2014**, pp. 375–9.

[115] S. Sharma et al., *Structural-mechanical characterization of nanoparticle exosomes in human saliva, using correlative AFM, FESEM, and force spectroscopy.* ACS nano, 4 (4) **2010**, pp. 1921–1926.

[116] T. A. Shtam et al., *Exosomes are natural carriers of exogenous siRNA to human cells in vitro*. Cell Communication and Signaling, 11 (1) **2013**, p. 88.

[117] A. Nicolet et al., *Inter-laboratory comparison on the size and stability of monodisperse and bimodal synthetic reference particles for standardization of extracellular vesicle measurements*. en. Measurement Science and Technology, 27 (3) **2016**, p. 035701.

[118] D. Gabriel et al., "Light- Scattering Methods to Characterize Extracellular Vesicles". In: *Extracellular Vesicles in Health and Disease*. Oxon, UK: Pan Stanford Publishing, May 2014, pp. 235–260.

[119] S. K. Brar and M. Verma, *Measurement of nanoparticles by light-scattering techniques*. TrAC Trends in Analytical Chemistry, 30 (1) **2011**, pp. 4–17.

[120] A. S. Lawrie et al., *Microparticle sizing by dynamic light scattering in fresh-frozen plasma.* Vox sanguinis, 96 (3) **2009**, pp. 206–212.

[121] C. Gardiner and R. Dragovic, "Nanoparticle Tracking Analysis". In: *Extracellular Vesicles in Health and Disease*. Oxon, UK: Pan Stanford Publishing, May 2014, pp. 261–283.

[122] Malvern, *NTA: Principles and Methodology (white paper)*. Tech. rep. Malvern Instruments Limited, 2015, p. 239.

[123] Malvern, *NanoSight LM10*. 2016.

[124] C. Gardiner et al., *Extracellular vesicle sizing and enumeration by nanoparticle tracking analysis.* Journal of extracellular vesicles, 2 **2013**, p. 19671.

[125] E. van der Pol, *Refractive Index Determination of Nanoparticles in Suspension Using Nanoparticle Tracking Analysis*. Nano letters, 14 (11) **2014**, pp. 6195–6201.

[126] E. van der Pol et al., *Optical and non-optical methods for detection and characterization of microparticles and exosomes.* Journal of thrombosis and haemostasis, 8 (12) **2010**, pp. 2596–607.

[127] R. van der Meel et al., *Toward routine detection of extracellular vesicles in clinical samples*. International Journal of Laboratory Hematology, 36 (3) **2014**, pp. 244–253.

[128] D. K. Jeppesen et al., *Comparative analysis of discrete exosome fractions obtained by differential centrifugation.* Journal of extracellular vesicles, 3 **2014**, p. 25011.

[129] F. A. W. Coumans et al., *Reproducible extracellular vesicle size and concentration determination with tunable resistive pulse sensing*. en. Journal of Extracellular Vesicles, 3 **2014**, p. 25922.

[130] S. L. N. Maas et al., *Possibilities and limitations of current technologies for quantification of biological extracellular vesicles and synthetic mimics.* Journal of controlled release, 200 **2015**, pp. 87–96.

[131] Izon Science Ltd, *Webinar: Characterizing Extracellular Vesicles from Biological Fluids*. 2016.

[132] E. L. C. J. Blundell, R. Vogel, and M. Platt, *Particle-by-Particle Charge Analysis of DNA-Modified Nanoparticles Using Tunable Resistive Pulse Sensing.* Langmuir, 32 (4) **2016**, pp. 1082–90.

[133] Z. Varga et al., *Towards traceable size determination of extracellular vesicles.* Journal of extracellular vesicles, 3 **2014**, p. 23289.

[134] M. D. Shah et al., *Flow cytometric measurement of microparticles: pitfalls and protocol modifications.* en. Platelets, 19 (5) **2008**, pp. 365–372.

[135] R. Lacroix et al., "Flow Cytometry". In: *Extracellular Vesicles in Health and Disease*. Oxon, UK: Pan Stanford Publishing, May 2014, pp. 201–222.

[136] E. Crompot et al., *Avoiding False Positive Antigen Detection by Flow Cytometry on Blood Cell Derived Microparticles: The Importance of an Appropriate Negative Control.* PloS one, 10 (5) **2015**, e0127209.

[137] J.-M. Freyssinet and F. Toti, *Membrane microparticle determination: at least seeing what's being sized!* Journal of thrombosis and haemostasis, 8 (2) **2010**, pp. 311–4.

[138] H. S. Leong et al., *Validation of flow cytometric detection of platelet microparticles and liposomes by atomic force microscopy.* Journal of thrombosis and haemostasis, 9 (12) **2011**, pp. 2466–76.

[139] S. Robert et al., *Standardization of platelet-derived microparticle counting using calibrated beads and a Cytomics FC500 routine flow cytometer: a first step towards multicenter studies?* Journal of thrombosis and haemostasis, 7 (1) **2009**, pp. 190–7.

[140] E. Shantsila et al., *Circulating microparticles: challenges and perspectives of flow cytometric assessment.* Thrombosis and haemostasis, 111 (6) **2014**, pp. 1009–14.

[141] C. Göhner et al., *A New Enzyme-linked Sorbent Assay (ELSA) to Quantify Syncytiotrophoblast Extracellular Vesicles in Biological Fluids.* American journal of reproductive immunology, 73 (6) **2015**, pp. 582–588.

[142] S. G. Patching, *Surface plasmon resonance spectroscopy for characterisation of membrane protein–ligand interactions and its potential for drug discovery*. Biochimica et Biophysica Acta (BBA) - Biomembranes, 1838 (1, Part A) **2014**, pp. 43–55.

[143] D. L. M. Rupert et al., *Determination of exosome concentration in solution using surface plasmon resonance spectroscopy.* Analytical chemistry, 86 (12) **2014**, pp. 5929–5936.

[144] L. Zhu et al., *Label-Free Quantitative Detection of Tumor-Derived Exosomes through Surface Plasmon Resonance Imaging*. Analytical Chemistry, 86 (17) **2014**, pp. 8857–8864.

[145] H. Im et al., *Label-free detection and molecular profiling of exosomes with a nano-plasmonic sensor.* Nature biotechnology, 32 (5) **2014**, pp. 490–495.

[146] N. Koliha et al., *A novel multiplex bead-based platform highlights the diversity of extracellular vesicles*. en. Journal of Extracellular Vesicles, 5 **2016**, p. 29975.

[147] M. Jørgensen et al., *Extracellular Vesicle (EV) Array: microarray capturing of exosomes and other extracellular vesicles for multiplexed phenotyping.* Journal of extracellular vesicles, 2 **2013**, p. 20920.

[148] M. M. Jørgensen, R. Bæk, and K. Varming, *Potentials and capabilities of the Extracellular Vesicle (EV) Array.* Journal of extracellular vesicles, 4 **2015**, p. 26048.

[149] P. Gagni et al., *Combined mass quantitation and phenotyping of intact extracellular vesicles by a microarray platform.* Analytica chimica acta, 902 **2016**, pp. 160–7.

[150] T. Akagi et al., *On-chip immunoelectrophoresis of extracellular vesicles released from human breast cancer cells.* PloS one, 10 (4) **2015**, e0123603.

[151] Z. Zhao et al., *A microfluidic ExoSearch chip for multiplexed exosome detection towards blood-based ovarian cancer diagnosis*. Lab on a Chip, 16 (3) **2016**, pp. 489–496.

[152] T. Mahmood and P.-C. Yang, *Western blot: technique, theory, and trouble shooting.* North American journal of medical sciences, 4 (9) **2012**, pp. 429–434.

[153] E. Milbank et al., *Microparticles from apoptotic RAW 264.7 macrophage cells carry tumour necrosis factor-a functionally active on cardiomyocytes from adult mice*. en. Oct. 2015.

[154] N. S. Barteneva et al., *Circulating microparticles: square the circle.* BMC cell biology, 14 **2013**, p. 23.

[155] M. He et al., *Integrated immunoisolation and protein analysis of circulating exosomes using microfluidic technology.* Lab on a chip, 14 (19) **2014**, pp. 3773–80.

[156] A. L. Capriotti et al., *Proteomic characterization of human platelet-derived microparticles.* Analytica chimica acta, 776 **2013**, pp. 57–63.

[157] O. Østergaard et al., *Quantitative Proteome Profiling of Normal Human Circulating Microparticles*. Journal of Proteome Research, 11 (4) **2012**, pp. 2154–2163.

[158] O. Østergaard et al., *Unique Protein Signature of Circulating Microparticles in Systemic Lupus Erythematosus*. Arthritis & Rheumatism, 65 (10) **2013**, pp. 2680–2690.

[159] P. Diehl et al., *Microparticles: major transport vehicles for distinct microRNAs in circulation.* Cardiovascular research, 93 (4) **2012**, pp. 633–44.

[160] R. J. Simpson, H. Kalra, and S. Mathivanan, *ExoCarta as a resource for exosomal research*. Journal of Extracellular Vesicles, 1 **2012**, p. 18374.

[161] S. Mathivanan and R. J. Simpson, *ExoCarta: A compendium of exosomal proteins and RNA*. PROTEOMICS, 9 (21) **2009**, pp. 4997–5000.

[162] S. Mathivanan et al., *ExoCarta 2012: database of exosomal proteins, RNA and lipids*. Nucleic Acids Research **2011**, pp. 1–4.

[163] S. Keerthikumar et al., *ExoCarta: A Web-Based Compendium of Exosomal Cargo*. Journal of Molecular Biology, 428 (4) **2016**, pp. 688–692.

[164] B. Woodhams, "Procoagulant Assays". In: *Extracellular Vesicles in Health and Disease*. Oxon, UK: Pan Stanford Publishing, May 2014, pp. 159–180.

[165] J. Amiral, "Capture- Based Assays for Extracellular Vesicles within the Blood". In: *Extracellular Vesicles in Health and Disease*. Oxon, UK: Pan Stanford Publishing, May 2014, pp. 181–199.

[166] J. Amiral and J. Seghatchian, *The diagnostic usefulness of capture assays for measuring global/specific extracellular micro-particles in plasma.* Transfusion and apheresis science, 53 (2) **2015**, pp. 127–36.

[167] K. Aupeix et al., *The significance of shed membrane particles during programmed cell death in vitro, and in vivo, in HIV-1 infection.* Journal of Clinical Investigation, 99 (7) **1997**, pp. 1546–1554.

[168] C. F. Reich and D. S. Pisetsky, *The content of DNA and RNA in microparticles released by Jurkat and HL-60 cells undergoing in vitro apoptosis.* Experimental cell research, 315 (5) **2009**, pp. 760–8.

[169] A. J. Ullal and D. S. Pisetsky, *The release of microparticles by Jurkat leukemia T cells treated with staurosporine and related kinase inhibitors to induce apoptosis.* Apoptosis, 15 (5) **2010**, pp. 586–96.

[170] J. Simák, K. Holada, and J. G. Vostal, *Release of annexin V-binding membrane microparticles from cultured human umbilical vein endothelial cells after treatment with camptothecin.* BMC cell biology, 3 **2002**, p. 11.

[171] M. L. Heinemann et al., *Benchtop isolation and characterization of functional exosomes by sequential filtration.* Journal of chromatography. A, 1371C **2014**, pp. 125–135.

[172] ATCC, *CRL-1730 morphology and culture condition*. 2014.

[173] J. Kabir, M. Lobo, and I. Zachary, *Staurosporine induces endothelial cell apoptosis via focal adhesion kinase dephosphorylation and focal adhesion disassembly independent of focal adhesion kinase proteolysis*. en. Biochemical Journal, 367 (1) **2002**, pp. 145–155.

[174] M. Heller et al., *The effect of extracellular matrix proteins on the cellular response of HUVECS and HOBS after covalent immobilization onto titanium.* Journal of biomedical materials research. Part A, 103 (6) **2015**, pp. 2035–44.

[175] I. F. Amaral et al., *Fibronectin-mediated endothelialisation of chitosan porous matrices.* Biomaterials, 30 (29) **2009**, pp. 5465–75.

[176] S. Johansson, *Fibronectin-integrin interactions*. Frontiers in Bioscience : a Journal and Virtual Library, 2 **1997**, pp. 126–146.

[177] K. Tashiro et al., *The RGD containing site of the mouse laminin A chain is active for cell attachment, spreading, migration and neurite outgrowth.* Journal of cellular physiology, 146 (3) **1991**, pp. 451–9.

[178] A. S. Shet, *Characterizing blood microparticles: technical aspects and challenges.* Vascular health and risk management, 4 (4) **2008**, pp. 769–774.

[179] M. C. Larson et al., *Calcium-phosphate microprecipitates mimic microparticles when examined with flow cytometry.* Cytometry. Part A, 83 (2) **2013**, pp. 242–250.

[180] E. Cocucci, G. Racchetti, and J. Meldolesi, *Shedding microvesicles: artefacts no more.* Trends in cell biology, 19 (2) **2009**, pp. 43–51.

[181] A. S. Leroyer et al., *Endothelial-derived microparticles: Biological conveyors at the crossroad of inflammation, thrombosis and angiogenesis.* Thrombosis and haemostasis, 104 (3) **2010**, pp. 456–63.

[182] B. Laffont et al., *Activated platelets can deliver mRNA regulatory Ago2 microRNA complexes to endothelial cells via microparticles.* Blood, 122 (2) **2013**, pp. 253–61.

[183] E. I. Buzas et al., *Emerging role of extracellular vesicles in inflammatory diseases.* Nature reviews. Rheumatology, 10 (6) **2014**, pp. 356–64.

[184] J. Gong et al., *Microparticles in Cancer: A Review of Recent Developments and the Potential for Clinical Application*. Seminars in Cell & Developmental Biology, 40 **2015**, pp. 35–40.

[185] L. Ayers et al., *Measurement of circulating cell-derived microparticles by flow cytometry: Sources of variability within the assay*. Thrombosis Research, 127 (4) **2011**, pp. 370–377.

[186] W. L. Chandler, W. Yeung, and J. F. Tait, *A new microparticle size calibration standard for use in measuring smaller microparticles using a new flow cytometer.* Journal of thrombosis and haemostasis, 9 (6) **2011**, pp. 1216–24.

[187] G. N. Chironi et al., *Endothelial microparticles in diseases.* Cell and tissue research, 335 (1) **2009**, pp. 143–51.

[188] C. M. Boulanger, N. Amabile, and A. Tedgui, *Circulating microparticles: a potential prognostic marker for atherosclerotic vascular disease.* Hypertension, 48 (2) **2006**, pp. 180–186.

[189] M. P. Gelderman and J. Simak, *Flow cytometric analysis of cell membrane microparticles.* Methods in molecular biology, 484 **2008**, pp. 79–93.

[190] N. Rozlosnik, M. C. Gerstenberg, and N. B. Larsen, *Effect of Solvents and Concentration on the Formation of a Self-Assembled Monolayer of Octadecylsiloxane on Silicon (001)*. Langmuir, 19 (4) **2003**, pp. 1182–1188.

[191] C. Gardiner et al., *Extracellular vesicles, tissue factor, cancer and thrombosis - discussion themes of the ISEV 2014 Educational Day.* Journal of extracellular vesicles, 4 **2015**, p. 26901.

[192] E. Fernandes et al., *A bacteriophage detection tool for viability assessment of Salmonella cells.* Biosensors & bioelectronics, 52 **2014**, pp. 239–46.

[193] S. S. Martins et al., "Waterborne Pathogen Detection Using a Magnetoresistive Immuno-Chip". English. In: *Molecular Biological Technologies for Ocean Sensing SE - 13*. Ed. by S. M. Tiquia-Arashiro. Springer Protocols Handbooks. New York City, NY, USA: Humana Press, 2012, pp. 263–288.

[194] A. M. Rieger et al., *Modified annexin V/propidium iodide apoptosis assay for accurate assessment of cell death.* Journal of visualized experiments, (50) **2011**, e2597.

[195] K. S. Kim et al., *AFM-detected apoptotic changes in morphology and biophysical property caused by paclitaxel in Ishikawa and HeLa cells.* PloS one, 7 (1) **2012**, e30066.

[196] N. G. Ordóñez, *Immunohistochemical endothelial markers: a review.* Advances in anatomic pathology, 19 (5) **2012**, pp. 281–95.

[197] N. Bardin, *Identification of CD146 as a component of the endothelial junction involved in the control of cell-cell cohesion*. en. Blood, 98 (13) **2001**, pp. 3677–3684.

[198] R. G. Bagley et al., *Endothelial precursor cells as a model of tumor endothelium: characterization and comparison with mature endothelial cells.* Cancer research, 63 (18) **2003**, pp. 5866–5873.

[199] R. Bertrand et al., *Induction of a common pathway of apoptosis by staurosporine.* Experimental cell research, 211 (2) **1994**, pp. 314–321.

[200] G. Vilas Shelke et al., *Importance of exosome depletion protocols to eliminate functional and RNA-containing extracellular vesicles from fetal bovine serum*. Journal of Extracellular Vesicles, 3 **2014**, p. 24783.

[201] J. Castillo-León, "Microfluidics and Lab-on-a-Chip Devices: History and Challenges". In: *Lab-on-a-Chip Devices and Micro-Total Analysis Systems: A Practical Guide*. Ed. by J. Castillo-León and E. W. Svendsen. Cham, Switzerland: Springer International Publishing, 2015, pp. 1–15.

[202] J. P. Brody and P. Yager, *Diffusion-based extraction in a microfabricated device*. Sensors and Actuators A: Physical, 58 (1) **1997**, pp. 13–18.

[203] K. K. Fleming Glass, E. K. Longmire, and A. Hubel, *Optimzation of a microfluidic device for diffusion-based extraction of DMSO from a cell suspension.* International journal of heat and mass transfer, 51 (23-24) **2008**, pp. 5749–5757.

[204] V. Arima, P. Watts, and G. Pascali, "Microfluidics in Planar Microchannels: Synthesis of Chemical Compounds On-Chip". In: *Lab-on-a-Chip Devices and Micro-Total Analysis Systems: A Practical Guide*. Ed. by J. Castillo-León and E. W. Svendsen. Cham, Switzerland: Springer International Publishing, 2015, pp. 197–239.

[205] W. E. Svendsen, "Basic Microfluidics Theory". In: *Lab-on-a-Chip Devices and Micro-Total Analysis Systems: A Practical Guide*. Ed. by J. Castillo-León and E. W. Svendsen. Cham, Switzerland: Springer International Publishing, 2015, pp. 17–26.

[206] H. Bruus, *Theoretical microfluidics*. Oxford, UK: Oxford University Press, 2007.

[207] N. N.-T. Nguyen and S. T. Wereley, *Fundamentals and applications of microfluidics*. London, UK: Artech House, 2002, p. 471.

[208] J. P. Beech, "Microfluidics separation and analysis of biological particles". phd. Lund University, Lund, Sweden, 2011.

[209] J. P. Brody et al., *Biotechnology at low Reynolds numbers.* Biophysical journal, 71 (6) **1996**, pp. 3430–3441.

[210] M. R. Holl et al., *Optimal design of a microfabricated diffusion-based extraction device*. American Society of Mechanical Engineers, 59 **1996**, pp. 189–196.

[211] M. Dimaki, "Design and Simulation of Lab-on-a-Chip Devices". In: *Lab-on-a-chip Devices and Micro-total Analysis Systems*. Ed. by J. Castillo-León and W. E. Svendsen. Heidelberg, Germany: Springer International Publishing, 2015, pp. 27–51.

[212] H. P. Erickson, *Size and shape of protein molecules at the nanometer level determined by sedimentation, gel filtration, and electron microscopy.* Biological procedures online, 11 **2009**, pp. 32–51.

[213] S. Hossain, M. Ansari, and K.-Y. Kim, *Evaluation of the mixing performance of three passive micromixers*. Chemical Engineering Journal, 150 (2-3) **2009**, pp. 492–501.

[214] C.-Y. Lee et al., *Microfluidic mixing: a review.* International journal of molecular sciences, 12 (5) **2011**, pp. 3263–87.

[215] A. Pfreundt et al., *An easy-to-use microfluidic interconnection system to create quick and reversibly interfaced simple microfluidic devices*. en. Journal of Micromechanics and Microengineering, 25 (11) **2015**, p. 115010.

[216] P.-C. Chen et al., *An experimental study of micromilling parameters to manufacture microchannels on a PMMA substrate*. The International Journal of Advanced Manufacturing Technology, 71 (9-12) **2014**, pp. 1623–1630.

[217] I. R. G. Ogilvie et al., *Reduction of surface roughness for optical quality microfluidic devices in PMMA and COC*. en. Journal of Micromechanics and Microengineering, 20 (6) **2010**, p. 065016.

[218] L. Uriarte, J. Eguia, and F. Egaña, "Micromilling Machines". In: *Machine Tools for High Performance Machining*. Ed. by L. N. López de Lacalle and A. Lamikiz. London, UK: Springer, 2009, pp. 369–397.

[219] I. Ogilvie et al., "Solvent processing of PMMA and COC chips for bonding devices with optical quality surfaces". In: *14th International Conference on Miniaturized Systems for Chemistry and Life Sciences*. The Printing House for Chemical and Biological Microsystems Society, Oct. 2010.

[220] I. R. G. Ogilvie et al., *Solvent vapor bonding and surface treatment methods*. Nov. 2012.

[221] Thermo Fisher Scientific, *Protein Absorbance Measurements using the Thermo Scientific NanoDrop™ 2000/2000c Spectrophotometers*. Tech. rep. 2009, p. 1.

[222] Thermo Fisher Scientific, *Protein Measurement Accuracy and Reproducibility*. Tech. rep. 2010, p. 1.

[223] G. D. Kipling, S. J. Haswell, and N. J. Brown, "A Considered Approach to Lab-on-a-Chip Fabrication". In: *Lab-on-a-Chip Devices and Micro-Total Analysis Systems: A Practical Guide*. Ed. by J. Castillo-León and E. W. Svendsen. Cham, Switzerland: Springer International Publishing, 2015, pp. 53–82.

[224] A. P. F. Turner, *Biosensors: sense and sensibility.* en. Chemical Society reviews, 42 (8) **2013**, pp. 3184–3196.

[225] S. Cherré and N. Rozlosnik, "Polymer Based Biosensors for Medical Applications". In: *Advanced Polymers in Medicine*. Ed. by F. Puoci. Cham, Switzerland: Springer International Publishing, 2015. Chap. 17, pp. 513–537.

[226] D. L. Graham, H. A. Ferreira, and P. P. Freitas, *Magnetoresistive-based biosensors and biochips.* Trends in biotechnology, 22 (9) **2004**, pp. 455–62.

[227] P. P. Freitas et al., *Magnetoresistive sensors*. Journal of Physics: Condensed Matter, 19 (16) **2007**, p. 165221.

[228] J. Germano et al., *A portable and autonomous magnetic detection platform for biosensing*. en. Sensors, 9 (6) **2009**, pp. 4119–4137.

[229] P. P. Freitas et al., *Spintronic platforms for biomedical applications.* en. Lab on a chip, 12 (3) **2012**, pp. 546–557.

[230] V. C. Martins et al., *Challenges and trends in the development of a magnetoresistive biochip portable platform*. Journal of Magnetism and Magnetic Materials, 322 (9-12) **2010**, pp. 1655–1663.

[231] H. Ferreira et al., *Detection of cystic fibrosis related DNA targets using AC field focusing of magnetic labels and spin-valve sensors*. IEEE Transactions on Magnetics, 41 (10) **2005**, pp. 4140–4142.

[232] V. C. Martins et al., *Femtomolar limit of detection with a magnetoresistive biochip.* Biosensors & bioelectronics, 24 (8) **2009**, pp. 2690–2695.

[233] E. Fernandes et al., "Development of a multiplexed system for ischemic stroke using a magnetoresistive (MR) biochip platform". In: *nanoPT 2016 - NanoPortugal International Conference*. Braga, Portugal, 2016.

[234] J. F. Tait and D. Gibson, *Phospholipid binding of annexin V: Effects of calcium and membrane phosphatidylserine content*. Archives of biochemistry and biophysics, 298 (1) **1992**, pp. 187–91.

[235] U. Trahtemberg et al., *Calcium, leukocyte cell death and the use of annexin V: fatal encounters.* Apoptosis : an international journal on programmed cell death, 12 (10) **2007**, pp. 1769–80.

[236] BD Pharmingen, *Technical Data Sheet FITC Annexin V Apoptosis Detection Kit I*. 2008.

[237] Miltenyi Biotec GmbH, *Annexin V MicroBead Kit*. 2012.

[238] C. Tong et al., *An Annexin V-based biosensor for quantitatively detecting early apoptotic cells.* Biosensors & bioelectronics, 24 (6) **2009**, pp. 1777–82.

[239] P.-H. Huang et al., *Increased circulating CD31+/annexin V+ apoptotic microparticles and decreased circulating endothelial progenitor cell levels in hypertensive patients with microalbuminuria.* Journal of hypertension, 28 (8) **2010**, pp. 1655–65.

[240] J.-M. Sinning et al., *Circulating CD31+/Annexin V+ microparticles correlate with cardiovascular outcomes.* European heart journal, 32 (16) **2011**, pp. 2034–41.

[241] Y. Yoshioka et al., *Comparative marker analysis of extracellular vesicles in different human cancer types.* Journal of extracellular vesicles, 2 **2013**.

Part VI

Appendix

Appendix A

Additional data

A.1 Calibration curve for the ELISA assay for the measurement of the CD31 concentration

To measure the expression of CD31 on the surface of the MVs, an ELISA assay was performed. This appendix presents the standard curve obtained for this measurement. The CD31 measurement was presented in the article 1 (see chapter 4 on page 45).

A.1.1 Material and methods

We used a one-step ELISA kit (Abcam, United Kingdom). A standard curve was measured between the concentrations of 4.4 and 50 ng/ml CD31 according to the manufacturer's instructions.

A.1.2 Results

Figure A.1 shows the standard curve for the different concentrations related to the OD_{450} corrected for the blank value. The linear region was limited to the concentrations 4.4 to 22.2 ng/ml CD31 and the corresponding OD_{450} 0.27 to 2.17. The standard curve was fitted with a linear fit to obtain the regression equation used for the samples.

A.2 Measurement of 100 nm polystyrene beads with NTA

The performances of the NTA were verified by the measurement of polystyrene beads of 100 nm in diameter.

A.2.1 Material and methods

Fluoresbrite polystyrene beads of 100 nm in diameter (Polysciences, Inc., USA) were diluted in milliQ water with a dilution factor 10^5. The stock concentration was 2.6% solid which corresponds to $4.73{\times}10^{13}$ beads/ml. The beads suspension was measured by NTA (LM10, Nanosight, United Kingdom) with a camera level of 11 and a threshold of 4. Three videos of 60 s were recorded.

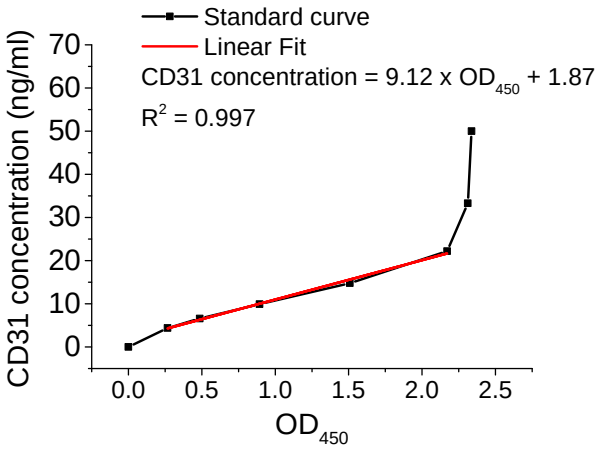

Figure A.1: Standard curve of ELISA assay for the measurement of the CD31 concentration on MVs A CD31 standard was measured between the concentrations of 4.4 and 50 ng/ml. The standard curve was fitted by a linear fit in the linear region, i.e. between 4.4 and 22.2 ng/ml. The linear fit and the corresponding equation are displayed on the figure.

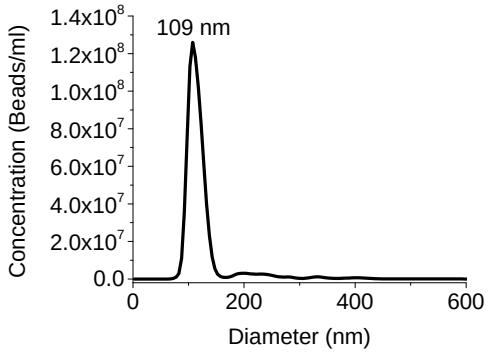

Figure A.2: NTA measurement of 100 nm beads The size distribution shows a main peak around 109 nm.

A.2.2 Results and discussion

Figure A.2 shows the size distribution of a sample of latex beads of 100 nm in diameter measured by NTA. The mean of the three measurements was 124 nm (SD +/- 12.4) and the modes were 116, 103 and 108 nm respectively. The mean concentration was $8.8{\times}10^8$ beads/ml. This was approximately 1.86 times higher than expected.

Due to the difference in refractive indexes between polystyrene beads (1.59-1.60 [63]) and MVs (1.37 [125]) the calibration for the concentration measurement is hampered. A measurement of silica beads would be more appropriate.

A.3 Calibration curves for the measurements of concentration of the polystyrene beads and the IgG

For the development of the H-filter, fluorescently polystyrene beads and IgG antibodies conjugated to FITC were used as representative samples. To measure their concentration after sorting

through the H-filter, it was required to measure a calibration curve to relate the concentration and the fluorescent intensity of each type of analyte.

A.3.1 Material and methods

Dilution series of the Fluoresbrite polystyrene beads (1 µm, 100 and 50 nm, Polysciences, Inc., USA) and of the Anti Rabbit IgG, FITC conjugated (from goat, Sigma Aldrich, Germany) were prepared in PBS with dilution steps of 10. 100 µl of each solutions were dispensed in the wells of a 96 black well plate (flat bottom). Each dilution step was measured in triplicate. The fluorescence intensity was measured with a plate reader (excitation: 485 nm, emission: 535 nm, exposure time: 0.1 s). A blank (PBS) was measured. The corrected fluorescence intensity (fluorescence intensity of the blank subtracted from the fluorescence intensity) was represented over the concentration. After identification of the linear range, a linear fit was calculated using the software OriginPro 9 (OriginLab, USA).

A.3.2 Results

Figure A.3 shows the calibration curves for the fluorescently labelled polystyrene beads with a diameter of 1 µm (figure A.3D), 100 nm (figure A.3C) and 50 nm (figure A.3B), as well as for the FITC conjugated IgG (figure A.3A). In the insets, we show the measurements of the small concentrations. When the concentration is too low the relation between fluorescence intensity and concentration is not linear anymore and the particle concentration cannot be measured properly with this technique. For each analyte the lowest measurable concentration was the lowest concentration of the linear range. The linear fit was calculated only for the particle concentration within the linear range. Table A.1 reports the lowest measurable concentration and the linear regression equation for each analyte.

A.4 Calibration curve for the measurement of the NaCl concentration

The concentration of NaCl diluted in water correlates to the conductivity of the solution. To measure the concentration of the NaCl solutions after sorting throught the filter, we established a calibration curve relating the conductivity to the concentration of NaCl solutions using a home-made conductimeter developed by Julie Kirkegaard.

A.4.1 Material and methods

A chamber for liquid was cut in a PMMA plate using a CO2 laser (Epilog Mini 18, Epilog Laser, USA). The dimensions of the chamber were 8x5 mm^2 and 5 mm deep (total volume: 200 µl). Using double sided tape, it was assembled onto a flat PMMA plate and adhesive conductive tape was fixed on the shorter edges of the chamber. The conductive tape was connected to a potentiostat (IM6, Zahner-elektrik, Germany) via crocodile clamps. Figure A.4A shows a photograph of the conductimeter. A 1% NaCl (Sigma Aldrich, Germany) solution was prepared

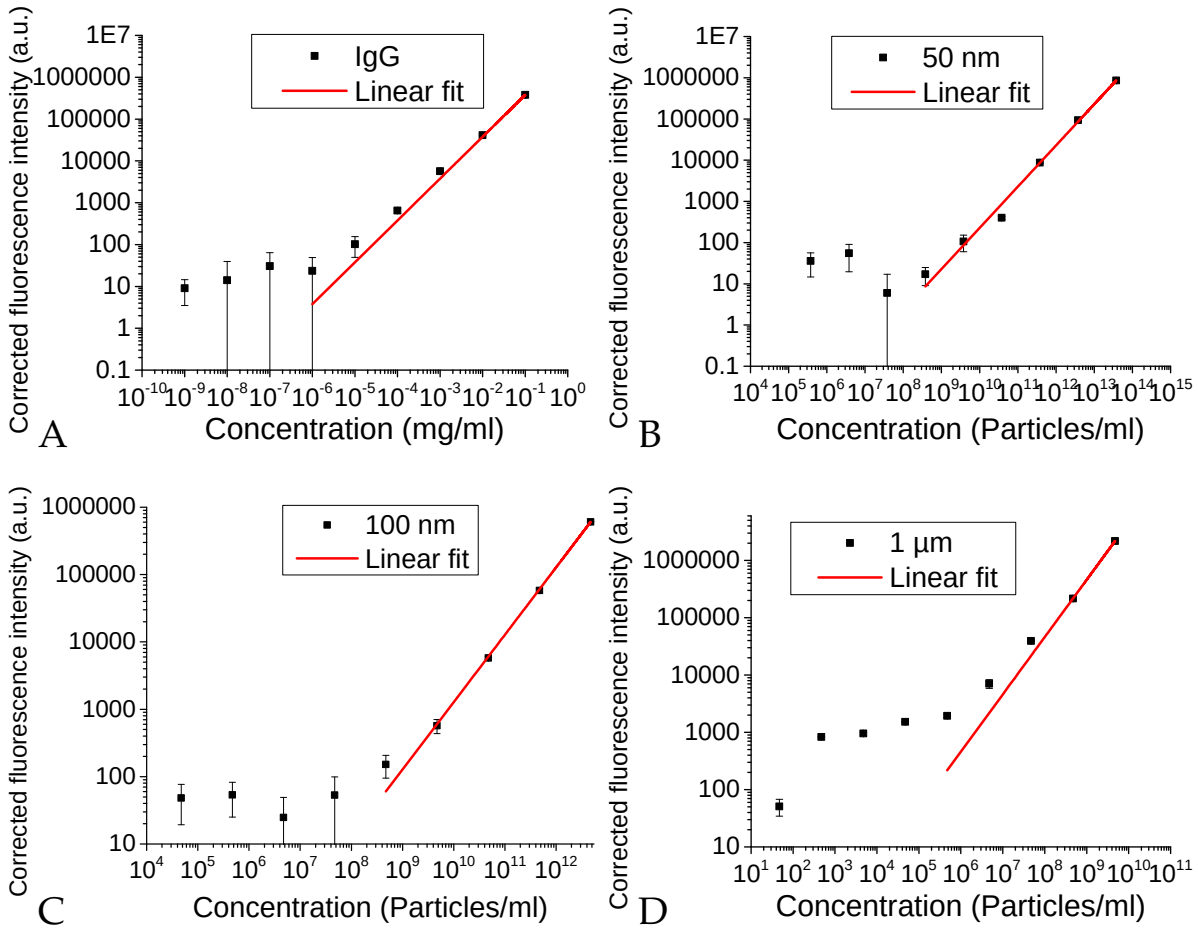

Figure A.3: Calibration curves for the measurement of the beads concentration via fluorescence. Dilution series of the fluorescent polysterene beads were prepared and the fluorescence of each suspension was measured. The linear range was determined and a linear fit was applied. The equations of the linear fit are presented in table A.1.

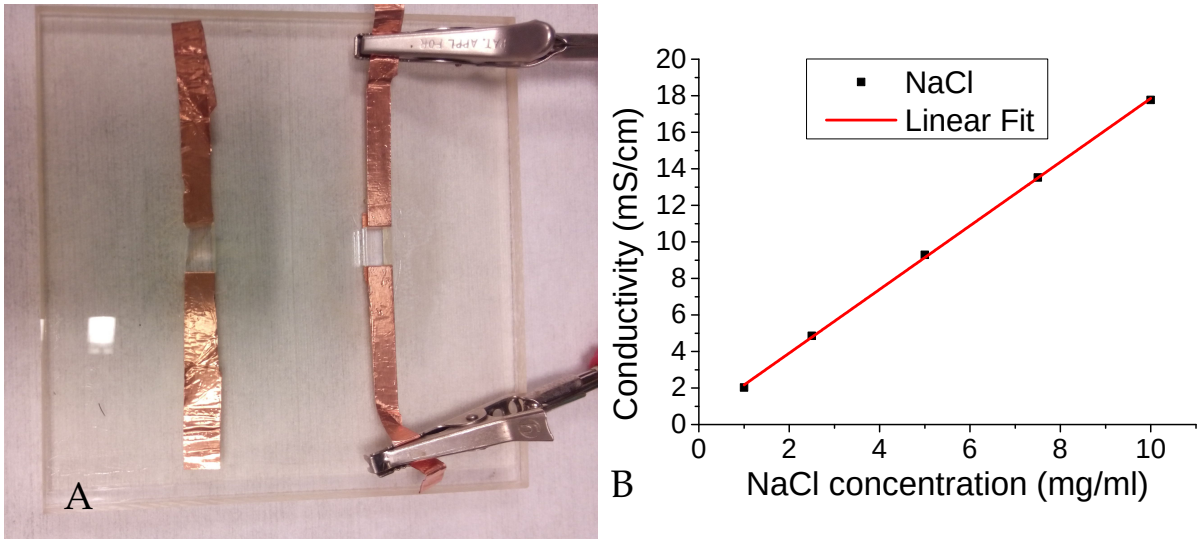

Figure A.4: Conductimeter (figure A) Two chambers (volumes respectively 300 and 200 µl) were cut in a PMMA plate. Adhesive conductive tape was fixed at the shorter edges and was connected to the potentiostat through crocodile clamps. **NaCl calibration curve (figure B**

in milliQ water. Five dilution steps in milliQ water were made. The resistance (R in Ohm) of each solution was measured with the potentiostat and the conductivity (σ in mS/cm) was calculated according to the following formula:

$$\sigma = \frac{\text{length of chamber}}{R \times \text{width} \times \text{depth}} \tag{A.1}$$

A linear fit was calculated (OriginPro 9, OriginLab, USA).

A.4.2 Results

Figure A.4B shows the calibration curve of the NaCl concentration over the conductivity. The conductivity increased linearly with the NaCl concentration in the range of 1% to 0.1% NaCl in milliQ water. A linear fit was calculated and the regression equation is reported in table A.1.

Table A.1: Equations of calibration for the fluorescently labelled particles, the IgG (FITC conjugated) and NaCl. The measurements of dilution series were fitted with a linear fit. For the fluorescence measurements, the intercept was fixed to 0. The table presents the equations of regression with the general formula FI = slope × Concentration with FI the corrected fluorescence intensity, and for NaCl σ = slope × Concentration + intercept with σ the conductivity in mS/cm.

Analyte	slope	intercept	R^2	lowest concentration detectable
NaCl	1.74	0.42	0.99953	1%
IgG	3.77E6	0	0.99987	1×10^{-6} mg/ml
50 nm particles	2.28e-8	0	0.99993	3.78×10^{8} particles/ml
100 nm particles	1.28e-7	0	0.99998	4.73×10^{8} particles/ml
1 µm particles	4.61e-4	0	0.99991	4.73×10^{5} particles/ml

Appendix B

Manuscripts

B.1 Article 1: Generation and characterization of cell-derived microvesicles from HUVECs

This is the original manuscript that has been submitted for publication in International Journal of Molecular Sciences, special issue "Focus on extracellular vesicles".

MDPI

Article

Generation and characterization of cell-derived microvesicles from HUVECs

Solène Cherre [1], Mathilde Granberg[1], Ole Østergaard[2], Niels H. H. Heegaard [2,3] and Noemi Rozlosnik [1]*

[1] Department of Micro- and Nanotechonolgy, Technical University of Denmark, Produktionstorvet 423, 2800 Kgs. Lyngby, Denmark; Noemi.Rozlosnik@nanotech.dtu.dk
[2] Statens Serum Institut, Artillerivej 5, 2300 Copenhagen, Denmark; nhe@ssi.dk
[3] Department of Clinical Biochemistry and Pharmacology, Odense University Hospital, University of Southern Denmark, Søndre Blvd. 29, DK-5000 Odense C, Denmark.
* Noemi.Rozlosnik@nanotech.dtu.dk, telephone +4545255691, fax +4545887762

Academic Editor: name
Version February 22, 2016 submitted to Int. J. Mol. Sci.; Typeset by LaTeX using class file mdpi.cls

Abstract: *Background and aim:* Microvesicles (MV) have gained a large interest in the biomedical field as novel diagnostics biomarkers. However MV research is still impaired by the lack of standardization of the analysis methods. In this study, our goals were to develop a method for the reproducible generation MV population from cell culture as a tool for standardization and validation of novel analysis methods, compare the sizing of MV by atomic force microscopy (AFM) and nanoparticle tracking analysis (NTA) and develop an MV array allowing the sizing and phenotyping of MV simultaneously.
Methods: MV were isolated from apoptotic Human Umbilical Vein Endothelial Cells (HUVECs) by high speed centrifugation. Size and concentration of the MV were characterized by AFM and NTA. The endothelial surface markers were analysed by an enzyme-linked immunosorbent assay (ELISA) and by the newly developed MV array, where MV were captured according to their phenotype and imaged per AFM.
Results: MV isolated from the cells undergoing apoptosis had a mean size of 115 nm as measured by AFM and of 197 nm as measured by NTA. MV isolated from apoptotic and control HUVECs could not be distinguished by their size ($p>0.05$). HUVECs and their released MV shared the same phenotype (positive for the endothelial markers CD31 and CD146 and negative for the platelet marker CD42b).
Conclusion: Our method generated MV with a concentration reproducible within 20% range. This is a relevant model systems for medical applications. The size of the MV was slightly larger as measured per NTA compared to AFM. The MV array proved to be an efficient tool to characterize the surface markers of MV and has the potential to identify the profile of MV in patient samples.

Keywords: cell-derived microvesicles; extracellular vesicles; atomic force microscopy; nanoparticle tracking analysis

1. Introduction

Cell-derived microvesicles (MV), also called cell-derived microparticles are a type of extracellular vesicles discovered in 1967 by Wolf, who named them "platelet dust" [1]. In contrast to exosomes which are formed inside the cells and released by exocytosis [2,3], MV are shed from cells by an outward blebbing of the cell membrane [4]. They are characterized by their diameter ranging from 50 to 1000 nm and the expression of receptors of the cell of origin on their surface. MV

play a central role in the cell-cell communication [5] and in the transfer of signal molecules such as microRNA from cell to cell [6,7].

In the recent years, numerous studies have been published that showed that the concentration of MV in the blood is altered in various pathological conditions such as systemic lupus erythematosus [8] and inflammatory diseases [9]. Therefore it has been proposed that MV could be implemented as novel diagnostics markers [4]. Moreover the analysis of MV could help to provide new insight in the pathogenesis of the diseases [10].

The main method used for MV analysis is flow cytometry, a method where the size and fluorescently stained surface molecules of each object are measured. Flow cytometry is a widely used analysis method with instruments available in most laboratories. However, flow cytometry is limited to measure objects larger than approximately 200 nm. Moreover lack of standadization in the measurement protocol leads to large variation in the results [11]. Therefore, other analysis methods have been developed to better understand and validate the potential of MV as biomarkers. On one hand, attempts have been made to improve the flow cytometry techniques to adapt it to MV such as the use of calibration beads [12,13]. On the other hand, techniques based on light scattering such as dynamic light scattering (DLS) [14] and nanoparticle tracking analysis (NTA) [15] are attractive alternatives for MV measurement. NTA in particular was shown to be more sensitive than flow cytometry and could detect vesicles as small as 50 nm [16]. Imaging methods based on electron microscopy [17] and atomic force microscopy (AFM) [18] have been developed for MV and allow a precise and accurate size and shape determination of MV. The surface proteins of MV can be accurately measured by an enzyme-linked immunosorbent assay (ELISA) and their pro-coagulatant function can be evaluated by a pro-thrombinase assay [19]. However solid phase assay such as ELISA do not deliver information concerning the particle size. Proteomics methods [20] are also available to characterize the protein content of MV. The reader is referred to recent reviews [4,21,22] for a broader overview of the analysis techniques for MV.

The development of new analysis methods for MV requires their test, optimization and validation. For this purpose, standard MV populations are required. Synthetic beads such as polysterene or silica beads have been developed as standards for the calibration of instruments measuring extracellular vesicles [13,23]. However those can only be used for size and concentration calibration. Previous studies used urine MV as standard sample in the comparison of different analysis techniques [24,25]. Using *in vitro* cell lines to release MV is a great tool to obtain defined MV populations harbouring the phenotype, i.e. the surface markers, of the cells of origin. Apoptosis is one of the processes by which the release of MV is induced [26,27] and it can be implemented easily *in vitro* to activate cells. Combes *et al.* were able to activate the MV release from Human Umbilical Vein Endothelial Cells (HUVECs) using tumour necrosis factor-α (TNF-α)[28]. Similarly Šimák *et al.* studied the release of endothelial MV when inducing the apoptosis in HUVECs with camptothecin [29]. Staurosporine induced apoptosis was used to activate Jurkat cells to release MV [30,31].

In the present study, we aimed at developing a standard method for the reproducible *in vitro* generation of a population of MV derived from HUVECs. We focused on sizing and characterizing the MV as well as on the reproducibility of the protocol. This well-characterized MV population can then be used to test and validate new analysis methods. The second aim of the study was compare the sizing of MV by AFM and NTA. To our knowledge, this is the first report comparing AFM and NTA sizing of biological MV. Moreover we combined the array from Jørgensen *et al.* [32,33] and of the AFM imaging of MV captured on antibodies by Yuana *et al.* [18] to obtain an MV array to characterize the MV phenotype as well as the size of the MV.

2. Materials and Methods

All chemicals have been purchased from Sigma Aldrich, Denmark, except if stated otherwise. All antibodies have been purchased from Abcam, United Kingdom. The buffer phosphate buffered saline (PBS) used for all experiments with MV was filtered through a 0.1 μm filter (VWR, Denmark).

2.1. Cell culture

HUVEC-C (Human umbilical vein endothelial cells, CLR-1730, ATCC, Germany) were purchased from ATCC and were cultivated in complete growth medium composed of Ham's F-12K nutrient mix (Gibco, Denmark) supplemented with 10% FBS, 50 μg/ml Endothelial cell growth supplement (ECGS), 0.1 mg/ml heparin and 1% penicillin/streptomycin (Stock concentration: 10000 Units penicillin/10 mg streptomycin per ml). The cells were seeded at a cell density of 1x10^4 cells/cm^2. The medium was changed every alternate day and cells were passaged when 80% confluency was reached (approximately twice a week).

2.2. Apoptosis detection assay of the HUVECs

HUVECs were seeded in a 24 well plate with 2.5x10^4 cells/well. 48 hours after seeding, the apoptosis was induced with medium supplemented with 5 μM staurosporine. After 4 and 8 hours, a well was stained with the Annexin V-FITC and PI (FITC Annexin V Apoptosis Detection Kit I, BD Pharmingen) with 5 μl of each dye in 1X binding buffer incubated for 15 min in the dark at room temperature. The cells were imaged using a fluorescent microscope (Nikon Eclipse Ti-S, DFA A/S, Denmark) with a 20X objective.

2.3. Atomic force microscopy of the apoptotic HUVECs

After rinsing with milliQ water, fragments (2x2 cm^2) of silicon wafer (Topsil, Denmark) were placed in 70% ethanol for 15 min for sterilization. They were then placed in a 24 well plate and coated with fibronectin (10 μg/ml in PBS) for three hours at room temperature. HUVECs were seeded on the fragments of silicon wafer at a density of 2x10^4 cell/well. 48 hours after seeding, apoptosis was induced as previously described (see 2.2). Samples were taken after 0, 4 and 8 hours. The cells were rinsed twice with PBS, then fixed in formaldehyde (3.7% in PBS) for 30 min at room temperature. The cells were then dehydrated in increasing concentrations of ethanol (30, 40, 50, 60, 70, 80, 90 and 99% (two times)) and finally dried in air. The cells were imaged with an AFM system (XE-150, Park Systems, Korea) in tapping mode. The images had a resolution of 512x512 pixel (scan area: 50x50 μm^2) and were acquired with a scan rate of 0.25 Hz. The AFM probe had a force constant of 40 N/m and a resonance frequency of 300 kHz (Budget Sensor, Bulgaria). The capture and analysis software were respectively XEP (version 1.7.70) and XEI (version 1.8.0) (Park Systems, Korea). The images were flatten using the linear regression method.

2.4. Immunostaining of HUVECs

An immunostaining assay was performed to verify the expression of the endothelial markers CD31 (Platelet endothelial cell adhesion molecule (PECAM-1)) and CD146 (Melanoma cell adhesion molecule (MCAM) or MUC18 or S-endo) on HUVECs. HUVECs were seeded on cover glasses. After two days of incubation, the cells were fixed in 3.7% formaldehyde for 30 min at room temperature. After rinsing twice in PBS, the remaining binding sites were blocked with 1% Bovine Serum Albumin (BSA) in PBS+0.1% tween-20 (PBST) for 30 min. The HUVECs were incubated with the primary antibodies anti-CD31 (Anti-CD31 antibody [JC/70A]) or anti-CD146 (Anti-CD146 antibody [P1H12]) at 4°C over night. As isotype control an anti-CD42b antibody was used. The primary antibodies were diluted in 1% BSA in PBST to a concentration of 1 μg/ml (anti-CD146), 2 μg/ml (anti-CD42b) and 1 to 100 diluted for anti-CD31 antibodies. A negative control was prepared without primary antibodies. After rinsing (three times in PBS 5 min under gentle agitation (120 rpm)), the cells were

incubated with a secondary antibody goat anti-mouse IgG1 FITC diluted in 1% BSA in PBST for one hour under gentle agitation (120 rpm). After rinsing the cells were counterstained with the DNA staining dye 2-(4-Amidinophenyl)-6-indolecarbamidine dihydrochloride (DAPI, final concentration 0.5 μg/ml) for one minute. The cells were rinsed twice in PBS and imaged right away in a confocal microscope (LSM 700, Zeiss, Germany) using a 50X objective.

2.5. Preparation of MV from HUVECs

HUVECs were seeded in a cell flask at a density of 8x10^3 cells/cm^2. 5 days after seeding, when the confluence had reached approximately 70%, the cell medium was changed to cell medium supplemented with 5 μM staurosporine, an apoptosis inducing chemical. 24 hours later, the supernatant containing the apoptotic MV was collected. The MV were purified from the cell culture supernatant using a procedure adapted from the literature [8,34,35] to specifically isolate MV. A first centrifugation step at 1250g for 5 min removed the large cell debris. The MV were then pelleted by centrifugation at 18800g for 30 min. 95% of the supernatant was removed and the MV were resuspended in PBS. The MV were then pelleted a second time. After removal of 95% of the supernatant, the pellet was resuspended into a volume corresponding to 10% of the initial volume. The aliquots were stored at -20°C. Each aliquot was thawed only once, directly before analysis. Control samples were prepared in the same way with complete medium.

2.6. Measurement of the MV with AFM in tapping mode

According to [36], fragments (2x2 cm^2) of p-doped single sided polished silicon wafer (Topsil, Denmark) were coated with N-(6-Aminohexyl)aminopropyltrimethoxysilane (1 ml in 40 ml isopropanol and 1 ml milliQ water, Abcr GmbH, Germany) for three hours at room temperature. The fragments were rinsed in isopropanol and milliQ water and blow dried. 10 μl MV solution was placed on a fragment of silicon wafer for 1 min. The MV solution was then rinsed with milliQ water three times and blow dried with air. The MV were imaged with AFM in tapping mode using cantilevers and software as previously described (see 2.3). The image size was 5x5 cm^2 with 256x256 pixel and a scan rate of 1 Hz was used. After flattening of the image, the MV were detected using the upper threshold method. Assuming that the MV were spherical, the diameter of the particles was calculated from the measured volume with the following formula : $d = 2 * (\frac{3V}{4\pi})^{\frac{1}{3}}$

2.7. Measurement of the MV with NTA

Samples of MV were diluted 10 times in PBS to suit into the recommended concentration range for NTA, i.e. between 2 to 10x10^8 MV/ml [16,37]. Samples were then introduced manually with a 1 ml syringe into the chamber of the Nanoparticle Tracking Analysis intrument (LM10, Nanosight, United Kingdom). The instrument was equipped with a laser with a wavelength of 638 nm and with the NTA software version 3.1. The camera level was adjusted to 11. For each samples, three videos of 60 s with a frame rate of 30 frames/second were recorded. For the analysis, the threshold level was set at 3, blur size was automatic. Between each measurements, the chamber was dismounted and washed thoroughly with milliQ water. For verification of the measurements, latex beads (size: 1000 to 50 nm , Molecular probes, USA) were used (data not shown).

2.8. ELISA assay for CD31 detection on the MV

An enzyme-linked immunosorbent assay (ELISA) was performed to measure the level of CD31 (PECAM1) on the isolated MV. A one step ELISA kit (Abcam, United Kingdom) according to the manufacturer's instruction. Briefly, the CD31 standard was reconstituted by adding 500 μl of sample diluent NS. A dilution serie of the standard was prepared from 50 to 4.4 ng/ml. MV samples were thawed. 50 μl of MV sample or standard aliquot was added to the wells of the pre-coated 96 well plate. A blank (only sample NS dilluent) was also prepared. Each measurement was made in

duplicate. 50 μl of antibody cocktail was added into each well. After one hour incubation on a shaker (400 rpm), the wells were rinsed three times with 1X wash buffer (diluted in milliQ water). 100 μl of 3,3',5,5'-Tetramethylbenzidine (TMB) substrate was added to each well and incubated for 10 min in the dark on a shaker (400 rpm). 100 μl of stop solution was then added and mixed for one minute on a shaker (400 rpm). The absorbance was then measured at 450 nm with a plate reader (Victor3, Perkin Elmer, USA).

2.9. MV array imaged by AFM to characterize the surface markers of MV

To determine the surface markers present on the surface of the MV, a MV array was developed with three antibodies (two antibodies against endothelial markers (Anti-CD31 antibody [JC/70A] and anti-CD146 antibody [P1H12]) and one antibody against a platelet marker (Anti-CD42b antibody [VM16d]) according to the experimental setup shown on figure 1. 10 nm titan and 100 nm gold were deposited on a silicon wafer using Wordentec QCL 800. The silicon wafer were diced with a dicing saw (Disco Automatic dicing saw, model DAD321). Antibodies were immobilized onto the gold surface according to the procedure described by Fernandes *et al.* [38] and Martins *et al.* [39]. Briefly, the gold substrate was cleaned for three times 10 min in a UV/ozone photoreactor (UVP, USA). The linker sulfo-LC-SPDP (sulfosuccinimidyl 6-(3'-(2-pyridyldithio)propionamido)hexanoate, ThermoFisher Scientific, USA) was incubated on the gold substrate for 20 min in a humid chamber at room temperature. The concentration of the sulfo-LC-SPDP linker was 2 mg/ml in PBS. The gold substrate was rinsed with PBS and milliQ water and blow-dried. The antibodies were spotted manually (with a pipette) on the gold substrate with a concentration of 250 μg/ml. Each spot had a volume of 1.5 μl. The incubation of the antibodies was performed overnight at 4°C. The gold substrate was rinsed in PBS. The remaining binding sites were blocked in BSA (1% in PBS) for 30 min at room temperature in a humid chamber. After rinsing in PBS, apoptotic MV (10 times diluted in PBS) were incubated on the functionalized gold substrate for 15 min at room temperature. The excess of MV was rinsed with PBS and milliQwater. The gold substrate was blow-dried and immediately imaged by non-contact AFM (Park Systems, Korea). Each spot was imaged on at least three representative positions. The images had a a scan size of 5x5 μm^2 and a resolution of 256x256 pixels.

2.10. Statistical analysis

The data representation and statistical analysis were performed using the software OriginPro 9.0.0 (OriginLab, USA). The normality of the samples was tested with a Kolmogorov-Smirnov test ($p<0.05$). The comparison of means was performed with a one-way ANOVA test. The difference was determined statistically significant if $p<0.05$. SD denotes the standard deviation. We also indicated the standard deviation as the ratio between the standard deviation and the mean value.

3. Results

3.1. Morphological changes of HUVECs undergoing apoptosis induced by staurosporine

Stauropsporine, a potent protein kinases inhibitor was used to induce apoptosis in HUVECs. Throughout the study, we aim to compare HUVECs treated with staurosporine (apoptotic HUVECs) with non-treated HUVECs (control HUVECs). Figure 2 shows HUVECs undergoing apoptosis. In the phase contrast images (2A to 2C) the changes in morphology of the HUVECs can be observed, while the pictures 2D to 2F show the corresponding fluorescence images of the standard fluorescent apoptosis assay including the component annexin V-FITC (fluorescein isothiocyanate) and propidium iodide (PI). In those images, the green staining corresponds to annexin V-FITC binding to the membrane phospholipid phosphatidylserine (PS), when it is translocated out of the cell, indicating an early apoptosis stage [40]. The red color corresponds to PI, that is able to stain the DNA inside the cells, only when the cell membrane has been perforated in late apoptosis stages [41]. At the time of apoptosis induction (figures 2A and 2D), the cells were well spread on the surface and no

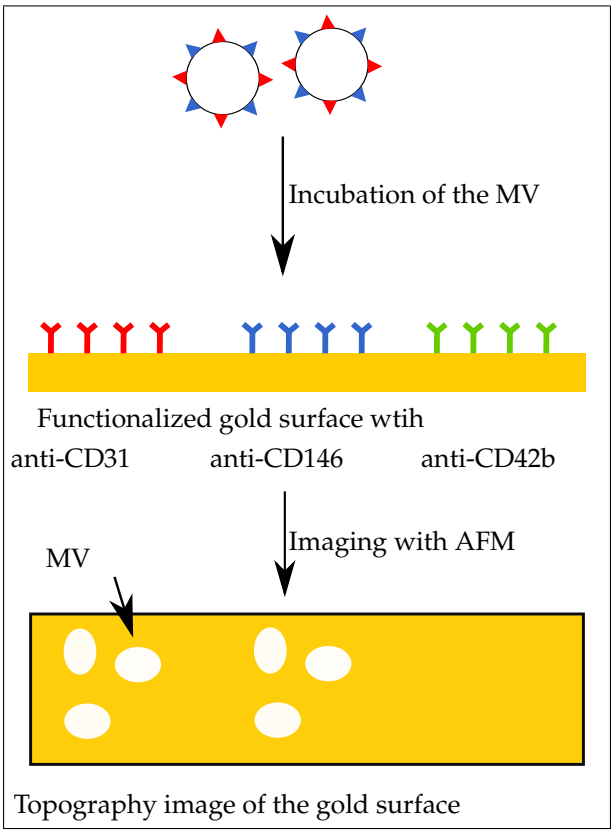

Figure 1. Experimental setup of the MV array A gold surface is functionalized in discrete spots with antibodies anti-CD31, anti-CD146 and anti-CD42b. MV are incubated over the functionalized surface. The bound MV are imaged by AFM.

fluorescence signal could be detected. In the sample taken after four hours (figures 2B and 2E), we could observe that the cells have shrunk and some cells showed a positive signal for annexin V-FITC due to the exposure of phosphatidylserine outside of the cells. Eight hours after the beginning of the treatment, we could see that the cells had shrunk further (figure 2C). More HUVECs had become positive for AnnexinV-FITC and PI signal could also be detected indicating that the cell membrane was perforated at this stage (figure 2F). In summary, treated with 5 μM of staurosporine the cells were in early apoptosis phase in the sample taken after four hours and had already reached a late apoptosis phase eight hours after the addition of staurosporine.

To confirm our findings of the annexin V-FITC/PI apoptosis detection assay, we imaged the HUVECs undergoing apoptosis using AFM in non-contact tapping mode. Figures 2G to 2I shows the topography image of HUVECs undergoing apoptosis. At the time point of the addition of the drug (figure 2G), the cells were widely spread on the surface showing numerous extensions and adhesion points evenly spread around the nucleus. After four hours of treatment with staurosporine, the membrane had lost many of these anchoring points and it seems that the cells had started to retract on themselves as illustrated by the representative cell presented on figure 2H. Moreover, protrusions appeared (highlighted in the red circles) that might indicate a blebbing of vesicles. Holes in the cell membrane had appeared which is a characteristic change of cells undergoing apoptotis [42]. The cells imaged after eight hours of treatment (figure 2I) had further retracted around the nucleus. The other structures on the surface corresponded to residues of the cell membrane.

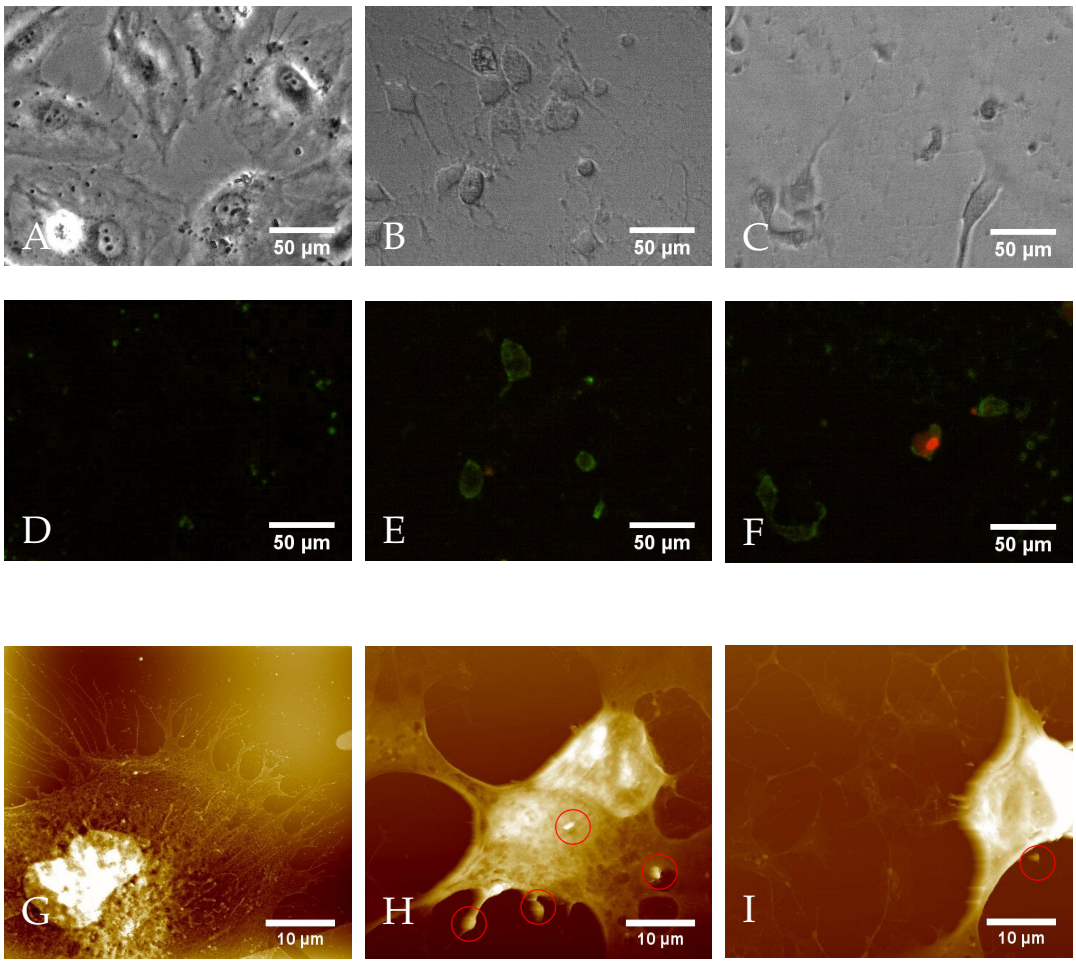

Figure 2. Morphological changes of HUVECs undergoing apoptosis induced by staurosporine after 0, 4 and 8 hours of treatment. (A to F) An Annexin V/PI apoptosis detection assay (Brightfield images with phase contrast: A to C and their corresponding fluorescence pictures: D to F) showed annexin V-FITC (green color) bound to the cells after four hours of treatment (E), showing that the exposure of phosphatidylserine started few hours after the addition of staurosporine. PI (red color) stained the DNA of some cells after eight hours (F). (G to I) The morphological changes of HUVECS were also observed by non-contact tapping mode AFM. The images represent the topography of a typical cells after 0 h (G), 4 h (H) and 8 h (I) of treatment. The color is reprensentative for the height where the darkest color shows the lowest region and white the highest regions. HUVECs that were widely spread on the surface (G) lost their adhesion sites and shrunk around the nucleus (H and I) while undergoing apoptosis. The red circles indicate protrusion on the apoptotic cells that could correspond to the blebbing of MV. The resolution of the images was 512x512 pixel.

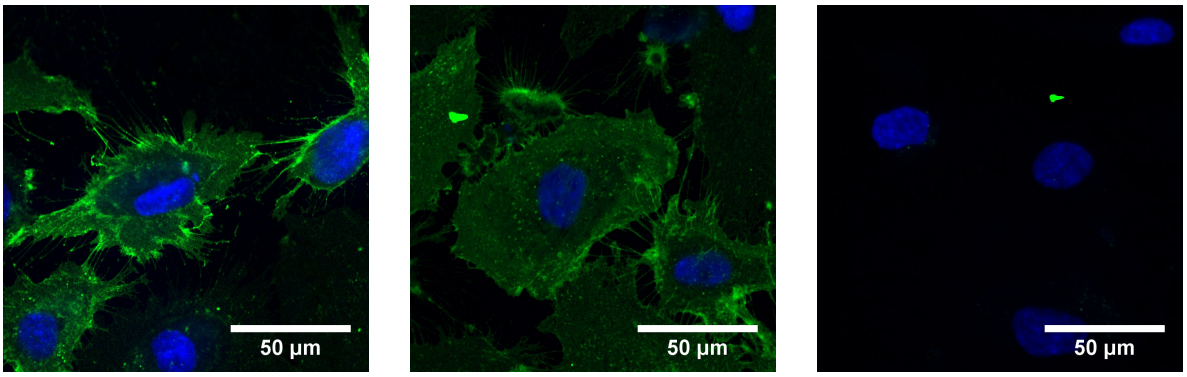

Figure 3. Expression of endothelial markers CD31 and CD146 on HUVECs The cells were double stained for the endothelial markers CD31 (green, A) or CD146 (green, B) and DNA (blue). As isotype control, a platelet marker CD42b (C) was used and was negative on the HUVECs. The images were obtained with a confocal microscope.

3.2. Expression of CD31 and CD146 on HUVECs

The expression of CD31 (Platelet endothelial cell adhesion molecule 1 (PECAM1)) and CD146 (melanoma cell adhesion molecule (MCAM)) on the surface of HUVECs was verified by an immunoassay. Those two markers were chosen as they are often used to show the presence of endothelial cells [43,44]. A secondary antibody conjugated to FITC was used so that the expression of the surface markers is indicated by the green color. The DNA of the cells was counterstained by 4',6-diamidino-2-phenylindole (DAPI) represented in blue. Figure 3A shows the expression of CD31 and figure 3B the expression of CD146. Both CD31 and CD146 were expressed on the surface of the HUVECs. The highest intensity was detected on the borders of the cells and also on the elongations of the cell membrane reaching to the neighbouring cells. The isotype negative control used was an antibody against a platelet surface marker (Platelet glycoprotein Ib alpha chain, CD42b) which was not expressed on HUVECs (figure 3C).

3.3. Release of MV from HUVECs over time

The release of MV over time was evaluated by collecting samples of cell culture supernatant at several times (1, 4, 8 and 24 hours) after addition of the medium supplemented with staurosporine. The samples were processed to collect the MV according to the centrifugation procedure described in 2.5. Figure 4 shows the concentration of MV in the different samples for the apoptotic MV and conrol MV. Until eight hours of treatment with staurosproine, the concentrations of isolated MV in both apoptotic and control MV aliquots were similar. After 24 hours, the concentration of apoptotic MV reached $1.3x10^{10}$ MV/ml, while the concentration of MV from the control cells was $5.9x10^{9}$ MV/ml, only slightly higher than one hour after the medium was changed. The size distributions of the apoptotic MV (figure A.2) shows that the MV that increased most had a diameter around 200 nm. For the control MV (figure A.2(a)), no significant change in the size distribution can be seen over the time.

3.4. Size characterization of MV from HUVECs

Many methods for characterization of MV are available as reviewed in [4,21,22]. In this work an imaging method (AFM) and a Brownian motion based method (NTA) were used to characterize and quantify MV released from control and apoptotic HUVECs.

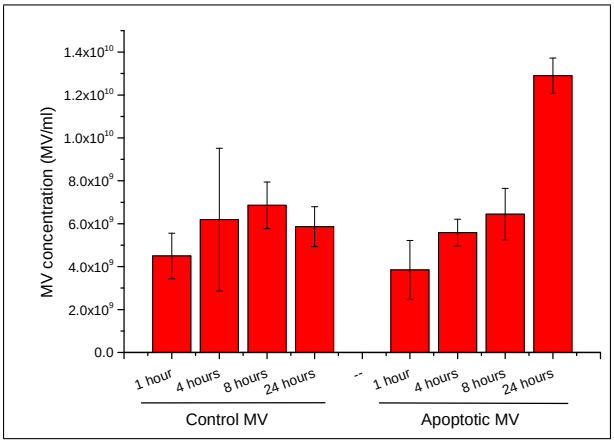

Figure 4. Release of MV over time The concentration of MV isolated from apoptotic and control HUVECs after 1, 4, 8 and 24 hours was measured by NTA. In the first eight hours, the MV concentration in apoptotic and control samples was comparable. After 24 hours, the concentration of the apoptotic samples was clearly higher than in the control samples. We present an average of three measurements of a representative samples.

Measurement of MV with AFM

AFM was previously used to characterize extracellular vesicles from cell culture supernatant as well as extracellular vesicles isolated from complex body fluids [18,45,46]. AFM provides highly precise sizing of the vesicles. The sample preparation is relatively fast (up to five minutes) and does not require any specific equipment. Figure 5 shows the topography images of MV on a silicon wafer measured by AFM. Those images provide structural information about the vesicles, which appeared as bell-shaped structures. Both apoptotic (figure 5A) and control MV (figure 5B) appeared as round to rod-shaped structures. The MV had a height of more than 50 nm.

A blank sample free of MV (PBS buffer) was prepared and imaged in the same way as sample with MV to verify for contamination. Figure 5C shows a representative topography image of a blank sample. No objects with a size similar to the MV were found. Few contamination could be imaged on the surface but their height (below 10 nm) was far lower than the threshold size for MV.

Six independent samples (MV from apoptotic and control HUVECs) were prepared and analysed by AFM. Around 200 MV were imaged in each sample. The images were taken at representative positions on the sample. An average of five images were acquired per sample. Figure 6A shows the mean size distribution of each six samples with bin width of 50 nm. The mean size of apoptotic MV was 115 nm (SD +/- 19, range: 12 to 409 nm), while the mean size of control MV was 139 nm (SD +/- 34, range: 26 to 393 nm). The mean sizes of the apoptotic and control MV were not significantly different from each other ($p = 0.16$).

Measurement of the MV with NTA

The size of the MV released from apoptotic and control HUVECs was also determinded using NTA. With this technique the size of the vesicles is calculated from their brownian motion in an analysis chamber. Figure 6A shows the average size distribution of six independent samples with bin width of 50 nm. Similar to the AFM, the size distribution of the apoptotic and control MV were overlapping each other. Compared to the size distribution obtained by the AFM analysis, the NTA analysis lead to a more polydisperse size distribution evidenced as a wider peak in the size distribution graph. The maximum of the peak was located around 125 to 175 nm. The mean size of the apoptotic MV as measured per NTA was 197 nm (SD +/- 28, range: 17 to 1381 nm) and the mean size of the control MV was 192 nm (SD +/- 29, range: 13 to 959 nm). The difference between the mean sizes of apoptotic and control MV measured with NTA was not significantly different ($p = 0.7$).

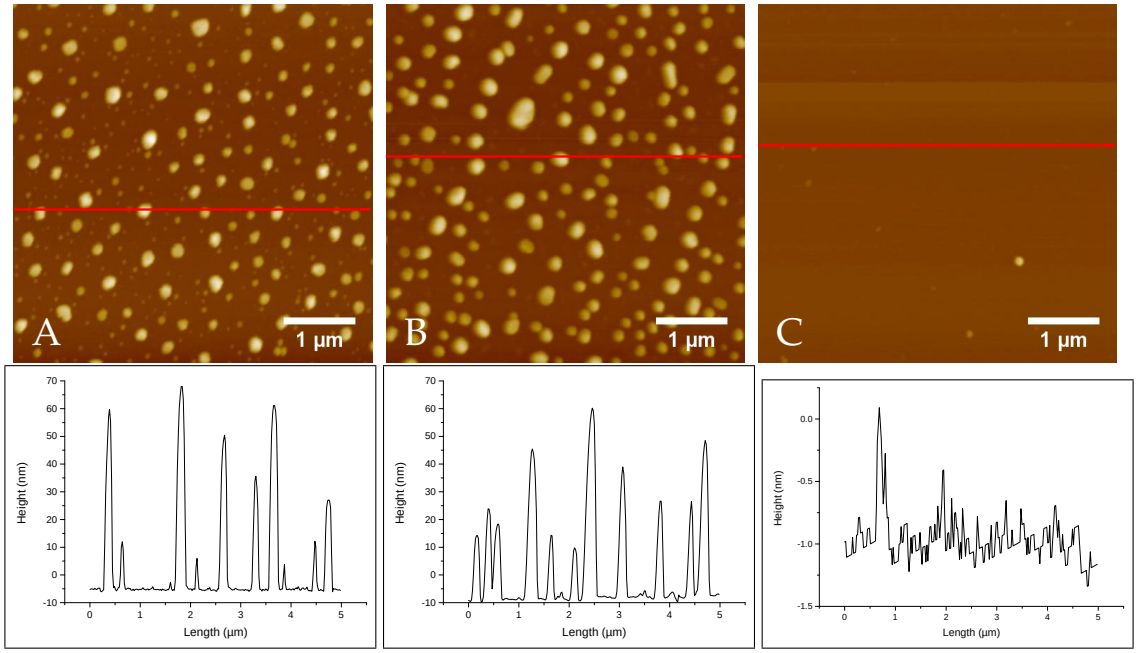

Figure 5. AFM imaging of MV Topography images of MV derived from apoptotic HUVECs (A) and from healthy HUVECs (B) acquired with an AFM in tapping mode. A height profile along the red lines was represented for each AFM image. MV isolated from HUVECs showed a height around 40 to 60 nm. Image C is the topography image of a blank sample (only buffer). No contamination was found in the buffer. The resolution of the images was 256x256 pixel.

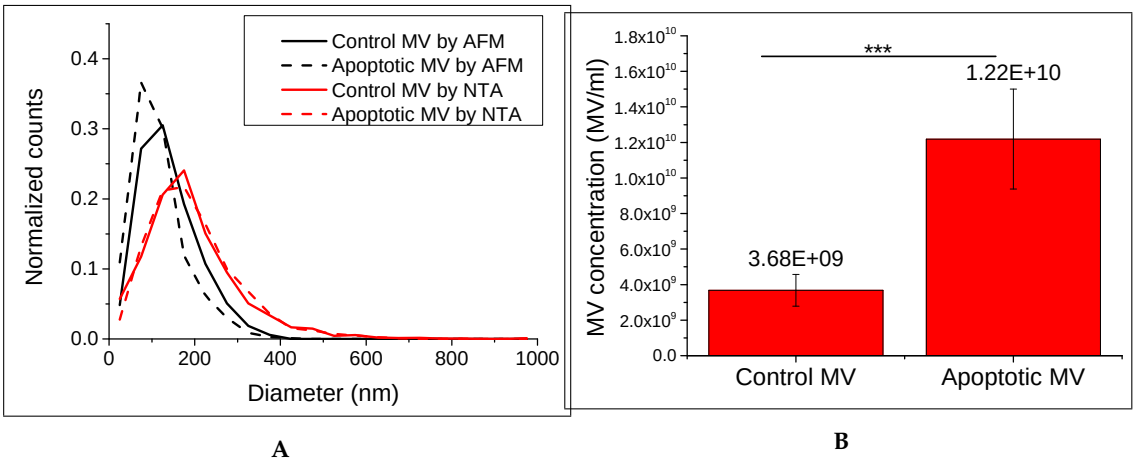

Figure 6. Size and concentration of HUVECs MV The size distribution (A) of MV isolated from apoptotic and control HUVECs was measured by AFM and NTA for six independent samples. The average size distributions are presented. The size distributions for MV measured by AFM and the size distribution of MV measured by NTA respectively overlap each other. The size distribution obtained per NTA is wider and the mean larger than the size distribution obtained per AFM. Figure B reports the average concentration of MV in the apoptotic and control aliquots for five independent samples. The measured concentration of apoptotic MV was 3.3 fold higher than the control MV concentration. The concentrations were significantly different ($p=2x10^{-4}$). The error bars represent the standard deviation. *** : $p < 0.001$

3.5. Measurement of the MV concentration by NTA

NTA measurements give information not only about the size of the vesicles in the samples, but also about the concentration of the vesicles. Figure 6B reports the average MV concentration in five independent samples of MV purified from control and apoptotic HUVECs. In the apoptotic samples, 1.22x10^{10} MV/ml (SD +/- 2.8x10^{9}, corresponding to 23%) MV were isolated, while 3.7x10^{9} MV/ml (SD +/- 9x10^{8}, corresponding to 24%) were isolated from the cell culture supernatant of control HUVECs. Thus, in the apoptotic samples, 3.3 times more MV could be measured compared to the control samples. The difference in concentration was statistically different with p = 2x10^{-4}.

The complete growth medium and four of its components followed individually the same centrifugation protocol like the cell culture supernatants in order to evaluate if MV or MV like structures could be isolated from the complete growth medium used to cultivate the cells. As shown in appendix A and on figure A.1, the concentration of MV in the complete growth medium corresponded to approximately 15% of the concentration of apoptotic MV and most of those vesicles came from the FBS.

As we measured the MV in the complete growth medium before incubation with the cells (see 6B), we can subtract the contaminating MV (or background MV) to calculate the MV released per cell and we obtain that the concentration of apoptotic MV and control MV without the contaminating MV from the medium were respectively 1x10^{10} MV/ml and 1.9x10^{9} MV/ml. Using the number of cells seeded in a cell flask (8000 cell/cm^2) of 75 cm^2 ($N_0 = 8000 \times 75 = 6 \times 10^5$) together with the number of days in culture (five days) and an estimated population doubling time of 30 hours [47], we could estimate the number of cells at the time of the apoptosis induction (N_{ind}) as follows:

$$N_{ind} = N_0 \times 2^{\frac{duration}{doubling\ time}} = 6 \times 10^5 \times 2^{(\frac{5 \times 24}{30})} = 9.6 \times 10^6\ cells \quad (1)$$

Using the average MV concentration in the apoptotic and control aliquots (with contaminating MV subtracted), the up-concentration factor of the aliquots compared to the cell flask corresponding to UF=10, the total volume of the cell flask (V=15 ml), we obtain the number of MV released per cell (MV_{cell}) as follow:

$$MV_{cell} = \frac{MV\ concentration \times V}{UF \times N_{ind}} \quad (2)$$

which corresponded to 1625 MV/cell for the apoptotic sample and 281 MV/cell for the control samples, which was 5.8 fold more MV released by an apoptotic cell compared to a healthy cell. Considering that the size distribution of the MV had a maximum of the peak at 150 nm (considered as diameter of MV (d_{MV}) as measured by NTA and that the HUVECs had a diameter (d_{cell}) of 15 μm, we can calculate the part (P_{MV}) of cell membrane used for the MV as the ratio of the surface area of all the MV released by one cell to the surface area of one cell, assuming that the cell is a sphere (surface area of a sphere=$4\pi r^2$):

$$P_{MV} = \frac{MV_{cell} \times area_{MV}}{area_{cell}} = \frac{MV_{cell} \times 4\pi(\frac{d_{MV}}{2})^2}{4\pi(\frac{d_{cell}}{2})^2} \quad (3)$$

We obtain that the released MV corresponded approximately to 16% of the total surface area of a HUVECs in the apoptotic samples and 3% of the total surface area of a HUVECs in the control samples.

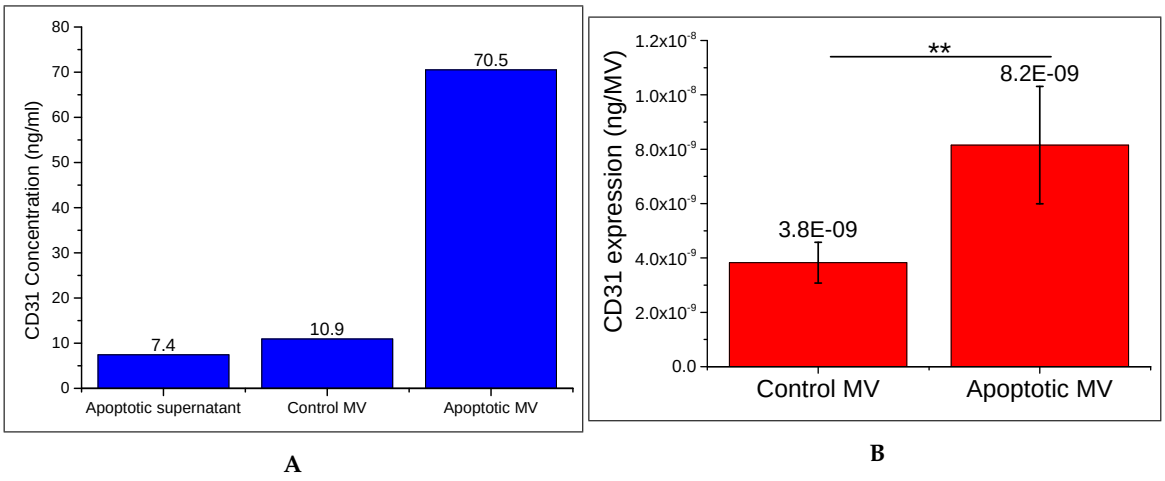

Figure 7. CD31 expression on the surface of the MV derived from HUVECs measured. Figure A represents the concentration of CD31 as measured per ELISA in a representative sample: in the apoptotic supernatant before isolation of MV and in the MV (control and apoptotic) preparation after isolation. The CD31 concentration was approximately ten fold higher in the MV aliquots compared to the apoptotic cell supernatant. This corresponded to the up-concentration factor of MV during the isolation procedure. Figure B reports the expression of CD31 per MV for five independent samples. The expression of CD31 was two fold higher on the apoptotic MV compared to the control MV. The error bars show the standard deviation. The difference of means was statistically significant ($p = 0.0029$). **: $p < 0.01$

3.6. Characterization of the surface markers on the surface of the cell-derived microvesicles

ELISA assay to measure the expression of CD31 on the MV

A one-step ELISA assay (see 2.8) was performed to measure the expression of CD31 (PECAM-1) on the surface of the MV. The analysis was performed for five independent apoptotic and control samples. The cell culture supernatants (after first centrifugation at 1250g to remove larger debris) as well as washing steps after each centrifugation steps at 18800g were measured for a representative sample. The absorbance values measured for the supernatant of the control sample as well as all the washing steps were below the lowest value of the standard curve. Therefore it can only be concluded that the CD31 concentration in those samples was below 4.4 ng/ml, the lowest concentration measured in the standard curve. Figure 7A shows that in the apoptotic supernatant 7.4 ng/ml of CD31 was present, while after isolation of the MV, the concentration of CD31 in the MV preparation (70.5 ng/ml) was 9.53 times higher than in the apoptotic supernatant.

Figure 7B shows the average expression of CD31 per MV in apoptotic MV and control MV preparations. Surprisingly the expression of CD31 was two fold higher on the apoptotic MV ($8.3x10^{-9}$ ng/ml, SD +/- $2.2x10^{-9}$ corresponding to 27%) than on the control MV ($3.8x10^{-9}$ ng/ml, SD +/- $7.5x10^{-10}$ corresponding to 20%). The difference between apoptotic and control MV was statistically significant (p=0.0029).

Characterization of the surface markers of the MV by a MV array

To further characterize the surface markers present on the membrane of the MV derived from HUVECs, antibodies were immobilized on a gold surface at discrete spots to create a MV array. After incubation of MV isolated from apoptotic HUVECs, the functionalized gold surface was imaged by true non-contact mode AFM. Three positions were imaged in each antibody spot and the experiment was repeated with three independent MV samples. Figure 8 shows the topography images of the

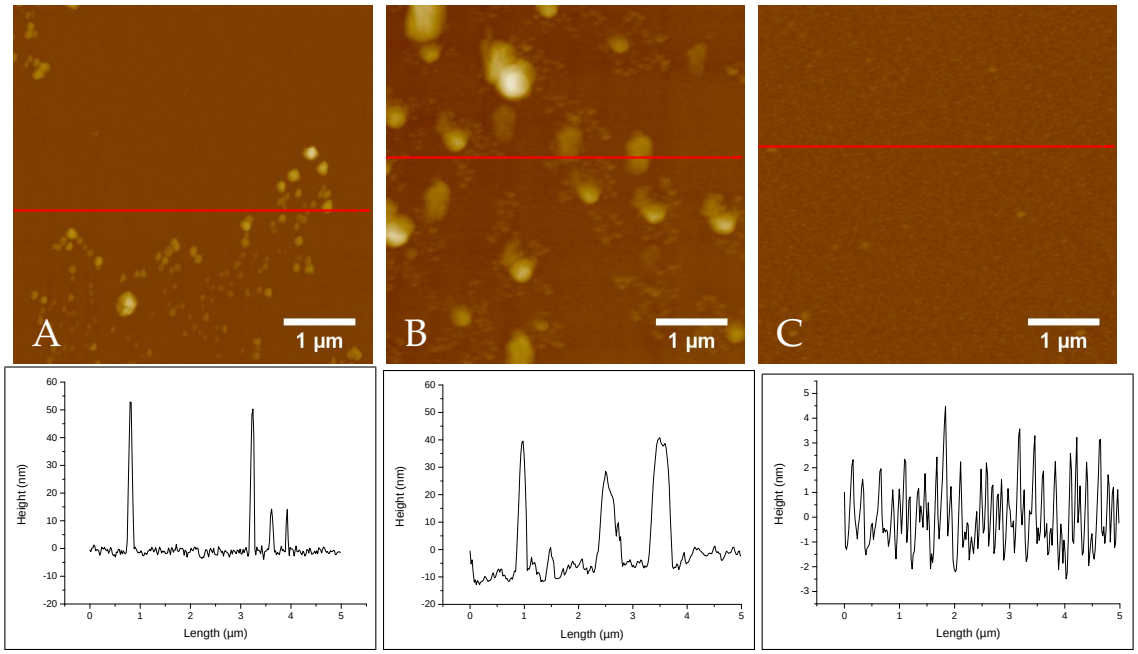

Figure 8. MV array Topography AFM images of MV derived from apoptotic HUVECs captured on a surface coated with antibodies against the endothelial markers anti-CD31 (A)and anti-CD146 (B). As negative control, a platelet marker anti-CD42b (C) was used and no MV were detected on this spot. The height profile across each image is also shown. The captured MV had a height of 40 to 60 nm. The resolution of the images was 256x256 pixel.

representative regions on the substrate. Figures 8A and 8B are regions functionalized with antibodies against the endothelial markers CD31 and CD146. We found MV captured on those regions. The MV imaged here had a height of 40 to 60 nm, which is similar to the MV imaged earlier without functionalization (see figure 5). This indicates that MV carried on their surface CD31 as well as CD146. The region shown in figure 8C was functionalized with antibodies against the platelet marker CD42b. The profile of figure 8C shows a height of 2 to 3 nm. No MV could be found on this marker in any of the independent experiments. This indicates that the MV did not express CD42b as they were not captured by an anti-CD42b antibody.

4. Discussion

As MV gain more and more significance in the biomedical field, adequate analysis methods are required. Great efforts are made to improve existing methods such as flow cytometry and to develop new characterization instruments with the objective of a rapid and reliable MV analysis. Our aim was to create a MV population that could be used as a reference for the testing of new analysis methods. When investigating MV released from a cell line, the complete system can be analysed, meaning that the precise phenotype (surface markers) of the parental cells can be determined, the release process of the MV can be monitored and finally MV can be isolated and characterized (size, concentration, surface markers). Therefore this is a very useful method to understand the biology behind the release of MV.

4.1. Apoptosis as the mechanism to release MV

In the present work, the release of the MV was induced by incubating the endothelial cells (HUVECs) with 5 μM staurosporine for 24 hours. Staurosporine is known to induce apoptosis [48] and was previously used to activate jurkat cells to produce MV [30,31]. HUVECs were sensitive to staurosporine and went into apoptosis few hours after the start of the treatment as detected by the

apoptosis assay (Figure 2). An homogeneous reaction was observed throughout the cell layer. In our experiments we could show by optical microscopy and AFM that the cells treated with staurosporine presented very clear morphological changes already few hours after the beginning of the treatment as previously shown by other studies [49,50]. Perforation of the cell membrane was observed. This was similar to the results presented by Kim *et al.* [42]. A shrinkage of the HUVECs as well as the loss of their adherence to the cell culture substrate were later observed (see figure 2). These observations were in good agreement with the results presented by Kabir *et al.* [50], who described the effect of staurosporine on endothelial cells as a focal adhesion disassembly. Imaging cells in tapping mode AFM provided very detailed information regarding the morphology change of the cells. In our experiments, the blebbing of the cells could not be clearly imaged, even though this is characteristic for cells in apoptosis. The difficulty of observing the blebbing might be due to the preparation of the cells (fixing and drying) prior to imaging.

4.2. MV in the cell growth medium

Contamination of the complete growth medium with vesicles prior to contact with the HUVECs was investigated. Our results showed that the vesicle concentration in the complete cell culture medium corresponded to less than 15% of the MV concentration in aliquots of apoptotic MV (figures A.1 and 6B). The concentration of MV in FBS was approximately ten times higher than in the complete growth medium (figure A.1). As FBS is diluted ten times in the complete growth medium, we can conclude that those vesicles seemed to originate from the FBS used. The size distribution had a peak at 160 nm. The analysis was only performed by NTA. Further analysis with imaging methods should investigate the proper nature and shape of those NTA events. Removal of the contaminating vesicles prior to induction of MV release could be achieved by overnight centrifugation at 120000g [51]. However the effect of this vesicle removal on the cell vitality needs to be assessed.

4.3. Concentration of MV released: comparison between apoptotic and control samples

In the present study, MV were released from HUVECs. Up to eight hours after the beginning of the incubation with staurosporine, the tendency was that the concentrations of MV isolated from the control and the apoptotic cell culture supernatant were similar (figure 4). Ullal and Pisetsky reported an increase of the MV released by jurkat cells within 20 min of treatment with staurosporine [31]. In our work, after 24 hours of treatment, a significant difference between the concentration of apoptotic and control MV was found (figure 6B). Approximately three times more MV could be isolated from the apoptotic cell supernatant than from the control cell supernatant. As measured by NTA, we obtained an average of 1625 MV per apoptotic cell and an average of 281 MV per control cell. In a previous study, Šimák *et al.* [29] measured using flow cytometry around 130 annexin V binding vesicles released per HUVEC activated with camptothecin and 20 annexin V binding vesicles from HUVECs treated with 0.5% DMSO. However, not all MV are annexin V positive [52] and van der Pol [25] showed that flow cytometry underestimates MV counts from 300 (standard flow cytometer) to 15 fold (dedicated flow cytometer) compared to NTA. The ratio of apoptotic MV compared to control MV was approximately 5.8, while Šimák *et al.* [29] found 6.5 in their work. Thus, the results of this study are comparable with previously reported work. The standard deviation corresponded to 23% of the mean MV concentration for the apoptotic MV samples and 24% for the control MV samples. This shows that our protocol can generate a population of MV with a reproducible concentration.

4.4. Characterization of the size of MV by AFM and NTA: a comparison

The size of MV was characterized using two methods: AFM and NTA. No significant difference was found between the mean diameter of the apoptotic MV and the mean diameter of the control MV sized by AFM and NTA. Apoptotic MV and control MV could not be distinguished by their sizes. However, the difference in the mean sizes measured by AFM compared to the mean sizes measured by NTA were significantly different (figure 6). MV measured by NTA were larger than MV measured

by AFM and showed a slightly broader size distribution. Both AFM and NTA measure objects that either have a certain topography (in case of the AFM) or scatter light (in the case of NTA). That is why the results have to be interpreted carefully. For instance our measurements showed that the smallest objects measured were below 30 nm. It raises the concern if those events really are vesicles and more particularly MV. They may instead correspond for instance to protein aggregates or small protein debris. Other methods such as electron microscopy would be able to identify if those very small objects are vesicles. However, those objects accounted for less than 5% of the total population. Since we followed a protocol with a centrifugation speed (18800g) generally accepted to pellet MV, we can thrust that the larger objects were MV. To image MV with AFM, the vesicles have to be deposited on a substrate. As previously described [12], MV deposited on a surface are subject to a morphology change that causes the vesicles to collapse (reduce height) while spreading on the surface. This means that the height is under-representative of the diameter while the area would overestimate the diameter of the MV. However we can assume that the volume remained the same. Therefore sizing the MV can be done by evaluating the volume of the measured MV and calculating the diameter from this value [12,18]. Apart from the size, AFM also provides structural information about the MV. Other drawbacks of MV study by AFM are the need of trained experimentators and the time required to image enough MV for a representative analysis. Compared to AFM, NTA measures more vesicles per sample in a shorter time. However, NTA does not allow to verify that the scattered events tracked by the software really correspond to single MV. Aggregates can therefore be reported as single vesicle and contribute to measurement of a larger MV population. Moreover it has been reported that NTA overestimate larger MV [25]. This might be the reason why the sizes of the MV measured are generally larger than with AFM (figure 6). However compared to AFM, the MV measured by NTA were in liquid, i.e. in their native state. The MV underwent no change before analysis and therefore their size distribution was less subject to artefacts due to preparation. Sizing MV is always subjected to the advantages and drawbacks of each methods. The use of several characterization methods is therefore highly recommendable to gain a proper estimation of the size of the different MV populations.

4.5. Characterization of the surface markers of the MV

Further, we assessed if the surface markers present on the surface of the HUVECs could be detected on the surface of the MV. As expected, CD31 and CD146 were detected on the membrane of HUVECs, while CD42b , a platelet marker was absent from the membrane of HUVECs. First, the concentration of CD31 on MV from HUVECs was measured with an ELISA (figure 7). The CD31 concentration in apoptotic supernatant was approximately ten times lower than the CD31 in the apoptotic MV aliquot after isolation by centrifugation (figure 7A). This factor of approximately 10 corresponds to the up-concentration factor of the MV preparation (see 2.5). Since the washing steps did not contain a high concentration of CD31 (below detection limit of 4.4 mg/ml), this result suggests the CD31 measured in the non-centrifuged supernatant was only associated with the MV pelleted during the isolation procedure and did not correspond to free CD31 in the cell culture supernatant. Moreover this result suggests that more than 95% of the MV expressing CD31 in the supernatant could be isolated by the high-speed centrifugation protocol used.

The MV array presented in this study provided a method to determine the phenotype of MV by imaging MV captured on a surface functionalized with antibodies against surface markers of MV. Thanks to the read-out by AFM, MV can also be enumerated and sized. In the present work, MV were captured on antibodies against CD31 and CD146 and were not captured on antibodies against CD42b, which is a platetelet marker. The height profile on the CD42b spot showed structures around 2 to 4 nm which corresponds to the height of an antibody coated surface as reported in [18]. Thus, we can conclude that the MV released from apoptotic HUVECs expressed the endothelial markers markers CD31 and CD146 and did not express CD42b. This expression pattern was also shown on the HUVECs (figure 3). According to literature [35,53], the combination of markers CD31 positive and CD42b negative confirms the endothelial origin of the MV. Therefore we can conclude that

the MV present in the MV preparations had been released from the endothelial cells HUVECs. As endothelial MV play a very central role in biological processes [53], our *in vitro* MV population is highly interesting and relevant for medical applications. Further investigation of the phenotype of the MV should include the expression of phosphatidylserine. This further investigation can be performed by the MV array presented here thanks to its flexibility in the surface functionalization.

5. Conclusions

In the present study, we showed that our method could generate MV from HUVECs in a reproducible way. This validate the use of this MV population for the testing and optimization of novel analysis methods for MV. AFM and NTA gave comparable results in the sizing of MV. Combining the two methods helps to gain a correct idea of the size of the MV. Moreover we introduced the use of an MV array to characterize simultaneously the phenotype (i.e. the surface proteins) and the size of MV. With further development, this analysis tool will become very relevant to characterize MV isolated from different type of body fluids.

Acknowledgments: The author would like to thank Mark Holm Olsen for the preparation of the gold substrates, and proof-reading, as well as Julie Kirkegaard for proof-reading. This work has been supported by the Technical University of Denmark.

Author Contributions: Solène Cherre, Ole Østergaard, Niels H.H. Heegaard and Noemi Rozlosnik conceived and designed the experiments; Solène Cherre performed all experiments except the AFM based MV array experiments which were performed by Mathilde Granberg. Solène Cherre analyzed the data and wrote the paper. All authors participated in reviewing the paper

.

Conflicts of Interest: The authors declare no conflict of interest.

Abbreviations

The following abbreviations are used in this manuscript:

MDPI: Multidisciplinary Digital Publishing Institute
AFM: Atomic Force Microscopy
BSA: Bovine Serum Albumin
CD: Cluster of Differentiation
DAPI: 4′,6-diamidino-2-phenylindole
ELISA: Enzyme-linked Immunosorbent Assay
FBS: Fetal Bovine Serum
FITC: Fluorescein isothiocyanate
HUVECs: Human Umbilical Vein Endothelial Cells
MV: Microvesicles
NTA: Nanoparticle Tracking Analysis
PBS: Phosphate buffered Saline
PBST: Phosphate-buffered saline + 0.1% Tween-20
PI: Propidium iodide
PS: Phosphatidylserine
SD: standard deviation

Appendix A: Characterization of the complete growth medium for HUVECs culture

The different components of the complete growth medium of HUVECs were processed like the cell culture supernatants (centrifugation protocol described in 2.5) to assess if MV or MV like particles were present in the complete growth medium before culture with the cells. Figure A.1(a) shows the concentration of MV detected in the processed aliquots of the medium components as measured with

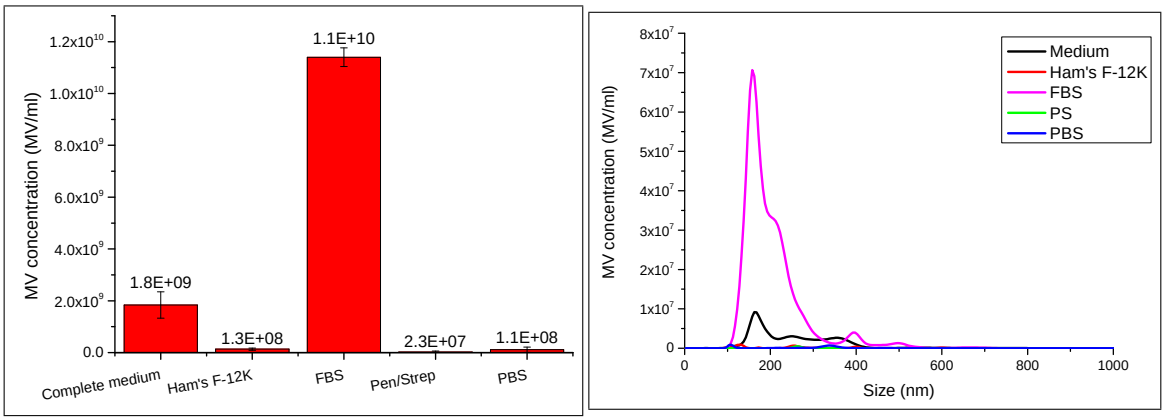

Figure A.1. Concentration (a) and size distributions (b) of MV isolated from the different components of the cell growth medium. The concentration and size distribution were obtained by NTA and are an average of three measurements of a representative sample. The error bars represent the standard deviation. The concentration of MV found in the complete growth medium was approximately ten times lower than in the FBS, which corresponded to the dilution factor FBS in the complete growth medium. For the FBS and the complete growth medium, the size distributions were overlapping with both a peak around 160 nm. This suggests that the MV from the medium were coming from the FBS. The other components did not contain a significant amount of MV.

NTA. In the complete growth medium, $1.8x10^9$ MV/ml (SD +/- $5x10^8$, corresponding to 28%) were detected. The levels of MV measured in Ham's F12K and the penicillin/streptomycin solution were below 10% of the level of MV in the complete growth medium. However the level of MV in the fetal bovine serum (FBS) reached $1.1x10^{10}$ MV/ml (SD +/- $3.6x10^8$, corresponding to 3%), that was approximately 10 times more than in the complete medium. The size distributions of the MV from the complete growth medium and from the FBS (figure A.1(b)) show both a main peak at 160 nm. Note that the buffer used (phosphate buffered saline, PBS) was filtered through a 0.1 μm syringe filter prior of use and also had a low level of MV ($1.1.^8$ MV/ml).

Appendix B: Size distributions of MV released over time

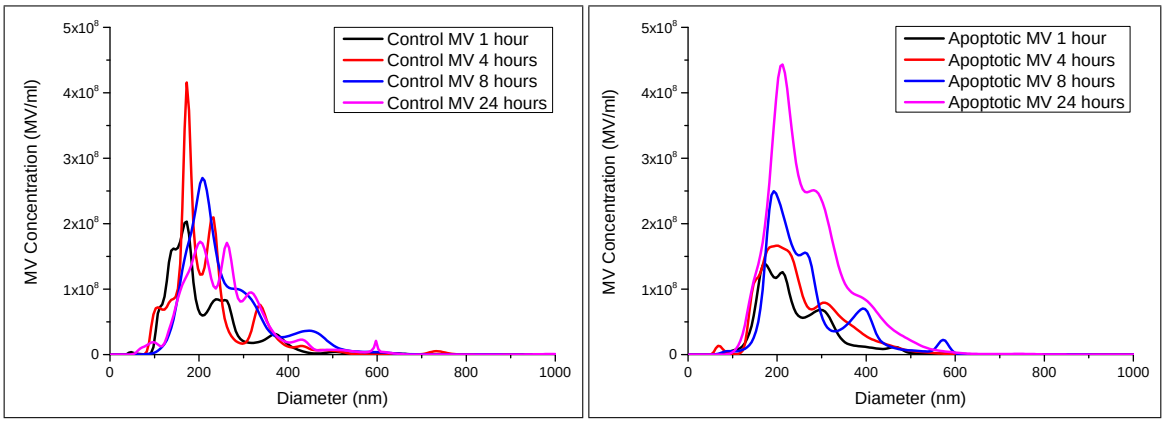

Figure A.2. Size distributions of MV isolated from control ((a)) and apoptotic ((b)) HUVECs after 1, 4, 8 and 24 hours of treatment with staurosporine. The size distribution was obtained by NTA and is an average of three measurements of a representative samples.

Bibliography

1. Wolf, P. The Nature and Significance of Platelet Products in Human Plasma. *British Journal of Haematology* **1967**, *13*, 269–288.
2. Liga, A.; Vliegenthart, A.D.B.; Oosthuyzen, W.; Dear, J.W.; Kersaudy-Kerhoas, M. Exosome isolation: a microfluidic road-map. *Lab Chip* **2015**, *15*, 2388–2394.
3. György, B.; Szabó, T.G.; Pásztói, M.; Pál, Z.; Misják, P.; Aradi, B.; László, V.; Pállinger, E.; Pap, E.; Kittel, A.; Nagy, G.; Falus, A.; Buzás, E.I. Membrane vesicles, current state-of-the-art: emerging role of extracellular vesicles. *Cellular and molecular life sciences : CMLS* **2011**, *68*, 2667–88.
4. Burger, D.; Schock, S.; Thompson, C.S.; Montezano, A.C.; Hakim, A.M.; Touyz, R.M. Microparticles: biomarkers and beyond. *Clinical science (London, England : 1979)* **2013**, *124*, 423–41.
5. Cocucci, E.; Racchetti, G.; Meldolesi, J. Shedding microvesicles: artefacts no more. *Trends in cell biology* **2009**, *19*, 43–51.
6. Leroyer, A.S.; Anfosso, F.; Lacroix, R.; Sabatier, F.; Simoncini, S.; Njock, S.M.; Jourde, N.; Brunet, P.; Camoin-Jau, L.; Sampol, J.; Dignat-George, F. Endothelial-derived microparticles: Biological conveyors at the crossroad of inflammation, thrombosis and angiogenesis. *Thrombosis and haemostasis* **2010**, *104*, 456–63.
7. Laffont, B.; Corduan, A.; Plé, H.; Duchez, A.C.; Cloutier, N.; Boilard, E.; Provost, P. Activated platelets can deliver mRNA regulatory Ago2{middle dot}microRNA complexes to endothelial cells via microparticles. *Blood* **2013**, *122*, 253–61.
8. Nielsen, C.T.; Østergaard, O.; Johnsen, C.; Jacobsen, S.; Heegaard, N.H.H. Distinct features of circulating microparticles and their relationship to clinical manifestations in systemic lupus erythematosus. *Arthritis and rheumatism* **2011**, *63*, 3067–77.
9. Buzas, E.I.; György, B.; Nagy, G.; Falus, A.; Gay, S. Emerging role of extracellular vesicles in inflammatory diseases. *Nature reviews. Rheumatology* **2014**, *10*, 356–64.
10. Gong, J.; Jaiswal, R.; Dalla, P.; Luk, F.; Bebawy, M. Microparticles in Cancer: A Review of Recent Developments and the Potential for Clinical Application. *Seminars in Cell & Developmental Biology* **2015**, *40*, 35–40.
11. Ayers, L.; Kohler, M.; Harrison, P.; Sargent, I.; Dragovic, R.; Schaap, M.; Nieuwland, R.; Brooks, S.A.; Ferry, B. Measurement of circulating cell-derived microparticles by flow cytometry: Sources of variability within the assay. *Thrombosis Research* **2011**, *127*, 370–377.
12. Leong, H.S.; Podor, T.J.; Manocha, B.; Lewis, J.D. Validation of flow cytometric detection of platelet microparticles and liposomes by atomic force microscopy. *Journal of thrombosis and haemostasis : JTH* **2011**, *9*, 2466–76.

13. Chandler, W.L.; Yeung, W.; Tait, J.F. A new microparticle size calibration standard for use in measuring smaller microparticles using a new flow cytometer. *Journal of thrombosis and haemostasis : JTH* **2011**, *9*, 1216–24.
14. Lawrie, A.S.; Albanyan, A.; Cardigan, R.A.; Mackie, I.J.; Harrison, P. Microparticle sizing by dynamic light scattering in fresh-frozen plasma. *Vox sanguinis* **2009**, *96*, 206–12.
15. Gardiner, C.; Ferreira, Y.J.; Dragovic, R.A.; Redman, C.W.G.; Sargent, I.L. Extracellular vesicle sizing and enumeration by nanoparticle tracking analysis. *Journal of extracellular vesicles* **2013**, *2*.
16. Dragovic, R.A.; Gardiner, C.; Brooks, A.S.; Tannetta, D.S.; Ferguson, D.J.P.; Hole, P.; Carr, B.; Redman, C.W.G.; Harris, A.L.; Dobson, P.J.; Harrison, P.; Sargent, I.L. Sizing and phenotyping of cellular vesicles using Nanoparticle Tracking Analysis. *Nanomedicine : nanotechnology, biology, and medicine* **2011**, *7*, 780–8.
17. Issman, L.; Brenner, B.; Talmon, Y.; Aharon, A. Cryogenic transmission electron microscopy nanostructural study of shed microparticles. *PloS one* **2013**, *8*, e83680.
18. Yuana, Y.; Oosterkamp, T.H.; Bahatyrova, S.; Ashcroft, B.; Garcia Rodriguez, P.; Bertina, R.M.; Osanto, S. Atomic force microscopy: a novel approach to the detection of nanosized blood microparticles. *Journal of thrombosis and haemostasis : JTH* **2010**, *8*, 315–23.
19. Gheldof, D.; Hardij, J.; Cecchet, F.; Chatelain, B.; Dogné, J.M.; Mullier, F. Thrombin generation assay and transmission electron microscopy: a useful combination to study tissue factor-bearing microvesicles.
20. Østergaard, O.; Nielsen, C.T.; Iversen, L.V.; Jacobsen, S.; Tanassi, J.T.; Heegaard, N.H.H. Quantitative Proteome Profiling of Normal Human Circulating Microparticles. *Journal of Proteome Research* **2012**, *11*, 2154–2163.
21. van der Pol, E.; Hoekstra, A.G.; Sturk, A.; Otto, C.; van Leeuwen, T.G.; Nieuwland, R. Optical and non-optical methods for detection and characterization of microparticles and exosomes. *Journal of thrombosis and haemostasis : JTH* **2010**, *8*, 2596–607.
22. Sunkara, V.; Woo, H.K.; Cho, Y.K. Emerging techniques in the isolation and characterization of extracellular vesicles and their roles in cancer diagnostics and prognostics. *The Analyst* **2015**, *141*, 371 – 381.
23. Nicolet, A.; Meli, F.; van der Pol, E.; Yuana, Y.; Gollwitzer, C.; Krumrey, M.; Cizmar, P.; Buhr, E.; Pétry, J.; Sebaihi, N.; de Boeck, B.; Fokkema, V.; Bergmans, R.; Nieuwland, R. Inter-laboratory comparison on the size and stability of monodisperse and bimodal synthetic reference particles for standardization of extracellular vesicle measurements. *Measurement Science and Technology* **2016**, *27*, 035701.
24. Coumans, F.A.W.; van der Pol, E.; Böing, A.N.; Hajji, N.; Sturk, G.; van Leeuwen, T.G.; Nieuwland, R. Reproducible extracellular vesicle size and concentration determination with tunable resistive pulse sensing. *Journal of Extracellular Vesicles* **2014**, *3*.
25. van der Pol, E.; Coumans, F.A.W.; Grootemaat, A.E.; Gardiner, C.; Sargent, I.L.; Harrison, P.; Sturk, A.; van Leeuwen, T.G.; Nieuwland, R. Particle size distribution of exosomes and microvesicles determined by transmission electron microscopy, flow cytometry, nanoparticle tracking analysis, and resistive pulse sensing. *Journal of Thrombosis and Haemostasis* **2014**, *12*, 1182–1192.
26. Chironi, G.N.; Boulanger, C.M.; Simon, A.; Dignat-George, F.; Freyssinet, J.M.; Tedgui, A. Endothelial microparticles in diseases. *Cell and tissue research* **2009**, *335*, 143–51.
27. Boulanger, C.M.; Amabile, N.; Tedgui, A. Circulating microparticles: a potential prognostic marker for atherosclerotic vascular disease. *Hypertension* **2006**, *48*, 180–6.
28. Combes, V.; Simon, A.C.; Grau, G.E.; Arnoux, D.; Camoin, L.; Sabatier, F.; Mutin, M.; Sanmarco, M.; Sampol, J.; Dignat-George, F. In vitro generation of endothelial microparticles and possible prothrombotic activity in patients with lupus anticoagulant. *The Journal of clinical investigation* **1999**, *104*, 93–102.
29. Simák, J.; Holada, K.; Vostal, J.G. Release of annexin V-binding membrane microparticles from cultured human umbilical vein endothelial cells after treatment with camptothecin. *BMC cell biology* **2002**, *3*, 11.
30. Reich, C.F.; Pisetsky, D.S. The content of DNA and RNA in microparticles released by Jurkat and HL-60 cells undergoing in vitro apoptosis. *Experimental cell research* **2009**, *315*, 760–8.
31. Ullal, A.J.; Pisetsky, D.S. The release of microparticles by Jurkat leukemia T cells treated with staurosporine and related kinase inhibitors to induce apoptosis. *Apoptosis : an international journal on programmed cell death* **2010**, *15*, 586–96.

32. Jørgensen, M.; Bæk, R.; Pedersen, S.; Søndergaard, E.K.L.; Kristensen, S.R.; Varming, K. Extracellular Vesicle (EV) Array: microarray capturing of exosomes and other extracellular vesicles for multiplexed phenotyping. *Journal of extracellular vesicles* **2013**, *2*.
33. Jørgensen, M.M.; Bæk, R.; Varming, K. Potentials and capabilities of the Extracellular Vesicle (EV) Array. *Journal of extracellular vesicles* **2015**, *4*, 26048.
34. Angelot, F.; Seillès, E.; Biichlé, S.; Berda, Y.; Gaugler, B.; Plumas, J.; Chaperot, L.; Dignat-George, F.; Tiberghien, P.; Saas, P.; Garnache-Ottou, F. Endothelial cell-derived microparticles induce plasmacytoid dendritic cell maturation: potential implications in inflammatory diseases. *Haematologica* **2009**, *94*, 1502–12.
35. Gelderman, M.P.; Simak, J. Flow cytometric analysis of cell membrane microparticles. *Methods in molecular biology (Clifton, N.J.)* **2008**, *484*, 79–93.
36. Rozlosnik, N.; Gerstenberg, M.C.; Larsen, N.B. Effect of Solvents and Concentration on the Formation of a Self-Assembled Monolayer of Octadecylsiloxane on Silicon (001). *Langmuir* **2003**, *19*, 1182–1188.
37. Gardiner, C.; Harrison, P.; Belting, M.; Böing, A.; Campello, E.; Carter, B.S.; Collier, M.E.; Coumans, F.; Ettelaie, C.; van Es, N.; Hochberg, F.H.; Mackman, N.; Rennert, R.C.; Thaler, J.; Rak, J.; Nieuwland, R. Extracellular vesicles, tissue factor, cancer and thrombosis - discussion themes of the ISEV 2014 Educational Day. *Journal of extracellular vesicles* **2015**, *4*, 26901.
38. Fernandes, E.; Martins, V.C.; Nóbrega, C.; Carvalho, C.M.; Cardoso, F.A.; Cardoso, S.; Dias, J.; Deng, D.; Kluskens, L.D.; Freitas, P.P.; Azeredo, J. A bacteriophage detection tool for viability assessment of Salmonella cells. *Biosensors & bioelectronics* **2014**, *52*, 239–46.
39. Martins, S.S.; Martins, V.; Cardoso, F.; Freitas, P.; Fonseca, L. Waterborne Pathogen Detection Using a Magnetoresistive Immuno-Chip. In *Molecular Biological Technologies for Ocean Sensing SE - 13*; Tiquia-Arashiro, S.M., Ed.; Springer Protocols Handbooks, Humana Press, 2012; pp. 263–288.
40. Elmore, S. Apoptosis: a review of programmed cell death. *Toxicologic pathology* **2007**, *35*, 495–516.
41. Rieger, A.M.; Nelson, K.L.; Konowalchuk, J.D.; Barreda, D.R. Modified annexin V/propidium iodide apoptosis assay for accurate assessment of cell death. *Journal of visualized experiments : JoVE* **2011**.
42. Kim, K.S.; Cho, C.H.; Park, E.K.; Jung, M.H.; Yoon, K.S.; Park, H.K. AFM-detected apoptotic changes in morphology and biophysical property caused by paclitaxel in Ishikawa and HeLa cells. *PloS one* **2012**, *7*, e30066.
43. Ordóñez, N.G. Immunohistochemical endothelial markers: a review. *Advances in anatomic pathology* **2012**, *19*, 281–95.
44. Bardin, N. Identification of CD146 as a component of the endothelial junction involved in the control of cell-cell cohesion. *Blood* **2001**, *98*, 3677–3684.
45. Ashcroft, B.A.; de Sonneville, J.; Yuana, Y.; Osanto, S.; Bertina, R.; Kuil, M.E.; Oosterkamp, T.H. Determination of the size distribution of blood microparticles directly in plasma using atomic force microscopy and microfluidics. *Biomedical microdevices* **2012**, *14*, 641–9.
46. Hardij, J.; Cecchet, F.; Berquand, A.; Gheldof, D.; Chatelain, C.; Mullier, F.; Chatelain, B.; Dogné, J.M. Characterisation of tissue factor-bearing extracellular vesicles with AFM: comparison of air-tapping-mode AFM and liquid Peak Force AFM, 2013.
47. Bagley, R.G.; Walter-Yohrling, J.; Cao, X.; Weber, W.; Simons, B.; Cook, B.P.; Chartrand, S.D.; Wang, C.; Madden, S.L.; Teicher, B.A. Endothelial precursor cells as a model of tumor endothelium: characterization and comparison with mature endothelial cells. *Cancer research* **2003**, *63*, 5866–73.
48. Bertrand, R.; Solary, E.; O'Connor, P.; Kohn, K.W.; Pommier, Y. Induction of a common pathway of apoptosis by staurosporine. *Experimental cell research* **1994**, *211*, 314–21.
49. Hessler, J.A.; Budor, A.; Putchakayala, K.; Mecke, A.; Rieger, D.; Banaszak Holl, M.M.; Orr, B.G.; Bielinska, A.; Beals, J.; Baker, J. Atomic force microscopy study of early morphological changes during apoptosis. *Langmuir : the ACS journal of surfaces and colloids* **2005**, *21*, 9280–6.
50. Kabir, J.; Lobo, M.; Zachary, I. Staurosporine induces endothelial cell apoptosis via focal adhesion kinase dephosphorylation and focal adhesion disassembly independent of focal adhesion kinase proteolysis. *Biochemical Journal* **2002**, *367*, 145–155.
51. Vilas Shelke, G.; Lässer, C.; Gho, Y.S.; Lötvall, J. Importance of exosome depletion protocols to eliminate functional and RNA-containing extracellular vesicles from fetal bovine serum. *Journal of Extracellular Vesicles; Vol 3 (2014) incl supplements* **2014**.

657 52. Latham, S.L.; Tiberti, N.; Gokoolparsadh, N.; Holdaway, K.; Olivier Couraud, P.; Grau, G.E.R.; Combes,
658 V. Immuno-analysis of microparticles: probing at the limits of detection. *Scientific reports* **2015**, *5*, 16314.
659 53. Dignat-George, F.; Boulanger, C.M. The many faces of endothelial microparticles. *Arteriosclerosis,*
660 *thrombosis, and vascular biology* **2011**, *31*, 27–33.

B.2 Conference proceeding: Analysis of Cell-Derived Microparticles with Highly Precise Nanotechnological Methods

This is the original conference proceeding that has been published in Journal of Nanomaterials & Molecular Nanotechnology.

Cherré et al., J Nanomater Mol Nanotechnol 2014, S2
http://dx.doi.org/10.4172/2324-8777.S2-004

Journal of Nanomaterials & Molecular Nanotechnology

Conference Proceedings

A SCITECHNOL JOURNAL

Analysis of Cell-Derived Microparticles with Highly Precise Nanotechnological Methods

Solène Cherré[1*], Ole Østergaard[2], Niels H. H. Heegaard[2], Noemi Rozlosnik[1]

Abstract

Cell-derived microparticles have gained a broad interest in the past years. Being released by blood cells upon activation or induction of apoptosis, they have a great potential as novel diagnostic markers and their investigation can bring new knowledge into the pathogenesis of various diseases. However, new analysis methods are required to correctly and reliably investigate these small biological particles (between 50 and 1000 nm). In this work, we aimed at developing an *in vitro* population of cell-derived microparticles from endothelial cells. The size of the microparticles was analysed by atomic force microscopy.

Keywords

Cell-derived microparticles; Atomic force microscopy; Apoptosis

Introduction

Cell-derived microparticles (MPs), also called extracellular vesicles, were described for the first time as platelet dust by Wolf in 1967 [1], and have gained a large interest in the biomedical field. They were considered for a long time as cell debris, but recently it has been shown that their investigation can provide valuable information about cellular events like stimulation or apoptosis and that they play a considerable role in the cell-cell communication [2]. MPs are small vesicles (50 to 1000 nm in diameter) and can be found circulating in the blood. They arise from membrane blebs on activated or apoptotic cells. All types of blood cells (erythrocytes, platelets, endothelial cells, etc) produce MPs. The membrane blebbing is indeed part of the remodelling of the cell membrane. Later on in the process, the blebs are released and form the cell-derived microparticles. Studies have shown that the concentration and types of microparticles present in the blood differs between healthy controls and patients of cardiovascular, inflammatory or autoimmune diseases, and in cancer [3]. Therefore, MPs have been proposed as novel diagnostic and prognostic biomarkers [4]. Moreover the investigation of MPs can provide new insights into the pathogenesis of various diseases.

The main problem in developing MPs as diagnostic tools is the difficulty of separating and characterizing them qualitatively and quantitatively in the complicated molecular and cellular environment of blood. The current methods for the analysis of MPs are not well adapted to meet those requirements [5]. Currently, the most widely used method is flow cytometry [5]. In this method a flow of particles is focused so that each particle passes in front of a laser as a single particle. Due to light scattering, the objects can be detected. Flow cytometers are excellent and widely used tools for the study of cells (diameter 10 to 15 μm). However the properties of the instruments are not well adapted for the study of MPs, which are smaller than the wavelength of the laser light. Other investigation methods includes the immunoassays ELISA (enzyme-linked immunosorbent assay) or PLA (proximity ligation assay) [5], as well as proteomics methods like mass spectrometry [6]. However any information relating to the size of the particles cannot be provided using those methods. Optical methods based on light scattering such as dynamic light scattering or combined with the Brownian motion of the particles such as the state-of-the-art nanoparticle tracking analysis (NTA) are also used for the study of cell-derived microparticles.

The aim of this work is to develop a population of cell-derived MPs from the endothelial cell line HUVEC-C and to develop a characterization method for MPs. We will use the highly precise imaging method atomic force microscopy (AFM) to obtain a picture of the microparticles. We will then develop an ImmunoAFM assay in order to characterize the surface antigens on the particles.

Material and Methods

Unless stated otherwise, all chemicals were purchased from Sigma Aldrich, Schnelldorf, Germany.

Cell culture

Human Umbilical Vein Cells C (HUVEC-C, ATCC® CRL-1730™, LGC standard, Borås, Sweden) were cultivated in Ham's F12K (Life Technologies, Nærum, Denmark), 10% fetal bovine serum (Geyer, Roskilde, Denmark), 100 units/ml penicillin/0.1 mg/ml streptomycin, 0.1 mg/ml heparin and 50 μg/ml endothelial cell growth supplement. The cells were passaged every two to three days when the confluence had reached 80%.

Production of cell-derived microparticles

HUVEC-C cells were seeded in a T25 cell flask with a density of $6x10^3/cm^2$. After 48 h of incubation, apoptosis was induced with the addition of 5 μM staurosporine into the cell medium. 24 h after induction of apoptosis, the cell supernatant was collected and centrifuged at 1200 g for 5 min in order to remove the cell debris. The supernatant was then centrifuged at 18900 g for 30 min according to [7] in order to pellet the MPs. 95% of the supernatant was removed and the MPs were resuspended in phosphate buffered saline (PBS). The MPs were pelleted at 18900 g for 30 min and resuspended in PBS. The PBS was filtered (0.22 μm pore size) before use. The cell-derived microparticles were stored at -20°C until further analysis.

Analysis of the cell-derived microparticles by atomic force microscopy (AFM)

10 μl of cell-derived MPs suspension were deposited on a clean silicon surface coated with N-(6-Aminohexyl)

***Corresponding author:** Solène Cherré, Technical University of Denmark, Department of Micro- and Nanotechnology, Oersteds Plads 345 East, DK-2800 Kongens Lyngby, Denmark, Tel: +45 914 184 34; E-mail: solch@nanotech.dtu.dk

Received: April 23, 2014 **Accepted:** July 22, 2014 **Published:** July 25, 2014

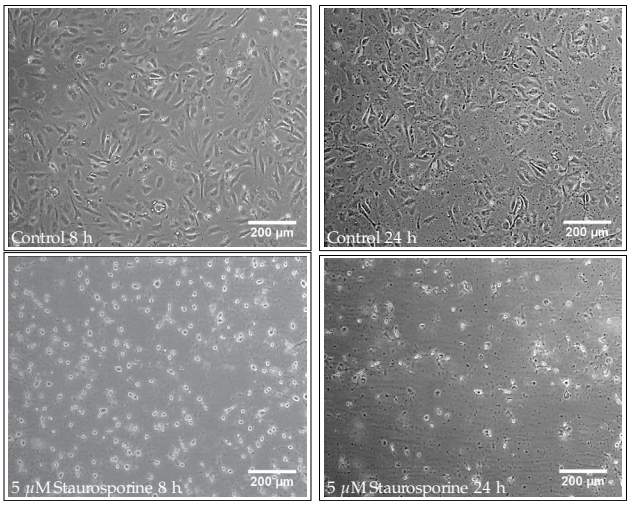

Figure 1: Generation of in-vitro endothelial microparticles. HUVEC-C cells were incubated for 24 h with 5 μM staurosporine so that apoptosis was induced in the cells as well as the release of endothelial microparticles. The pictures were taken with an optical microscope (phase contrast,10X).

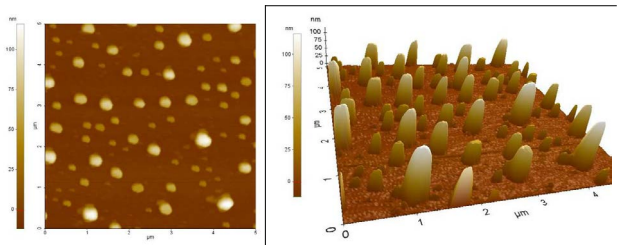

Figure 2: Topography picture of a sample of cell derived microparticles Cell-derived microparticles were produced by induction of apoptosis in HUVEC-C cells. The sample was scanned in non-contact taping mode by AFM. The picture on the right shows a 3D projection of the 2D picture. The picture is a scan of 5x5 μm.

aminopropyltrimethoxysilane (ABCR, Karlsruhe, Germany). After 1 min of absorption, the sample was rinsed with 200 μl milliQ water (filtered against 0.22 μm pore size) three times. The sample was then dried under air flow within 1 min. The sample was scanned using the AFM system XE 150 (Park Systems, Suwon, Korea) in tapping mode (non-contact intermittent mode). The cantilever (Tap300Al-G, BudgetSensor, Sofia, Bulgaria) had a force constant of 40 N/m and a resonance frequency of 300 kHz with a tip radius of curvature below 10 nm. The topography of the sample was registered using the software XEP and the images were analysed with the software XEI (Park Systems, Suwon, Korea).

Results

Development of a system model for the study of cell-derived microparticles

Since the aim of this project is to work on the methodology for analysis of cell-derived microparticles, it is a main concern to work with a defined and characterized population of cell-derived microparticles in order to validate the new methods. We cultivated HUVEC-C cells according to standard cell cultivation procedures. When the cells had reached 70% confluency, 5 μM staurosporine was

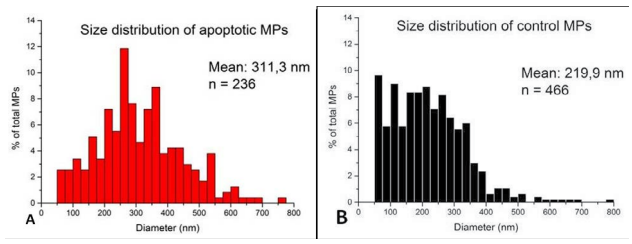

Figure 3: Size distribution of cell-derived microparticles (MPs) Control cell-derived microparticles are particles collected from non-treated cells, while apoptotic cells were collected from cells which had been treated with the apoptosis inducting chemical staurosporine. The mean diameter of the apoptotic cell-derived microparticles was larger than the one of control cell-derived microparticles.

added to the medium in order to induce apoptosis. Staurosporine is an inhibitor of protein kinases. It induces apoptosis in endothelial cells by breaking the focal adhesion sites by dephosphorylation of focal adhesion kinase [8]. Figure 1 shows the effects of the chemical compound staurosporine. The pictures in the first row of Figure 1 show HUVEC-C cells that have not been treated with staurosporine. 8 hours as well as 24 hours after the beginning of the experiment, the cells had conversed a morphology characteristic for HUVEC-C cells, that is to say that the cells were attached on the bottom of the cell culture flask and were spread and elongated. The cells treated with staurosporine are shown in the second row of Figure 1, 8 hours and 24 hours after addition of staurosporine. Already 8 hours after addition of staurosporine, the morphology of the HUVEC-C cells had changed completely. The cells were round and had detached from the surface of the cell culture flask, which is characteristic for cells undergoing apoptosis. Therefore we could conclude that the treatment with staurosporine was efficient to induce apoptosis in the HUVEC-C cells. The supernatant was collected and purified by high speed centrifugation in order to resuspend the cell-derived microparticles in the phosphate buffer PBS.

Analysis of the cell-derived microparticles by atomic force microscopy

The cell derived microparticles collected from the cell supernatant were analyzed by atomic force microscopy (AFM) in order to determine the size distribution of the sample. Figure 2 shows a representative picture of the scanned microparticles. Using the upper threshold method, the projected areas of each of the microparticles were obtained and the diameter was calculated according to the following formula: $d = 2 \times \sqrt{\frac{area}{\pi}}$. The data were represented in a histogram (Figure 3). Figure 3A shows the size distribution for MPs collected from the supernatant of apoptotic cells (apoptotic MPs), while Figure 3B shows the size distribution of MPs collected from non-treated cells (control MPs). The relative change of the mean diameter was 42% and the distributions were found to be significantly different according to the non-parametric Kolmogorov-Smirnov Test with p=0.05. These data suggested that the induction of apoptosis in HUVEC-C cells had an effect on the size of the MPs released from those cells. AFM was well suited for the study of these small biological objects. Using AFM objects with a broad size range could be analysed in the same experiment and a clear picture of the samples could be obtained.

Conclusion and Outlook

We have established a model system of cell-derived microparticles

in vitro. It was very easy to collect the microparticles and purify them to obtain a solution for analysis. The characterization of the cell-derived microparticles was performed by atomic force microcospy, a method well adapted to the size of those objects. This lay down the basement of a new analytical method for cell-derived microparticles. AFM will be further used in combination with microparticle specific capture molecules such as antibodies, so that the surface antigens can also be characterized.

Acknowledgments

This work was supported by the Technical University of Denmark.

References

1. Wolf P (1967) The Nature and Significance of Platelet Products in Human Plasma. Brit J Haematol 13: 269-288.
2. Mause SF, Weber C (2010) Microparticles Protagonists of a Novel Communication Network for Intercellular Information Exchange. Circ Res107: 1047-1057.
3. Hugel B, Martínez MC, Kunzelmann C, Freyssinet JM (2005) Membrane microparticles: two sides of the coin. Physiology 20: 22-27.
4. Simak J, Gelderman MP (2006) Cell membrane microparticles in blood and blood products: potentially pathogenic agents and diagnostic markers. Transfus Med Rev 20: 1-26.
5. Shet AS (2008) Characterizing blood microparticles: technical aspects and challenges. Vasc Health Risk Manag 4: 769-774.
6. Østergaard O, Nielsen CT, Iversen LV, Jacobsen S, Tanassi JT, Heegaard NH (2012) Quantitative Proteome Profiling of Normal Human Circulating Microparticles. J Proteome Res 11: 2154-2163.
7. Nielsen CT (2012) Circulating microparticles in systemic Lupus Erythematosus. Dan Med J 59: B4548.
8. Kabir J, Lobo M, Zachary I (2002) Staurosporine induces endothelial cell apoptosis via focal adhesion kinase dephosphorylation and focal adhesion disassembly independent of focal adhesion kinase proteolysis. Biochem J 367: 145-155.

Author Affiliations

Top

[1]*Technical University of Denmark, Department of Micro- and Nanotechnology, Oersteds Plads 345 East, DK-2800 Kongens Lyngby, Denmark*

[2]*Statens Serum Institut 5 Artillerivej, DK-2300 Copenhagen S, Denmark*

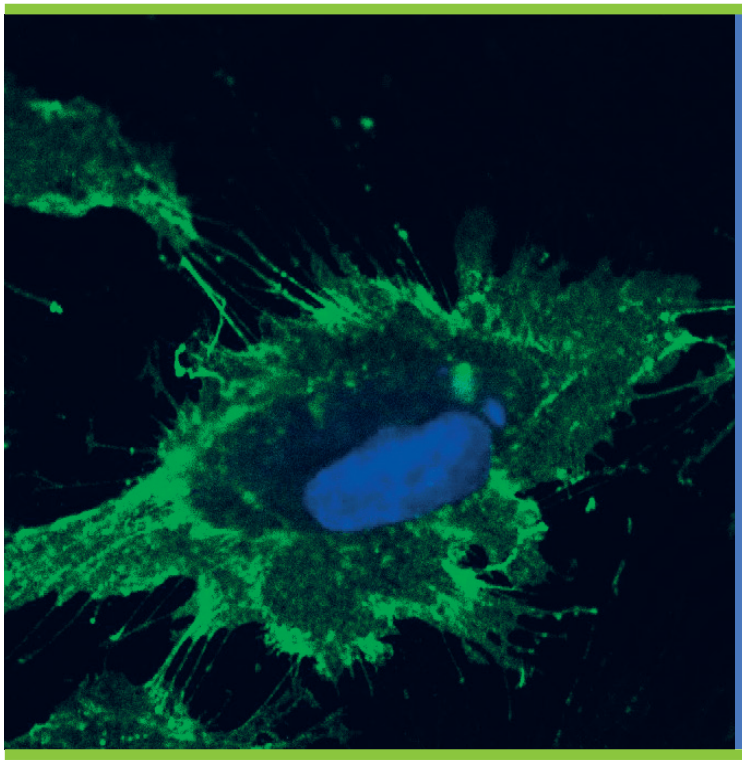

Published by:
DTU Nanotech
Department of Micro- and Nanotechnology
Technical University of Denmark
Ørsteds Plads, building 345C
DK-2800 Kgs. Lyngby

DTU Nanotech
Department of Micro- and Nanotechnology